

# Energy performance and ecological potential of solar thermal façade collectors made of ultra-high performance concrete (UHPC) for a CO<sub>2</sub> neutral heat supply

Lotta Margarete Koch

Vollständiger Abdruck der von der TUM School of Engineering and Design der Technischen  
Universität München zur Erlangung einer  
Doktorin der Ingenieurwissenschaften (Dr. -Ing.)  
genehmigten Dissertation.

Vorsitz: Prof. Andreas Hild

Prüfer\*innen der Dissertation:

1. Prof. Thomas Auer
2. Prof. Dr.-Ing. Tillmann Klein

Die Dissertation wurde am 20.10.2022 bei der Technischen Universität München eingereicht  
und durch die TUM School of Engineering and Design am 24.01.2023 angenommen.



# Contents

	.PAGE
Summary .....	iii
Danksagung .....	vii
Nomenclature .....	ix
1. Overview .....	1
1.1. Introduction .....	1
1.2. Background .....	2
1.3. Problem .....	2
1.4. Objective .....	5
1.5. Social and scientific relevance .....	5
1.6. Hypothesis .....	7
1.7. Research question .....	7
1.8. Scope .....	8
1.9. Methodology and Chapter Overview .....	9
2. Architecture and solar thermal .....	13
2.1. Contribution of building-integrated solar thermal (BIST) to urban heat transition .....	13
2.1.1. Challenge .....	13
2.1.2. Energy transition and area needed for solar technology .....	14
2.1.3. Decentralization/location .....	15
2.1.4. Visibility .....	16
2.1.5. Status quo of visible solar components .....	17
2.1.6. Aspects of consumer behavior .....	17
2.1.7. Façade and solar thermal markets .....	18
2.1.8. Architectural integrability .....	18
2.2. Former and ongoing product development and research in BIST .....	21
2.2.1. Overview of literature .....	21
2.2.2. Different approaches to BIST .....	22

2.2.3.	Exemplary own retrospective.....	24
2.2.4.	Barriers to deployment of BIST.....	28
2.3.	Pull vs. push or piggy-backing strategies for BIST.....	29
2.4.	Background theses for further assessment of BIST.....	30
2.5.	Qualitative evaluation factors for BIST collectors.....	31
3.	Towards sustainability assessment of BIST collectors.....	35
3.1.	Reasons for sustainability assessment of BIST collectors.....	35
3.2.	System boundaries.....	38
3.3.	Fundamentals of sustainability assessment of products.....	40
3.3.1.	Benefit analysis (BA).....	40
3.3.2.	Life cycle assessment (LCA).....	41
3.3.3.	Life cycle costing (LCC).....	44
3.3.4.	Social life cycle assessment (S-LCA).....	44
3.3.5.	Sustainability assessment methodology.....	45
3.4.	Overview of the literature about LCA of solar thermal systems.....	45
3.5.	Functional unit for BIST.....	49
3.5.1.	General remarks.....	49
3.5.2.	Description of functional unit and the system boundaries for BIST.....	50
4.	Solar thermal collectors made of UHPC.....	55
4.1.	Fundamentals and state of the art of solar thermal collectors.....	55
4.1.1.	Classification.....	55
4.1.2.	State of the art of glazed and unglazed flat plate collectors.....	56
4.1.3.	Description of solar yield.....	60
4.2.	Particularities of UHPC collectors.....	64
4.2.1.	Architectural possibilities for UHPC collectors.....	65
4.2.2.	Description of production technology and properties.....	67
4.3.	Modeling UHPC collectors.....	73
4.3.1.	Overview of existing models and their limits.....	74
4.3.2.	FEM modeling approach for wind and infrared-sensitive UHPC collectors.....	76
4.3.3.	Glazed UHPC collectors.....	97
4.4.	Summary and discussion of results.....	104
4.5.	Further research.....	105
5.	Solar thermal systems with UHPC collectors.....	107
5.1.	Fundamentals.....	107
5.1.1.	Solar thermal systems.....	107
5.1.2.	Heat pump systems.....	110

5.1.3.	Solar-assisted heat pump systems .....	114
5.2.	Modeling of solar thermal and reference systems .....	115
5.2.1.	General remarks .....	115
5.2.2.	Selection of reference systems .....	116
5.2.3.	Modeling environment and language .....	117
5.2.4.	System configurations .....	117
5.3.	Description and modeling of reference house .....	119
5.3.1.	Heating load .....	119
5.3.2.	Site selection and weather data .....	123
5.3.3.	Domestic hot water and circulation .....	124
5.4.	Components and dimensioning of heating systems .....	125
5.4.1.	Solar collectors .....	125
5.4.2.	Ice storage .....	125
5.4.3.	Heat pumps .....	127
5.4.4.	Borehole heat exchanger .....	131
5.4.5.	Hot storages .....	133
5.4.6.	Heat distribution .....	135
5.4.7.	Control .....	135
5.5.	Results of energy simulations and discussion .....	137
5.5.1.	Performance figures .....	137
5.5.2.	Test solar direct systems “Col-Dir area and wind influence” .....	139
5.5.3.	Test solar direct systems “Col-Dir north façade” .....	143
5.5.4.	Test solar direct systems “Col-Dir store-hot” .....	144
5.5.5.	Test solar ice systems “Col-Ice south and north façade” .....	148
5.6.	Summary and discussion of results .....	153
5.7.	Further research .....	154
6.	Life cycle assessment of systems with UHPC collectors .....	157
6.1.	Inventory analysis .....	157
6.1.1.	Data collection and quality .....	157
6.1.2.	Lifetime .....	158
6.1.3.	Façade components .....	159
6.1.4.	System components .....	172
6.1.5.	Use phase .....	174
6.2.	Life cycle impact assessment (LCIA) and discussion .....	174
6.2.1.	LCIA of components .....	174
6.2.2.	LCIA of life cycle .....	180
6.3.	Summary and discussion of results .....	187

6.4. Further research .....	189
7. Life cycle cost assessment of systems with UHPC collectors.....	191
7.1. Methodology .....	191
7.2. Cost assumptions of façade components .....	191
7.3. Results and discussion .....	193
7.3.1. Glazed UHPC collector .....	193
7.3.2. Unglazed UHPC collector .....	195
7.4. Further research .....	199
8. Discussion of results, conclusion, and further research .....	201
8.1. Summary and discussion of results .....	201
8.2. Conclusion.....	204
8.3. Further research .....	208
Bibliography .....	209
Appendix A. ....	225
List of Figures .....	251
List of Tables .....	265

## Summary

One of the greatest challenges society is facing today is climate change. The central task for Germany in addressing the effects of climate change is the transformation of our energy systems. A large share of energy consumption in Germany is attributable to the building sector. In order to achieve the heat transition, the adoption of renewable energy sources is required. During this transformation, heat pumps will play an important role in providing the amount of energy needed from renewable sources for this sector.

In combination with heat pumps or other heat suppliers, it is expected that solar thermal energy will be relied on increasingly as a, mostly secondary, heat supply. There are currently several types of solar thermal collectors on the market. Due to their architectural flexibility, unglazed façade collectors made of ultra-high performance concrete (UHPC) seem to be a promising solution for increasing adoption of solar thermal in the building sector. This thesis investigates the use of these collectors as a source for heat pumps. Using a whole life cycle analysis (LCA), the carbon emissions of different renovation pathways are compared for a multi-family home in Potsdam, Germany. System and component simulations are conducted and serve as an input to the LCA.

The adoption of both heat pumps and solar thermal is proceeding more slowly than necessary to achieve Germany's climate targets (climate-neutrality in 2045); in building renovations, the share of heat pumps is just under six percent.

High investment cost may be the largest barrier to installing heat pumps on a large scale. Especially in narrow urban areas other counter-arguments come on top or become more important: local conditions may not allow for the use of geothermal, and/or noise pollution, regulations and distance from adjacent buildings may impede using ambient heat. However, systems with façade collectors that serve as a source for a heat pump neither require a borehole nor involve the acoustic emissions of outdoor air units. Thus, it is possible that these systems could close a gap in the market for heat pumps and thus accelerate the heat transition.

In order to generate sufficient energy from renewable sources, large areas are needed. For photovoltaics and solar thermal collectors, building envelope surfaces are also suitable. The more façade surfaces are used for energy generation, in addition to roof surfaces, the more visible the technical components are and the more important good

architectural integration becomes. The interrelations between architecture and solar thermal energy are clarified in this thesis, and the existing obstacles for a successful architectural integration are summarized from the literature. It is made clear that in the case of large solar active surface areas in the façade, the energy system of the building can no longer be considered separately from the building itself. The system boundaries for an ecological and economic consideration should include both.

In this context, the extension of the product range by collectors, for example those made of UHPC, is considered positive for a better architectural integrability. Depending on how visible the material is in the built-in façade collector, the result is a more-or-less obvious expansion of the product range. The most direct material contact is effected by unglazed, uncoated collectors. However, such unglazed and uncoated collectors cannot provide a temperature level sufficient for direct heating support or to provide domestic hot water. Collectors with an uncoated absorber and a Low-E glazing allow for a more indirect visual contact with the material, but they can achieve higher temperature levels.

In this work, a major focus is placed on the use of unglazed solar thermal façade collectors made of UHPC as an alternative source for a heat pump. The system is a so-called serial system. UHPC collectors with glazings with or without Low-E layer may be used in more established parallel systems with an air- or a ground-source heat pump or gas as a second heat provider. For these glazed types of collector, only a short efficiency study is carried out. The considerations are based on the *TABSOLAR*<sup>®</sup> concept, which currently only exists for the production of flow-through elements made of UHPC and is still under development. No pilot installation exists so far.

For the characterization of these UHPC collectors, existing models for the simulation of a heat gain curve of glazed and insulated solar thermal collectors are extended with the help of the finite element method for unglazed, non-insulated collectors. With the developed model, boundary effects and thermal bridge effects due to fastenings are quantified, and different installation situations are analyzed. This study also investigates whether it is possible for uncoated UHPC collectors with a Low-E glazing to achieve the funding conditions of the MAP<sup>1</sup> currently in force in Germany. Depending on the width of the edge area, this possibility is assessed as difficult but not ruled out completely. For UHPC collectors with spectrally selective coating, the MAP criteria is met with the parameters of a simulated heat gain curve.

Based on the retrofit of a medium-sized apartment building in Potsdam, Germany, the simulations show that a system with unglazed collectors as a direct source for a heat pump can achieve similar or better system efficiencies compared to air-source heat pumps, depending on the installed area. However, in these systems the collector mainly

---

<sup>1</sup>Marktanreizprogramm



acts as an ambient heat exchanger, convective gains dominate, and solar gains can hardly be used. If additionally an ice storage tank is used, the usable solar thermal heat increases significantly, and system efficiencies in the range of ground source heat pumps can be achieved. In combination with a large ice storage tank, water can be used as the heat transfer fluid in the collector.

In order to show advantages in system efficiency in the consideration of primary energy and CO<sub>2</sub> emissions over the entire life cycle, the respective emissions of a kilowatt hour of the German electricity mix are assumed to be constant. The energy advantages are then retained in this consideration as well. If a dynamic development of the CO<sub>2</sub> emissions of a kilowatt hour of the German electricity mix is assumed, savings are lower, but can still be achieved.

Economically, a system with an active rear-ventilated façade as the source for a heat pump offers no advantages over an economic benchmark defined as a system with an external thermal insulation composite system on the façade and an air-source heat pump. The differences in investment costs of the façade system are too high compared to the relatively low energy cost savings. Systems with ice storage show greater operational cost savings, but are not currently economically advantageous due to a low level of standardization. Since most ice storage units are buried in the ground, high digging costs must be considered. If a system with a passive rear-ventilated façade and air source heat pump is used as a reference, the façade collector system may be advantageous depending on the additional cost of the solar system.

Overall, it can be seen that systems with UHPC façade collectors as sources for heat pumps can be architecturally attractive alternatives to other heat pump systems that are favorable in terms of energy, primary energy, and CO<sub>2</sub> emissions. Solar thermal collectors (i.e., those that can also provide usable temperature levels directly in the heating system and thus temporarily take over the function of the heat pump), adapted heat pumps, and other storing concepts and control strategies potentially offer further savings and may improve the economic efficiency.



## Danksagung

Ich danke Prof. Tina Wolf für die Bereitschaft, meine Dissertation zu betreuen. Prof. Thomas Auer und Prof. Tillmann Klein danke ich für die Übernahme meiner Betreuung. Ihre konstruktive, unkomplizierte Art meine Dissertation zu begleiten hat mir sehr geholfen. Michael Hermann danke ich für die fachliche Begleitung und Betreuung meiner Dissertation seitens des Fraunhofer ISE. Die vielen Stunden Gespräche über Solarthermie und die Zukunft der Energieversorgung mit ihm, sein Ideenreichtum, die gründliche Korrekturlese und seine wertschätzende, vertrauensvolle und mitnehmende Art haben wesentlich zum Gelingen dieser Arbeit beigetragen.

Meiner Kollegin Katharina Morawietz danke ich für eine sehr gute gemeinsame Bürozeit als Promovierende. Christoforos Pouloupoulos danke ich für seine Arbeit und das gemeinsame Eintauchen in die Welt von Life Cycle Assessment. Jeannette Wappler danke ich für den Austausch über ihr fundiertes Wissen über Wärmepumpen. Auch den vielen anderen, freundlichen, hilfsbereiten und inspirierenden MitarbeiterInnen vom Fraunhofer ISE und den Projektpartnern aus den Projekten TABSOLAR I, II und III, die mich auf dem Weg der Dissertation begleitet haben, möchte ich herzlich danken. Insbesondere konnte ich auf den Arbeiten von Manuel Lämmle und VorgängerInnen und MitarbeiterInnen an den verschiedenen Kollektormodellen und auf den Arbeiten der MitarbeiterInnen des Projektes Lowex-Bestand ([www.lowex-bestand.de/](http://www.lowex-bestand.de/)) aufbauen. Vielen Dank dafür!

Außerdem möchte ich mich beim Fraunhofer ISE für die finanzielle Unterstützung im Rahmen des Doktorandinnen-Programms bedanken.

Mit der englischen Korrekturlese haben mir Ana Gauche, Anne Kovach-Hebling und Usch Engelmann geholfen. Vielen Dank!

Ohne die immerwährende Unterstützung meiner Eltern und meiner Familie wäre ich niemals bis hier gekommen. Danke dafür! Meinen drei Kindern danke ich für den Ausgleich und viel Freude neben der Dissertation. Ganz besonders danke ich Konrad Völkel.



## Nomenclature

$\alpha$	Absorptance	
$\dot{Q}_{demand,biv,heat+DHW}$	Thermal capacity needed to cover the heating demand and the demand for DHW at the bivalent temperature	kW
$\dot{Q}_{demand,biv,heat}$	Thermal capacity needed to cover the heating demand at the bivalent temperature	kW
$\dot{Q}_{demand,biv}$	Short form of $\dot{Q}_{demand,biv,heat+DHW}$	kW
$\dot{Q}_{heat,MB-scaled,nom}$	Nominal thermal capacity of the scaled model base heat pump	kW
$\dot{Q}_{heat,MB}(\vartheta_{biv})$	Capacity of model base heat pump in bivalent point	kW
$\dot{Q}_{useful}$	Useful heat flux from collector	W
$\eta_0$	Thermal conversion factor	
$\lambda$	Thermal conductivity	$\text{W m}^{-1} \text{K}^{-1}$
$(\tau\alpha)_{eff}$	Effective transmittance-absorptance product	
$\mu$	Dynamic viscosity	$1 \times 10^{-6} \text{kg m}^{-1} \text{s}^{-1}$
$\nu$	Kinematic viscosity	$1 \times 10^{-6} \text{m}^2 \text{s}^{-1}$
$\rho$	Density	$\text{kg m}^{-3}$
$\sigma$	Stefan-Boltzmann constant	$\text{W m}^{-2} \text{K}^4$
$\Theta$	Incidence angle	
$\varepsilon_{100^\circ\text{C}} = \varepsilon$	Emissivity at $100^\circ\text{C}$	
$\vartheta_{abs,m}$	Mean absorber temperature	$^\circ\text{C}$
$\vartheta_{amb}$	Ambient temperature	$^\circ\text{C}$
$\vartheta_{biv}$	Temperature in bivalent point	$^\circ\text{C}$
$\vartheta_{fluid,m}$	Mean fluid temperature	$^\circ\text{C}$
$\vartheta_{limit,heating}$	Heating limit temperature	$^\circ\text{C}$
$\vartheta_{room}$	Room temperature	$^\circ\text{C}$
$\vartheta_{stand,out}$	Standard minimum outside temperature	$^\circ\text{C}$
$A_{ap}$	Aperture area of collector	$\text{m}^2$

$A_f$	Net heated floor area	$\text{m}^2$
$b_0$	Collector specific constant for calculating the incidence angle modifier	
$b_1$	linear heat loss coefficient for unglazed collectors	$\text{W s m}^{-3} \text{K}^{-1}$
$b_2$	wind dependent linear loss coefficient for unglazed collectors, equation (4.1.2)	$\text{W m}^{-2} \text{K}^{-1}$
$b_u$	wind dependent thermal conversion factor for unglazed collectors, equation (4.1.2)	$\text{m}^{-1} \text{s}$
$c_1$	Linear heat transfer coefficient	$\text{W m}^{-2} \text{K}^{-1}$
$c_2$	Quadratic heat transfer coefficient dependent on temperature	$\text{W m}^{-2} \text{K}^{-2}$
$c_3$	Heat transfer coefficient dependent on wind speed	$\text{J m}^{-3} \text{K}^{-1}$
$c_4$	Heat transfer coefficient dependent on sky temperature	
$c_5$	Effective heat capacity	$\text{J m}^{-2} \text{K}^{-1}$
$c_6$	Thermal conversion factor dependent on wind speed	$\text{s m}^{-1}$
$c_7$	IR radiation exchange dependent on wind speed	$\text{W m}^{-2} \text{K}^{-4}$
$c_8$	Radiation losses	$\text{W m}^{-2} \text{K}^{-4}$
$C_{eff}$	Total thermal capacity	$\text{kJ K}^{-1}$
$c_{eff}$	Specific thermal capacity	$\text{kJ m}^{-2} \text{K}^{-1}$
$cp$	Specific heat capacity	$\text{kJ kg}^{-1} \text{K}^{-1}$
$E_L$	Long-wave irradiance ( $\lambda > 3 \mu\text{m}$ )	$\text{W m}^{-2}$
$F'$	Collector efficiency factor	
$f_{sav}$	Fractional energy savings	
$G$	Hemispherical solar irradiance	$\text{W m}^{-2}$
$G''$	Net hemispherical solar irradiance	$\text{W m}^{-2}$
$h$	Heat transfer coefficient	$\text{W m}^{-2} \text{K}^{-1}$
$K_{\Theta}$	Incident angle modifier	
$m$	Mass	$\text{kg}$
$q$	Specific heat flux	$\text{W m}^{-2}$
$Q_{coll,MAP}$	Collector output calculated with equation (4.1.7)	$\text{kWh m}^{-2}$
$T$	Temperature	$\text{K}$

$T_{out}$	Temperature towards radiation is occurring	K
$T_{sky}$	Sky temperature	K
$U_{abs,fluid}$	Internal heat transfer coefficient between mean absorber temperature and mean fluid temperature	$\text{W m}^{-2} \text{K}^{-1}$
$U_{loss}$	Overall heat loss coefficient	$\text{W m}^{-2} \text{K}^{-1}$
$u_{wind}$	wind velocity	$\text{m s}^{-1}$
Nu	Nusselt number	
Pr	Prandtl number	
Re	Reynolds number	
T	Temperature	K

### Definitions

Parallel system	Solar thermal collectors and other heat source work separately, compare figure 5.1.4.
Serial system	Solar thermal collectors are used as a direct source for a heat pump, compare figure 5.1.4.

### Subscript

abs	Absorber
aux	Auxiliary
biv	bivalent
con	Condenser
cond	Conductive
conv	Convective
DHW	Domestic hot water
el	Electrical
eva	Evaporator
HC	Heating circuit
HP	Heat pump
rad	Radiative
tot	Total

**Abbreviations**

<i>wcf</i>	Wind correction factor
ASHP	Air-source heat pump
BA	Benefit analysis
BAST	Building added solar thermal
BIPV	Building-integrated photovoltaic
BIST	Building integrated solar thermal
Col-Dir	Systems with collectors as only source for a heat pump
Col-Ice	Systems with collectors in combination with an ice storage as sources for a heat pump
COP	Coefficient of performance
CPC	Compound parabolic concentrator
DE	Dataset for Germany
DHW	Domestic hot water
EnEV	Energieeinsparverordnung, Engl.: German Energy Saving Ordinance
EPD	Environmental product declaration
ETICS	External thermal insulation composite system
EYR	Energy yield ratio
FEM	Finite element method
FRP	Fiber reinforced plastic
GLO	Global dataset
GSHP	Ground-source heat pump
GWP 100a	Global warming potential with a time horizon of 100 years
HVAC	Heating, ventilation, and air conditioning
LCA	Life cycle assessment
LCC	Life cycle cost
LCIA	Life cycle impact assessment
LCOE	Levelized cost of energy
MFH	Multi-family home
PCE	Polycarboxylate-ether based
PED	Primary energy demand
PP	Polypropylene



PV	Photovoltaics
PVT	Photovoltaic thermal
RER	Dataset for Europe
RoW	Dataset for rest of the world, corresponds to GLO
S-LCA	Social life cycle assessment
SAHC	Solar and ambient heat collector
SDG	Sustainable Development Goal
SFH	Single-family home
SPF	Seasonal performance factor
STS	solar thermal system
SVF	Sky view factor
TABS	Thermo-active building element
TCO	Total cost of ownership
UHPC	ultra-high performance concrete
WISC	Wind and Infrared Sensitive Collector



## CHAPTER 1

# Overview

### 1.1. Introduction

Solar thermal energy is considered one of the key technologies for the energy transition. Although façades are well suited for solar thermal energy applications for a variety of reasons, they are rarely used for this purpose. In order to generate sufficient energy from renewable sources, large areas are needed. The fact is that the façade area suitable for renewable energy generation exceeds the amount of suitable roof area, especially in urban areas. Compared to roof-integrations, the total energy gain is lower for façade-integrated systems. However, due to the more homogenous gain profile with a lower peak in the summer, they match the typical load profile better. Usually, high demand occurs during the winter and low demand during the summer, in the northern hemisphere.

Building-integrated solar thermal systems is still a niche market. Besides the legal, technical, distribution and cost issues, the low amount of flexibility in the shape, color and surface structure of the available systems impedes the use of solar thermal in façades today. In contrast to fossil fuel heating systems, solar systems are always visible on the building exterior and influence the design of the building envelope. Façades are particularly sensitive to design interventions, as they represent the faces of the building. However, if architectural integration is aesthetically pleasing and synergies can be exploited through the multifunctionality of the façade, the market for façade-integrated solar thermal systems could open up. The façade market is nearly four orders of magnitude larger than the solar thermal market (market data from Germany, 2017). Together with good heating systems, activated high quality façades could help to reduce the energy demand of buildings. Overall, the total energy savings and the CO<sub>2</sub> emissions reductions in the building sector depend on both the savings in each individual building as well as the market penetration of highly energy-efficient buildings.

In this thesis façade-integrated solar thermal collectors made of ultra-high performance concrete are investigated. Their energetic and ecological potential for urban heat transition in Germany is estimated on the base of component and system simulation and life cycle assessment. The focus is on unglazed UHPC collectors as a source for a heat pump with and without a combination with an ice storage.

## 1.2. Background

One approach to increase architectural integration was pursued in the two German research projects TABSOLAR I and II [74, 75] and the follow-up project TABSOLAR III. In these projects, the material ultra-high performance concrete (UHPC) is the basis for prefabricated fluid-carrying façade elements for different types of façades (rear-ventilated, thermal insulation composite system (ETICS), sandwich-wall). A heat carrier fluid flows through the channels of the UHPC element and collects the heat for usage. Inside the building, corresponding elements are planned as thermo-active building elements (TABS), possibly in combination with classical concrete core activation. The flow channels are fabricated by a so-called membrane vacuum deep-drawing process developed by Fraunhofer ISE.

Three product families of the *TABSOLAR*<sup>®</sup> collectors are planned and under development: *Premium*, *Economy* and *Design*. Each family has a different solar gain, maximum temperature, cost and design, in order to serve different applications. *TABSOLAR*<sup>®</sup> *Premium* and *Economy* have glazings for higher solar gains and temperature levels. *TABSOLAR*<sup>®</sup> *Design* is designed for lower temperature levels, e. g., as a source for a heat pump or for heating swimming pools, and therefore can remain unglazed. It also offers free surface design through structuring and/or coloring to match market available passive cladding elements. Although *TABSOLAR*<sup>®</sup> is not yet available on the market, a trademark has been registered.

This work deals with UHPC collectors. At the time this work was carried out, no other UHPC collector concepts existed. Therefore “UHPC collector” refers to one type of the *TABSOLAR*<sup>®</sup> collector family. The focus is on *TABSOLAR*<sup>®</sup> *Design*, but the context explains which type of the *TABSOLAR*<sup>®</sup> collector family is meant. Figure 1.2.1 shows some impressions from the trade fair BAU and figure 1.2.2 presents the *TABSOLAR*<sup>®</sup> concept ([www.tabsolar.de](http://www.tabsolar.de)).

## 1.3. Problem

A big advantage of UHPC is its high flexibility with respect to surface texture and color. Personal feedback from architects regarding the *TABSOLAR*<sup>®</sup> concept was positive, for the most part, during the trade fair BAU in Munich in 2017 and 2019 and project work. However, no scientific feedback study was conducted. The material properties of UHPC are interesting for façades, however, the properties are quite different than those of state-of-the-art absorbers, which are mostly made from copper or aluminum.

The properties of UHPC come along with some disadvantages for common collector or absorber design. Higher material usage along with higher thermal capacity, two orders of magnitude lower thermal conductivity, thermal bridges on fixing points influence



(A)



(B)



(C)

FIGURE 1.2.1. Impression of trade fair BAU 2019: (A, left) *TABSOLAR*<sup>®</sup> *Premium* with spectrally selective coating and (A, right) *TABSOLAR*<sup>®</sup> *Design* unglazed in two colors. (B) The little cutout demonstrates a possible surface structure. Depending on the point of view the contrast of the pattern varies. (C) Backside of the collector with cutout of the back insulation (Source: Fraunhofer ISE).

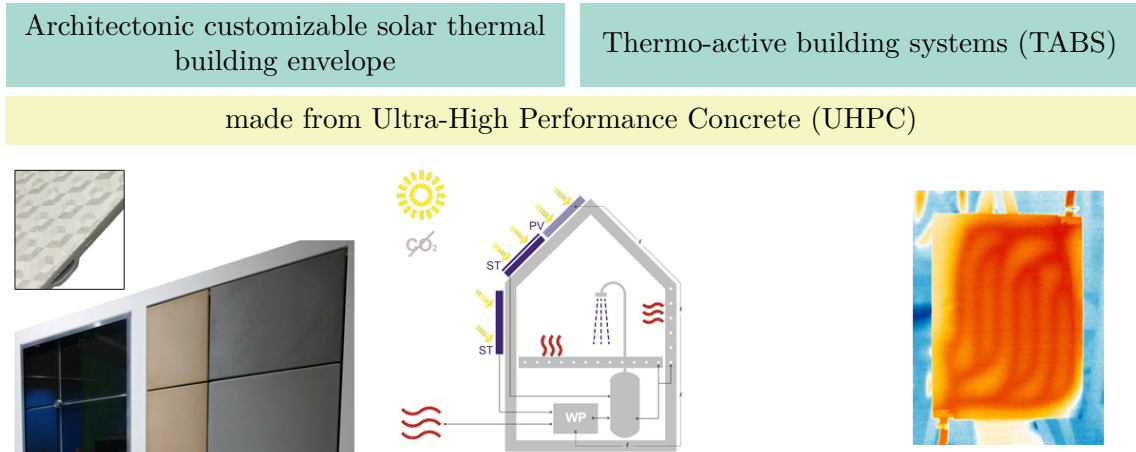


FIGURE 1.2.2. *TABSOLAR*<sup>®</sup> concept. Left: impression of trade fair BAU 2019 (Source: Fraunhofer ISE). Center: schematic of possible system configuration (Source: Priedemann Facade-Lab GmbH). Right: thermographic image of small a *TABSOLAR*<sup>®</sup> sample (Source: Fraunhofer ISE).

the efficiency. Spectrally selective coatings used to reduce heat loss in state-of-the-art absorbers may have lower quality but higher cost when applied to UHPC absorbers. The UHPC material is very dense and watertight, in contrast to normal concrete, and therefore no additional metal or plastic pipes are necessary for the flow channels. Most collectors are operated with a mixture of water and antifreeze.

Antifreeze fluid based on propylene glycol is not highly toxic, but releases into the environment should be minimized [154].

It is not known if very small amounts of antifreeze could pass the UHPC material during operation. In case of a possible passing of antifreeze through the UHPC, an internal sealing coating could be applied. Another solution can be to operate the UHPC collector with pure water. The operating temperature of the collector must then be restricted to temperatures above the freezing temperature of water.

All these aspects of UHPC lead to a completely redesigned collector and system.

To assess the efficiency of new absorber or collector concepts, different validated models exist that can simulate characteristic heat gain curves. For a solar and ambient heat collector (SAHC) like *TABSOLAR*<sup>®</sup> *Design*, current modeling strategies reach their limits as they work with simplifications that are only valid for insulated collectors. In particular, the unglazed and uninsulated variant of *TABSOLAR*<sup>®</sup> *Design* cannot be accurately described using the actual node models.

Nonetheless, with an insulation, adequate design and glazing as for *TABSOLAR*<sup>®</sup> *Economy* or with an additional spectrally selective coating as for *TABSOLAR*<sup>®</sup> *Premium*,

thermal efficiencies which are comparable to state-of-the-art collectors may be reached. Thus, both collector variants will probably be able to provide heat for common heating systems. If funding is to be applied for in Germany, the eligible criteria need to be met. Whether all variants will meet the eligible criteria for current funding in Germany is not known.

The collector family *TABSOLAR<sup>®</sup> Design*, which consists in a pure absorber without glazing, will probably not, or only for a short period in summer, be able to directly provide heat for domestic hot water or heating. Heat losses will be too high. However, heat from those absorbers can still be used as a source for a heat pump. The effect that the coatings, insulation, thermal bridges or back ventilation has on the achievable temperature level of *TABSOLAR<sup>®</sup> Design*, and thus on its capability to deliver heat directly to the building, is not known. When using the collector as direct source for a heat pump it is not known which part of the needed energy can be provided by solar gains and which by ambient heat gains.

It is also not known whether collectors that are not able to operate below 0°C collector temperature are sufficient as a single source for a heat pump or whether a cold storage is necessary between the collectors and the heat pump. Also it is not known how systems with uncovered UHPC collectors as source for a heat pump are to be designed and how much energy can be saved compared to other solutions.

Beyond that, it is uncertain if the cement-based *TABSOLAR<sup>®</sup>* collector families can be favorable in terms of primary energy and CO<sub>2</sub> emission reductions compared to other solutions. No life cycle inventory for the systems considered, especially for the UHPC collectors, were available.

#### 1.4. Objective

This work is intended to estimate the energetic and ecological potential of unglazed solar thermal and ambient façade collectors made of UHPC as source for a heat pump for the renovation of multi-family homes in Germany. Comparisons with other systems that form adequate benchmarks shall be made possible.

#### 1.5. Social and scientific relevance

For the urban heat transition, renovation of the building stock towards higher energy efficiency and the transition to renewable energy are very important topics. Different systems must be able to be compared with respect to primary energy and CO<sub>2</sub> emissions so that the customer can make intelligent choices.

Also, the importance of life cycle assessment (LCA) is increasingly recognized. In its final report “Urban energy transition” [85], the German Energy Agency dena attaches

increasing importance to considering the energy used in the manufacture, maintenance and end-of-life of new buildings and renovations, known as “embodied energy”, since 30 % to 40 % of the environmental impact comes from these phases of a building’s life cycle.

LCA plays an important role in various building certification processes. Bruce-Hyrkäs et al. [14] found that 84 % of all people interviewed said that a certification is the main incentive for doing a whole-building LCA. As part of the building envelope, building-integrated solar thermal (BIST) should also be included in the LCA. To compare BIST with other systems, not only the energy generated but the whole life cycle, i.e. materials, processing, transports, use phase and end-of-life, should be assessed. Up to now life cycle assessments of BIST collectors are extremely rare and the strategies for assessment differ greatly. The ecological impact of UHPC collectors has never been studied except for C. Pouloupoulos’ master’s thesis [134] supervised by the author of this thesis.

For purchase decisions, additional factors like cost and qualitative factors play a role. A strategy that assesses BIST holistically is lacking.

In this work, a strategy for a holistic assessment of *TABSOLAR*<sup>®</sup> collectors, which can be transferred to other BIST collectors, is outlined and executed. This includes the discussion of the adequate functional unit and the reference system for the multifunctional BIST components, which is necessary for the LCA evaluation as well as for the life cycle cost assessment (LCC).

There are very few systems built with collectors as a source for a heat pump. Such systems have been rarely studied on a scientific base. Scientific and practical experience was gathered with a spectrally selective uncovered steel absorber in combination with different ice storage systems. First promising investigations on photovoltaic-thermal collectors also exist. They mainly focused on the dual use of the area of photovoltaics and solar thermal energy. To the knowledge of the author, the joint consideration of architectural quality and system efficiency of systems that use collectors as a source for a heat pump was not in the scientific focus up to now. This work explores the interrelation of architecture and solar systems, especially solar thermal systems and explains why systems with solar thermal collectors as a source for a heat pump may support the urban heat transition. The energetic performance of such systems is assessed with detailed dynamic system simulation and allows for comparison with other heat pump systems.

For a climate-neutral heat provision to residential buildings, heat pumps in combination with a renewable electricity mix become increasingly important. If collectors as a source for a heat pump work well and such systems disseminate, solar ambient heat collectors will gain importance, increasingly different models will appear on the market.



As up to now solar ambient heat collectors were rather marginalized, the modeling is less detailed and fewer experiences exist, compared to the modeling of high-efficiency collectors that operate at a higher temperature level. Modeling of such collectors is rather complex as it depends on local ambient conditions. In this work, experiences with the modeling of such collectors is detailed.

### 1.6. Hypothesis

Rear-ventilated façade systems with unglazed UHPC collectors as cladding can serve as a source for a heat pump. They can be the single source or work together with an ice storage. The primary energy demand and CO<sub>2</sub> emissions during lifetime of such architecturally integrated system combinations can be lower than those of an economic benchmark.

Through their low energy demand without a need of a visible outside air unit, these architecturally integrated system combinations can increase attractiveness of rear-ventilated high-quality façade systems and, at the same time, lead to significant national CO<sub>2</sub> savings.

### 1.7. Research question

Can a renovation with a rear-ventilated façade system with unglazed UHPC collectors as cladding elements that serve as a source for a heat pump be an economically competitive and sustainable restructuring plan for existing multi-family homes in Germany?

#### Questions to be addressed

- (1) What are the qualitative parameters of solar thermal for good architectural integration? →Chapter 2
- (2) What is the functional unit and the reference system to fairly assess architecturally integrated, technical renovation plans? →Chapter 3
- (3) How can systems with unglazed UHPC collectors be designed and which energy demand do they have? →Chapter 5
- (4) How can UHPC collectors be simulated depending on the existence of a back insulation and glazings and what is their heat output? →Chapter 4
- (5) What is the primary energy demand and the CO<sub>2</sub> emissions for materials, processing, transport, use phase, and end-of-life of the architecturally integrated, technical systems considered? →Chapter 6

- (6) What are the life cycle costs of the architecturally integrated, technical systems considered? →Chapter 7

### 1.8. Scope

To position the researched systems in the context of established systems, their performance is compared with benchmark systems in terms of primary energy demand and global warming potential.

A rear-ventilated façade structure was chosen for the façade structure of the researched architecturally integrated, technical system with UHPC façade collectors. In terms of interchangeability of single façade collector elements in case of damage it seemed to be the best façade system for a reliable system operation.

As the researched system can be compared with systems that have a similar appearance, an architectural benchmark is defined with a similar façade structure, the same cladding material and without a visible outside air unit. For a comparison with the most economic heat pump system with the most economic façade structure, an economic benchmark and for a comparison with other unglazed façade collectors that were already used in buildings as a source for a heat pump a technical benchmark is defined.

These different benchmarks were chosen to represent different main focuses of possible consumers and to compare the UHPC collector with a commercial collector in the same system. As case study, the renovation of multi-family homes in Germany was chosen. The refurbishment plans include the façade renovation and the heating supply. Figure 1.8.1 shows the representative house with the system of research (left) and the economic benchmark (right). The following systems were chosen for the research object and the benchmark:

- (1) Research subject: Rear-ventilated façade system with unglazed UHPC collectors as cladding elements that serve either as a single source or together with ice storage for a heat pump
- (2) Architectonic benchmark: Rear-ventilated façade system with passive, commercially available UHPC-elements as cladding combined with a ground-source heat pump
- (3) Economic benchmark: ETICS façade system combined with an air-source heat pump
- (4) Technical benchmark: Rear-ventilated façade system with unglazed stainless steel collectors as cladding elements that serve as a single source for a heat pump

The decision for the case study was made in favor of the renovation of multi-family homes in Germany for the following reasons:

- (1) 80 % of the building stock in Germany is older than 30 years old, 40 % is older than 60 years. Therefore, the work concentrates on renovation, even if the general concept could be applied to new buildings as well.
- (2) Rear-ventilated façade systems might be especially interesting for investors of multi-family homes, as high-quality façades can lead to higher rents on the long-term. Higher invests are minor issues for large investors. One-family houses are therefore excluded from this work, but may be interesting in the future.
- (3) The simulations carried out in this work are restricted to the reference location in Germany (Potsdam, reference since EnEV 2014). For other climatic regions, the dimensioning needs to be adapted.

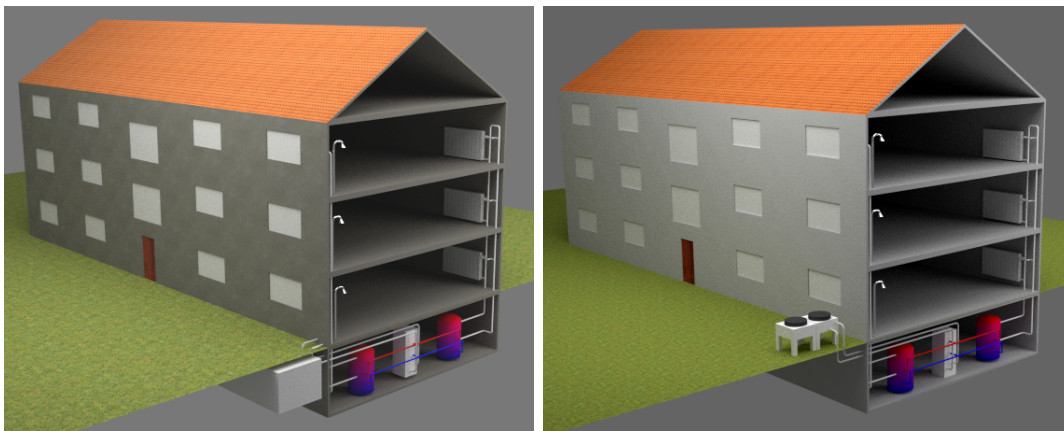


FIGURE 1.8.1. Visualization of a representative multi-family home with a *TABSOLAR*®/ice storage system (left) and the economic benchmark with air heat pump and ETICS façade (right), schematically

### 1.9. Methodology and Chapter Overview

Figure 1.9.1 outlines the organization, inter-dependencies and results of the thesis. As a first step a literature study with focus on the relationship of architecture and solar thermal was made. A possible role of building integrated solar thermal (BIST) for the urban heat transition is discussed. Existing BIST projects and actual barriers are briefly summarized and qualitative evaluation factors for the UHPC collectors are derived.

Chapter 3 introduces possibilities of sustainability assessment and describes the life cycle assessment (LCA) methodology based on ISO 14040 in detail. On the basis of previous LCA studies, possibilities are discussed for its application to UHPC collectors. A strategy and a functional unit is worked out for the assessment in this thesis. This strategy is not limited to UHPC collectors but can be understood as a proposal for LCA of BIST in general. This study evaluates primary energy and global warming

potential. Other evaluation factors can be investigated outside of this study based on the conclusions made in this work. The inventories include the materials and processing of the components (façade components and the respective heat generation systems), transportation, the energy demand during lifetime and an end-of-life scenario. As LCA might not be the single decisive factor, the possible ways for a holistic sustainability assessment are outlined and discussed, based on the findings described in the previous chapter.

The energy demand during use phase is calculated with dynamic system simulations using Modelica modeling language [116] in the Dymola environment of Dassault Systèmes. The weather data was generated with the Software Meteonorm. All questions regarding the system design, the necessary developments and simulations results are presented in chapter 5. Collectors are modeled with characteristic curves following DIN EN ISO 9806. During this work none of the necessary parameter measurements of *TABSOLAR*<sup>®</sup> collectors existed, therefore the system simulations are based on simulations of the characteristic curves.

In chapter 4, *TABSOLAR*<sup>®</sup> collector families are described in detail. It is shown that existing node models for modeling characteristic curves of collectors are not sufficient to accurately describe the uncovered, non-insulated variant of *TABSOLAR*<sup>®</sup> collectors. A modeling approach using the finite element method (FEM) is presented. This was used to generate the characteristic curves used in chapter 5.

In chapter 6 all inventories used are described and the results of primary energy consumption and global warming potential within the life cycle of the different systems are demonstrated. The data collection was carried out in collaboration with the project partners of *TABSOLAR* I and II and with the support of a master's thesis [134], as well as through literature studies and personal information exchange [38, 86]. The software Umberto<sup>®</sup>, in combination with the Ecoinvent database version 3.6 [164], was used.

As an important part of sustainability assessment, a short life cycle cost (LCC) assessment is included and described in chapter 7. Because *TABSOLAR*<sup>®</sup> collectors are, as of now, not on the market, only rough estimates of realizable prices can be made. Large ice storage systems are for the most part, customized and therefore not a mass product. Therefore, the price estimates remain somewhat vague.

Chapter 8 summarizes the results and the discussions. Subsequently, it presents the conclusions and recommendations for further research.

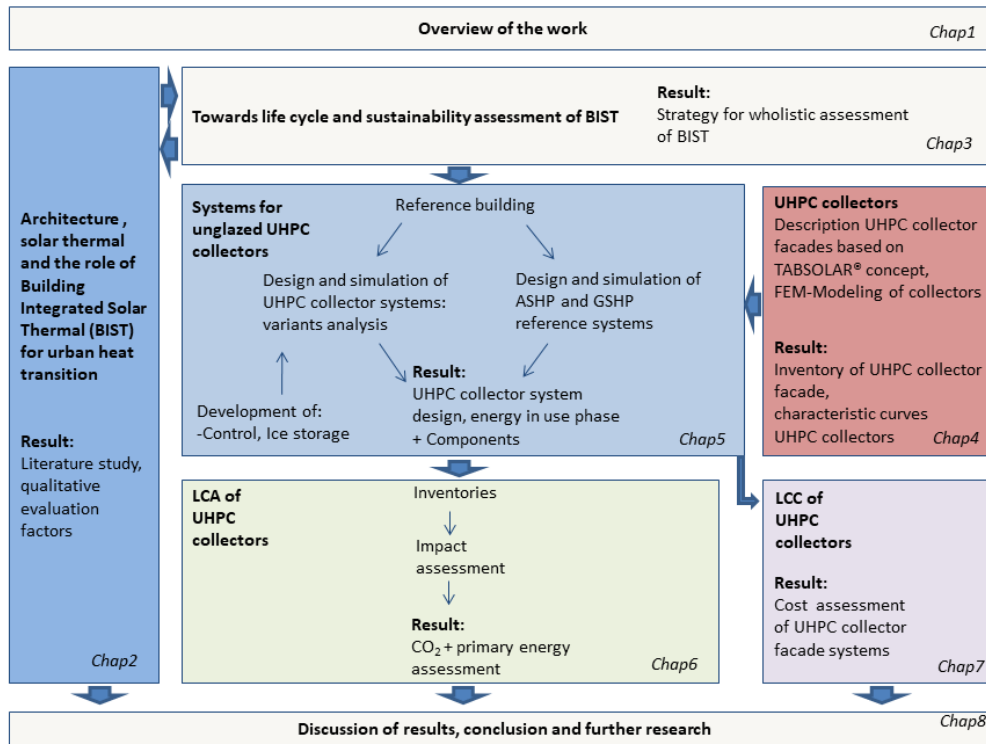


FIGURE 1.9.1. Overview of thesis chapter organization



## CHAPTER 2

### Architecture and solar thermal

In this chapter, a line of argumentation is presented to show the possible influence of building-integrated solar thermal (BIST) on the transition towards Co<sub>2</sub> neutral heating. A short review of the literature follows, and a review of the status quo and the possible obstacles to building-integrated solar thermal are described. Push and pull strategies of BIST are briefly discussed, and a few theses that form the basis of this work are summarized. Finally, evaluation factors for BIST are concluded.

#### **2.1. Contribution of building-integrated solar thermal (BIST) to urban heat transition**

##### **2.1.1. Challenge**

On September 25th 2015, countries adopted the 2030 Agenda for Sustainable Development and its 17 Sustainable Development Goals (SDGs), among them “Clean and affordable energy” (Goal 7) and “Climate action” (Goal 13). Besides the two goals concerning energy generation and decarbonization, SDGs comprise other goals such as no poverty, zero hunger, good health and well-being, and all goals must to be thought of and pursued in tandem.

However, as Prof. Dr. Ernst Ulrich von Weizsäcker candidly stated in November 2017 in a DBU’s Symposium on the occasion of awarding the German Environmental prize (German: Deutscher Umweltpreis): “There is no coherence between the different SDGs.” He further states that the ecological goals are the loser of the agenda 2030. Fulfilling the other goals would imply a massive increase in environmental damage. In their report “Future of spaceship earth” [66], DNV, a global quality assurance and risk management company, evaluates the likelihood of meeting the 17 Sustainable Development Goals in five world regions. Climate actions (Goal 13) – sometimes considered as the game-changing goal – is the least likely goal to be reached in all regions.

Regarding such a negative foresight, the challenge is to find new ways to meet the climate goals together with the other SDGs.

### 2.1.2. Energy transition and area needed for solar technology

The energy transition is a key factor in meeting the climate targets. Energy transition means transition from energy reliant on fossil fuels to renewable energy. Several studies have been conducted to determine the procedural steps needed to create a 100 % renewable energy system and what the energy mix will look like in such a system. Henning and Palzer [70] studied the entire energy system, including the power sector, the heating and cooling sector, and the mobility sector.

The leading question in this study asks what a cost-optimal transformation of the German energy system will look like, considering all energy carriers and consumption sectors. Different scenarios that all meet the climate targets in 2050 are described.

Although the authors restrict the potentially usable area for photovoltaics (PV) and solar thermal to an upper limit they assumed to be acceptable, the calculated area for PV in 2050 varies from four to seven times the PV area installed in 2015, and the area for solar thermal increases more than tenfold until 2050 (between 133 GW and 159 GW in 2050).

The authors present one promising scenario (85 %-Scenario) in detail, and its development of solar thermal is presented in figure 2.1.1. Individual buildings (decentralized) have the biggest share of the installed capacity of solar thermal energy plants. It increases to about a factor of six within this time span.

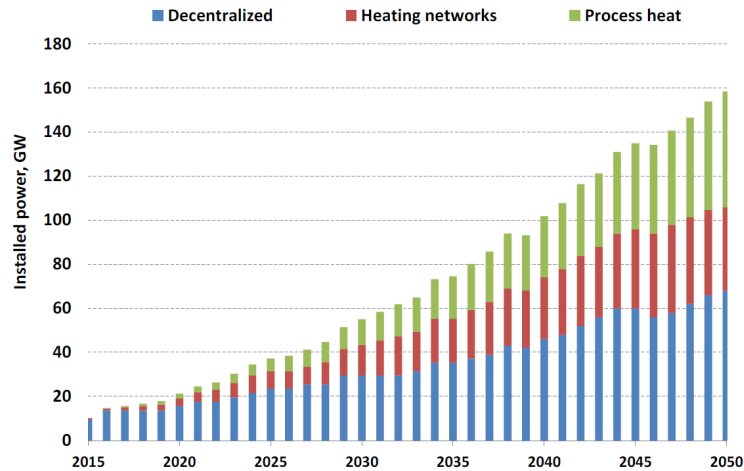


FIGURE 2.1.1. Development of the installed capacity of solar thermal energy plants for the provision of low temperature heat in individual buildings (decentralized), in connection with heating networks, and in trade and industrial processes [70].

A more recent study of Sterchele et al. [130] sheds light on the German energy system transformation in the context of social behaviors. Within the scenario they call



“Persistence”, the development of solar thermal remains about the same as presented in figure 2.1.1. Within other scenarios, the growth of solar thermal is lower but still requires a multiplication of the actual installed capacity.

It is not known how far the assumptions like price development and life expectancy for all technologies will prove true. For example, for decentral solar thermal, cutting costs into half and a life expectancy of 30 years is foreseen [70].

These studies indicate that a) there is enough available area for energy transition in Germany and b) it is probable that solar thermal will be part of the future energy system.

Cost will likely be the main decision maker, but will it be the only one?

One could argue that if the studies’ recommendations [70, 130] had been put into action, market share should have raised significantly by now, but in reality shares were trending downwards for solar thermal since 2008 for EU28 and Switzerland. Only in 2018 and 2019 did the newly installed capacity begin to rise again slightly [163]. So, what are the reasons for this deviation?

### 2.1.3. Decentralization/location

Even if large, centralized, renewable energy parks existed, the general character of renewable energy generation is much more decentralized than that of fossil fuel energies with almost exclusively large centralized power plants. Due to the low energy density of renewable energies, there is a high demand for land, and the generation has to be distributed over a large number of locations (i.e., it is decentralized). Thus, renewable energy can also be used in a decentralized manner.

PV panels and solar thermal collectors naturally face the sun. In an urban setting, where large areas for ground-mounted power plants are rarely available, installations are usually situated in the building envelope. Regarding land sealing and land occupation aspects, it is also advantageous to use the sealed areas of existing, as well as future, buildings for energy generation. The building sector is one of the main energy consumers and could be the means for future power plants.

The two solar technologies for the building sector, PV and solar thermal both rely on solar irradiation. So, they compete for the same area. Solar gains are highest on tilted areas facing south. However, typical load profiles of buildings such as those shown in figure 2.1.2 are opposite to the irradiation profile presented in figure 2.1.3, so over-production of larger systems in the summertime must be either stored, used for other needs, or is wastefully dissipated. In the case of solar thermal, using the generated heat for other purposes is more challenging as it relies on channels with fluid instead of power cables and – contrary to PV – usually has no access to a grid. The lower total gain

but more even gain profile of façades makes it especially interesting for solar thermal, whereas PV can better use the higher gains on the roof.

In order to generate sufficient energy from renewable sources, large areas are needed. The fact is, façade areas suitable for renewable energy generation exceed suitable roof areas, especially in urban areas.

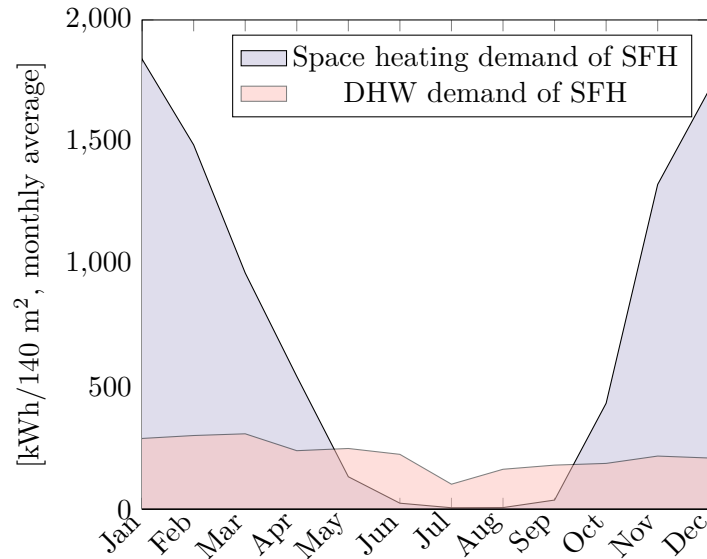


FIGURE 2.1.2. Exemplary loadfile for the demand of space heating of a single-family home (SFH) with 140 m<sup>2</sup> according to Task 32 SFH 60 (60 kWh/(m<sup>2</sup>a)) and the demand for domestic hot water according to DHWcalc, location Würzburg (Germany).

#### 2.1.4. Visibility

Increasing the energy providing area in urban regions to the extent needed requires using not only the roofs but the façades as well. Consequently, energy providing elements are more visible and thus it is more important to integrate them into the urban environment in an appealing way.

One can assume that consumers will be drawn to more attractive, culturally adapted energy providing elements. We know that “[t]he better visible, the more important are symbolic values for purchase decisions” [60]. Architectural quality is a means of communicating with the surroundings, i.e. a symbolic value of building envelopes.

In other words, the relevance of the criterion “architectural integrability” for the purchase decision increases if the visibility of the technical components increases (e. g., by positioning the technical components on the façade or by increasing the used area).

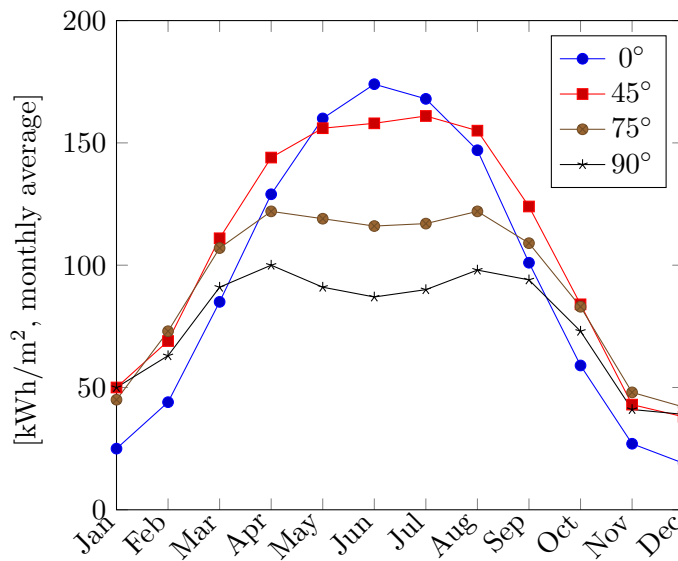


FIGURE 2.1.3. Global Irradiation on tilted surface per square meter ( $0^\circ$ ,  $45^\circ$ ,  $75^\circ$  and  $90^\circ$ ), monthly averages, orientation: south, location Würzburg (Germany).

That means poor aesthetics can be a criterion that excludes solar technologies from the decision process, while good aesthetics could be a reason for a purchase decision.

If integration of energy components in urban environments does not succeed, acceptance problems may result. If energy components in urban environments are not accepted, the energy transition risks failure.

### 2.1.5. Status quo of visible solar components

Up until now, solar thermal collectors have had a relatively homogeneous appearance: although their frames are slightly different, their sizes are similar (the majority are about  $2\text{m}^2$ ), they are black or dark blue in color, and they have a glass cover. Similarly, PV panels are generally homogeneous in appearance. Mass production and certain technical issues have led to low flexibility of appearance. For the most part, both energy providing components are sold and perceived as technical. Components must be placed where they are most productive and little consideration can be given to the architectural design.

### 2.1.6. Aspects of consumer behavior

An analysis of motives, obstacles, and target groups for an energy-focused building refurbishment of private homes reveals that “[r]enovators have predominantly a high emotional bond to their house” [147].

This fact indicates that at least those who renovate their homes are not purely concerned with the cost-effectiveness of certain measures taken on their homes.

From the perspective of a cultural scientist, Thorsten Raabe gives the following general judgment with regard to sustainability marketing: “The purchase and usage behavior of private consumers follows traditional patterns of behavior in many consumer sectors and is rarely ecologically motivated. [...] Thus, there is little doubt that cultural influences are essential for the implementation of sustainable consumption patterns.” [136]. From the perspective of consumer research, therefore, purely ecological advantages are usually not sufficient to motivate a purchase decision. Applied to solar thermal energy, this would mean that pure CO<sub>2</sub> savings alone will rarely lead to a purchase decision for a solar thermal system. Relevant cost savings could be a motivation. For a considerable economic success, the building-added solar thermal collector, or, figuratively speaking, “postal stamp on the roof”<sup>1</sup>, that is often seen today would probably need more cultural adaptivity.

### 2.1.7. Façade and solar thermal markets

Figure 2.1.4 contrasts the current market for solar thermal and for façades in Germany. Scenario A in figure 2.1.5 visualizes a potential market merging, while total market sizes remain the same, graphically expressed through translation. Scenario B in figure 2.1.5 demonstrates a possible growth of solar thermal if Germany realizes a cost-efficient energy transition up to 2050 (85 % scenario [70]). The area of the dashed circle represents the size of the market in 2050 foreseen in that scenario. The intersection set in this scenario is unknown. Looking at the huge façade market in Germany alone, the potential for solar thermal growth into that market seems enormous. The key question is whether it is possible for solar thermal to tap into this market, and if so, how.

### 2.1.8. Architectural integrability

Architects consider the lack of suitable products as one of the three most important barriers for the widespread integration of solar thermal elements in architecture, as found out Farkas et al. in a international survey (n=613) in 2012 [48] and underlined by Prieto et al. in 2017 [135]. They are used to being able to choose from a variety of different

<sup>1</sup>Quote from Detlef Koenemann: <https://www.solarserver.de/2021/03/19/solarthermie-als-jahrbuch/>. In many solar thermal roof installations, the area of the roof is not fully used and the collector covers only a small part of the roof, like a stamp on a letter.

<sup>2</sup>During TABSOLAR II a team, consisting of M. Hermann, P. Di Lauro, L. Koch (Fraunhofer ISE) and P.-R. Denz (Facade-Lab), participated at FDays<sup>®</sup> - Fraunhofer Days. FDays<sup>®</sup> serve the entrepreneurial, systematic development and evaluation of business models based on Fraunhofer technology/competence. A 12 week acceleration model functioned as a stress test for the market, team, and technology. The team developed and presented a pitch for TABSOLAR<sup>®</sup> collectors and received coaching.

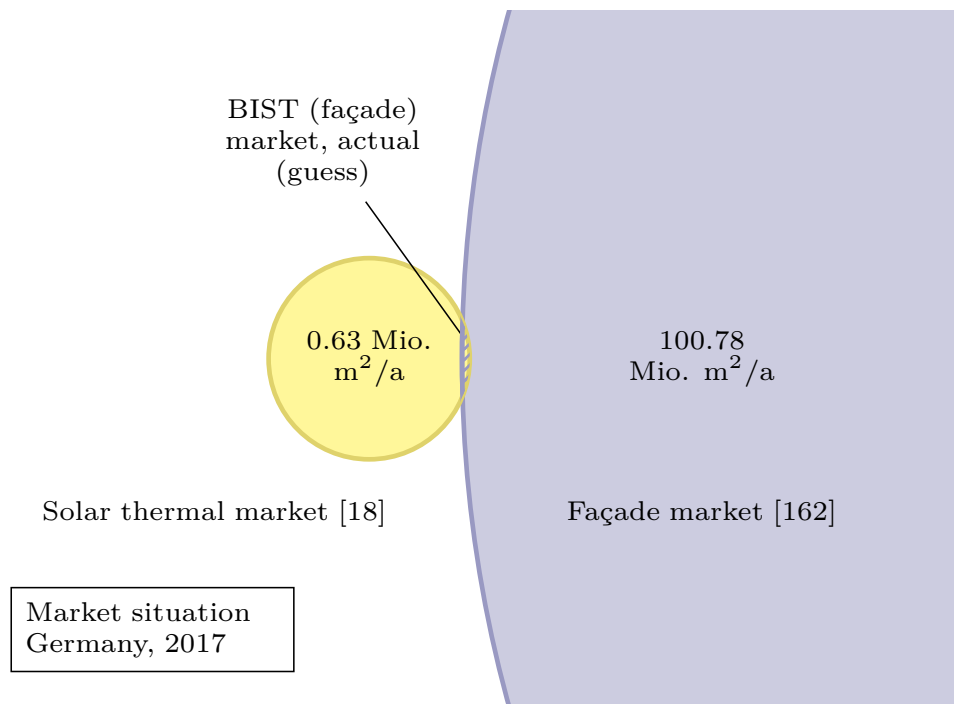


FIGURE 2.1.4. Visualization of actual markets of solar thermal and façades in Germany with intersecting set BIST façades. Each market is represented with a circular area representing the size of the market. As the façade market (blue) is far larger than the solar thermal market (yellow) only a cutout of its representing circular area is shown. The graphic was developed during FDays<sup>®2</sup>.

materials, surface textures, colors, sizes, and jointing for their building envelopes. Increasing these design possibilities increases architectural integrability as could be shown by Munari Probst [119]. She also investigated the architectural integration quality of ten different installations (six glazed and four unglazed) [121]. All installations were assessed by architects as well as engineers and façade manufacturers. Among the four best rated installations were one glazed and three unglazed. Since the sample is small, it cannot be concluded that unglazed collectors are generally better to integrate. The disproportionately high share of unglazed collectors with good ratings is at most an indication that these collectors can be integrated well architecturally.

However, changing the present design towards a higher architectural integrability can imply a decrease in efficiency and reachable temperature level.

In the case of PV, a decrease in efficiency can be compensated with area. This does not hold true for solar thermal; lowering the efficiency of solar thermal not only

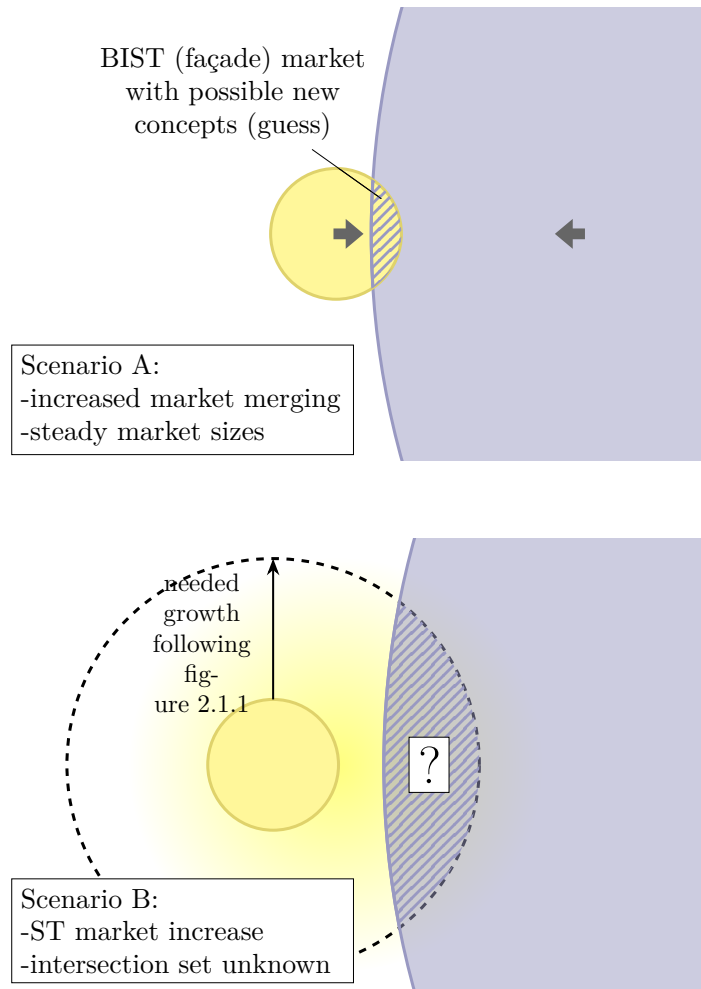


FIGURE 2.1.5. Possible Scenarios for the development of solar thermal and façade markets shown in figure 2.1.4. Scenario A: possible future intersecting set of markets of solar thermal and façades if markets merge together and sizes stagnate; Scenario B: Visualization of needed market growth up to 2050 following figure 2.1.1.

implies a loss of gain per area. If the higher integrability is achieved by taking the glazing off, the dependency of the efficiency from ambient temperature increases. This also means that the reachable temperature level above the ambient temperature at a given fluid temperature decreases (compare section 4.1.3). Especially in colder periods of the year from autumn to spring the generated energy cannot be used anymore for its most common application: preparation of domestic hot water. Even direct heating can be impossible, depending on the temperature level needed. In that case, an increase in area does not lead to an increase of energy savings compared to a fossil fuel system.

If such solar collectors have a high potential of contributing toward good quality architecture, like it is shown in [121] for some unglazed collectors, the system developer may find ways of using them to make highly efficient sustainable energy systems by using their high energy providing potential at low temperatures.

There are two possibilities to still use the collected and transformed energy at lower temperature levels. The first is to change the application and use it, for example, to pre-heat swimming pools. The second is to change the system configuration and combine it with another system; for example, a heat pump that can lift the temperature level to the needed temperature.

Given the increased importance of “architectural integrability”, the collector developer must answer the following questions: 1) how can architectural integrability be increased while minimizing the loss of efficiency? 2) if decreased efficiency is unavoidable, how much is tolerable without losing the collector’s *raison d’être* in a specific system configuration? and 3) under which circumstances does the collector have a *raison d’être*?

While the first question requires detailed knowledge of relevant physics and engineering of solar thermal systems, the last two can only be answered with a detailed sustainability assessment. Within the next chapter, an approach for a sustainability assessment for solar thermal systems is presented. This first question will be addressed within chapters 4 and 5.

## 2.2. Former and ongoing product development and research in BIST

### 2.2.1. Overview of literature

Maurer et al. [110] give a very good overview of the progress of BIST systems that had been made by 2017. In addition to the state of research, a presentation of the commercially available products is given in the introduction. Many of the results presented in that paper were collected during the German/Austrian project AKTIFAS - Fassadenintegrierte Solarthermie: Bestandsaufnahme und Entwicklung zukunftsfähiger Konzepte (Engl. Façade-integrated solar thermal energy: Inventory and development of sustainable concepts) [25]. Within the COST action<sup>3</sup> “TU1205 Building Integration of Solar Thermal Systems (BISTS)”, another very large overview of BIST state of the art, models and applications was published in 2015 [133]. For an overview of existing innovative solar products for building integration, a website can be consulted. It was started in 2013 and was last updated in 2016 [82]. Krippner et al. discuss building-integrated solar technologies available in 2016 in the series of DETAIL Green books, giving a good introduction to the topic and presenting case studies, though only four are

---

<sup>3</sup>COST (European Cooperation in Science and Technology) is a funding organisation for research and innovation networks. <https://www.cost.eu/>

solar thermal [8]. The project (task) “Building Integrated Solar Envelope Systems for HVAC and Lighting” (task 56) of the International Energy Agency (IEA) in the solar heating and cooling programme (SHC) provides the most recent state-of-the-art report on building integrated solar envelope systems [11]. In order not to repeat the comprehensive work, this topic is addressed here by an exemplary retrospective, accompanied with examples of BIST, one of building-integrated PV (BIPV), and two of passive façade examples. Picture (A) in figure 2.2.1 depicts a very old and frequently referenced example of BIST with unglazed, curved collectors serving as a roof. Munari Probst and Roecker [120] allow various professional groups (engineers, façade designers, architects) to assess the quality of architectural integration. This example is among the best rated in all professional groups. Picture (B) causes dissent between the professional groups in the mentioned study. While architects judge the architectonic integration to be unsuccessful, the colored collectors have positive impact on engineers who rate the integration quality as high. The pictures in (C) show a polymer façade collector. Picture (D) is not an example of BIST, but for BIPV technology. The colored panels make up the design of the whole building. Even the north façade, with almost no gains, is covered with these panels. This example demonstrates the importance of architectonic integrability; the overall impression must be coherent. Picture (E) shows the “Haus der Bauern” (Engl. House of the farmers) in Freiburg, Germany, and (F) shows the Headquarters of the Cambridge Water Company. Both examples present different façade materials that are presented through the glazing. These last two examples illustrate how glazed solar thermal collectors with non-black absorber surfaces, different materials, and/or different textures can be architecturally interesting.

Before presenting the author’s own retrospective, different approaches to active solar thermal energy generation in buildings are presented to better understand the difficulties revealed through past work and to present a possible solutions to overcome these difficulties.

### 2.2.2. Different approaches to BIST

Figure 2.2.2 outlines three different approaches to active solar thermal energy generation in the context of sustainable buildings. Usually, the engineer enters the building design process via the building technology (left) whereas the architect via the building envelope (right). Both approaches, with its respective entry points, represent different professions, different knowledge backgrounds, different ways of thinking, and usually different entrance times in the building design process. The engineer is responsible for the building technology. A partial goal of its energetic optimization is the optimization of the heat generation and distribution (Energieatlas p.113, B 4.11 [68]). The architect is responsible for the building envelope. One partial goal of the energetic optimization,



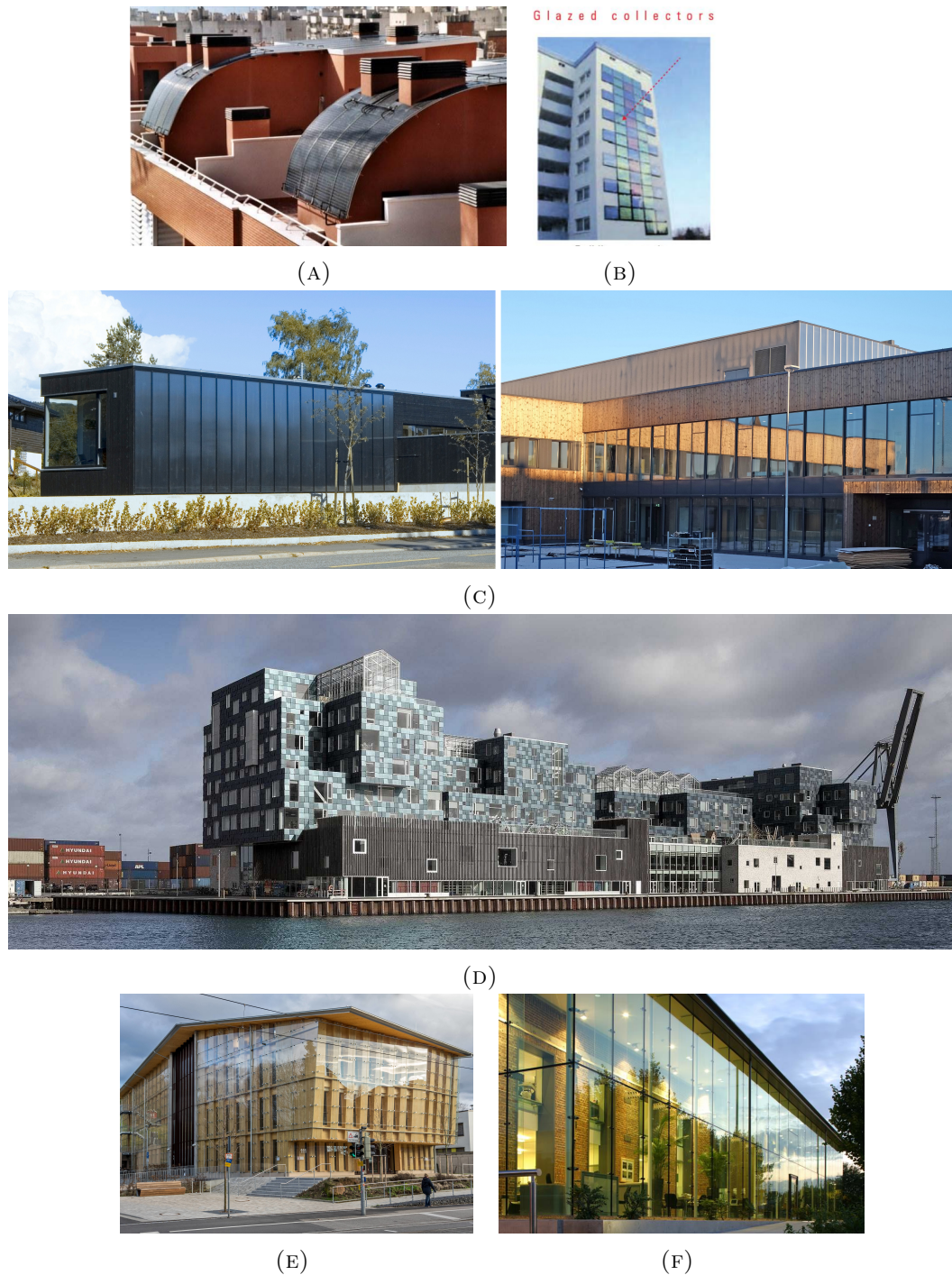


FIGURE 2.2.1. Examples for BIST, BIPV and glazed materials. (A) Villanova (Spain) [119], (B) Solarsiedlung Köln-Bocklemünd (Germany) [119], (C) left: Multi-family atrium house in Oslo (Norway), right: Bjørkelangen school (Norway) [115], (D) Copenhagen-International-School-Nordhavn (Denmark), Adam Mørk, (E) Haus der Bauern (Freiburg, Germany), Joergens.mi/Wikipedia, (F) Cambridge Water Company Headquarters (England), Pilkington.

following Energieatlas p.85, B 3.7 [68], is the optimization of heat conservation and generation. So from both sides, the engineer's and the architect's, a possible technical solution can be found in active solar thermal energy generation. The different entry points may rather lead to systems that neglect either architectonic quality or system efficiency. Within the exemplary scoring of the graphic, architectonic quality is assigned to "Baukultur and design quality", whereas system efficiency is assigned to "Sustainable development goals". "Sustainable development goals" could also include "Baukultur and design quality", but in the scoring context of this graphic, only the environmental aspect of the SDGs is addressed. In contrast to the architect's and engineer's approach, the interdisciplinary approach, is a synthesis of the two. A scoring could be high in both categories. Possibly a slightly lower scoring compared to the top scoring 'green' is indicated by 'light green'. In the context of the German Sustainable Building Council (DGNB - Deutsche Gesellschaft für Nachhaltiges Bauen), the goal is to achieve high scoring in every core topic. Included with the seemingly contrary topics of "Baukultur and design quality" and "Sustainable development goals"(i. e., in the context of the scoring within this graphic), are the topics "Innovation", "Circular Economy", "EU-conformity" and "People focus", and these also need to be addressed.

So, finding and applying sustainability criteria that consider the whole building is assumed to be crucial for success of solar thermal in building envelopes, especially the façades.

### 2.2.3. Exemplary own retrospective

Solar thermal product development has been mainly driven by pioneer companies and companies coming from the heating sector. The aim is to offer environmentally friendly heating systems. In cooperation with research institutes, the companies involved have developed highly efficient solar thermal collectors using the "engineer's approach" shown in figure 2.2.2. Only a few exceptions follow a more architectural or interdisciplinary approach. One example is SOLARroof from the German pioneer company Wagner & Co. This product is designed to replace a complete roof and is suitable for façades. The idea is innovative and interdisciplinary. However, with the exception of the photo of the architectonic integration in the roof, the technical information [161] seems to be addressed to a more technologically minded consumer, highlighting are big installation areas rather than excellent architecture (see excerpt in figure 2.2.3). Quite a few installations were made, but finally this product disappeared from the market. The word pair "Solar Roof" is now linked to a new product from TESLA, Inc., a PV tile that generates electric power. This product is not yet on the market, but the advertisement, which states "Solar Roof complements your home's architecture while turning sunlight into electricity..." [152] positions architecture as central selling feature. The visual language

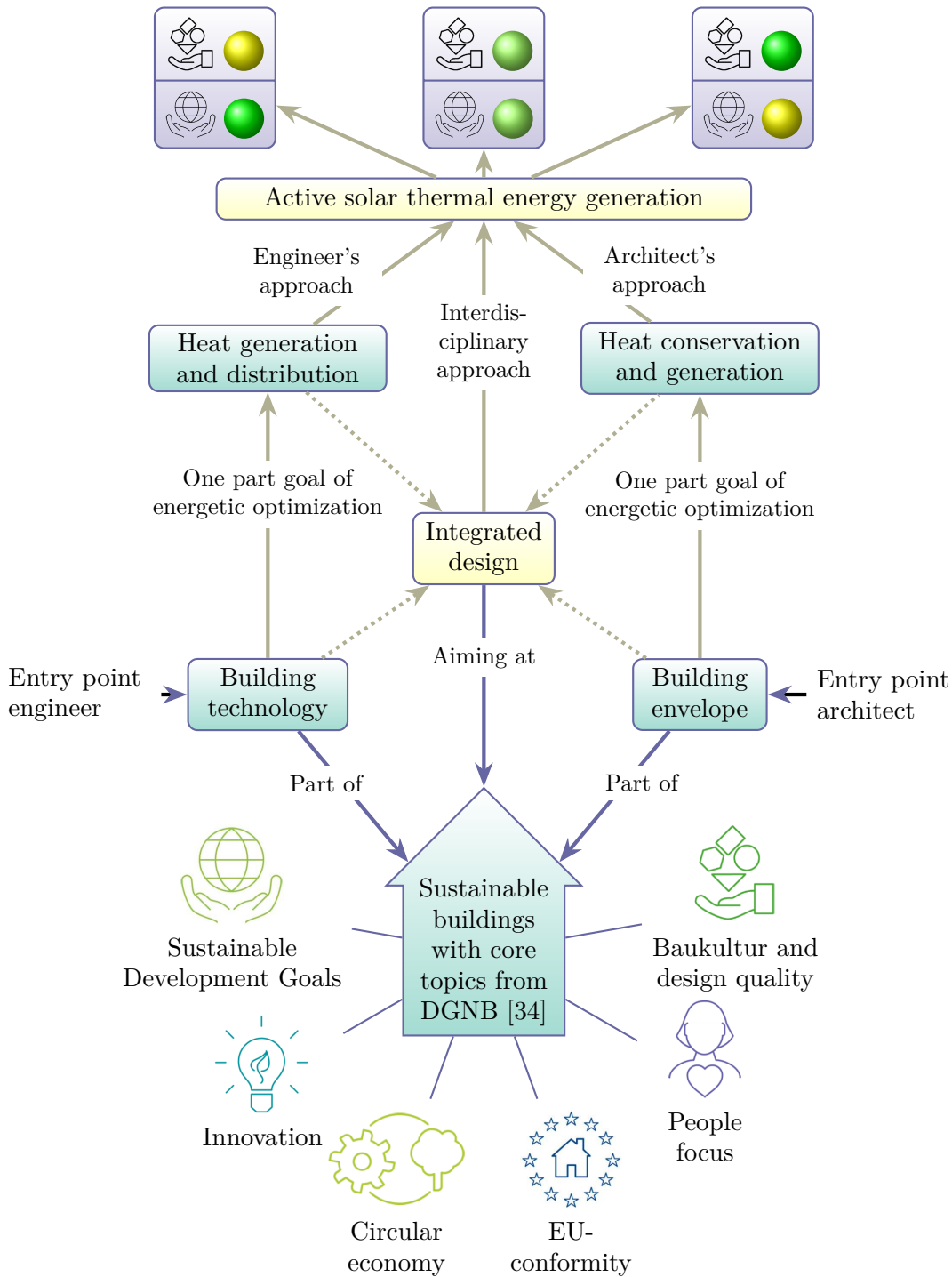


FIGURE 2.2.2. Three approaches to active solar thermal energy generation in context of sustainable buildings with different possible scores in “Baukultur and design quality” and “Sustainable development goals”, in this graphic’s context referred to decarbonization (Yellow = mediocre, green = good, light green = good with small restrictions).



FIGURE 2.2.3. SOLARroof of Wagner & Co, excerpt of technical information from 2007 [161]

alone (see figure 2.2.4) illustrates that this tile is not going to be sold as a technical component, but as piece of your life. The buyers choice of tile design will depend on the planned architecture rather than on differences in heat gain curves.

Another BIST product development in which architects were project leaders is based on vacuum tubes combined with semitransparent CPC reflectors. The production of vacuum tubes is highly automatized, and flexibility of length in current production lines is low. The team made a virtue out of necessity by developing a comb principle that enhanced the flexibility of length, see figure 2.2.5. The project partners were honored with the Intersolar Award in 2010. Further information about this product can be found in the dissertation of architect Prof. Bettina Wolf, born Volz, who was part of the developing team [166] and in the dissertation of architect Philipp Molter [117]. Until now, only one demonstration installation of this product existed. One can only speculate why this innovative product was not installed in more projects: low consumer confidence, high product expense, insufficient marketing structure, something else, or a conglomerate of it all.

These examples illustrate that innovative products alone are not the only key factor to success. We still do not know the market success of Tesla's Solar Roof. But an

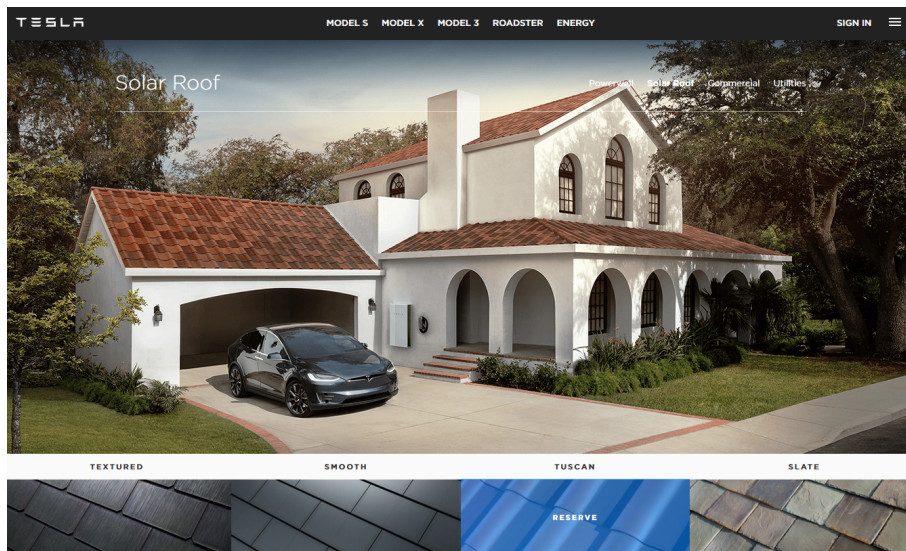


FIGURE 2.2.4. Planned Solar roof of Tesla, Inc. [152]



FIGURE 2.2.5. Mock-up of semitransparent BIST element [166]

important thing has changed: The advertisement promotes (system) solutions as value proposition or product instead of individual components.

#### 2.2.4. Barriers to deployment of BIST

In 2020, Maurer et al. presented and described the known barriers preventing the deployment of BIST, BIPV, and natural lighting control solutions according to the experts of Task 56 “Building integrated Solar Envelope Systems” [111]. The following barriers were identified:

- (1) **Technical barriers:** Different specialist disciplines need to work together (installer for heating, ventilation, and air conditioning (HVAC); façade installer), changing or maintaining the components can be more complex. Peak temperatures of high efficiency components can reach up to 200 °C, and components must be designed for these temperatures. Vapor transfer within wall construction must be considered. Hydraulics need space and should respect the Tichelmann principle. Shading during operation needs to be identified. The system has to be well controlled.
- (2) **Regulations:** In addition to the common regulations for solar thermal components, BIST collectors need to comply with all regulations and codes for buildings components. Test methods developed for standard components may not account for special needs.
- (3) **Design support tools:** Solar technologies must be incorporated into the façade design and construction process from the start, allowing for closer collaboration between the different disciplines involved.
- (4) **Architectural barriers:** During workshops and interviews about innovative solar envelope components, architects have expressed a clear wish for more versatility in shapes, colors, textures, and sizes. There is also a perceived lack of suitable, ready-to-use components available on the market.
- (5) **Economic barriers:** Economic barriers for solar envelope systems not only are due to the components being more expensive, but also in some cases because of a mismatch between the design budget and the construction budget. Another issue arises if the investor is not the one who benefits from building improvements. Solar envelope systems should be evaluated on the basis of life-cycle costs (LCC) or total cost of ownership (TCO) instead of, for example, capital costs or the levelized cost of energy (LCOE). Good financial concepts need to be developed.
- (6) **Social barriers:** New technologies in general need some time to enter the market (diffusion of innovation, Rogers, 1962). Regarding building technology, participants might be more conservative than about average products as failure can lead to considerable costs.

Regarding the weighting of the different barriers, some surveys were conducted within the past years. In 2017, Prieto et al. [135] ask participants (Sample size  $n = 79$ , among them engineers 44% and architects 39%) to name the main barriers for a widespread integration of solar technologies into the building envelope. In a word cloud of answers, “costs” stood out particularly. Thereafter, participants could name 3 barriers out of 7 and rank them. Within first ranked barriers, “Economy” (not economically justifiable and lack of governmental incentives) was the most frequent, followed by “Product” (lack of products suitable for quality building integration and complementary building components). Summing up all named barriers, the most frequently named was the category “Product”. As this category seemed to be of special interest, it was further analyzed and split into the subcategories “Performance”, “Aesthetics”, “Durability”, “Technical complexity” and “Availability” (in the order of frequency of total mentions). Variation between these subcategories were between 7 and 16 mentions, with differences being almost equidistant. This survey delivers similar results to a former survey from 2012 [48] with a bigger sample size; only the lack of knowledge and interest of BIST and BIPV systems seems to have become less important.

In 2014, Cappel et al. [26] find through a qualitative survey, literature review and expert workshops that economic issues are the number one problem preventing broader adoption of BIST, just like of solar thermal technology in general, followed by a lack of knowledge of BIST components and systems by all stakeholders. The fact that BIST, in contrary to the fear and experience of the stakeholders, can today be a more economical choice than the usual BAST (Building added solar thermal) systems, is shown by Cappel et al. [25] in 2015 by means of three built examples: Up to almost 30% were saved compared to usual BAST systems. The examined projects were all prototypes, so further cost reduction potential of about 40% to 50% through standardization in planning and construction is estimated by the architect and the involved companies.

### **2.3. Pull vs. push or piggy-backing strategies for BIST**

“Ultimately, the harmony between building and solar technology and the attractiveness of the emerging architecture will determine the acceptance and success of these technologies on a broad scale” [68].

Creating that harmony requires suitable products, knowledge, and creativity. Lacking one of these three elements, architecture will possibly be only mediocre. Mediocre architecture does hardly win competitions. Fuchs finds that, currently, ecological or sustainable assessment criteria are hardly decisive in architecture competitions and developed guidelines for sustainability-oriented architecture competitions [56]. In a six-step

process (“Preparation” over “Offer of a reward”, “Check back + colloquium”, “Preliminary review”, and “Jury” to “Completion of the competition”) Fuchs lists the “definition of essential sustainability goals” as a task in the first step and includes the refinement of the sustainability goals in every process step. This process chain illustrates that sustainability issues like solar thermal should be pursued from the very beginning of the planning process.

Such sustainability-oriented architecture competitions could be a means to increase demand for knowledge acquisition and suitable products. This would be a pull strategy as it generates a market need which can initiate developments. Other approaches that follow the same goal are legal obligations like the Energy Performance of Buildings Directive, EPBD [47] or obligations on a national level. Even if those legal obligations are very successful, they have a disadvantage: they can be against human preferences. Feeling obliged to do something can provoke a negative response from the general public. Many people react with only doing the minimum amount required. A ‘push strategy’, that is, offering products that evoke a big desire to have them, could avoid that dilemma. Metaphorically expressed: Combining the attractiveness of the iPhone with the sustainability approach of the Fairphone would be a sustainable push product development strategy. Entering in the façade market with a solar thermal collector orientated on the requirements of façades has also aspects of a piggy-backing strategy, as the distribution channels of a far broader market can be used to sell the new product.

#### **2.4. Background theses for further assessment of BIST**

The following theses are summarized thoughts that inspired this work.

- (1) Architectural integrability can be a key success factor for solar thermal and for (some) sustainable energy systems.
- (2) For a 100 % renewable energy system, low-temperature solar thermal can play an important role. If solar thermal is going to play this important role, the thermally active area has to be increased immensely.
- (3) In densely populated urban areas, the possibility for an open space installation is unlikely, and solar thermal system compete with PV for the available roof areas. The advantage of the roofs is that they can offer optimal orientation to the sun so that the highest amount of energy can be collected. With regard to time correlations of energy provision to energy demand in buildings, this advantage is especially significant if a solution can be found for using the overproduction of energy that can occur in the summer months. One solution might involve using the overproduction of electricity for power-to-gas and thus



store it. However, seasonal storage of solar thermal energy has proven challenging. Positioning solar thermal on the façade avoids huge useless summertime overproduction, avoids competition with PV installations, and the generation profile is advantageous for typical load profiles (low sun in heating period).

- (4) The classical solar thermal collector for a typical roof installation is highly developed and offers limited potential for optimization in the sense of efficiency and costs. Although the potential for cost reduction is low, it does exist, for example, with polymer or steel absorbers in mass production. However, such cost reductions are not attractive enough to realize their complete potential for reducing environmental impact of energy production in future energy systems.
- (5) Façades are the faces of buildings, and culture plays an important role in changing consumer behavior so that solar thermal collectors on façades are desirable options. The more visible a product is, the more important the symbolic values are for purchase decisions [60]. So, façades have a highly symbolic value. Conceivably, collectors with a higher freedom of design or a broader palette of collectors would better meet the requirements of façades and the interests of consumers.
- (6) Measures to increase the freedom of design of solar thermal could lead to a decrease of its thermal performance. Thus, a minimum criterion for thermal performance is needed, and the environmental impact should be held in focus.
- (7) It is possible to make efficient systems with low efficient solar thermal collectors, given that they have other properties that compensate for it, for example, multifunctionality. Determining which properties are important depends on the system.
- (8) There is a need for a life cycle assessment and an environmental product declaration for solar thermal.

### 2.5. Qualitative evaluation factors for BIST collectors

From the literature and requirements regarding the meeting of standards and the installation and maintenance processes, a grouped, not exhaustive list of different evaluation parameters for BIST was compiled and is presented in figure 2.5.1. Some parameters do not belong to one group, but are related to some or all groups. Some parameters can only have two values (yes/no), some can have a range of values. The most important evaluation parameter is the thermal yield, highlighted in red. It is the main function of solar thermal collectors and, thus, is assigned to the group Functionality. The (solar) thermal yield also is essential for the groups Economics and Environmental aspects. Another example for a parameter that does not clearly fit into one group is lifetime:

it is a clear functional parameter, but it is crucial as well for life cycle costings as for life cycle impact assessment. Also aesthetics and lifetime can be interrelated: timeless architecture can prolong the lifetime of the building or the façade and thus has influence of the (required) lifetime of the collector. The collector in turn should not impede good architecture but at best support it. All of these parameters are influenced by the product design parameters Production technology and Materials.

A comprehensive assessment of BIST should address all these point. Prioritizing special issues or determining which limitations are to be set should be discussed individually for each project.

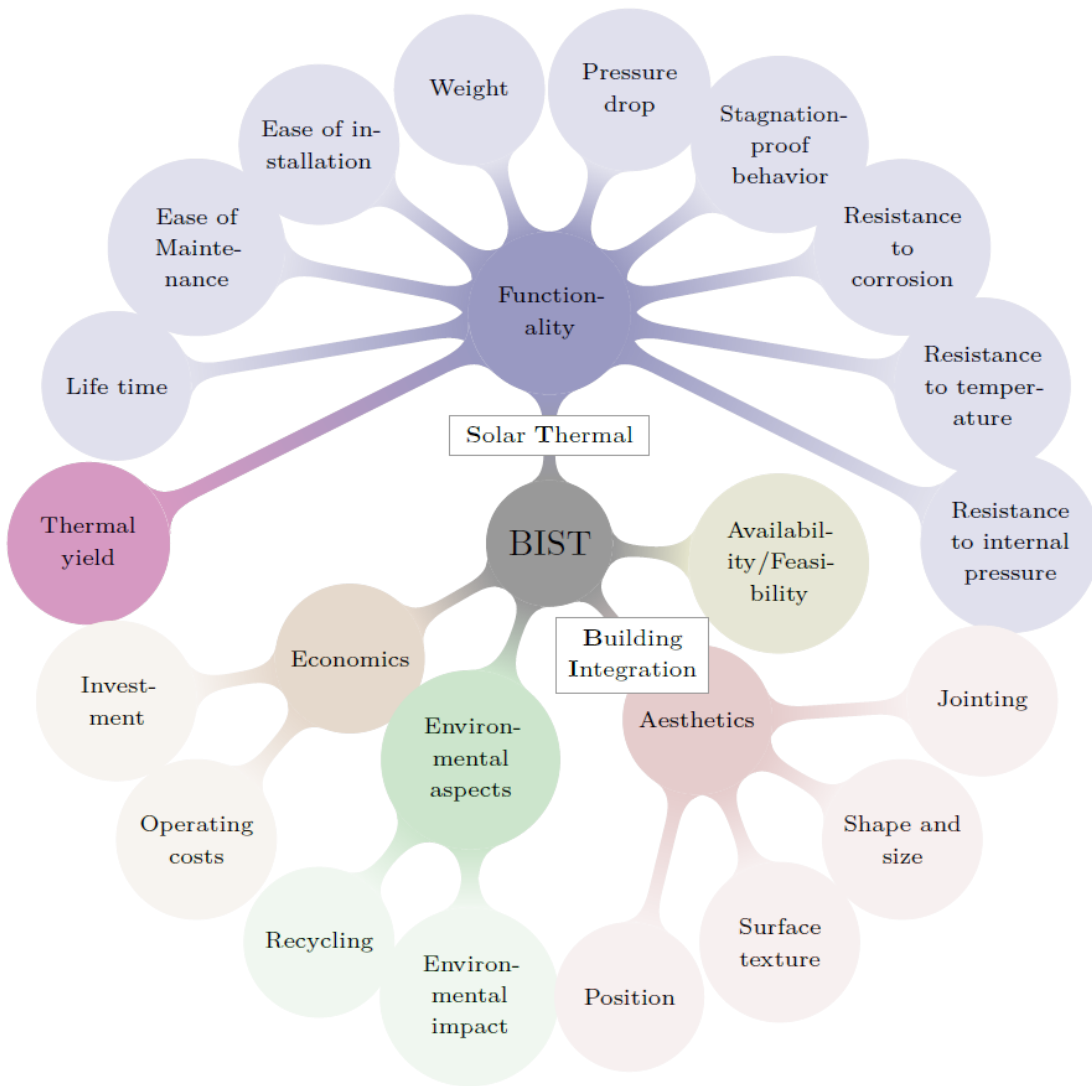


FIGURE 2.5.1. Evaluation parameters for BIST, first level based on Maurer et al. [109], second level “Aesthetics” based on Munari Probst and Roecker [119].



## CHAPTER 3

### **Towards sustainability assessment of BIST collectors**

This chapter describes a methodology how sustainability aspects of BIST can be evaluated, which of the different aspects are considered, and how they were evaluated in this work. The evaluation of sustainability can be structured into the following questions:

- (1) Why?
- (2) What?
- (3) How?

The first question asks for the intention, the target group for which an evaluation is made, and the overall goal. The second question aims at the system boundaries and defines possible reference systems. These depend on the intentions, the research question, i.e. on the objective, and define the scope. The third question focuses on the evaluation criteria and methodology.

In the following, all these questions are addressed step by step. The first section outlines reasons why sustainability assessment of BIST collectors might be desirable, followed by a section evaluating which system boundaries can be assumed for BIST and which purposes can be fulfilled with each. After that, a section describing the fundamentals of sustainability assessment with a focus on life cycle assessment (LCA) follows. LCA is applied in more detail in this work, and the final results with the inputs of chapters 4 to 6 are presented in chapter 6. A brief overview of the sparse literature on LCA of BIST is then given before describing the functional unit defined in this work and the different methods used to compare the primary energy and CO<sub>2</sub> emissions of systems with UHPC collectors and reference systems.

#### **3.1. Reasons for sustainability assessment of BIST collectors**

- (1) Why?

Based on the two premises of increasing areas and acceptance needed for its realization, former, rather technical assessment and development criteria for energy components like PV and solar thermal systems may no longer prove sufficient. “Architectural integrability” of solar active components is becoming a more central aspect. Coming from the building industry, a huge variety of materials for energy components are imaginable. But what happens if the materials usually used are replaced by others? What influence

does this have on efficiency, costs, environmental impact, flexibility of production and possible appearance in the building envelope? How do all these properties influence each other? Are there minimal criteria for some or all properties, and if so, which? Are there mechanisms in place to prevent unsustainable solar thermal systems from being sold or installed? Is there something like an optimum, and what is the variable to be optimized?

To answer this question, the concept of sustainability can be taken as a framework. There is a lot of discussion on what sustainability means, and many definitions of the concept exist. The Brundtland Commission of the United Nations on March 20, 1987, defined the following: “Sustainable development is development that meets the needs of the present without compromising the ability of future generations to meet their own needs”.

What does sustainable mean in the context of energy-providing elements? Are PV or solar thermal energy sustainable per se? A minimum sustainability criterion for energy-producing elements can be defined as follows: “The energy produced during lifetime must exceed the energy used for its production several times.”

Kleine defined the integrated sustainability model presented in figure 3.1.1, left. It permits the continuous integration of the three dimensions of sustainability, the environmental, economic, and social dimension. In figure 3.1.1, right, this model was applied to solar thermal collectors with example terms.

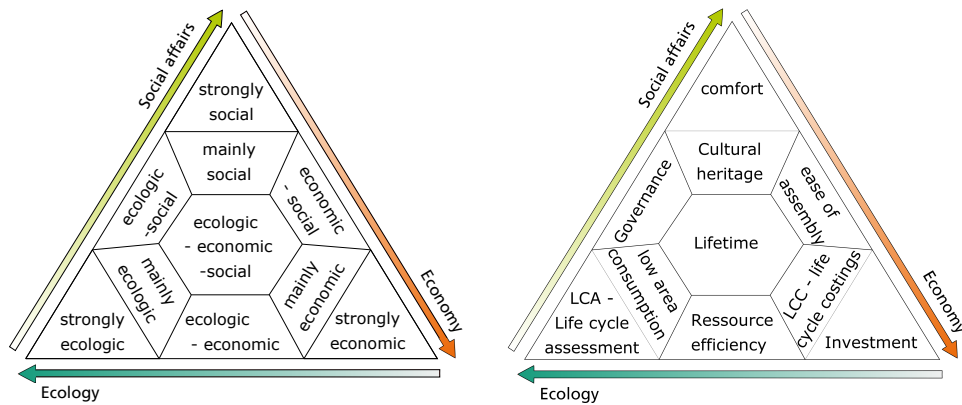


FIGURE 3.1.1. Left: theory of an integrated sustainability model, visualized following [89], right: exemplary application to solar thermal collectors following [91]

We need to pursue many different goals simultaneously to develop more sustainable solar collectors that can be part of a more sustainable energy system.

The question of what exactly is a sustainable energy system can also be answered in a variety of ways. The goals for a sustainable energy system must be clarified on the level of components, as well: does a sustainable energy system mean that everything is produced with renewable energy sources independently of the environmental, social, and economic impact of the components? At least some of the economic aspects of the different technologies are included in most definitions of a sustainable energy system. More holistic and – in the view of the author – more expedient definitions would consider data from life cycle assessment (LCA), broad economic analyses with influences on the gross domestic product (GDP) as well as employment, social life cycle assessment, and acceptance research. However, the question of the whole energy system is a broader discussion that is far beyond the scope of this work. Nevertheless, the more holistic definition serves as a vision for this work.

In order to pursue the different goals for the sustainable development of solar thermal energy, the existing interdependencies must be clear. Optimizing for only one variable (efficiency) has proven to be insufficient. There actually is a seal of approval for solar thermal systems to guarantee a certain quality of components, planning, execution of service, and operation (RAL 966) [32]. Initially, this seal of approval was not well received due to high certification requirements for the executing craftsmen [149], and, for some time, it was even unavailable. However, the seal has been usable again since 2018. The criteria of this certification are used in particular as a reference for craftsmen. However, this quality mark is not adapted to the requirements of building-integrated solar thermal systems.

The evaluation parameters for BIST, as shown in figure 2.5.1 have some parallels to the Sustainable Development Goals (SDGs) of the UN. Prof. Dr. Ernst Ulrich von Weizsäcker's previously mentioned critique of the SDGs concerning their missing coherence may not apply in the same way, but the different BIST properties seem oppositional, as well. Today, the task is to enable a simultaneous pursuing of all SDGs or – broken down to BIST – a simultaneous pursuing of all evaluation parameters considered relevant. To enable such simultaneous persecution, the systems under consideration must be evaluated under all relevant sustainability criteria. The outcome can be used for an iterative, interdisciplinary development towards a broader palette of more sustainable BIST for sustainable buildings. This work aims to contribute to the awareness of this challenge in the context of solar thermal collectors.

### 3.2. System boundaries

#### (2) What?

The purpose or the goal of an assessment of a solar thermal collector can vary depending on the context. Figure 3.2.1 provides an overview of the different goals of the assessment of solar thermal collectors. The different goals and system boundaries are explained on the basis of life cycle assessment, but they similarly apply to the assessment of the other parts assessments of sustainability presented in the next section. As the function of a solar thermal collector is generating energy, a minimal requirement in the context of LCA would be that the energy generation over lifetime exceeds its gray energy several times. Strictly speaking, a component that recovers its energy even proportionally is already more sustainable than a passive component if nothing else changes. Assuming that this minimal requirement is fulfilled, the goal can be to identify an environmental hotspot in the production process or the material selection of a special component. In this case, the pure “environmental back pack” per unit represented with adequate indicators such as global warming potential, primary energy demand or others can suffice (figure 3.2.1, 1). If the goal is to compare different solar thermal collectors with different efficiencies, the pure “environmental backpack” is not enough to decide which component is environmentally friendlier: The collector with the heavier backpack might lead to a higher energy gain over a lifetime. Both the components as well as the delivered energy would have to be considered (figure 3.2.1, 2a). The purpose could also be to compare different collectors on a defined area (figure 3.2.1, 2b) or collectors that deliver a specific amount of energy (figure 3.2.1, 2c).

If the system boundaries are extended to the whole building, the whole heat supply system needs to be considered (figure 3.2.1, 3). If the collector is integrated into the building envelope, a credit for the replaced part of the building envelope has to be given (figure 3.2.1, 4). This credit depends, of course, on the replaced component and can have a high impact on the results. This case has to be looked at carefully as this impacts the architectural quality of the building. As BIST collectors are part of the building envelope and the heating system, this system boundary should be chosen. From an esthetic point of view, the system boundary can also vary, and components can be assessed piecewise or per area. But the decisive aspect is the appearance of the whole building, which represents the system boundary not only for BIST collectors but also for BAST (building added collectors).

For the practice of LCA, this means that the environmental impact of all components should be available: The collector’s impact per unit with specified size, all components of the heat supply system, and the impact of the possibly replaced building component. In addition, the efficiency of the collector and, based thereupon, the yearly energy savings



	Purpose/Goal for LCA	System boundary
1	Identification of hot spots in the environmental impacts in the life cycle of a collector.	Production, materials and disposal of collectors
2	Comparison of different collectors with the same heat supply system and the same application	
2a	Different collector areas, different energy yields	Production, materials and disposal of collectors + energy yield in the utilization phase
2b	Same collector area	Production, materials and disposal of collectors + energy yield in the utilization phase
2c	Same collector energy gain	Production, materials and disposal of collectors (Not necessarily: energy yield in the utilization phase)
3	Comparison of different heat supply systems for a given application	Production, materials and disposal of the collectors (if any) and the heat supply system + Total energy demand in the use phase.
4	Comparison of different building envelopes with different heat supply systems	Production, materials and disposal of the building envelope and the heat supply system + Total energy demand in the utilization phase

FIGURE 3.2.1. Various LCA goals related to energy-producing building envelope elements (e.g., solar thermal collectors) with associated system boundaries.

of the system compared to a reference system need to be known. To avoid having to use a reference system, a good approach could be to consider the whole heat consumption of the building and the whole building envelope. This would allow a fair comparison of very different heating supply systems with different building envelopes.

### 3.3. Fundamentals of sustainability assessment of products

#### (3) How?

Saurat and Ritthoff published an overview of existing sustainability assessment methods and tools and of the relevant standards for the process industry[139]. Although their review is not exhaustive, it yielded a long list of methods (51) and tools (38) for sustainability assessment. Most methods include standardized life cycle analysis (LCA), but very few integrate all aspects of sustainability.

One of them is “PROSA – product sustainability assessment” by the Institute for Applied Ecology (Öko-Institut e. V.)[62], [61]. Besides the three fields of sustainability, it includes a benefit analysis as seen in the methodology’s general structure, shown in figure 3.3.1. The following first discusses the benefit analysis in more detail and then explains the basic methodology of life cycle assessment, the most standardized sub-method. This basic methodology is also used in the other sub-methods presented later on.

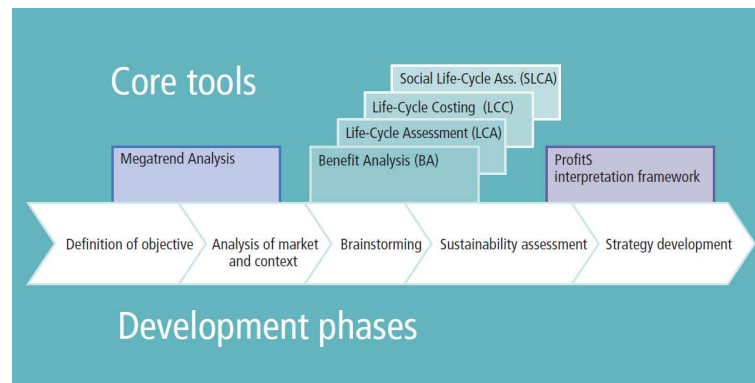


FIGURE 3.3.1. Basic structure of PROSA – product sustainability assessment [61]

#### 3.3.1. Benefit analysis (BA)

Benefits are purchase-deciding factors. A benefit analysis helps choose the correct reference system for a sustainability assessment. A more sustainable product only gains market acceptance if it has the same or similar benefits as the less sustainable alternative, see, for example, Fairphone and iPhone sales figures. According to Griebhammer, there

are three different types of benefits: practical, symbolic, and societal. The PROSA guideline provides checklists for every type of utility. In the case of BIST collectors, most of the benefits or evaluation criteria like functionality and availability represent a practical benefit. Aesthetics would be a more symbolic benefit, and climate protection would represent a societal benefit. Until now, the societal benefit of climate protection is usually of no or low (through funding measures) direct benefit for the investor. Instead, visibly demonstrating that the investor is doing something for the neighborhood or the whole of humankind (fighting against climate change) and, at the same time, having a very attractive building can be a direct benefit for the investor. This can be increased building value or better expression of own lifestyle and values. The latter could apply to a consumer group called LOHAS which stands for “Lifestyle of health and sustainability”. According to the consumer index for Germany [58], this consumer group grew by eight percentage points to a total share of 30 % from 2007 to 2016.

A solar thermal system that saves little or no energy would, of course, be greenwashing and hardly sustainable. The main benefit of solar thermal collectors is enabling systems that emit fewer greenhouse gases than the alternatives.

As mentioned, a BA can help define the right reference system and also the suitable functional unit. The functional unit defines the requirements. If high aesthetic requirements of a building envelope are defined for the functional unit, some solar thermal collectors are not even considered.

One requirement can also be to plan an energy-efficient heating system for a building. A heat pump would, in principle, come into question and – if applicable – even be the first choice. However, in a fictive scenario, regional conditions impede using geothermal heat as the source for a heat pump. An air heat pump might not be applicable either since distance regulations cannot be kept or there is no suitable place for a noise-emitting outside air unit. In this case, a solar thermal collector can represent an alternative heat source and thus make a heating system with an efficient heat pump possible. Therefore, in this scenario, the comparison must be made not with air or geothermal heat pump systems but rather with other possible systems that may emit significantly more greenhouse gas. It could also be that both air and geothermal heat pumps are possible, but a solar thermal collector would be favored due to additional benefits (low noise, synergies with planned façade renovation). In summary, it can be said that there are different and differently weighted benefits of ambient heat or solar thermal collectors depending on the application.

### **3.3.2. Life cycle assessment (LCA)**

Life cycle assessment or life cycle analysis (LCA) is a method to assess the environmental impact of a commercial product, process or service throughout all product life

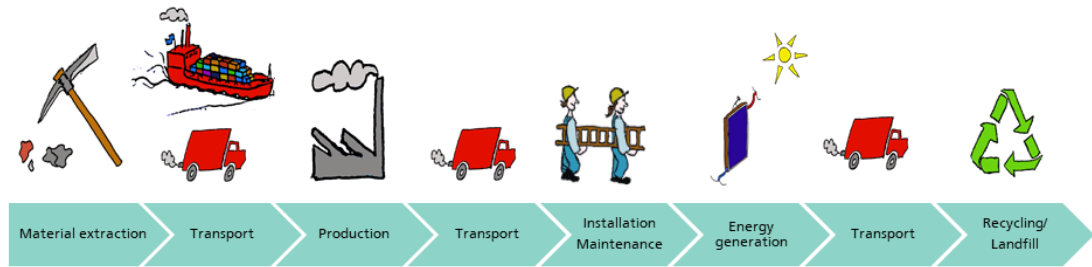


FIGURE 3.3.2. Exemplary life cycle stages of a solar thermal collector

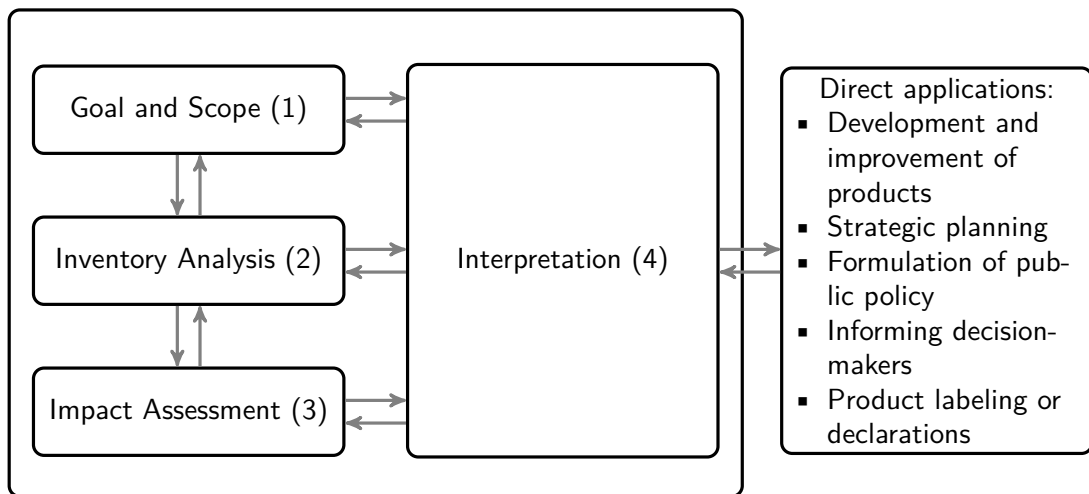


FIGURE 3.3.3. Framework of Life cycle assessment (LCA) [126]. The numbering indicates the order within the iterative process.

stages. An exemplary list of product life stages for a solar thermal collector is shown in figure 3.3.2.

Widely recognized procedures how to conduct an LCA are described in ISO 14044 (Requirements and guidelines) [127] and ISO 14040 (Principles and framework) [126]. The methodology is well developed and documented for practical use in the International Reference Life Cycle Data System (ILCD) Handbook [46].

The main phases of an LCA, together with possible applications, are depicted in figure 3.3.3 and shortly described in the following.

Lowering the environmental impact is gaining importance for all products (Environmental product declaration – EPD). The environmental impact of all parts must be known to calculate the environmental impact of a building. Until now, solar thermal collectors do not have to be included in such a calculation for a certificate of the Deutsche Gesellschaft für Nachhaltiges Bauen – DGNB e. V., for example. If substantial parts

of the building envelope consist of solar thermal collectors or photovoltaic modules, the regulations might be changed in future.

#### 3.3.2.1. *Goal and scope*

The so-called “functional unit” is defined in the goal and scope phase. The functional unit exactly defines and quantifies what is going to be studied.

Further, the system boundaries are fixed. They define which processes should be included and if other co-products need to be assessed.

Any assumptions and limitations of the study need to be clarified. The data quality requirements such as data range, completeness, county or region of study, etc. are stated.

The impact categories need to be selected. A vast set of impact categories and methods is available. They can be classified into midpoint and endpoint categories. Global warming potential, eutrophication, acidification or others would represent a midpoint category while “damage to human health”, “damage to ecosystem” and “damage to resource availability” of the ReCiPe-Method [81] would represent endpoint categories that summarize and weight different midpoint categories. The target group has to be specified.

#### 3.3.2.2. *Inventory analysis*

All process and product inputs and outputs within the system boundaries are compiled and quantified during this phase. Common databases like Ecoinvent [164], GaBi or others provide data for materials and processes with the respective emissions data. They also include some compiled data such as data for a complete heat pump or data for “1 kWh of heat produced by a heat pump system”. The data description serves to find the functional unit for the data set “1 kWh of heat produced by a heat pump system” and to check whether it is applicable or if the data set must be compiled manually based on existing materials and processes datasheets.

#### 3.3.2.3. *Impact assessment*

All products and processes are evaluated according to the requirements set in the goal and scope phase. This can be done with special software combined with the databases (e. g. Umberto, GaBi, SimaPro, OpenLCA), with the databases alone or – if available – with primary data from measurements. Impact assessment is often abbreviated with LCIA - life cycle impact assessment.

#### 3.3.2.4. *Interpretation*

The whole procedure is iterative, meaning that after every single phase, the requirements of the goal and scope have to be revised, interpreted and possibly adapted. The result has to be communicated adequately to the target group.

#### 3.3.3. **Life cycle costing (LCC)**

Life cycle costing (LCC) is used to ascertain the relevant costs arising for one or more actors in relation to a product and its alternatives in the course of a product life cycle. In this thesis, this topic is treated in chapter 7. Since the UHPC collectors under consideration are not finished products and other system parameters are not exactly known, only relatively rough estimates are made there.

#### 3.3.4. **Social life cycle assessment (S-LCA)**

A complete sustainability assessment includes a social life cycle assessment (S-LCA) that can be used to assess products' social and sociological aspects. A comprehensive S-LCA follows the framework of ISO 14040 illustrated in figure 3.3.3, but some aspects differ, are more common or are amplified at each phase of the study. The UNEP Guidelines for Social Life Cycle Assessment of Products [3] propose a methodology to develop life cycle inventories. A life cycle inventory is elaborated for indicators (for example, number of jobs created) linked to impact categories (for example, local employment) which are related to five main stakeholder groups (for example, worker, consumer, local community, society, and value chain actors). Figure 3.3.4 outlines the assessment system from categories to unit of measurement.

In this work, detailed S-LCA is not performed as it would go beyond the scope of this thesis. Nevertheless, some aspects of S-LCA, like cultural heritage and governance, are already mentioned in the previous chapter in section 2.2.4 section 2.5. So, sustainability considerations have already been made, even if they were not explicitly named as such. Also, figure 3.1.1 includes several social aspects. In this thesis, it is assumed that a UHPC collector supports a high rating in this area of sustainability due to the higher flexibility in size, surface texture and color, as well as the higher orientation of the development as a façade element. This is set as a boundary condition, so to speak, to investigate how the other areas can be evaluated. These ratings are put in relation to other systems that offer similar flexibility in terms of architectural integration. Thus, an architectural benchmark is defined as described in section 3.5 However, extensive empirical studies with representative interviews would be necessary for a scientifically robust comparative view of social influence.

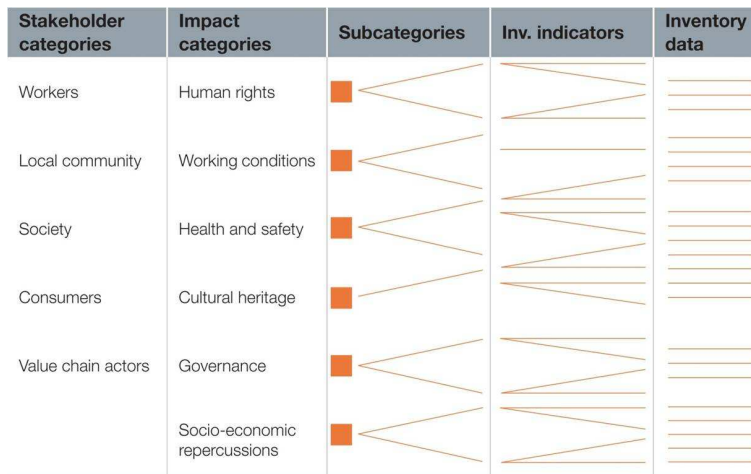


FIGURE 3.3.4. Framework of Social Life Cycle, assessment system from categories to unit of measurement. [3], p. 45.

**3.3.5. Sustainability assessment methodology**

A summarizing sustainability assessment can be done in different ways. If the main areas of sustainability – sometimes represented with pillars – are weighted in the goal and scope definition, and the respective area or pillar can be described by a single number, a single sustainability value or single score can be derived by adding up the three numbers.

However, in retrospect, this value can only be understood if the weighting and calculation of the individual factors are known. Usually, it is rather informative to look at the results individually, for example, in a spider diagram as shown in figure 3.3.5, or to look at combined factors such as the CO<sub>2</sub> avoidance costs or the costs for high architectural quality. After working through the basics of formal sustainability assessment, one may realize that decisions are often led by sustainability, or at least by some aspects thereof<sup>1</sup>. A benefit of such a formalization is using the same functional unit for all aspects. Through the different perspectives, the system boundaries can be sharpened and maybe more adequate reference systems can be found.

**3.4. Overview of the literature about LCA of solar thermal systems**

The LCA methodology is not standardized for solar thermal systems, with few case studies existing today. A technical study report on solar thermal technology LCIA methods and LCC models by Ehrismann [43] illustrates the small number of existing studies and the low comparability between those studies: 24 different studies of solar thermal systems are summarized; among them six about solar thermal electricity generation. 16

<sup>1</sup>Usually, at least the economic aspect of sustainability is taken into account. If this were to reflect the impact on the environment better, the ecological aspect would also receive more attention.

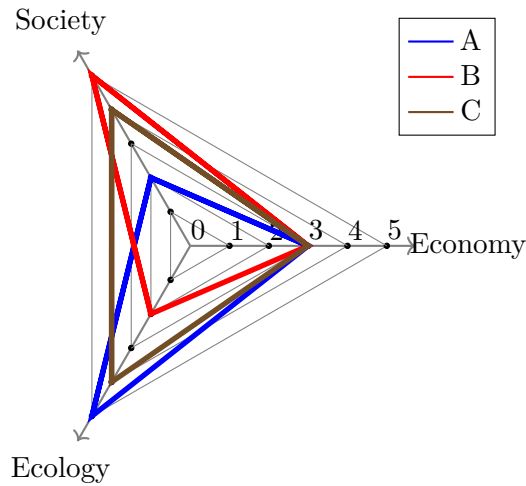


FIGURE 3.3.5. Evaluation of sustainability of three examples in a spiderweb chart. “A” could represent the evaluation of BIST conducted by the “engineer’s approach”, “B” the one of the “architect’s approach”, and “C” could represent the “interdisciplinary approach” in figure 2.2.2, of which the sum of all sustainability numbers is the highest.

studies treat active solar thermal systems or collectors for domestic hot water and heating. The functional unit varies from  $1 \text{ m}^2$  of collector area to a whole collector to a whole system to a certain amount of energy generation supplied. Most of the studies consider the efficiency or the harvested energy in some way, but the considered locations are spread across the whole world. Almost all studies consider a cradle-to-grave approach. Lifetimes of collectors vary from 10-30 years. Some studies consider different scenarios and compare solar thermal systems with other technologies.

Especially for BIST, the database is small: a review and perspectives on life cycle analyses of solar technologies with emphasis on building-integrated solar thermal systems were published in 2015 [104]. That paper only includes four BIST studies; three studies consider Trombe walls, and the fourth is by the authors of this study about a gutter-integrated solar collector. Different aspects of this gutter-integrated system are examined with LCA methods in [103, 105, 102]. In addition to this overview, the study of Lenz et al. in 2012 [106] should be mentioned: The authors examined façade integrated solar energy-producing elements for existing high-rise buildings. In their work, they used the gross energy yield per  $1 \text{ m}^2$  of south façade as the functional unit for the collectors. They also state that whole system simulations would be needed to assess the impact more accurately. They suggest a functional unit of energy savings in kWh per  $1 \text{ m}^2$  building net floor area for future work.



In 2015, C. Pouloupoulos presented his master’s thesis “Life Cycle Assessment of a Multifunctional Solar Thermal Façade System and a Reference Model” [134] which was written in the framework of the TABSOLAR project (see description in section 4.2) under the supervision of the author. Within this work, the functional unit was defined as a wall with embedded solar thermal collectors which can cover 23.8% of the total heat demand of a 140 m<sup>2</sup> single-family home in Freiburg, Germany, with an annual total heat demand of 10.3 MWh. Two variants of the *TABSOLAR*<sup>®</sup> collectors (Economy and Premium) were compared to a reference collector. The *TABSOLAR*<sup>®</sup> collector variants needed more area (15 m<sup>2</sup> and 8.56 m<sup>2</sup>) than the reference collector (7.65 m<sup>2</sup>), but the total impact in all investigated categories (primary energy demand, global warming potential, ozone layer depletion, acidification, eutrophication and photochemical ozone creation potential) was lower than the reference. This study shows that a selection based solely on the gross collector yield (highest for the reference collector) may not lead to the system with the lowest environmental impact.

Besides individual studies, the Ecoinvent database<sup>2</sup> contains inventories of different solar thermal systems. The inventory of Ecoinvent is based on the report by Jungbluth in 2007 [87]. An update to that report was presented in 2012 [150] but has not yet been included in the Ecoinvent database. As the description is very good, the different solar thermal collectors and systems can be modeled manually with Ecoinvent processes. It can serve as a reference.

In the book “Erneuerbare Energien – Systemtechnik, Wirtschaftlichkeit, Umweltaspekte” (English: Renewable energies – systems, economics and environmental aspects) [88] the authors present LCA of different classical solar thermal systems as described in section 5.1.1. The overview in this book is very informative as it uses the same functional unit (impact per Terra Joule needed for heating and hot water) for many systems (different combinations of solar thermal systems with oil or gas, different heat pump systems, and pure oil and gas systems). The authors consider the ecological and economic aspects of all systems. They do not consider combinations of heat pumps with solar thermal systems and no BIST collectors.

The recently initiated IEA SHC Working Group “Life cycle assessment for solar heating and cooling technologies” underlines that LCA for solar thermal systems is an important topic that lacks knowledge, standardization and common understanding. First approaches towards standardization of LCA of solar thermal systems were made in the European Union project “NEGST – New generation of solar thermal systems”: by presenting procedures for environmental performance assessment for solar thermal

---

<sup>2</sup>The international Ecoinvent database is a leading global data system by the Swiss Ecoinvent Center for central recording, calculation, administration, and offering of LCA data via the Internet with more than 4500 users in more than 40 countries [165].

systems [5]. The approach proposes a standardized data sheet for solar thermal collectors similar to the existing one of Solar Keymark. They propose that this environmental fact sheet presents the following:

- (1) a thorough presentation of the results from the solar thermal systems (STS) life cycle inventory with the use of resources such as energy and materials, emissions, waste, and recycling etc.,
- (2) the energy delivered by the STS in terms of annual collector energy output,
- (3) an immediate, objective, and easily understandable overview of the most important assessments of the STS's environmental impact. For this purpose, they propose the energy yield ratio and prevented global warming as basis for environmental assessment.

The energy yield ratio (EYR) describes how many times the energy invested is returned.

$$(3.4.1) \quad \text{EYR} = \frac{\left( \frac{E_{delivered}}{\eta_{conventional}} - E_{operation} \cdot \text{Lifetime}_{STS} \right)}{\text{Embodied energy}_{STS}}$$

with  $E_{delivered}$  being the energy delivered for domestic hot water or heating by the solar thermal system (STS) in kWh per year,  $E_{operation}$  being the operational energy needed by the STS (mainly the circulation pump) in kWh per year,  $\eta_{conventional}$  being the efficiency of the conventional system that the STS is replacing, and  $\text{Lifetime}_{STS}$  equaling the lifetime of the STS unit; often 10 to 30 years.

This approach would enable at least a reasonably fair comparison of different solar thermal systems. The first point is the basis for all life cycle assessments, providing it enables own calculations. The second point in the list requires annual collector output, which very much depends on the system, the orientation to the sun, and the local weather conditions. A first approach could include calculating the gross collector yield for a set of most common systems temperatures for different standard locations, possible with the freely available tool ScenoCalc. This would at least facilitate the comparison between different collectors. Still, the gross collector output does not reflect actual energy savings. They can only be determined with system simulations. The same is true for the energy yield ratio, which can only be calculated correctly with system simulations. Additionally, it refers to a conventional system that needs to be defined. The resulting EYR does not reveal the lifetime even if implicitly included. Other influencing factors such as maintenance effort may be included in the embodied energy. In a context where a particular lifetime is required, this can be stated in the functional unit. Assessing the amount of global warming that is prevented also implies the reference system, which is usually conceived as a gas or oil system. This might change in future.

In conclusion to this brief overview of LCA of BIST, a study should be presented that illustrates the importance of considering all life phases of energy-saving measures.

G. A. Blengini T. Di Carlo [10] investigated the carbon footprint and the life cycle energy of a low-energy family house in Italy. As the building was claimed to be sustainable based on its outstanding energy-saving performances, an ex-post LCA was set up to understand whether and to what extent the favorable judgment could be confirmed from a life cycle perspective. The study has confirmed that the initial goal of environmental sustainability was reached, but to a much lower extent than previously thought.

Compared to a standard house, the energy demand for heating was reduced by a factor of 10, while the primary energy demand of the building was only reduced by a factor of 2.1 and the carbon footprint by a factor of 2.2. This may be an isolated case, and the difference might not be as severe in other comparative calculations. Nevertheless, it becomes apparent that low energy consumption does not necessarily lead to an equally large improvement in total primary energy savings or carbon footprint. Accordingly, at least one typical example should be used to check how environmentally friendly an energy-saving measure really is.

### 3.5. Functional unit for BIST

#### 3.5.1. General remarks

For a full comparison of different building systems, it can generally be said that all differences should be compiled and checked whether they have to be included in the comparison or not to meet the requirements in the goal description. Thus, the first step for both new buildings and renovations is to determine the building systems to be compared. To classify new systems in a market environment, the typical market or at least one example case should be illustrated by means of reference systems. This allows later indirect comparison of other systems based on the deviation to the known reference system.

Then the differences and the intersection of the considered building systems have to be determined.

If the variation of a system's variable of interest (e. g. CO<sub>2</sub> emissions) is to be determined related to the overall system (e. g. a whole building), the intersection (foundation walls, the roof, all façades, etc.) must also be evaluated. If applicable, the intersection can be evaluated and varied individually, as long as it is independent of the considered systems.

The intersection can be omitted if differences between systems are to be determined, as it is only an offset.

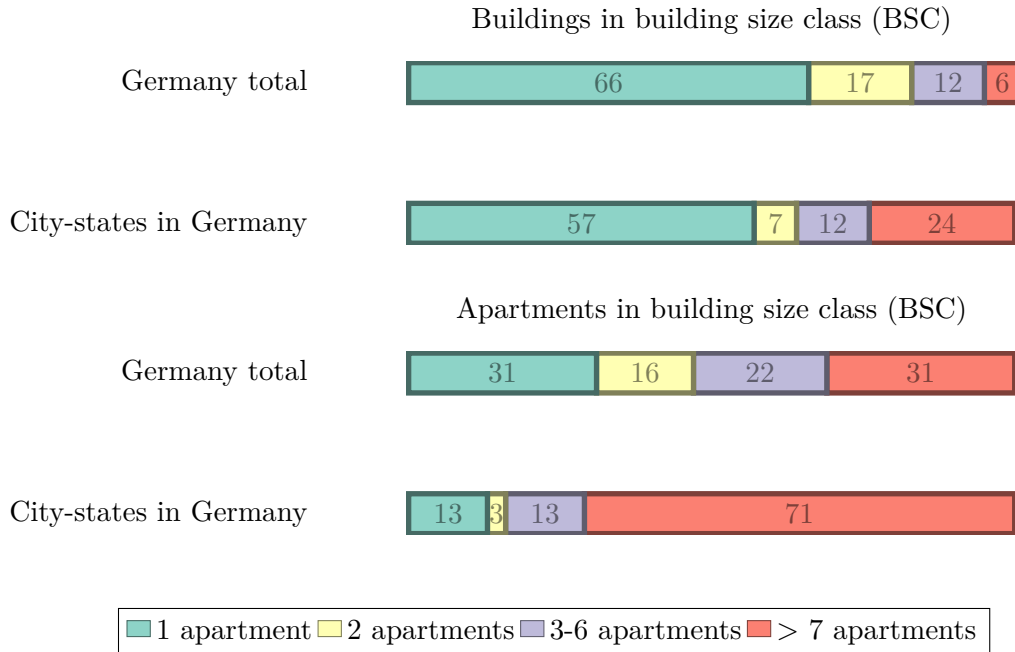


FIGURE 3.5.1. Above: residential buildings in building size classes (BSC) of 1, 2, 3-6 and more than 7 apartments in percent; below: shares of apartments in BSC. Evaluation for city-states (Hamburg, Bremen, Berlin) in Germany and all of Germany in 2011, own graphic based on [20].

### 3.5.2. Description of functional unit and the system boundaries for BIST

This work deals with the contribution of solar thermal façade collectors made of UHPC to the urban heat transition. An overview of urban building stock can be obtained, for example, from the building stock of the city-states of Hamburg, Berlin, and Bremen [20]. A comparison of the shares of residential buildings and apartments in the respective building size class (BSC) is shown in figure 3.5.1 for the city-states and Germany as a whole. According to this evaluation, the share of large buildings with more than seven apartments in the city-states is 24 % of the whole building stock, whereas the share of apartments in buildings with more than seven apartments is 71 %. In Germany as a whole, the share of large buildings is significantly lower, namely 6 %. Still, adding up the apartments in the BSC of 3-6 apartments (31 %) and those of BSC with more than seven apartments (22 %), more than 50 % of all apartments in Germany are in houses with more than three apartments.

The stock of apartment buildings in Germany was examined more closely in the project “LowEx im Bestand” (Engl. “LowEx in stock”) project [42]. An analysis brought

forth the definition of three typical building sizes from four building age classes. As the project is not yet concluded, this thesis is based on an intermediate status of the project.

Figure 3.5.2 shows the visualization of the medium-sized apartment building of the age class 1958–1978, which is the subject of the investigation in this work. A detailed description of this building can be found in chapter 5.

The visualization shown here shows the initial situation of the building before renovation. Different renovation paths are now to be compared with each other. It is assumed that the existing radiators were about 15 % oversized. By renovating the façade and the roof, the heat demand can be reduced. The remaining heat demand can then be covered with fewer or smaller radiators with the same supply temperature or with the existing number and size of the radiators with lower supply temperatures. As heat pumps with a given source temperature operate more efficient with a low supply temperature, the latter case is considered here. In addition to reducing the heat demand, the heating system is also to be renewed with a heat pump system.

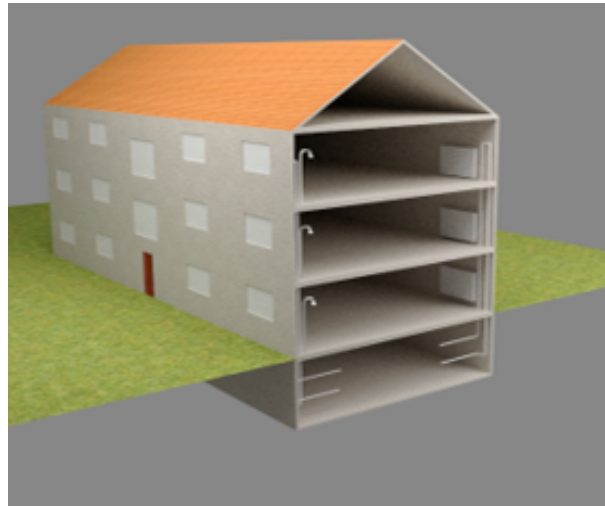


FIGURE 3.5.2. Visualization of an apartment building of the building age class 1958–1978. South side, east side in section, without heat generation system.

A system with an air heat pump, one with a geothermal heat pump and different combinations of a heat pump and UHPC collectors as a heat source with and without cold storage are to be compared. A system with a reference collector as a heat source serves as the technical reference. The chosen reference collector is the unglazed stainless steel collector used in the example in figure 2.2.1 (A). The economic benchmark for the collector-heat pump systems (Col-Ice and Col-Dir) illustrated in figure 3.5.3 (C) and (D) would be an air-source heat pump together with an External Thermal Insulation

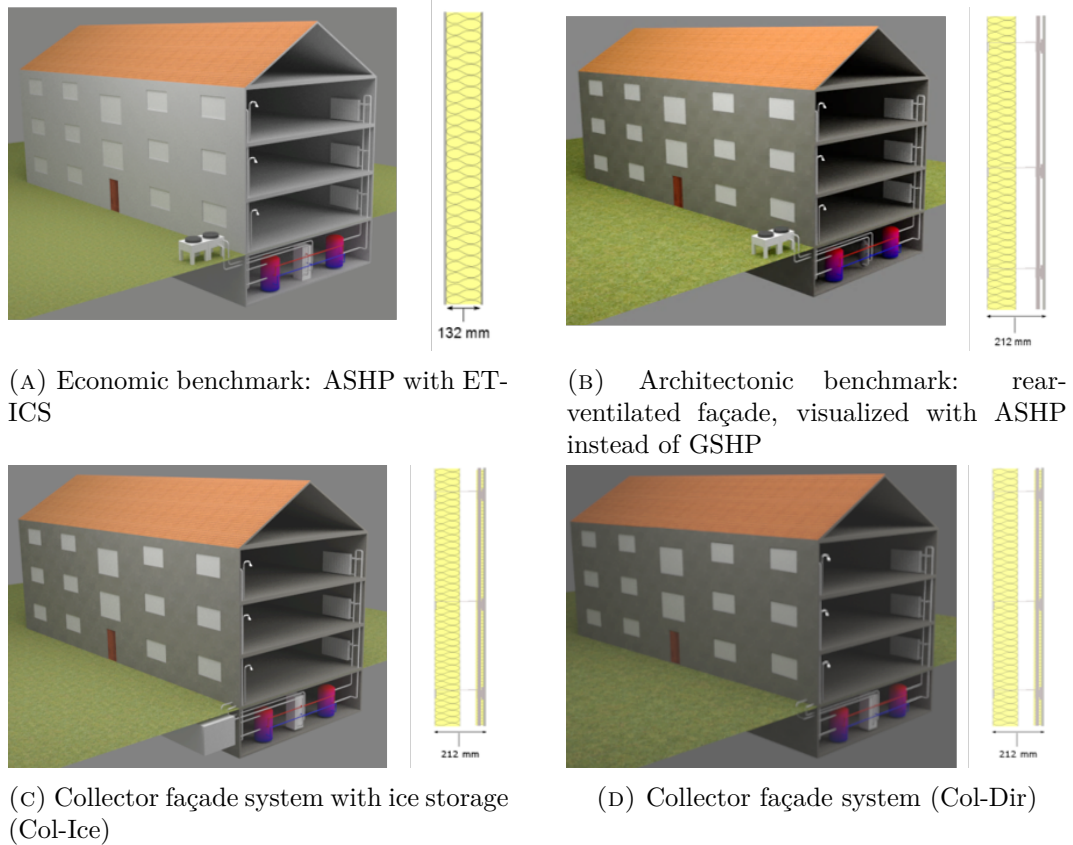


FIGURE 3.5.3. Visualizations of economic benchmark, architectural benchmark, and the solar systems

Composite System (ETICS), depicted in figure 3.5.3 (A). As the variation in the efficiency of air-source heat pumps is relatively high, two types were assumed and simulated.

As an architectural benchmark, a rear-ventilated façade with UHPC cladding together with a ground-source heat pump (B) was defined (picture shows an ASHP instead of a GSHP). The intersection of all renovation pathways (roof insulation, share of façades not covered by collectors in the solar systems) was not considered in this case.

These different renovation paths will now be evaluated in terms of primary energy and CO<sub>2</sub> emissions over their life cycle. This evaluation requires data for the various materials, processes, and transports used. The production facility for the UHPC collectors and the installation site are assumed to be located in Germany.

In addition, the respective energy required for heating and hot water preparation must be determined and evaluated with the primary energy factor and the factor for CO<sub>2</sub> equivalents.

The amounts of energy required in each system are determined using system simulations. The characteristic curves of the UHPC collectors required for the system simulations (compare chapter 5) are determined from the simulation of different operating points using 2D FEM simulation by regression (compare chapter 4). Figure 3.5.4 gives an overview of the workflow and the methods used to compare the primary energy consumption and CO<sub>2</sub> emissions of different systems. The inventory used and the resulting life cycle impact assessment is presented in chapter 6. The CO<sub>2</sub> emissions are evaluated according to the IPCC report 2013 – climate change, GWP 100a [148].

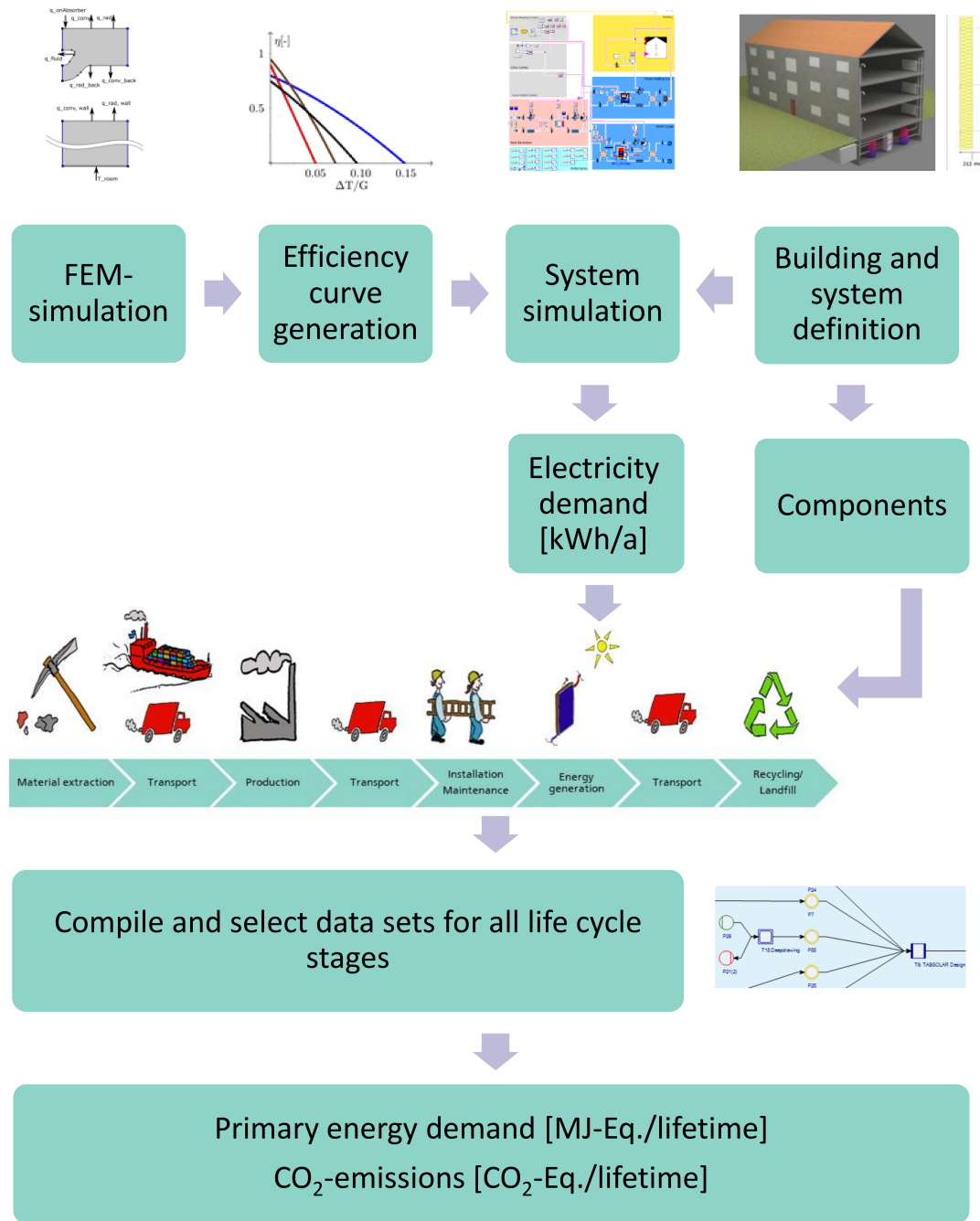


FIGURE 3.5.4. Overview and workflow of used methods within this work using the example of solar systems.



## CHAPTER 4

### Solar thermal collectors made of UHPC

This chapter introduces the reader to solar thermal collectors and provides a general overview of existing solar thermal collector concepts with a focus on flat plate collectors. The technical description of heat output and its influencing parameters are briefly summarized. This thesis investigates façade collectors made of UHPC due to their assumed architectural flexibility. Since no such product is currently in the market, a far developed concept, the *TABSOLAR*<sup>®</sup> concept (figure 1.2.2), is presented in detail. Questions arising concerning the modeling of the heat output of UHPC collectors are discussed based on this concept. As, on the one hand, the architectural flexibility of unglazed collectors is assumed to be particularly high and, on the other hand, modeling of unglazed collectors is least investigated, the details of modeling these collectors is investigated. As a result, a new methodology for modeling unglazed façade collectors with and without insulation is presented, as well as a proposal for the inclusion of margin effects.

As indicated by the examples (E) and (F) in figure 2.2.1, non-black glazed UHPC collectors might be of architectonic interest, too. Therefore, some design considerations for these collectors are presented in section 4.3.3. With the methodology developed, two exemplary heat gain curves for different UHPC collectors are generated for further use in system simulations.

#### 4.1. Fundamentals and state of the art of solar thermal collectors

##### 4.1.1. Classification

Solar thermal collectors transform solar radiation into useful heat and losses. Depending on the insulation towards the environment, collectors can also use heat from the ambient air if operated below ambient temperature. They can be classified depending on the operating temperatures. Figure 4.1.1 gives an indicative overview of solar thermal applications with a rough classification of solar thermal technologies. This work only considers the color-coded applications and collector concepts. PVT exist as unglazed and glazed variants. They are not included in this work. The different collector concepts are presented in the following, a more comprehensive overview of the colored applications is given in section 5.1.

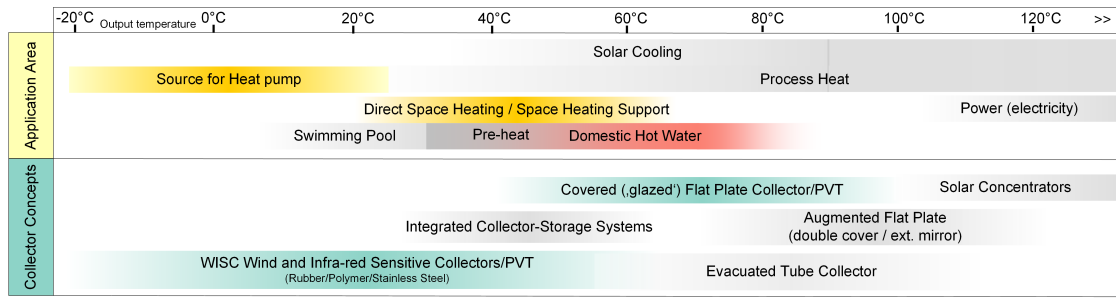


FIGURE 4.1.1. Indicative overview of solar thermal applications (based on output temperature) with a rough classification of solar thermal technologies. Grayed applications and collector concepts are not explicitly treated within this work. PVT stands for Photovoltaic thermal collectors [52].

#### 4.1.2. State of the art of glazed and unglazed flat plate collectors

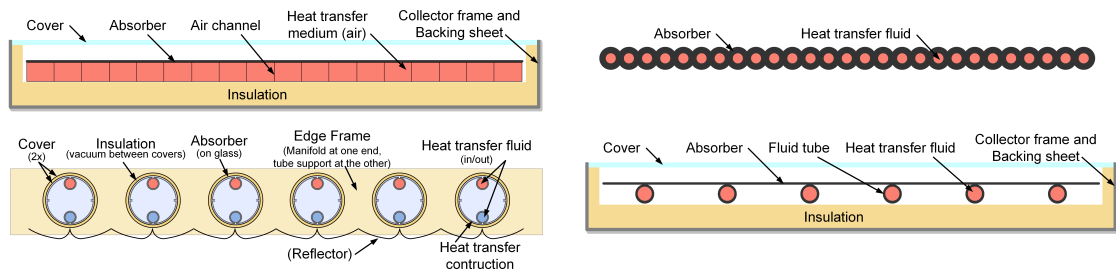


FIGURE 4.1.2. Cross-sections of different collectors: air collector (top, left), unglazed absorber (top, right), vacuum tube collector (bottom left) and flat plate collector (bottom, right) [52].

Figure 4.1.2 shows exemplary cross-sections of different low and medium temperature solar thermal collectors. The first example on the left-hand side depicts an air collector. Air has a far lower heat capacity than water or water-glycol, the heat carriers typically used in solar thermal collectors. The efficiency of air collectors is very dependent on mass flow and leakage. Larger pipes or channels are needed. The absorber of the depicted variant consists in a double-wall plate. The cross-section on the lower left demonstrates a vacuum tube collector. Vacuum is used to minimize the convective heat losses and to achieve higher temperatures. Both air collector and vacuum tube collectors are not further considered in this work.

The upper right-hand side shows a typical representation of an unglazed collector. These collectors are also called WISC - Wind and Infrared Sensitive Collectors. As the name indicates, they are very sensitive to wind velocities and infrared radiation. These

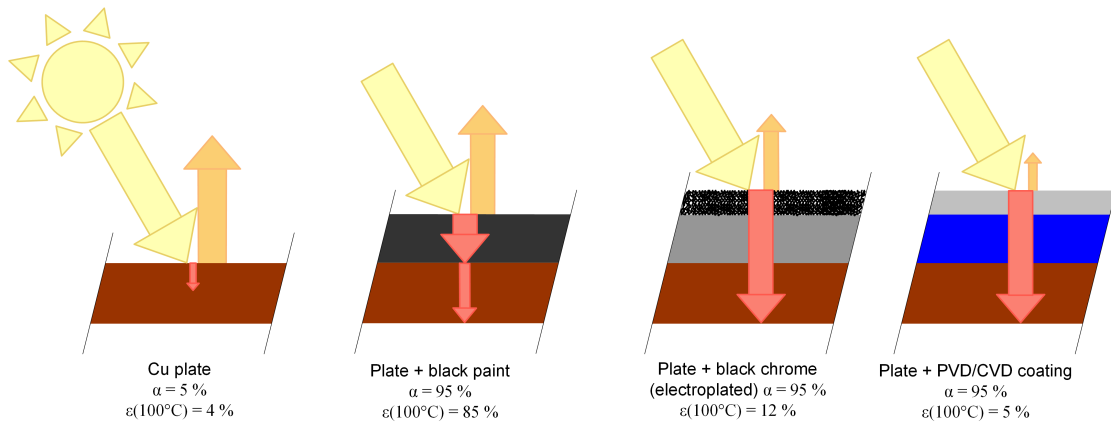


FIGURE 4.1.3. Absorption and emission factors for various absorber coatings [52].

collectors can also use heat from the ambient if operated below ambient temperature. The presented cross-section consists only of the fluid-carrying absorber; this variant has no insulation. The absorber can be seen as the core of any collector as this is the part where incoming radiation or ambient heat is converted into useful energy. The depicted variant is also called swimming pool absorber as the (pre-)heating of swimming pools is or was its main application. Meanwhile, they are also used as a low-temperature source, as described in the next paragraph. They are usually made from plastic or rubber. Unglazed collectors can also be made from steel or polymer. Stainless steel collectors are available as unglazed variants that can take over functions of the building envelope, such as a roof or façade as shown in the section 2.2 figure 2.2.1, (A). Unlike most unglazed absorbers, these stainless steel absorbers are coated with a spectrally selective layer like absorbers in state-of-the-art glazed collectors. Spectrally selective coatings have a high ability to absorb the solar spectrum (characterized by the absorptance  $\alpha$ ), and at the same time, they emit little infrared radiation at higher temperatures. This is also called IR mirror and is characterized by the emissivity at 100 °C  $\epsilon_{100^\circ\text{C}}$ . In the remainder of this work,  $\epsilon_{100^\circ\text{C}}$  is abbreviated as  $\epsilon$ . figure 4.1.3 provides an indicative overview of absorption and emission factors for various coatings. A spectrally selective coating leads to lower heat losses and higher achievable operating temperatures. So even if this collector has no glazing, it can be used for direct space heating or even domestic hot water support during times of high irradiation.

Unglazed collectors can also be used as a single source, bivalently in combination with ice storage or other sources for a heat pump like, for example, in a pilot plant in a kindergarten as described in [27].

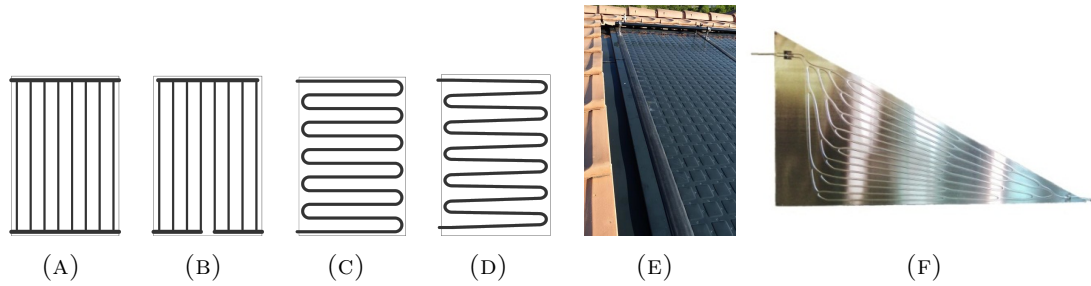


FIGURE 4.1.4. Different channel designs of classical absorbers: (A) harp, (B) double harp, (C) meander, (D) meander designed for drainback systems [52], cutout of unglazed pillow absorber, source: [www.energie-solaire.com](http://www.energie-solaire.com) (E), uncoated triangular sample with FracTherm<sup>®</sup> design built within the European project BIONICOL (F) [72]

A glazed solar thermal collector with a so-called fin-and-tube absorber is depicted below the pure absorber in figure 4.1.2. The absorber is embedded in insulation made of mineral wool or polyurethane and cased with a frame typically consisting of aluminum or wood. The casing is covered with a single or double glazing that can be equipped with an anti-reflection (AR) cover for higher transmittance. The classical fin-and-tube absorber for solar thermal collectors with function separation of absorption of solar radiation with subsequent heat transfer within thin fins or metal sheets and fluid transportation under pressure within tubes has been developed for a long time. The production technology, originally based on handcraft, is now widely automated, mostly with ultrasonic or laser welding as junction technology for the metal sheet and the tube. Whereas the tubes are still commonly made from copper, aluminum has mostly replaced copper as a material of the absorbers. Channel design varies between harp, meander and combinations of both, as shown in figure 4.1.4 (left). With current productions technologies, absorbers with special sizes, e. g. for triangular areas below a roof ridge, are very difficult to produce and much more manual work is needed. Usually, a meander with a rather high pressure drop is chosen as channel for a special size collector area. Harps have a lower pressure drop, but more connecting points to the bigger connecting pipes, which increases manual work. Another problem of a harp design is the mostly inhomogeneous flow distribution within the rising pipes. How different channel cross-sections influence the flow distribution in harp absorbers was investigated by the authoress in 2013 [97]. Greatly differing volume flows in the rising pipes can result in high temperature differences within the absorber. In worst cases, this leads to partial stagnation.

The cost reduction potential of fin-and-tube absorbers without efficiency reduction is exhausted almost entirely. Mass production technologies such as sheet metal forming

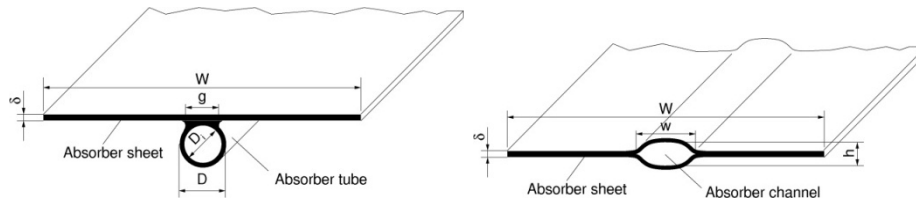


FIGURE 4.1.5. Schematic sketches of fin/sheet-and-tube absorber (left) and integrated absorber (right) [73]

processes, for example, promise both cost reduction by increasing the degree of automation and higher flexibility of shape of the outer dimensions of the absorber and the channel structure and cross-sections. Designs like pillow absorbers (figure 4.1.4, (E)) or the quasi fractal FracTherm<sup>®</sup> structures (figure 4.1.4, (F)) can be produced. The FracTherm<sup>®</sup> algorithm developed by M. Hermann [71] can create channel designs for various outer shapes, such as the depicted triangle. With an equal flow distribution and a low pressure drop, it combines the advantages of harp and meander design.

As the channel and the absorber made with sheet metal forming or other forming technologies form a unity, we call them “integrated absorbers”, see figure 4.1.5.

At Fraunhofer ISE, roll-bonding, hydroforming or deep-drawing are investigated as production technologies for solar thermal integrated absorbers. Challenges, opportunities, and experiences for steel absorbers are described by the author ([93, 94, 96, 97]) or in the final reports of the German projects SAPRES<sup>1</sup> [95] and STAHLABS<sup>2</sup> [146].

Besides changing the production technology, further cost reduction potential can be found in alternative materials like steel, polymers or Ultra-High Performance Concrete (UHPC). Due to the lower thermal conductivity, the absorber design has to be adapted to achieve the same or even better thermal efficiencies than state-of-the-art absorbers. The production technology of classical fin-and-tube absorbers may no longer be appropriate for these needs [92].

To the author’s knowledge, neither pure steel nor UHPC absorbers are currently on the market. The combination of material switch and mass production technology promises lower costs at high production volume. However, since total market volumes are still rather small, there is a high risk of not being able to sell the production volume.

<sup>1</sup>The SAPRES project was carried out with funds from the German Federal Ministry for the Environment, Nature Conservation and Nuclear Safety (BMU) according to a decision of the German Bundestag (FKZ 0325989A)

<sup>2</sup>The IGF project 339 ZN (STAHLABS) of the Research Association for Steel Application, FOSTA, Sohnstraße 65, 40237 Düsseldorf, was funded by AiF in the context of the program for support of Industrial Collective Research and Development (IGF) by the Federal Ministry of Economic Affairs and Energy on the basis of a decision by the German Bundestag.

Stainless steel absorbers are available as unglazed and glazed variants. And polymer collectors increasingly find their way into the market. An excellent overview of existing products was worked out within the framework of IEA-SHC Task 39<sup>3</sup>. Many questions concerning material switch and production technologies are similar for all new materials but must be answered individually. Polymer collectors lie outside the scope of this research work. A commercial, uninsulated, and unglazed stainless steel collector serves as a technical reference for the UHPC collectors.

#### 4.1.3. Description of solar yield

The performance of solar thermal collectors can be characterized by procedures for testing and subsequent parameter identification described by ISO 9806 [124].

A simple form of describing the instantaneous efficiency of glazed solar thermal collectors is given by

$$(4.1.1) \quad \eta = \eta_0 - c_1 \cdot \frac{(\vartheta_{fluid,m} - \vartheta_{amb})}{G} - c_2 \cdot \frac{(\vartheta_{fluid,m} - \vartheta_{amb})^2}{G},$$

where  $\eta_0$  stands for the thermal conversion factor,  $c_1$  and  $c_2$  for the the linear and the quadratic heat loss coefficient, and  $G$  for the normal irradiation.  $\vartheta_{fluid,m}$  is the mean collector temperature and  $\vartheta_{amb}$  the ambient temperature. The difference of  $\vartheta_{fluid,m}$  and  $\vartheta_{amb}$  divided by  $G$  is often noted shortly as the reduced temperature  $\Delta T/G$ . Measurements are conducted at wind velocities between 2 m/s and 4 m/s.

The efficiency of WISC (wind and infrared-sensitive collectors) strongly depends on wind velocities and ambient temperatures. In ISO 9806, the description of the instantaneous efficiency considers this with the wind dependent thermal conversion factor  $b_u$  and the wind dependent linear loss coefficient  $b_2$ . The linear heat loss coefficient  $b_1$  resembles  $c_1$  in equation (4.1.1) but is valid for  $u_{wind} = 0$  m/s. The same applies to  $\eta_0$  of WISC.

$$(4.1.2) \quad \eta = \eta_0 \cdot (1 - b_u \cdot u_{wind}) - (b_1 + b_2 \cdot u_{wind}) \cdot \frac{(\vartheta_{fluid,m} - \vartheta_{amb})}{G''}$$

with

$$(4.1.3) \quad G'' = G + \frac{\varepsilon}{\alpha} \cdot (E_L - \sigma T_{out}^4)$$

$T_{out}$  stands for the temperature towards where the radiation is occurring,  $E_L$  ( $\lambda > 3 \mu\text{m}$ ) for the long wave irradiance. During normative measurements,  $T_{out}$  usually means the sky temperature. In case of cloudy weather or a tilted area,  $T_{out}$  can also indicate the ambient temperature or something between the two. The term for the net long-wave irradiance ( $E_L - \sigma T_{out}^4$ ) is usually negative, as the effective sky temperature is lower than

<sup>3</sup><https://task39.iea-shc.org/publications>

the ambient temperature. The net long-wave irradiance of  $100 \text{ W/m}^2$  approximately corresponds to the conditions of the sky if  $\vartheta_{amb} = 20^\circ\text{C}$  and  $T_{sky} = 0^\circ\text{C}$ .

These characteristic values are usually retrieved from either indoor testing in a solar simulator under artificial sun and wind or outdoor testing under natural weather conditions. The norm allows for steady-state or quasi-dynamic test procedures. During the test procedure in the solar simulator, the collector is operated with different collector temperatures and different wind velocities, and the corresponding useful energy is measured. The needed parameters can then be derived from the measurement by regression. During the quasi-dynamic test procedure, collectors are exposed to the natural weather conditions outdoors. If certain test conditions are fulfilled, the characteristic curve can be derived from the measured data via parameter identification. As the test method is dynamic, the thermal capacity is included with the  $c_5$  term.

The heat output can then be described with the quasi-dynamic, instantaneous heat output described in ISO 9806 (2012) [124]. In ISO 9806 (2018) [36] this equation was amplified with the terms  $c_7$  and  $c_8$ . Furthermore, the wind velocity  $u_{wind}$  was replaced by  $u'_{wind} = u - 3 \text{ m/s}$ . The last replacement is only a change in representation and was left out in the following equation for better understanding:

$$(4.1.4) \quad \begin{aligned} \frac{\dot{Q}_{useful}}{A} = & \eta_0 \cdot (K_{\Theta,b}(\Theta) \cdot G_b + K_{\Theta,d}(\Theta) \cdot G_d) - c_1 \cdot (\vartheta_{fluid,m} - \vartheta_{amb}) \\ & - c_2 \cdot (\vartheta_{fluid,m} - \vartheta_{amb})^2 - c_3 \cdot u_{wind} \cdot (\vartheta_{fluid,m} - \vartheta_{amb}) + c_4 \cdot (E_L - \sigma T_{out}^4) \\ & - c_5 \cdot \frac{dT_m}{dt} - c_6 \cdot u \cdot G - c_7 \cdot u_{wind} \cdot (E_L - \sigma T_{out}^4) - c_8 \cdot \vartheta_{fluid,m}^4 \end{aligned}$$

with  $K_{\Theta,b}$  and  $K_{\Theta,d}$  being the incident angle modifier for beam and diffuse radiation,  $G_b$  and  $G_d$  being the respective part of the global irradiation. It also takes into account wind speed and long-wave irradiance. The reference area  $A$  can be either the aperture area  $A_{ap}$ , the absorber area  $A_{abs}$  or the gross collector area  $A_G$ .

The angular dependence of direct absorbed irradiance  $K_{\Theta,b}$  is symmetrical and can be expressed by equation (4.1.5):

$$(4.1.5) \quad K_{\Theta,b} = 1 - b_0 \cdot \left( \frac{1}{\cos(\Theta)} - 1 \right)$$

with the collector specific constant  $b_0$  and the incident angle  $\Theta$ .

Rearranging equation (4.1.2) with equation (4.1.3) results in:

(4.1.6)

$$\frac{\dot{Q}_{useful}}{A} = \eta_0 \cdot G + \eta_0 \cdot \frac{\varepsilon}{\alpha} \cdot (E_L - \sigma T_{out}^4) - G \eta_0 \cdot b_u \cdot u_{wind} - \eta_0 \cdot b_u \cdot u_{wind} \cdot \frac{\varepsilon}{\alpha} \cdot (E_L - \sigma T_{out}^4) - b_1 \cdot (\vartheta_{fluid,m} - \vartheta_{amb}) - b_2 \cdot u_{wind} \cdot (\vartheta_{fluid,m} - \vartheta_{amb}),$$

and by comparing coefficients with equation (4.1.4), the coefficients of equation (4.1.6) can be transformed as followed:

$c_1 = b_1$ ,  $c_2 = 0$ ,  $c_3 = b_2$ ,  $c_4 = \eta_0 \cdot \frac{\varepsilon}{\alpha}$ ,  $c_5 = 0$ ,  $c_6 = \eta_0 \cdot b_u$  and  $c_7 = \eta_0 \cdot b_u \cdot \frac{\varepsilon}{\alpha}$  and  $c_8 = 0$ . This method also allows to use equation (4.1.4) to represent unglazed collectors that were measured with the old standard ISO 9806 (2013).

Efficiency is often presented in relation to the reduced temperature  $\Delta T/G = (\vartheta_{fluid,m} - \vartheta_{amb})/G$ , as shown in figure 4.1.6 (left) for different typical collector types. This way of presenting collectors is rather complex and difficult to understand at a glance. Meanwhile, the presentation of the collector's heat gain in relation to the temperature difference of  $\vartheta_{fluid,m}$  and  $\vartheta_{amb}$  (figure 4.1.6 (right)) is more common, and certified test results are presented that way. The heat gain curve of two collector types is plotted at two different irradiances:  $750 \text{ W/m}^2$  represents a sunny day on the south façade, and  $250 \text{ W/m}^2$  represents a rather cloudy day. As the figure shows, with the lower irradiation of  $250 \text{ W/m}^2$ , some temperatures can not be achieved anymore as the x-axis is cut at lower temperature differences.

Collectors tested according to ISO 9806 [124] in certified test centers can receive the solar keymark certificate. This certificate comprises not only the heat output measurement but also a set of functional tests, among which internal pressure tests, inner and outer thermal shock tests, and impact from hail and mechanical load tests. This certificate is a seal of approval for the installer or end consumer as well as for many funding programs. So most collectors on the market are tested accordingly. For system simulations, these parameters can be fed into a model that works with the characteristic curve.

The annual collector output provides an orientation for the selection of a collector type. For its calculation, the Swedish Research Institute RISE developed the tool ScenoCalc based on Excel. It is now provided by Solar Keymark Network and can be downloaded for free. Based on standardized collector parameters, the tool calculates the maximum heat output for a constant operating temperature at a specific location. The Solar Keymark data sheet provides the annual collector outputs for the locations Athens, Davos, Stockholm, and Würzburg at the operating temperatures  $25^\circ\text{C}$ ,  $50^\circ\text{C}$  and  $75^\circ\text{C}$ .



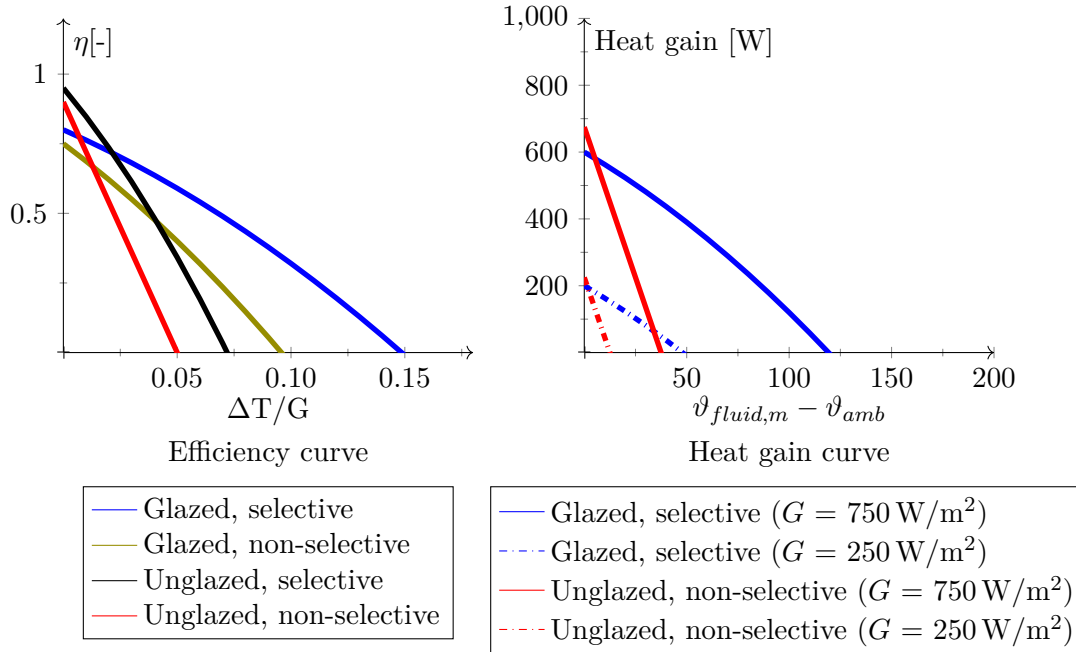


FIGURE 4.1.6. Typical instantaneous efficiency curves of various flat plate collector types with and without glazing and with and without spectrally selective coating (left). For two of the shown four collector types, the heat gain curve is given for two values of irradiation:  $G = 750 \text{ W/m}^2$  and  $G = 250 \text{ W/m}^2$  (right). Significant differences from actual collectors may occur ( $\eta$  = instantaneous thermal efficiency,  $\vartheta_{fluid,m}$  = medium collector temperature,  $\vartheta_{amb}$  = ambient temperature,  $G$  = Irradiation). Values are based on the aperture area of the collector. Values are based on measurement at  $G = 1000 \text{ W/m}^2$  and a wind velocity of  $u_{wind} = 3 \text{ m/s}$ .

The German market incentive program MAP (Marktanzreizprogramm) also uses ScenoCalc to define a benchmark  $Q_{coll,MAP}$  for eligible collectors. To represent a typical system for domestic hot water, a weighting function (equation (4.1.7)) was developed that considers the collector output at  $25^\circ\text{C}$  ( $Q_{coll,25^\circ\text{C}}$ ) and  $50^\circ\text{C}$  ( $Q_{coll,50^\circ\text{C}}$ ) as well as the specific capacity  $c_{eff}$  [16].

$$(4.1.7) \quad Q_{coll,MAP} = 0.38 \cdot Q_{coll,25^\circ\text{C}}/A_{ap} + 0.71 \cdot Q_{coll,50^\circ\text{C}}/A_{ap} - 1.09 \cdot c_{eff} \text{ kWh K/kJ}$$

The MAP benchmark for eligible collectors is  $525 \text{ kWh/m}^2$  at  $45^\circ$  inclination towards south at the location Würzburg. It can be considered a lower limit for collectors for domestic hot water preparation. For collectors serving as a source for a heat pump, the output at lower temperatures is decisive. They usually do not reach the MAP benchmark.

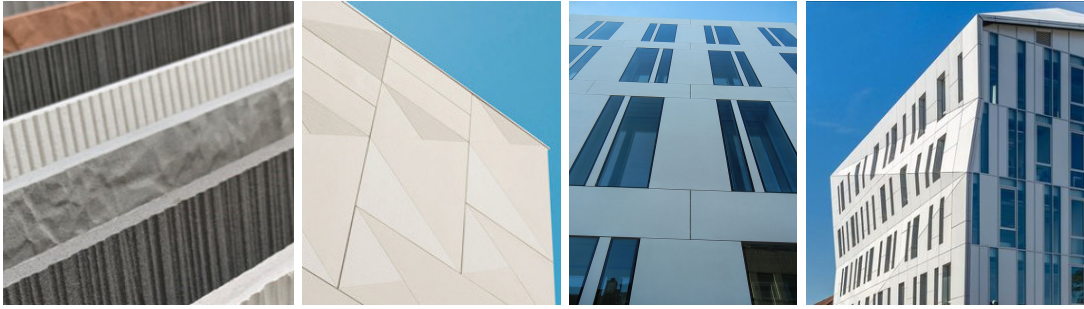


FIGURE 4.2.1. Impressions of TAKTL® elements (left, center left, source: [www.taktl-llc.com](http://www.taktl-llc.com)); Volksbank in Krefeld, Germany, with white UHPC cladding [39] (center right); ESTP - Cachan, Architect: Architecture Studio, source: <https://fehrgroup.com> (left)

#### 4.2. Particularities of UHPC collectors

Ultra-high performance concrete (UHPC) is developed for high structure density. Far higher strength ( $> 150 \text{ N/mm}^2$ ) than normal concrete can be achieved, which leads to remarkable material savings in product design. The different components of the material are locally available worldwide, and the production process casting is a low-energy process as it needs neither high temperatures nor high forces. Applications can be found in different areas like bridges, mechanical engineering, and façades. Two compendia about the research in UHPC were published in 2007 and 2014 [140], [141]. Figure 4.2.1 shows a set of samples of UHPC cladding and built examples.

UHPC cladding gains in importance. In the USA, quite a few projects have used UHPC elements by the company TAKTL®, and in Germany and other European countries, several companies offer UHPC cladding, too. The next step could be to thermally activate these cladding elements and use the incoming heat on the façade for building needs.

Two German research projects, TABSOLAR I and II<sup>4</sup>, pursued this idea, followed by TABSOLAR III (Duration: 2020-2023). Basic investigations into the production of UHPC elements with integrated channels and fluid connections for the application as solar thermal façades or thermo-active building elements inside the building (TABS) were conducted, and three product families were defined (see figure 4.2.2, top left) [74].

Different system concepts were developed, a transfer from laboratory production towards a pilot plant was initiated, and a demonstration house was planned (see figure 4.2.2, below) [75]. In the framework of TABSOLAR III, the main goal is to develop a whole value chain from concept phase to planning, production, and installation up to

<sup>4</sup><https://tabsolar.de/>

operation. Complete solutions for sustainable heating in new buildings and renovations should be developed; proofs of concepts are planned in demonstration installations.

The author is not aware of any other current collector concepts with UHPC. So arising challenges are discussed based on the status quo of the TABSOLAR projects.

#### 4.2.1. Architectural possibilities for UHPC collectors

##### 4.2.1.1. Collector variants

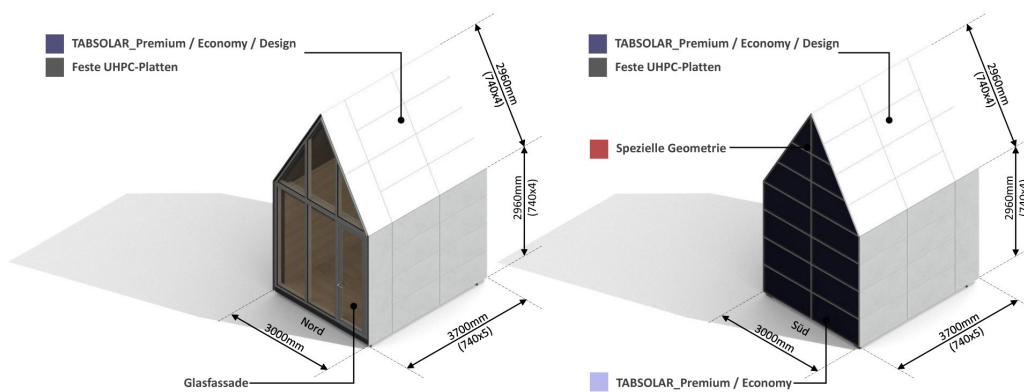
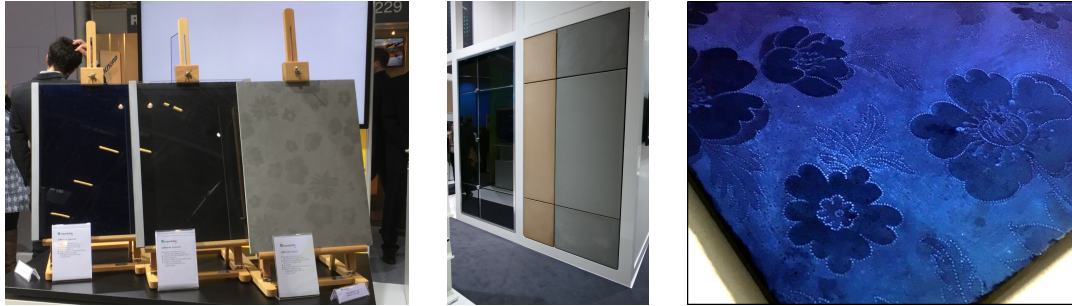


FIGURE 4.2.2. Exhibit of *TABSOLAR*<sup>®</sup> *Premium*, *Economy* and *Design* (left), Exhibit of *TABSOLAR*<sup>®</sup> *Premium* and *Design* on trade fair BAU 2019 in Munich (center, top), UHPC sample with spectrally selective coating (right), design of a planned mobile demonstration building, source: Priedemann Facade-Lab

As mentioned, three UHPC collector families were defined. *TABSOLAR*<sup>®</sup> *Premium* and *Economy* are both glazed and are designed for classical solar thermal applications like domestic hot water preparation and heating support. Since the family *Premium* has

a spectrally selective coating, efficiencies in the range of good state-of-the-art collectors can be achieved, as shown in the first simulations. These first simulations did not yet consider the large inactive margins. The family *Economy* has no spectrally selective coating but a commercially available Low-E coating on the glazing, which still allows for high efficiencies. Lower but still high solar fractions were achieved with the initial simulations. The family *Design* is developed for high architectural flexibility and low-temperature applications. The surface can be structured or colored, and it can be used for preheating or as a source for a heat pump. The collector could be insulated if higher temperatures are targeted. It can even have a spectrally selective coating that is currently in development. Typically, these coatings are susceptible to scratches, and the visual appearance can be destroyed easily. But they are protected with the glazing typically used. The current coating development works with layers of varnish that can protect the spectrally selective coating against environmental conditions. With this method, an emissivity of  $\varepsilon = 0.1$  was achieved at laboratory scale.

#### 4.2.1.2. Wall constructions

A set of different wall constructions for renovation and new buildings was defined in the framework of the TABSOLAR projects (see figure 4.2.3 for first drafts). ETICS or sandwich walls are principally possible; they offer additional synergies, as shown by I. Bergmann and W. Weiß [9], but the rear-ventilated façade offers better possibilities of replacing components in case of damage. It is, therefore, the preferred wall construction for the first buildings.

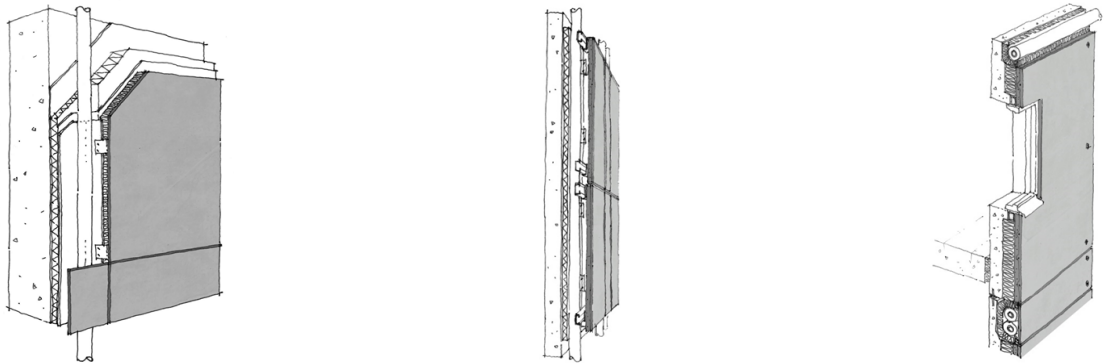


FIGURE 4.2.3. Different façade systems with fluid-carrying UHPC elements for renovation and new buildings: External thermal insulation composite system (ETICS) (left), rear-ventilated façade (center), sandwich wall (right) [75].

Figure 4.2.4, left, shows the size of a sample element. The agrafes to fasten the elements on the substructure are depicted in orange, and the space holder in blue. The

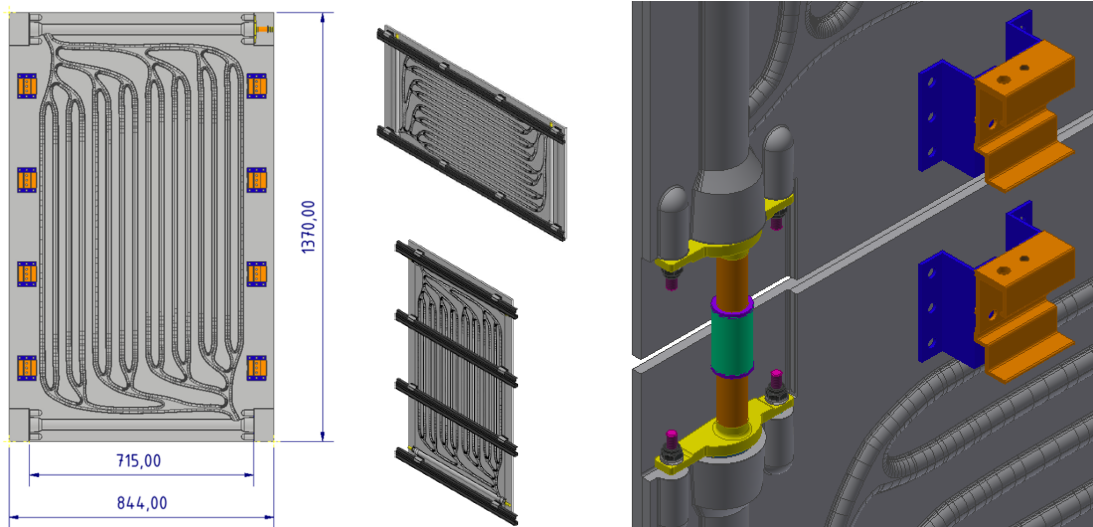


FIGURE 4.2.4. Schematic of UHPC element of current design (left). Principle possibilities to mount a UHPC element, piping structure adapted to vertical orientation (center). Schematic of two hydraulically connected UHPC elements with agrafes for fastening on traverse; view from the backside (left). Source: Fraunhofer ISE.

two possible orientations on the façade are depicted in the center of figure 4.2.4. The hydraulic connections can be seen on the right side of figure 4.2.4.

The gaps between the collectors on the façade can be designed differently: open gaps, frames or punctual connections are possible, as shown for glazing in figure 4.2.5. The variants (B) and (D) are depicted with sealing rubber and silicone (black). It needs to be investigated whether the sealing of the glazing could be left out. In the case of pure absorbers, no sealing would be applied, and the black part would indicate the open gap. If the gaps are open, the wind can pass through the elements, and convective losses can increase. It can be advantageous to operate the collector mainly below ambient temperatures. For common collector concepts and higher temperature levels, a closed frame would be preferable.

## 4.2.2. Description of production technology and properties

### 4.2.2.1. Production technology

The fluid-carrying *TABSOLAR*<sup>®</sup> elements are produced with a membrane vacuum deep-drawing process developed by Fraunhofer ISE. The different production steps can be seen in figure 4.2.6. First, the UHPC is applied on a membrane stretched over the mold containing the channel design (A). The membrane is then drawn into the mold through a vacuum pump, and the viscous concrete follows the form (B). The frame containing

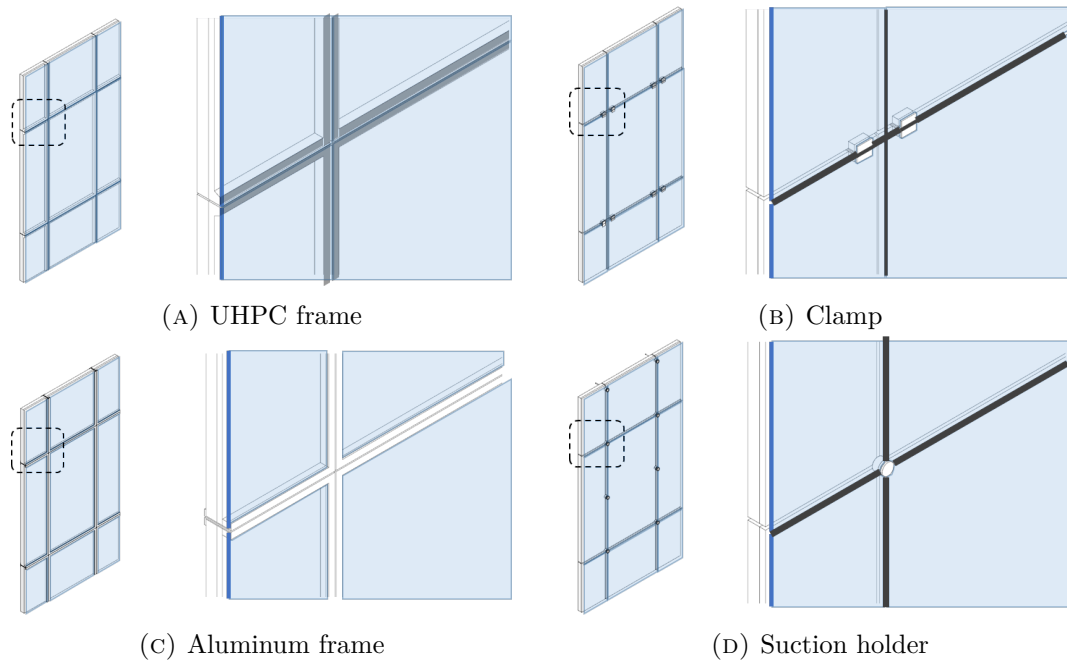


FIGURE 4.2.5. Variants of glazing for *TABSOLAR® Premium* and *Economy*. Variant (B) and (D) are depicted with sealing rubber and silicone (black). Source: Priedemann Facade-Lab.

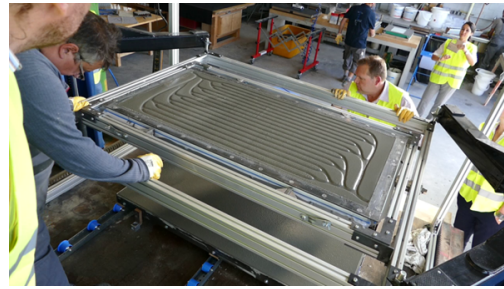
the deep-drawn concrete is then turned and pressed into a level fresh concrete plate. The upper and the lower part join in moist conditions and form a firm connection between the channels (C). After a drying phase, the mold can be removed (D). Impressions of a produced sample are given in figure 4.2.7.

#### 4.2.2.2. Fluid tightness

The dense structure of UHPC makes additional material for channels, such as capillary mats, dispensable. The channels are made from pure UHPC, as shown in figure 4.2.6 and figure 4.2.7. As tests indicate, the UHPC structure might not be completely water vapor-tight [74]. In a closed system, losses could lead to a fluid loss over the years, and the fluid needs to be refilled. In open-loop systems, so-called drainback systems (compare figure 5.1.2), the collector contains fluid only during operation. If the pump stops, the heat carrier drains into drainback tanks or heat storages by gravitation. Minor losses would not cause problems, and drainback systems can have additional advantages: Philippen et al. showed that a water drainback system could save 18% cost compared to a reference system [132]. Nevertheless, if drainback systems are operated with pure water without an antifreeze, the operation is limited to collector temperatures above



(A) Applying UHPC

(B) FracTherm<sup>®</sup> structure after deep-drawing and plain plate below

(C) Joining the upper and lower part



(D) Demolding

FIGURE 4.2.6. Production of *TABSOLAR*<sup>®</sup> elements with channels by membrane vacuum deep-drawing.

0 °C. This would lower operating times significantly if the collector is operated as a heat pump source.

For further system design, the following options are to be considered:

- (1) The vapor diffusion of the absorber is relatively high. It should only be operated with pure water without an antifreeze. Drainback systems would be needed. The operation is limited to collector temperatures above 0 °C.
- (2) The absorber is tight enough and can also be operated with propylene glycol. Open and closed systems could be used. The operating temperature of the collector is not limited.
- (3) The vapor diffusion is too high, and a coating is needed. This coating should be glycol-resistant and environmentally friendly. Regarding recycling and production, it would better be avoided. Nevertheless, open and closed systems could be used. The operating temperature of the collector is not limited.

#### 4.2.2.3. Pressure loss

On the one hand, the FracTherm<sup>®</sup> channel structure with its smooth curving and branching provides for minor pressure loss. On the other hand, the cross-section of the channels is not circular, the favorable cross-section in terms of pressure loss. The



FIGURE 4.2.7. *TABSOLAR*<sup>®</sup> element with channels

FracTherm<sup>®</sup> algorithm calculates a hydraulic balancing based on the hydraulic diameter and assumptions for the pressure loss of the bifurcations and adapts channel widths. These assumptions might not represent the ideal FracTherm<sup>®</sup> channels and bifurcations, and can lead to non-optimal hydraulic balancing in the final channel design. In addition, the production accuracy is probably insufficient to accommodate the small channel width corrections for the hydraulic balancing calculated by the algorithm. This chain of uncertainties makes measurements essential.

The pressure loss of the collector loops must be known to estimate the required pump power. In the case of *TABSOLAR*<sup>®</sup> collectors, it is not trivial to guess this as it requires detailed knowledge of pressure loss of every individually shaped Y-bifurcation. As this was unknown and measurements were not available, it was not considered within this work.

#### 4.2.2.4. *Thermal efficiency*

To achieve good thermal efficiency despite the low thermal conductivity, the geometry has to be adapted. The flexible production technology allows for very complex geometries. Using FEM simulations, the author was able to show that very good values



for the so-called collector efficiency factor  $F'$  (compare next section) can be achieved with UHPC absorbers [92].

Unfortunately, in the case of *TABSOLAR*<sup>®</sup> collectors, no prototype could be tested yet. A model to generate the required input parameters for system simulation was needed to assess the accessible heat gain from UHPC collectors.

#### 4.2.2.5. *Thermal capacity*

The specific effective thermal capacity  $c_{eff}$ , modeled as  $c_5$  and equal to the total thermal capacity  $C_{eff}$  referred to the collector area  $A$  in equation (4.1.4), is an obligatory part of the quasi-dynamic measurement procedure of ISO 9806 (2018)[36] and is determined simultaneously with all other collector parameters. ISO 9806 also presents a calculation method to determine the effective heat capacity  $C_{eff}$  of the collector. It is calculated as the sum of the total heat capacities of the collector parts  $m_i \cdot c_i$  with weighting factors  $p_i$  for different parts of the collector according to equation (4.2.1).

$$(4.2.1) \quad C_{eff} = \sum_i p_i \cdot m_i \cdot c_i$$

According to the weighting factors given in ISO 9806, the total thermal capacity of a glazed, insulated and an unglazed, uninsulated UHPC collector variant was calculated with the values given in table 4.2.1. The density of UHPC was determined with Archimedes' principle through immersion experiments and the thermal capacity by means of differential scanning calorimetry<sup>5</sup> during the *TABSOLAR I* project [74]. In this case, the collector area  $A$  was 1.75 m<sup>2</sup>, the thicknesses of the components were 12 mm (absorber), 50 mm (insulation) and 3.2 mm (glazing).

---

<sup>5</sup>[https://en.wikipedia.org/wiki/Differential\\_scanning\\_calorimetry](https://en.wikipedia.org/wiki/Differential_scanning_calorimetry)

TABLE 4.2.1. Calculation of the effective heat capacity of collector variants according to ISO 9806 (2018)[36] for a collector with  $A = 1.75 \text{ m}^2$ .

Component	Weight- ing factor $p$ [-]	Specific heat capac- ity $c_p$ $\left[ \frac{\text{kJ}}{\text{kg K}} \right]$	Den- sity $\rho$ $\left[ \frac{\text{kg}}{\text{m}^3} \right]$	Mass $m$ [kg]	Weighted capacity $C_{eff}$ $\left[ \frac{\text{kJ}}{\text{K}} \right]$	Weighted specific capacity $c_{eff}$ $\left[ \frac{\text{kJ}}{\text{m}^2 \text{K}} \right]$
Absorber	1	0.75	2400	50.4	37.8	21.6
Insulation	0.5	1.45	120	10.5	7.6	4.4
Heat carrier fluid	1	4.186	1000	2.3	9.5	5.4
Glazing	$0.01 \cdot c_1^6$	0.84	2500	14	0.5	0.3
Glazed, insulated UHPC collector				77.2	55.3	31.6
Unglazed UHPC collector				52.7	47.3	27

<sup>6</sup>according to equation (4.1.4), for this calculation 3.5

### 4.3. Modeling UHPC collectors

For the efficient development of solar thermal collectors, good physical models are needed that calculate important characteristics like efficiency curves. These models need to account for the different heat loss mechanisms to identify promising development paths via parameter variation. The most important loss mechanisms are depicted in figure 4.3.1.

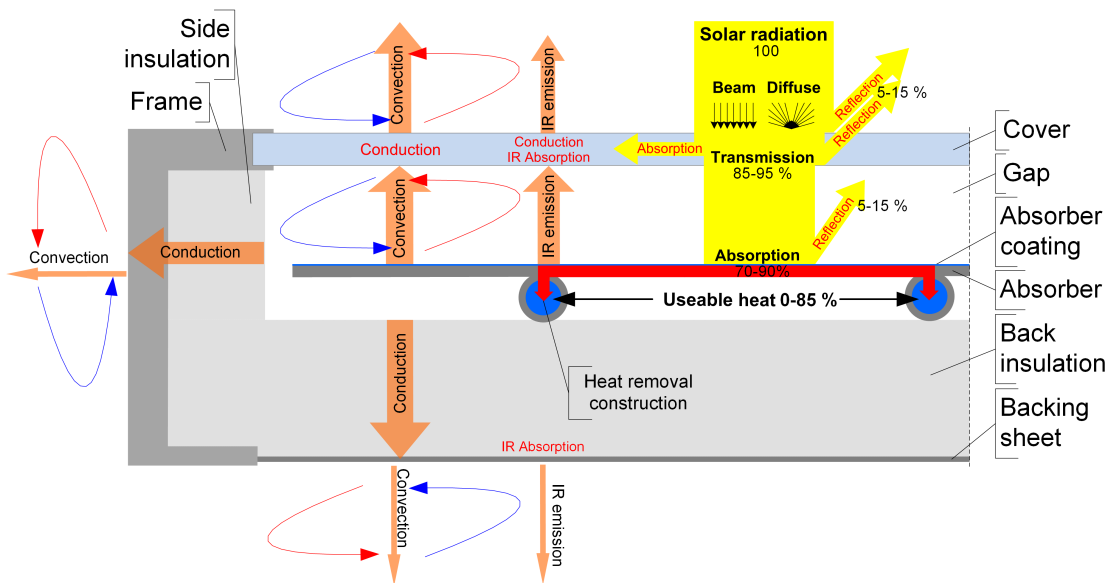


FIGURE 4.3.1. Heat loss mechanisms in a glazed solar thermal collector [52].

The following section gives an overview of existing models and outlines their limitations for absorbers without back insulation. An existing node model that was validated for collectors with back insulation is then compared to a model that uses the finite element method (FEM) for heat transfer for every operating point developed by the author (test “Model comparison”).

Different setups for UHPC façade collectors were tested within the test “Boundary condition”.

If absorbers without frames are directly mounted on the façade, there has to be a certain contact area for the suspension. A method to assess the influence of the margin on the overall efficiency is presented in the “Margin influence” test and applied to UHPC collectors.

### 4.3.1. Overview of existing models and their limits

Duffie and Beckman [40] established well-tested correlations for the thermal efficiency of state-of-the-art collectors with fin-and-tube absorbers. Different models based on Duffie and Beckman were developed. Kolektor 2.2 by Matuska [108] is one of the most widely used models for modeling characteristic curves of solar thermal collectors; it has been validated with much tested data [107].

Lämmle [101] elaborated a similar model that can be used for both PVT collectors and standard covered solar thermal collectors. It is implemented in Modelica<sup>®</sup>, a unified object-oriented language for system modeling. Comparisons with measurement data of a standard covered solar thermal collector and different covered and uncovered PVT collectors showed good agreement with this model. Figure 4.3.2 shows a reduced version of the resistance network to calculate the overall loss coefficient  $U_{loss}$  of Lämmle's model.

To couple the temperature of the absorber with the mean fluid temperature, Duffie and Beckman established the so-called collector efficiency factor  $F'$ . Together with the effective transmittance-absorptance product  $(\tau\alpha)_{eff}$  (calculation according to Dupeyrat et al. [41] with equation (4.3.2)), it builds the collector efficiency at  $\Delta T/G = 0 \text{ K m}^2/\text{W}$ . At this point, the mean fluid temperature equals the ambient temperature, but the absorber temperature is higher.  $F'$  accounts for the heat losses still occurring:

$$(4.3.1) \quad \eta_0 = F' \cdot (\tau\alpha)_{eff}$$

$$(4.3.2) \quad (\tau\alpha)_{eff} = 0.9542 \cdot \tau\alpha + 0.042$$

Duffie and Beckman defined  $F'$  as follows:

*At a particular location,  $F'$  represents the ratio of the actual useful energy gain to the useful gain that would result if the collector absorbing surface had been at the local fluid temperature.*

This can be expressed as:

$$(4.3.3) \quad F' = \frac{\dot{q}_{useful}}{\dot{q}_{(\vartheta_{abs}=\vartheta_{fluid})}}$$

with

$$(4.3.4) \quad \dot{q}_{useful} = G \cdot (\tau\alpha)_{eff} - U_{loss} \cdot (\vartheta_{abs,m} - \vartheta_{amb})$$

and

$$(4.3.5) \quad \dot{q}_{(\vartheta_{abs,m}=\vartheta_{fluid,m})} = G \cdot (\tau\alpha)_{eff} - U_{loss} \cdot (\vartheta_{fluid,m} - \vartheta_{amb}).$$

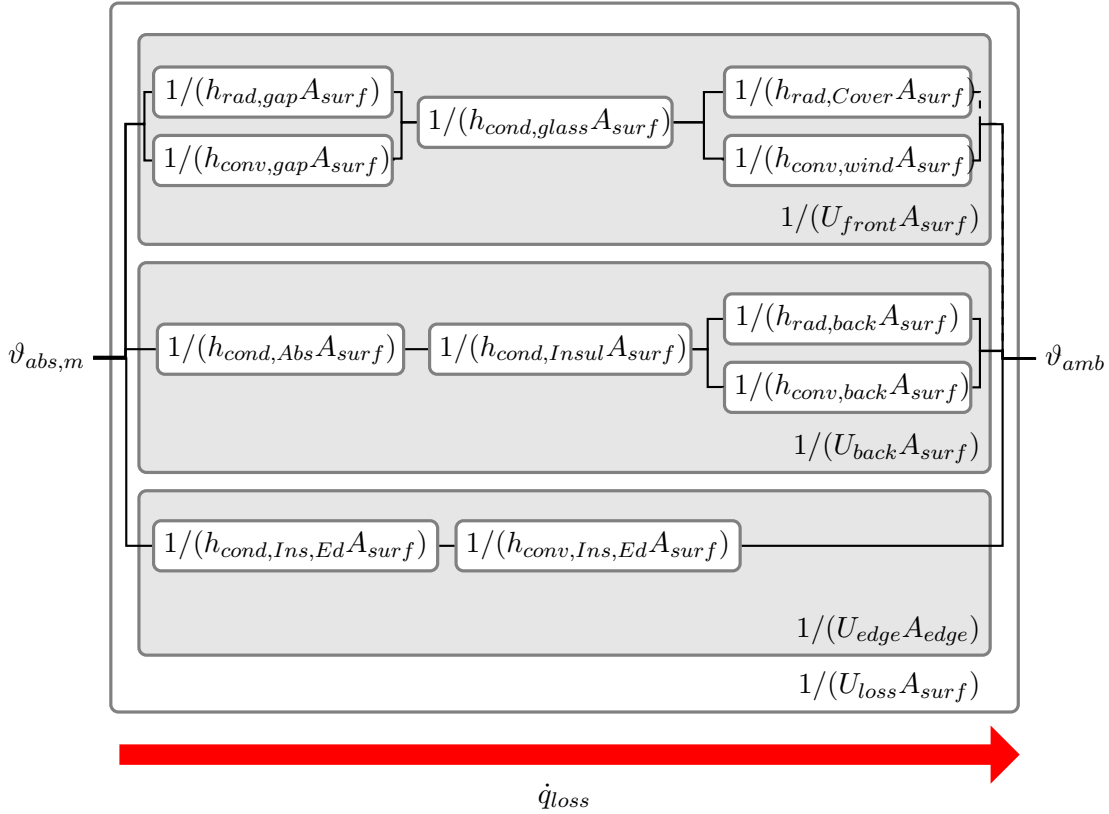


FIGURE 4.3.2. Thermal resistance network of the overall collector heat loss coefficient  $1/U_{loss}$  of a glazed collector. The dashed line between  $h_{rad,Cover}$  and  $\vartheta_{amb}$  indicates the differentiation between sky and ambient temperature. Graphic adapted from Lämmle [101].

The author investigated  $F'$  numerically for glazed collectors with a UHPC absorber. A comparison of the 1-D model of Duffie and Beckmann with the numerical 2-D model showed that the effect of 2-D heat transport leads to a discrepancy between a numerical and an analytical model of about 4% to 8%; a discrepancy that cannot be neglected for massive absorbers made from material with low thermal conductivity like UHPC. Even with thin, low-conductivity absorber plates, the discrepancy between numerical and analytical models are in the range of almost 3%. So it is worthwhile carrying out the numerical analysis of absorbers made from UHPC and from polymers. The model showed that good values for  $F'$  can be achieved with UHPC only by adapting the geometry. For a not yet optimized geometry, an  $F'$  of 96% was calculated [92], which, comparatively, are very good values. The value  $F'$  depends on the overall heat loss

coefficient  $U_{loss}$ . It must therefore be recalculated for every change in collector design that affects  $U_{loss}$ . Lämmle proposes to better use the internal heat transfer coefficient  $U_{abs,fluid}$  which describes the thermal heat transfer coefficient between mean absorber temperature and mean fluid temperature.

It comprises the thermal heat transfer coefficient between absorber and channel  $U_{abs,chan}$  (thermal conductance) and between pipe and fluid  $U_{chan,fluid}$  (convection) connected in series like shown in figure 4.3.3. The collector efficiency factor  $F'$  can be expressed with the internal heat transfer coefficient  $U_{abs,fluid}$  and the overall heat loss  $U_{loss}$ :

$$(4.3.6) \quad F' = \frac{U_{abs,fluid}}{U_{loss} + U_{abs,fluid}}$$

Using FEM simulations, he shows that this value remains constant with variations below 1% for varying irradiation, temperatures or heat loss coefficients as long as the backside and edge boundary condition is set to adiabatic. He concludes that this value can be simulated once for a given absorber geometry using a FEM simulation and then be used for the thermal resistance model (here referred to as node model).

In actual absorbers, there are no adiabatic boundary conditions. Still, a rather good backside and edge insulation allow for this simplification, as the comparisons of the model with the measurement data show [101].

The arising question is whether this simplification is also valid for absorbers made from poor thermal conductors like UHPC. Furthermore, it is to be investigated how to proceed with absorbers without any back insulation. In which range will the error be? And if the error is high, how to calculate heat gain curves for absorbers without back insulation?

#### 4.3.2. FEM modeling approach for wind and infrared-sensitive UHPC collectors

The node model described in the previous paragraph is validated with the internal heat transfer coefficient  $U_{abs,fluid}$  determined via FEM simulation under adiabatic boundary conditions. To test if this simplification is also valid a) for absorbers with low thermal conductivity and back insulation and b) for absorbers without back insulation, the node model is compared with a FEM setup as described in the test “Model comparison”.

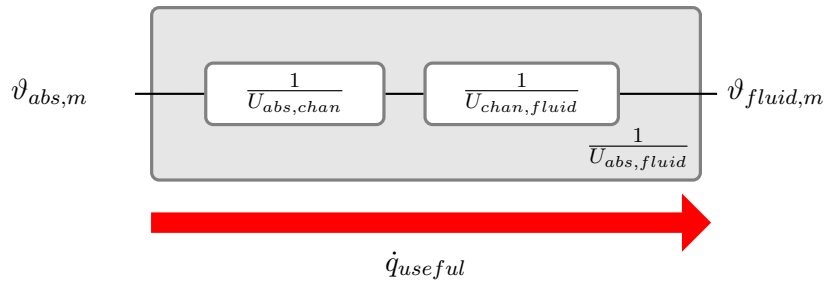
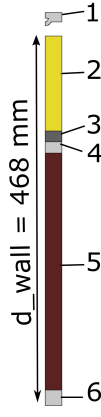


FIGURE 4.3.3. Equivalent thermal resistance network of the internal heat transfer coefficient  $U_{abs,fluid}$ . Graphic adapted from Lämmle [101].

#### 4.3.2.1. Test “Model comparison”

##### Setup

For absorbers without back insulation, the radiative back losses and possible gains become more important. The absorber is assumed to be installed as a rear-ventilated façade and faces backwards toward the insulated building wall. The building wall towards the room has a temperature condition (Dirichlet condition) of  $\vartheta_{room} = 20^\circ\text{C}$  representing a common room temperature inside the building. The node model was extended, as shown in figure 4.3.4 by the yellow colored nodes. The conduction node represents a series of conduction nodes representing the different layers of the assumed building wall. The exact construction of the wall can be found in table 4.3.1. Only the green colored nodes were used as no cover or edge losses were assumed. As two cases were of interest (with and without insulation), the node representing the thermal resistance of the insulation was colored in bright green. The heat output is calculated for the active area (marked red in figure 4.3.11), referring to the total area. As a conservative first guess, it is assumed that the margin does not contribute to the overall heat output at all.



Layer	Thermal conductivity $\lambda$ [W/(m K)]	Thickness $d$ [mm]
1 UHPC absorber	1.87	12
2 Insulation	0.035	120
3 Outer Mortar 1,	1.07	14
4 Outer Mortar 2	1.52	14
5 Brick	0.46	300
6 Inner Mortar	0.87	20

TABLE 4.3.1. Composition of a simulated building wall. It was assumed that an old building wall with a U-value of  $1.13 \text{ W}/(\text{m}^2 \text{ K})$  would be renovated with thermal insulation and a rear-ventilated façade. The U-value of the renovated wall construction is  $0.23 \text{ W}/(\text{m}^2 \text{ K})$ .

To determine  $U_{AbsFluid,fix}$  for the node model, a FEM simulation with the boundary conditions depicted in figure 4.3.5 as proposed by Lämmle [101] was conducted. For symmetry reasons, it is sufficient to simulate only half of the channel and set the cut area to adiabatic boundary conditions. The dimensions of the geometry can be derived from figure 4.3.6. The channels in the center and towards the inlet and outlet differ in cross-section and distance. For simplification, it is assumed that the specific heat output of the whole active area resembles the specific heat output of the cutout of the channel from the center. The backside of the absorber is also set to adiabatic boundary conditions.

$U_{AbsFluid,fix}$  is then fed into the node model as a constant value. The node model calculates the heat output for every operating point. The heat gain curve can then be calculated with linear regression.

The FEM test model calculates all operating points with 2-D heat transfer within the absorber and the wall with boundary conditions, as shown in figure 4.3.7.

The different energy flows indicated in figure 4.3.5 are calculated as described below.

The radiative loss  $\dot{q}_{rad}$  is calculated following equation (4.3.7). For façade collectors, the view factor related to the sky lies somewhere between 0 if the façade does not face the sky at all and 0.5 for a façade with an inclination of  $90^\circ$  that incurs no shading. The sky factor of roofs is close to 1. To identify the possible range, later simulations as part of the test “Boundary condition” were conducted with  $T_{out} = T_{amb}$  and  $T_{out} = T_{sky}$  using Swinbank’s equation (4.3.8) [151].



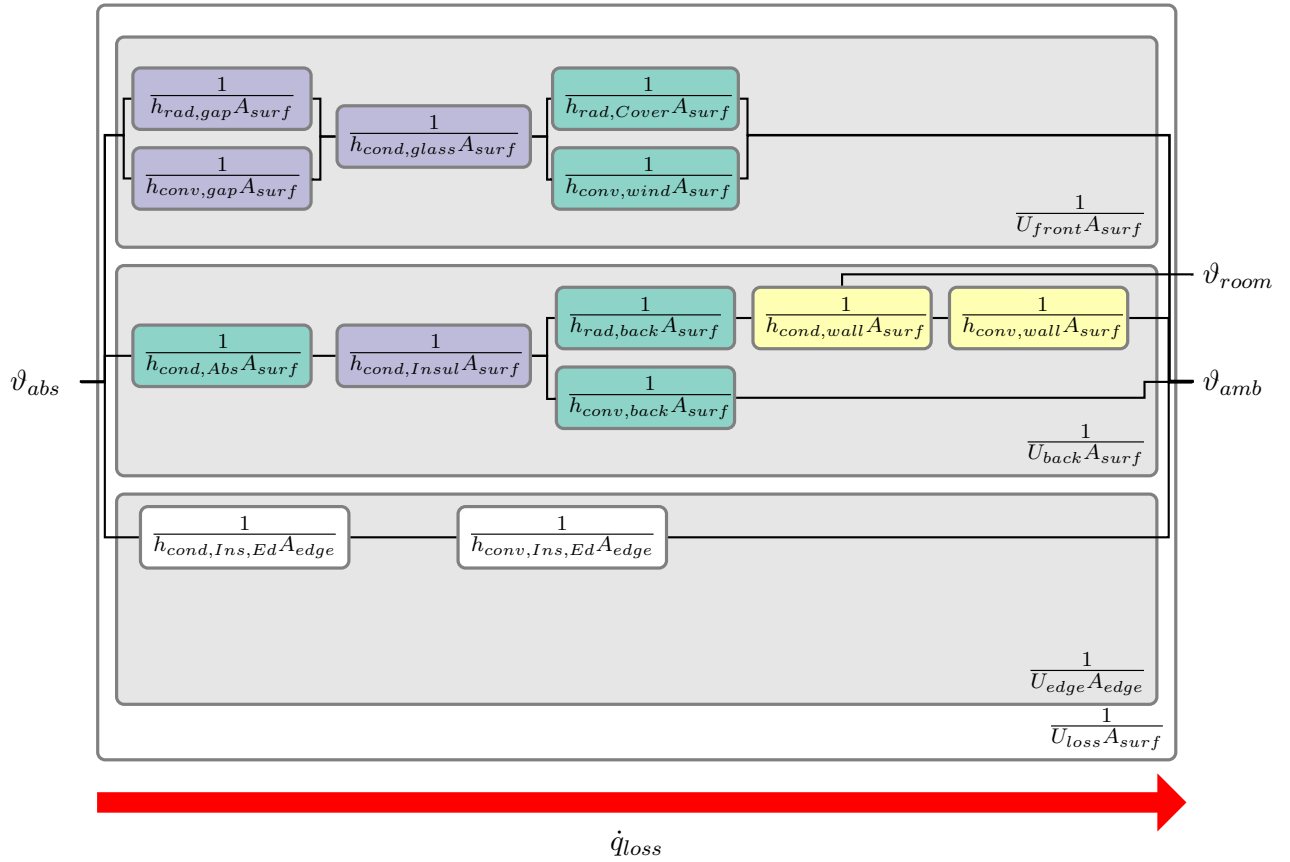


FIGURE 4.3.4. Thermal resistance network of the overall collector heat loss coefficient  $1/U_{loss}$  of a glazed façade collector. Green and yellow colored resistances were used for test “Model comparison”. For glazed collectors within test “Active area vs. channel distance” also the purple colored resistances were used. Graphic adapted from Lämmle [101].

Incident radiation greatly influences the sky view factor (SVF). Chatzipoulka et al. investigated the sky view factor of building façades in urban environments. Depending on the built density, it varied between 0.17 and 0.35 for the locations of Athens, London and Helsinki [28].

For the test “Model comparison”,  $T_{out}$  was set to  $T_{amb}$ .  $T_{abs,m}$  is the mean absorber surface temperature. The emissivity  $\varepsilon$  was assumed to be 0.95 for the gray surface. For the first tests of the spectrally selective absorber, the emissivity was assumed to  $\varepsilon = 0.2$  while further measurements showed that this can be optimized to  $\varepsilon = 0.1$ . This was used in the latest tests as indicated in the captions and the final calculation of the heat gain curve.

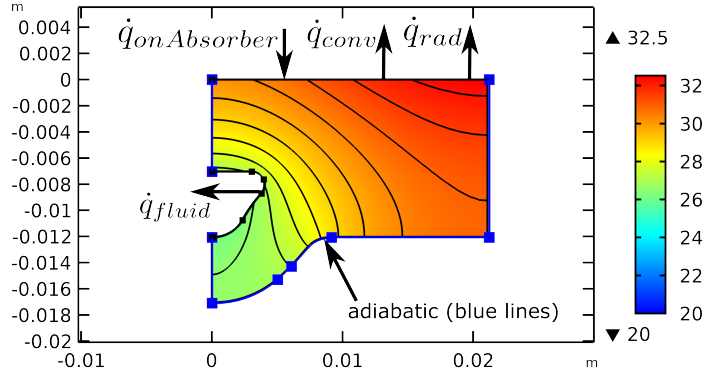


FIGURE 4.3.5. Geometry, boundary conditions, and temperature distribution to determine the heat transfer coefficient  $U_{Abs,Fluid,fix}$  with  $\varepsilon = 0.95$ ,  $\vartheta_{amb} = \vartheta_{fluid,m} = 25^\circ\text{C}$ ,  $G = 750\text{ W/m}^2$  and  $u_{wind} = 3\text{ m/s}$ . Adiabatic boundary conditions are shown in blue.

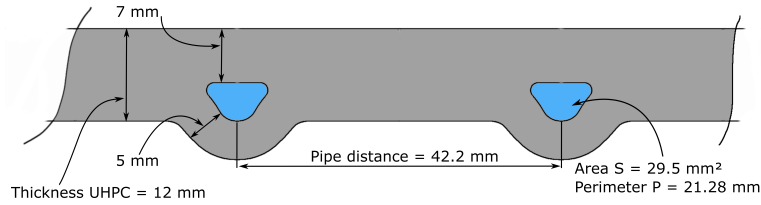


FIGURE 4.3.6. Cross-section of UHPC element, cutout with two channels

$$(4.3.7) \quad \dot{q}_{rad} = \varepsilon \cdot \sigma \cdot (T_{abs,m}^4 - T_{out}^4)$$

$\sigma$  is the Stefan-Boltzmann constant.

$$(4.3.8) \quad T_{sky} = 0.0552 \cdot T_{amb}^{1.5}$$

The convective losses  $\dot{q}_{conv}$  are calculated as follows:

$$(4.3.9) \quad \dot{q}_{conv} = h_{conv} \cdot (\vartheta_{abs} - \vartheta_{amb})$$

Matuska and Zmrhal compared several correlations for the heat transfer coefficient  $h_{conv}$ . McAdams' correlations following equation (4.3.10) [112] showed the best agreement from their numerical model to experimental data [108] and are also used in this

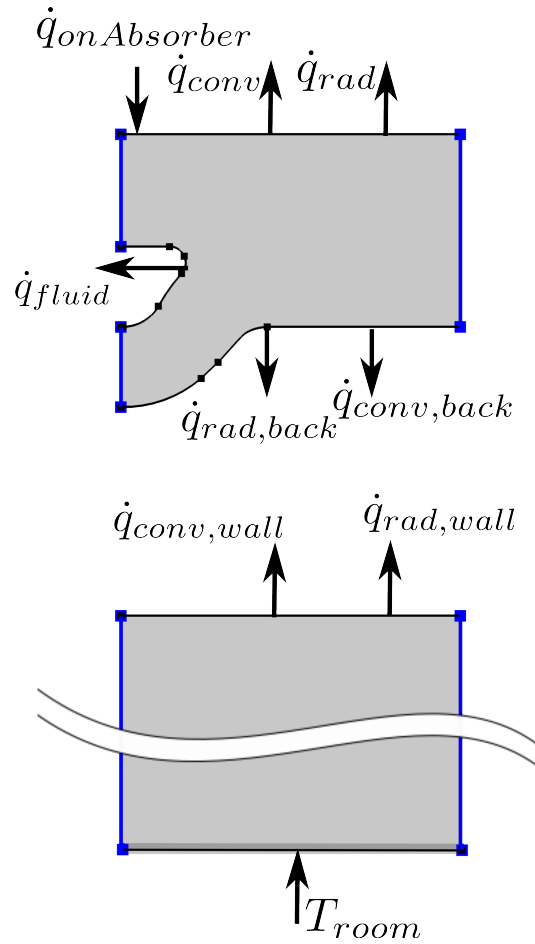


FIGURE 4.3.7. Geometry and boundary conditions for FEM simulation of partition Centre. Adiabatic boundary conditions are shown in blue.

study.

$$(4.3.10) \quad h_{conv} = 5.7 + 3.8 \cdot u_{wind} \quad \text{for} \quad u_{wind} < 5 \text{ m/s}$$

$$(4.3.11) \quad h_{conv} = 6.47 \cdot u_{wind}^{0.78} \quad \text{for} \quad u_{wind} \geq 5 \text{ m/s}$$

The irradiation is calculated with equation (4.3.12) with the transmittance of the glazing of  $\tau = 1$ , as no glazing with transmission loss was calculated. The absorption coefficient  $\alpha$  was set to 0.89 according to measurements of gray colored UHPC and to 0.95 for the spectrally selective absorber. The irradiation was set to  $750 \text{ W/m}^2$  for conditions on the façade.

$$(4.3.12) \quad \dot{q}_{onAbsorber} = G \cdot (\tau\alpha)_{eff}$$

The heat transferred to the fluid is calculated using equation (4.3.13).

$$(4.3.13) \quad \dot{q}_{fluid} = h_{channel,fluid} \cdot (\vartheta_{channel,mean} - \vartheta_{fluid,m})$$

The heat transfer coefficient  $h_{channel,fluid}$  is calculated with the mean Nusselt number  $Nu_m$ , the thermal conductivity  $\lambda$  and the inner diameter  $d_i$  in equation (4.3.14).

$$(4.3.14) \quad h_{channel,fluid} = Nu_m \cdot \lambda / d_i$$

The Nusselt number has different correlations for laminar, transient, and turbulent flow regimes. The absorber was assumed to be tested with the normative mass flow (72 kg/(h m<sup>2</sup>)). With the resulting flow velocity, the Reynolds number (equation (4.3.20)) for the calculated channel was below 2300 (exactly 447), so the flow can be considered laminar. The mean Nusselt number  $Nu_m$  was calculated with equations from the VDI heat atlas. Equation (25) in chapter ‘‘Heat Transfer in Pipe Flow’’ (here: equation (4.3.15)) describes the mean Nusselt number for thermally and hydrodynamically developed flows for all tube lengths with constant heat flux [59]:

$$(4.3.15) \quad Nu_{m,q} = \left\{ Nu_{m,q,1}^3 + 0.6^3 + (Nu_{m,q,2} - 0.6)^3 + Nu_{m,q,3}^3 \right\}^{1/3}$$

$$(4.3.16) \quad Nu_{m,q,1} = 4.364$$

$$(4.3.17) \quad Nu_{m,q,2} = 1.953 \cdot \sqrt[3]{Re \cdot Pr \cdot d_i / l}$$

$$(4.3.18) \quad Nu_{m,q,3} = 0.924 \cdot \sqrt[3]{Pr} \cdot \sqrt{Re} (d_i / l)$$

with Prandtl number  $Pr$ :

$$(4.3.19) \quad Pr = \mu \cdot c_p / \lambda$$

with  $\mu$  = dynamic viscosity,  $c_p$  = specific heat,  $\lambda$  = thermal conductivity

‘‘According to statements from the literature, the Nusselt numbers for heat transfer in turbulent flow in smooth straight channels of non-circular cross-section can also be calculated [...] using the hydraulic diameter of the channel in evaluating  $Nu$ ,  $Re$ , and  $d_i/l$ ’’[59]. Due to missing standard equations for laminar flow in pipes or channels of non-circular cross-section, the Reynolds number and the heat transfer coefficient  $\alpha$  is also calculated with the hydraulic diameter  $d_{hyd}$  for laminar flow. Together with the flow velocity  $w$  and the kinematic viscosity  $\nu$ , it is described by equation (4.3.20).

$$(4.3.20) \quad Re = w \cdot d_{hyd} / \nu \quad \text{with} \quad d_{hyd} = 4 \cdot S / P$$

where  $S$  is the flow cross-sectional area and  $P$  is the whetted perimeter of the channel. The values of  $S$  and  $P$  are indicated in figure 4.3.6.

With these parameters,  $U_{abs,fluid}$  could be determined with equation (4.3.21)

$$(4.3.21) \quad U_{abs,fluid} = \frac{\dot{q}_{useful}}{\vartheta_{abs,m} - \vartheta_{fluid,m}}$$

to  $80 \text{ W}/(\text{m}^2 \text{ K})$  for the given geometry and thermal conductivity  $\lambda = 1.87 \text{ W}/(\text{m K})$  of UHPC.

This value was then fed into the node model. The correlations used for the node model were similar to those described by Lämmle [101]. They are briefly described in the following.

The equations for convection on the front side were the same as for the determination of  $U_{abs,fluid}$  (equation (4.3.10)).

The radiative heat transfer coefficient  $h_{rad}$  was calculated with equation (4.3.22). For the radiation on the backside of the absorber, it was assumed that the absorber only faces the wall and vice-versa.

$$(4.3.22) \quad h_{rad} = \sigma \cdot \frac{(T_1^2 + T_2^2) \cdot (T_1 + T_2)}{\frac{1}{\varepsilon_1} + \frac{1}{\varepsilon_2} - 1}$$

The convective loss on the backside of the absorber and the wall is calculated with the same correlation as for the front (equation (4.3.10)), but the velocity  $u_{wind,back}$  was assumed to be  $u_{wind,front}/2$ . This was assumed in the calculations of convective back losses in the validated model by Lämmle [101].

The heat transfer coefficients for conduction are calculated with the thermal conductivity  $\lambda$  and the thickness  $d$  of the material using equation (4.3.23).

$$(4.3.23) \quad h_{cond} = \frac{\lambda}{d}$$

The FEM model uses almost the same formulæ as the node model. All boundary conditions are indicated in figure 4.3.7. As the wall thickness is  $0.468 \text{ m}$ , it is not fully depicted. Table 4.3.1, left, gives an impression of the dimensions wall-absorber. In the case of the FEM model, the equation for heat conduction is solved for every operating point within the given 2-D geometry.  $T_{abs,m}$  is the mean resulting absorber temperature,  $T_{abs,back}$  the mean absorber back temperature, and  $T_{wall}$  the mean outer wall temperature. So radiation on the front side is calculated using equation (4.3.7), on the backside equation (4.3.24) and the wall using equation (4.3.25). The emissivity  $\varepsilon$  of the wall was assumed to be the same as that of the absorber back  $\varepsilon_{abs,back} = \varepsilon_{wall} = 0.95$ .

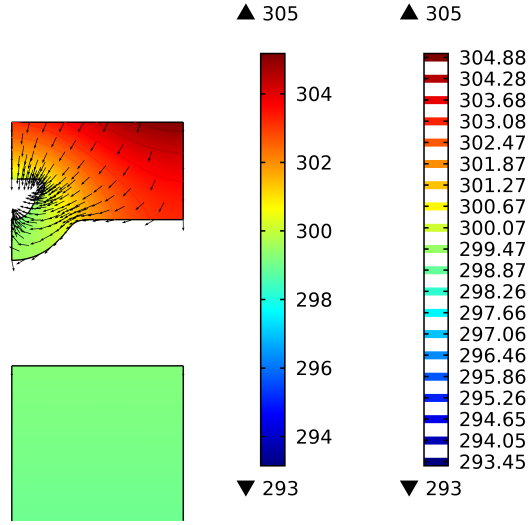


FIGURE 4.3.8. Calculated temperature distribution of FEM simulation in Kelvin for partition Center for  $\varepsilon = 0.95$ ,  $\vartheta_{amb} = \vartheta_{fluid,m} = 25^\circ\text{C}$ ,  $G = 750 \text{ W/m}^2$  and  $u_{wind} = 3 \text{ m/s}$ . Arrows indicate heat flow.

$$(4.3.24) \quad \dot{q}_{rad,back} = \varepsilon \cdot \sigma \cdot (T_{wall}^4 - T_{abs,back}^4)$$

$$(4.3.25) \quad \dot{q}_{rad,wall} = \varepsilon \cdot \sigma \cdot (T_{abs,back}^4 - T_{wall}^4)$$

### Results and conclusions

Figure 4.3.9 shows the resulting heat gain curves generated with the two models (FEM and node model) for wind velocities of  $u_{wind} = 3 \text{ m/s}$ . In the case without insulation, a discrepancy of both can be observed: The heat gain curve calculated with the FEM model is steeper than the one of the node model with constant  $U_{abs,fluid}$ . Both curves intersect at about 5 K difference of  $\vartheta_{fluid,m}$  and  $\vartheta_{amb}$ . Below, the heat output of the FEM model is higher, and above, it is lower than the heat gain curve of the node model. At  $-10 \text{ K}$ , the curve of the FEM model exceeds the curve of the node model by 46 W or 7.6%. At 10 K, the curve of the FEM model is 19 W or 11.1% lower than the curve of the node model for emission  $\varepsilon = 0.95$ . The differences for emission  $\varepsilon = 0.2$  are in the same range. Figure 4.3.8 shows the temperature distribution of the element at

$\vartheta_{amb} = \vartheta_{fluid,m} = 25^\circ\text{C}$  and the resulting vectors for heat flows. As expected, on the backside, they point outside the geometry.

However, if insulation of 0.05 m with thermal conductivity of  $\lambda = 0.035 \text{ W}/(\text{m K})$  is assumed, the differences of 4 W to  $-1 \text{ W}$  in the range of  $-10 \text{ K}$  to  $10 \text{ K}$  are below 1 %.

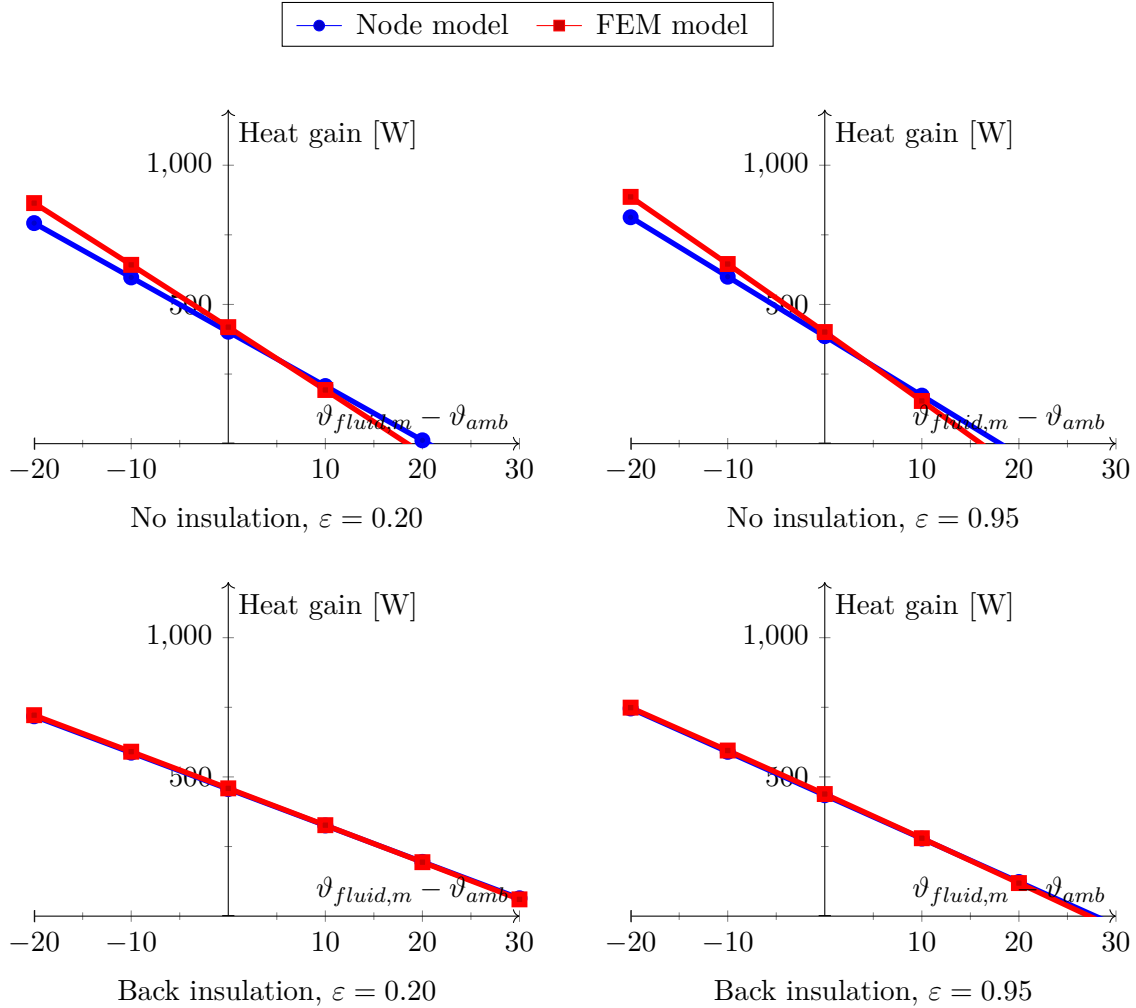


FIGURE 4.3.9. Comparison of heat gain curves simulated with different models for an unglazed UHPC absorber with  $G = 750 \text{ W}/\text{m}^2$ ,  $u_{wind} = 3 \text{ m}/\text{s}$  and radiation towards  $\vartheta_{amb}$ . Right:  $\varepsilon = 0.95$ , left:  $\varepsilon = 0.2$ , above without back insulation, below with back insulation. Heat gain calculated for an aperture area  $= 1.16 \text{ m}^2$  with an active area of  $0.98 \text{ m}^2$ .

The test showed that the simplification of a constant  $U_{abs,fluid}$  calculated with adiabatic boundary conditions at the backside is valid even for absorbers of the considered dimension with low thermal conductivity such as UHPC if they have back insulation

of 5 cm. The error is below 1%. If the absorber has no back insulation, the error is higher depending on the differences of operating fluid temperature  $\vartheta_{fluid,m}$  and ambient temperature  $\vartheta_{amb}$ . The results are similar for an emissivity of  $\varepsilon = 0.2$  and  $\varepsilon = 0.95$ . Since the FEM model is not validated against measurements, it is unclear how well it fits them. Nevertheless, it is expected to be more exact than the node model with a constant  $U_{abs,fluid}$ . The recommendation is, therefore, to use it for the calculation of heat gain curves of absorbers without back insulation.

#### 4.3.2.2. Test “Boundary conditions”

##### Setup

As indicated in section 4.3.2.1, an element on the façade partly faces the environment and partly the sky. So equation (4.3.7) was calculated for radiation against  $T_{amb}$  and  $T_{sky}$ .

Regarding the type of wall construction, two versions were considered. Case 1 is assumed to be an open, rear-ventilated façade. The wind flows through the open gaps between the absorbers, but the wind velocity is half of the velocity in front of the absorber as assumed for the convective back losses. It is assumed that the temperature in the gap between absorber and wall is ambient, and convective losses are calculated accordingly.

In case 2, the gaps between the absorber are assumed to be closed, and the wind velocity on the backside of the absorber to be zero. As no forced convective losses occur, convective losses are far lower but not zero. For detailed knowledge of the occurring convective losses, buoyancy should be calculated. Describing the setup more accurately would be quite complex as it depends a lot on the exact geometry, which is still unknown. Therefore, first approximations were made. As a first simplified guess, the temperature between the absorber and the wall was assumed to be the arithmetic mean of outer wall temperature and the mean backside temperature of the absorber. The wind-dependent heat transfer coefficient would be calculated according to equation (4.3.10) for both cases.

##### Results and conclusion

The influence of the temperature towards radiation losses occurred is almost negligible for the low-emissivity absorber, as shown in figure 4.3.10. The highly emitting absorber ( $\varepsilon = 0.95$ ) proves to be more sensitive to the facing temperature. The heat output is about  $50 \text{ W/m}^2$  to  $60 \text{ W/m}^2$  lower for all temperature differences if emitting



against  $T_{sky}$ . This corresponds to about 11% of the useful heat at  $\vartheta_{amb} = \vartheta_{fluid,m}$  with irradiation of  $750 \text{ W/m}^2$ .

For the described scenario with closed gaps between the absorbers, the heat gain curves are less steep, and higher temperatures can be achieved. If the absorber is operated far below ambient temperature ( $\Delta T > -3 \text{ K}$ ), the resulting heat output is lower.

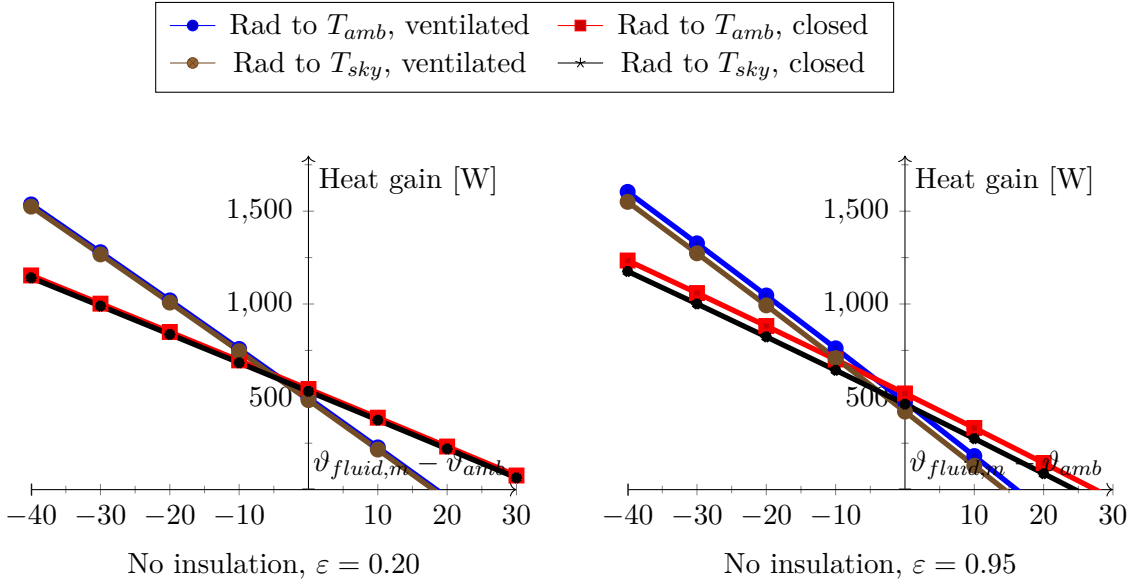


FIGURE 4.3.10. Comparison of heat gain curves simulated with different boundary conditions for an unglazed UHPC absorber with  $G = 750 \text{ W/m}^2$ ,  $u_{wind} = 3 \text{ m/s}$  and  $\vartheta_{amb} = 25 \text{ }^\circ\text{C}$ . Right:  $\varepsilon = 0.95$ , left:  $\varepsilon = 0.2$ , Heat gain calculated for aperture area  $= 1 \text{ m}^2$  without margin effects.

#### 4.3.2.3. Test “Margin influence”

##### Motivation

In the schematic of a common glazed collector in figure 4.3.1, the absorber has no contact with the frame. In reality, the absorber has to be fixed in the casing. In roof collectors, this is often ensured purely by the passage of the fluid connections through the housing. Collector designers minimize the contact areas and possible thermal bridges. The side losses can usually be calculated with sufficient accuracy with a node for side insulation conduction and a node for convective losses outside the frame.

Absorbers without frames have to be somehow fixed in the designated place. Contrary to the very thin absorbers in standard glazed collectors, they have to be stiff enough to withstand weather conditions without protective glazing. Depending on the

material, higher stiffness can lead to higher weight, in which case the suspension has to be designed for this weight. In the case of polymer absorbers, this might not be a problem, as the material is relatively light, and its thermal conductivity is even lower than that of UHPC. But for metal as well as UHPC absorbers, the suspension points can have a significant influence on the heat output. The reasons are: suspensions require channel-free space, so the active area is reduced, and suspensions can lead to significant thermal bridges.

Concerning the first issue, it is interesting to know how much the non-active margin contributes to the overall efficiency as it is still connected to the absorber, yet incoming heat has to travel further to reach the fluid. The second issue raises the question of what the actual goal is. If the absorber functions mainly as a heat exchanger with the environment, it might be good to thermally couple the absorber to the substructure, use this as an additional heat exchange area, and increase heat output. In contrast, if the absorber is also used for direct solar heating and the temperature level is important, it is better to thermally decouple absorber and substructure. The following section describes how the influence of the margins can be investigated.

## Setup

The described FEM model was set up for the margin design of the considered UHPC absorbers to analyze the influence of the margins.

The absorber with the current dimensions was split into four zones: the center area  $A_C$  and two margin areas  $A_{ML}$  and  $A_{MS}$  of different sizes, as shown in figure 4.3.11.  $A_{Agr,Infl}$  is a zone of the center area where the agrafes influence the heat output at high temperature differences, as is explained in the following. Figure 4.3.12 illustrates the model's boundary conditions. They resemble the boundary conditions for the center area very much and differ only in the geometry (channel cross-sections remain the same) and the edge loss  $\dot{q}_{conv,edge}$  which is calculated with the same equations and assumptions as  $\dot{q}_{conv,back}$  (compare equation (4.3.9)).

The margin area can be further split into zones with and without direct coupling to the façade construction. A setup, as shown in figure 4.3.13, was defined for direct coupling. It is based on the geometry shown in figure 4.2.4. The aluminum agrafe is fastened on the absorber with steel screws and thermally insulated as depicted. The agrafe is in contact with the substructure. Curves orthogonally to the depicted 2-D drawing are neglected. In an extreme case, the agrafe and the substructure would act as a frame. Such a setup does not reflect reality and would not be built. Actual contacts of agrafe

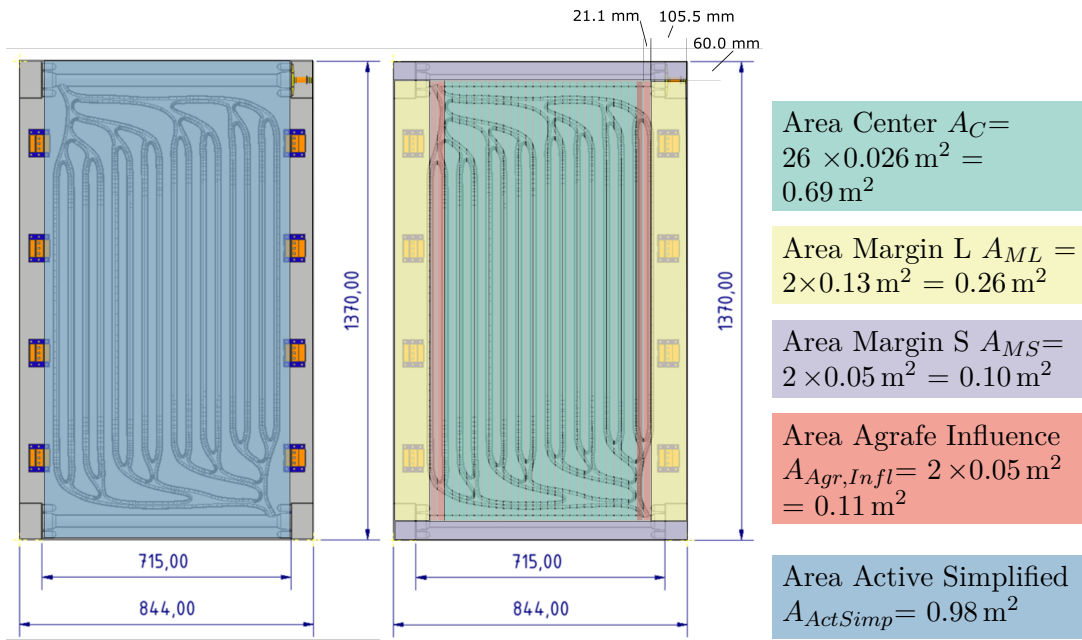


FIGURE 4.3.11. Areas of different efficiencies of UHPC collector, marked in colors.

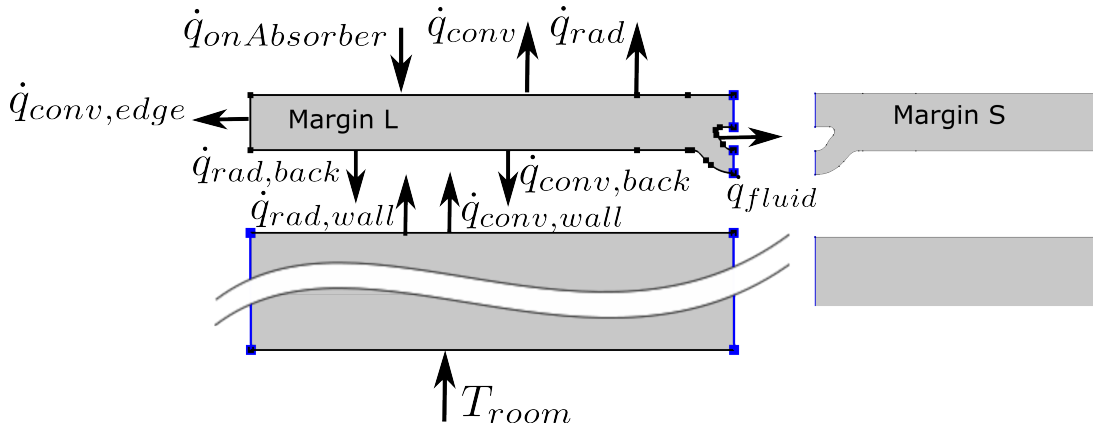


FIGURE 4.3.12. Boundary conditions for FEM calculation of margins L and geometry of margin S.

and substructure would be line contacts rather than whole-area contacts. The assumed cross-section serves as a “worst-case scenario” for thermal bridges. First simulations showed that, in case of high temperature differences, the influence of the agrafe goes beyond the first channel, which is why a center part was added to the geometry.

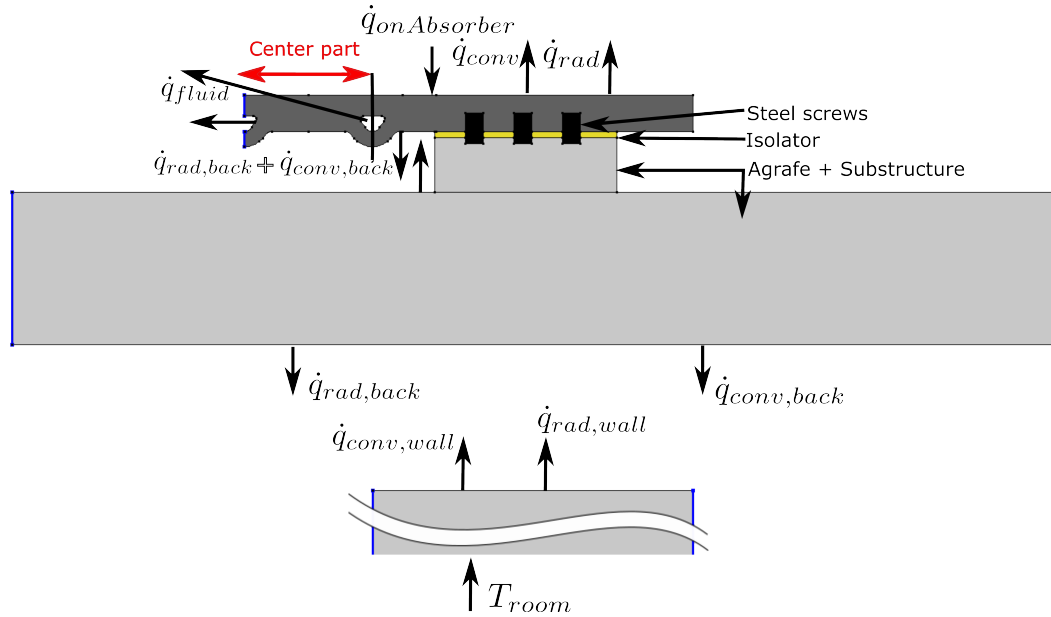


FIGURE 4.3.13. Boundary condition for margins with agrafe and part of the center area.

First, the heat output for all different geometries was calculated. To obtain the heat gain curve of the entire collector, the heat output was then calculated as the area-weighted sum of all heat outputs.

### Results and conclusions

The respective heat gain curves were calculated assuming that each geometry covers a total area of  $1 \text{ m}^2$ . The first calculation of margin L with agrafe was conducted without the center part indicated in figure 4.3.13. The result of the heat output calculation for the different geometries at  $G = 750 \text{ W/m}^2$ ,  $u_{wind} = 3 \text{ m/s}$ , and radiation towards  $\vartheta_{amb} = 25^\circ\text{C}$  can be seen in figure 4.3.14. It shows the significantly lower gain from the margin area due to the distance the heat has to travel from the surface to the channel through the poor thermal conductor UHPC. This indicates the importance of proper design, i. e. small channel distances.

Looking at the heat output of the margin with agrafe, it can be seen that 1) in the shown temperature difference range, the heat gain of the margin with agrafe is always the lowest. It could be assumed that at fluid temperatures below ambient temperature, the agrafe acts as an additional heat exchanger, and the performance is higher than that of a margin without agrafe. However, this is not the case. Figure 4.3.15 shows the

temperature distribution and the normalized heat flux of the margin with agrafe at a temperature difference of  $-10$  K for the simulated heat gain curve shown in figure 4.3.14, left.

It also shows that the incoming heat flux is dissipated via the screws. If there is no heat income from the sun, it is expected that the agrafe contributes positively to the heat transferred to the fluid. 2) Already at about a fluid temperature  $\vartheta_{fluid,m}$  that is only 8 K higher than ambient temperature  $\vartheta_{amb}$  the heat output is zero, so the incoming solar heat and the heat from the incoming fluid is dissipated through the screws to the substructure and then further to the ambient. This means that the incoming fluid cools down instead of heating up. As soon as this happens, the margin also influences part of the center area. A pure area-weighted sum of all heat outputs would be wrong for higher temperature differences. A new simulation of the margin, including parts of the center, is needed to identify how far the influence of the agrafes reaches.

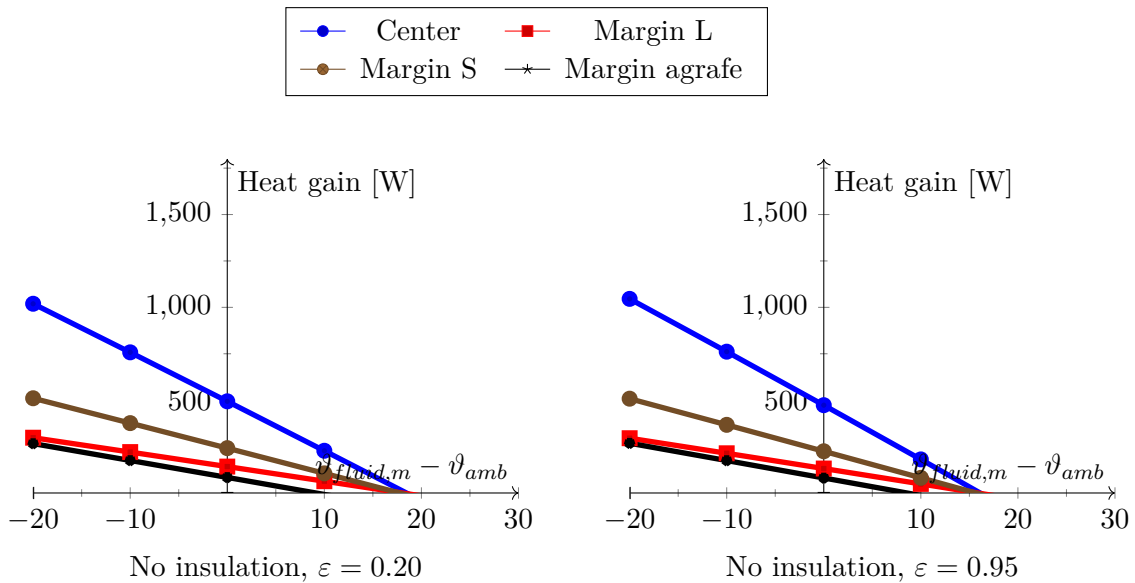


FIGURE 4.3.14. Comparison of heat gain curves simulated with different geometries for an unglazed UHPC absorber with  $G = 750 \text{ W/m}^2$ ,  $u_{wind} = 3 \text{ m/s}$  and radiation towards  $\vartheta_{amb} = 25^\circ\text{C}$ . Right:  $\varepsilon = 0.95$ , left:  $\varepsilon = 0.2$ , heat gain calculated for aperture area  $A_{ap} = 1 \text{ m}^2$ .

For the new simulation, a center part, as indicated in figure 4.3.13 was included in the geometry of margin L with agrafe. To test the influence of the agrafes at higher operating temperatures, simulations were also conducted for an insulated collector with an emissivity of  $\varepsilon = 0.2$  and an uninsulated collector with an emissivity of  $\varepsilon = 0.95$ .

The heat output for the uninsulated absorber was plotted at wind velocities of  $u_{wind} = 3 \text{ m/s}$ , figure 4.3.16, right. Compared to figure 4.3.14 the specific heat of the

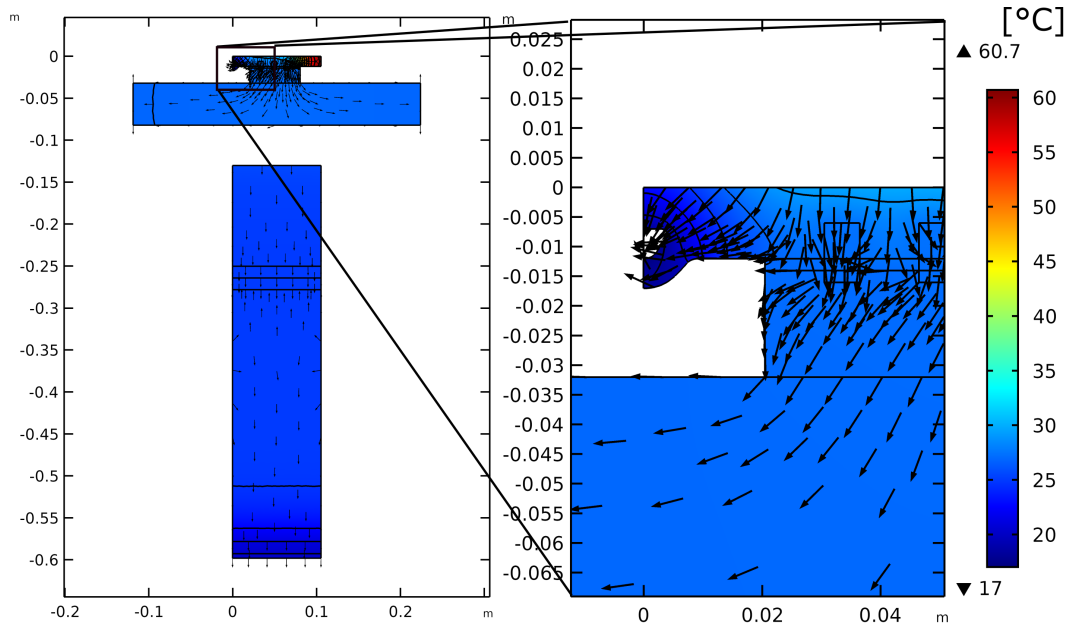


FIGURE 4.3.15. Temperature distribution for margin with agrafe (total and excerpt) calculated with  $\varepsilon = 0.2$ ,  $\vartheta_{amb} = 25^\circ\text{C}$ ,  $\vartheta_{fluid,m} = 15^\circ\text{C}$ ,  $G = 750\text{ W/m}^2$  and  $u_{wind} = 3\text{ m/s}$ . Arrows indicate normed total heat flux.

“margin agrafe” is higher as it includes parts of the center with higher efficiency. It intersects the x-axis in the same temperature difference range as the other curves.

The heat output for the insulated absorber was plotted at wind velocities of  $u_{wind} = 0\text{ m/s}$ , figure 4.3.16, left. A significantly higher impact of the agrafes can be observed. The heat gain curve of “margin agrafe” intersects the x-axis already at about  $\Delta T = 47\text{ K}$ . Figure 4.3.17 shows the temperature distribution together with arrows indicating the heat flux for the insulated margin with agrafe at two different fluid temperatures. The red line in the picture of  $\vartheta_{amb} = 85^\circ\text{C}$  indicates the point where the incoming heat separates. This red line is left of the center of the two margin channels indicated with the dash-dotted line. Right of that line, no incoming heat can be used as it is all dissipated. Only the incoming heat left of the red line, which includes an area smaller than half the channel distance, can still be used. In the graph of  $\vartheta_{amb} = 95^\circ\text{C}$ , all heat is dissipated. This means that up to a temperature difference of about  $\vartheta_{amb} = 85^\circ\text{C}$ , the area-weighted sum of all geometries is correct within the framework of the assumptions. At higher temperatures, the influence of the agrafe and the other margins grows more into the center area, and the resulting heat gain curve would be slightly lower. As the heat output at these temperature differences is very low, it was neglected in the final heat gain curve.

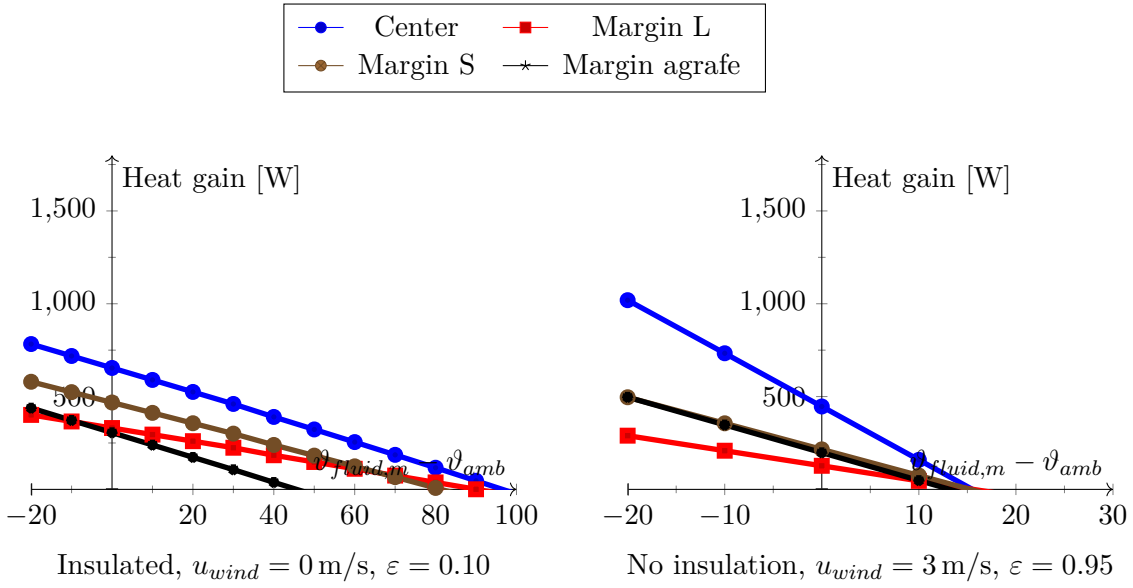


FIGURE 4.3.16. Comparison of heat gain curves simulated with different geometries for an unglazed UHPC absorber with  $G = 750 \text{ W/m}^2$  and sky view factor  $\text{SVF} = 0.5$ . Right: Insulated,  $\varepsilon = 0.1$ ,  $u_{wind} = 0 \text{ m/s}$ , left: uninsulated,  $u_{wind} = 3 \text{ m/s}$ ,  $\varepsilon = 0.95$ , heat gain calculated for aperture area  $= 1 \text{ m}^2$ .

A theoretical heat output curve was plotted in figure 4.3.18 to illustrate how significant the losses at the margins are. The uppermost line would indicate the heat output of the element if the whole area had the efficiency of the center area. The next line below would indicate the heat output of the element if it had neither a margin L nor any agrafes but margin S with  $A_{MS}$ . Assuming that the element did not have agrafes, the line below would indicate the result for the whole area. Assuming the worst case that agrafes were all along margin L, the lower line is the result.

This graphic illustrates two findings: The loss at margin L is high. If this margin area could be reduced, the heat output per area could be significantly increased. The larger the elements are, the lower the impact is and vice versa. Second, the influence of the agrafes on the margin is rather low for low temperature differences. Even if the effect is shown excessively – in reality, the agrafes cover only a small percentage of margin L – the difference to the margin without agrafes is not very high: in the case of  $\varepsilon = 0.95$  and  $u_{wind} = 3 \text{ m/s}$ , the difference is hardly visible.

The low impact of the agrafe compared to the margin without agrafe is caused not only by the low achievable temperatures but also by the low thermal conductivity of UHPC. For metal absorbers, this effect could be higher. The higher the temperature difference, the higher the influence of the agrafes. In the case of the insulated collector

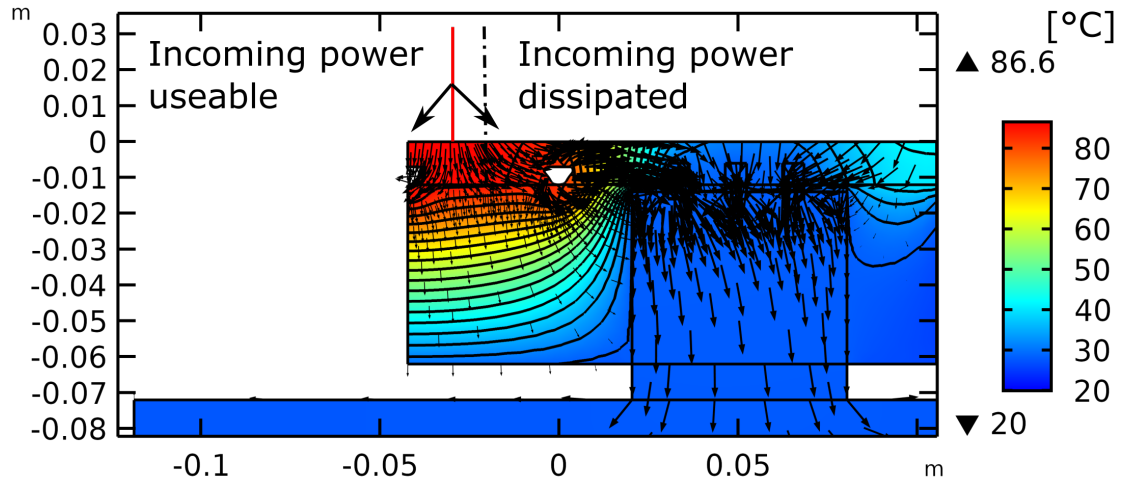
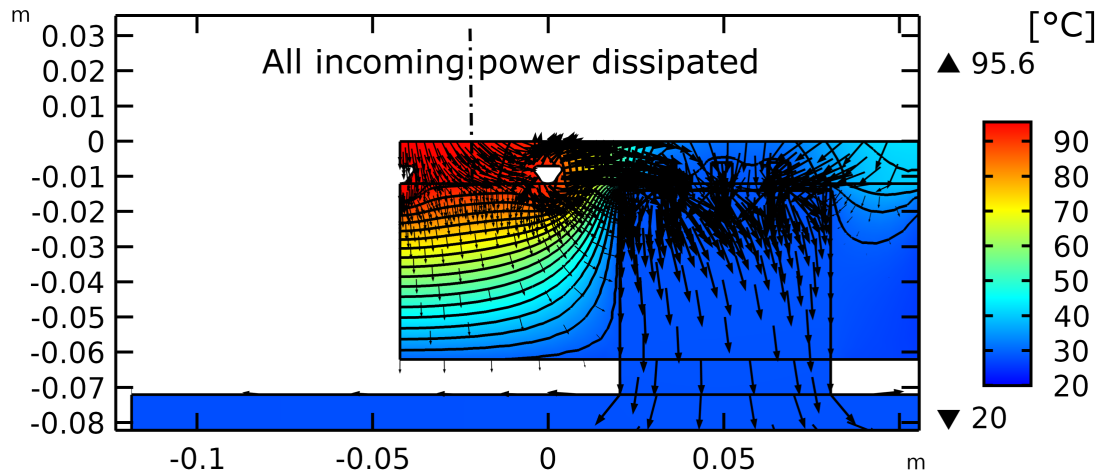
(A)  $\vartheta_{fluid,m} = 85^\circ\text{C}$ (B)  $\vartheta_{fluid,m} = 95^\circ\text{C}$ 

FIGURE 4.3.17. Temperature distribution for insulated margin with agrafe. The unit of temperature scale is  $^\circ\text{C}$ . It is calculated with radiation toward  $\vartheta_{amb}$ , ventilated,  $\vartheta_{amb} = 25^\circ\text{C}$ ,  $\varepsilon = 0.1$ ,  $u_{wind} = 0\text{ m/s}$ ,  $G = 750\text{ W/m}^2$ . Arrows indicate heat flow and are sized proportionally to the heat flux.

with  $\varepsilon = 0.10$  at  $u_{wind} = 0\text{ m/s}$ , the heat output at 50 K temperature difference could be 37% higher (of the resulting heat gain with all losses, 313 W instead of 229 W) if no losses would occur through the agrafes. Also, for the glazed, insulated UHPC collectors, the effect is expected to be higher due to the higher occurring temperatures.



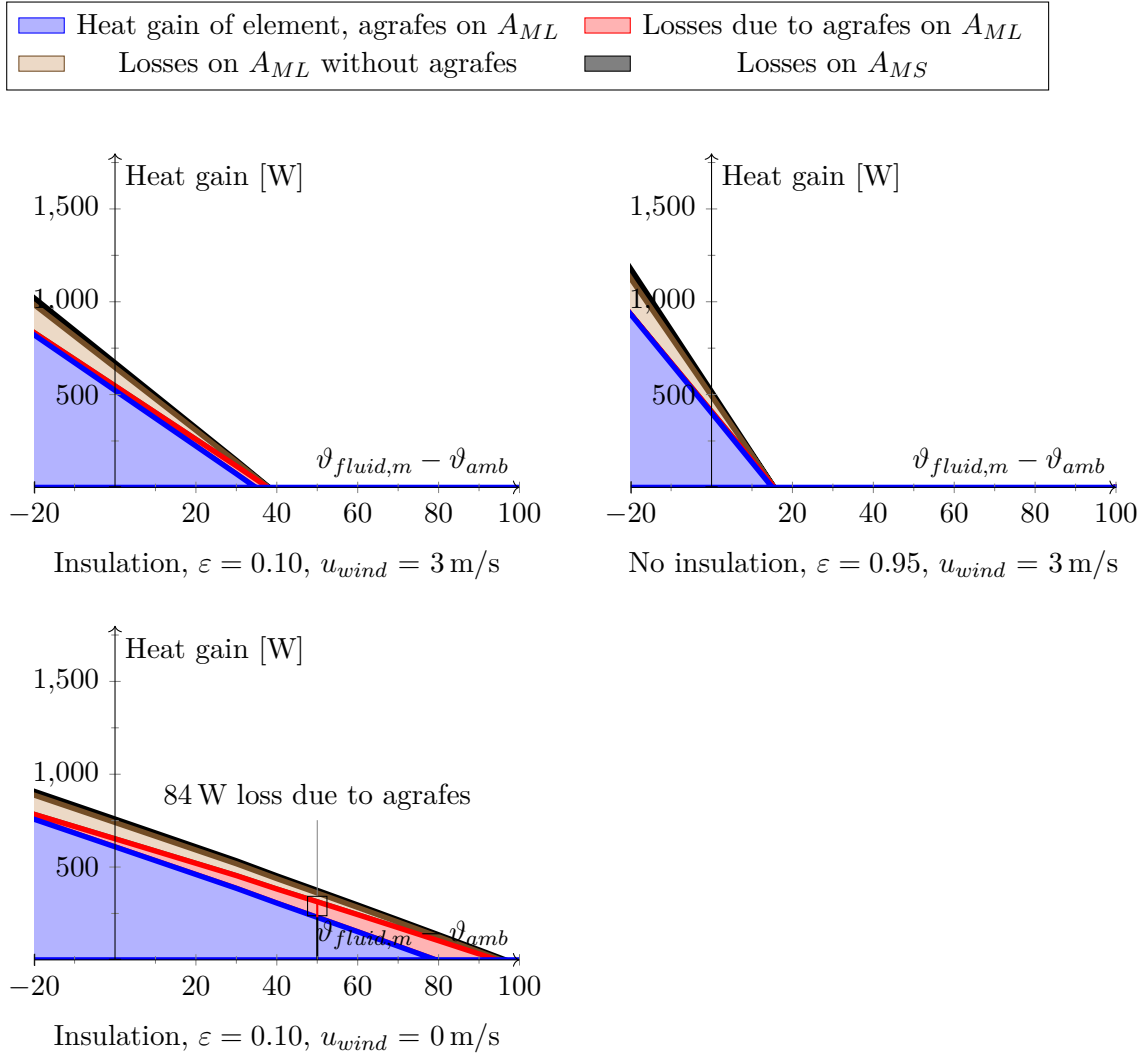


FIGURE 4.3.18. Influence of different margins on the total heat output of an unglazed UHPC absorber with an area of  $A = 1.16 \text{ m}^2$ . The uppermost line would be the heat gain curve if the element had no margins. Heat output calculated for  $G = 750 \text{ W/m}^2$  and sky view factor  $SVF = 0.5$ .

#### 4.3.2.4. Results of heat gain curve simulation

For the calculation of the necessary input parameters for the mathematical description of the efficiency following equation (4.1.2), a set of operational points were simulated with: wind velocities of 0 m/s, 1.5 m/s, and 3 m/s, irradiances of 500 W, 750 W, and 1000 W, fluid temperatures from  $-15^\circ\text{C}$  to  $115^\circ\text{C}$  in steps of 10 K at an ambient temperature of  $25^\circ\text{C}$ .

These points were calculated for all types of areas, and the heat output of the total area was calculated as the area-weighted sum of all heat outputs. With regression and substitution as in equation (4.3.26), the necessary parameter  $b_1$ ,  $b_2$  and  $b_u$  for equation (4.1.2) were calculated. As the simulation does not calculate with a solar spectrum, no correction for infra-red radiation has to be made, and  $G''$  in equation (4.1.2) is  $G$ .

$$(4.3.26) \quad \eta = p_1 \cdot x_1 - p_2 \cdot x_2 - p_3 \cdot x_3 + p_4 \cdot x_4 \text{ with}$$

$$(4.3.27) \quad p_1 = \eta_0 \rightarrow x_1 = 1$$

$$(4.3.28) \quad p_2 = \eta_0 \cdot b_u \rightarrow x_2 = u_{wind}$$

$$(4.3.29) \quad p_3 = b_1 \rightarrow x_3 = \Delta T / G$$

$$(4.3.30) \quad p_4 = b_2 \rightarrow x_4 = u_{wind} \cdot \Delta T / G$$

For further simulation it was assumed that the agrafes influence the heat along their length plus one times their length at each side. This corresponds to 33 % of the length of Margin L, which probably still overestimates the influence of the agrafes. By comparing of coefficients, the identified parameters  $\eta_0$ ,  $b_1$ ,  $b_2$ , and  $b_u$  were transformed to  $\eta_0$ ,  $c_1$ ,  $c_2$ ,  $c_3$ ,  $c_4$ , and  $c_6$  to fit equation (4.1.4). The capacity factor  $c_5$  was calculated as described in table 4.2.1. The collector-specific constant  $b_0$  was assumed to be similar to the uncovered, commercially available collector “Solardach AS” by Energie solaire SA [144]. The wind correction factor  $wcf$  was assumed to be 0.5 if not stated otherwise. As a technical reference, the commercially available, unglazed stainless steel collector “Solardach AS” is given as a reference. The parameters of the datasheet [144] were transferred to the definition of equation (4.1.4) with the described procedure of coefficient comparison. The capacity term  $c_5$  was calculated as described in table 4.2.1 with the masses given in table A.12. The “Solardach AS” was chosen as a technical reference as many of the well-integrated solar thermal collector examples were done with this collector (compare also figure 2.2.1 (A)). The collector has a spectrally selective pillow absorber with almost no margin. It has a corrugated plastic back sheet and an aluminum frame. These design parameters lead to a very high value for  $\eta_0$ . Table 4.3.2 lists the data used for further simulations.

TABLE 4.3.2. Input data for collector model in Modelica according to DIN EN ISO 9806 (2018)[36]. Col1 and Col2 were simulated and prepared for a collector with an aperture area of  $A = 1.16 \text{ m}^2$ . The reference steel collector (ColRef) has an aperture area of  $A = 2.03 \text{ m}^2$

Parameter	Unit	Gray NoInsu (Col1)	Spec- Sel Insu (Col2)	Solar- dach AS (ColRef)
$\eta_0$	[-]	0.6	0.77	0.95
$c_1$	[W/(m <sup>2</sup> K)]	17.61	6.65	9
$c_2$	[W/(m <sup>2</sup> K <sup>2</sup> )]	0	0	0
$c_3$	[J/(m <sup>3</sup> K)]	3.07	2.3	3.77
$c_4$	[-]	0	0	0.05
$c_5$	[J/(m <sup>2</sup> K)]	27000	31600	17900
$c_6$	[s/m]	0.031	0.04	0.01
$c_7$	[W/(m <sup>2</sup> K <sup>4</sup> )]	0	0	0.001
$c_8$	[W/(m <sup>2</sup> K <sup>4</sup> )]	0	0	0
$b_0$	[-]	0.018	0.018	0.018
$K_{\theta,d}$	[-]	0.95	0.95	0.95
$wcr$	[-]	0.5	0.5	0.5

### 4.3.3. Glazed UHPC collectors

#### 4.3.3.1. Test “Active area vs. channel distance”

##### Motivation

The production technology, as shown in figure 4.2.6, is, in principle, applicable to a wide variety of module sizes. Nevertheless, every single channel design needs its own mold. To save costs, it might be interesting to use a specific channel design for different module sizes by increasing the non-active area, the margins. In the case of FracTherm<sup>®</sup>

design, the sizing is also a question of channel distance: the algorithm bifurcates symmetrically and produces 2, 4, 8 or 16 ... channels in the center part. So, with a certain range of module widths, there will always be 16 channels. If, within this range, the possible active area – the activatable area – is fully used and the module size increases, the channel distance increases. This influences the heat transfer coefficient  $U_{abs,fluid}$ . A decrease in  $U_{abs,fluid}$  also lowers the thermal efficiency.

The heat gain curves of the differently structured modules can be compared to compare the effect of a lower  $U_{abs,fluid}$  and a smaller active area. To assess the collector quality, the criterion for funding, as explained in section 4.1.3, can also be applied and compared. Funding in Germany is only available for glazed collectors. So, for this test, only glazed UHPC collectors were considered. As collectors with non-black or dark blue absorber surfaces could increase the architectural variety, the focus was on non-selective absorbers with Low-E glazing. In addition, non-selective absorbers save the costs for spectrally selective coating. If these collectors do not reach the funding limit, this commercial advantage might be far lower or disappear.

### Setup

For a total module area of  $1.75 \text{ m}^2$  and the golden ratio the possible active area was determined according to the production boundaries which include margins to fasten the agrafes as well as space for hydraulic connectors. In figure 4.3.19 this is represented by active area A, which, in this case, is  $1.47 \text{ m}^2$  with a width of 871 mm. With 16 center channels a channel distance of 54.4 mm can be derived.

In a second step, assuming a minimal producible channel distance of 40 mm, the width of the active area was determined to be 640 mm, leading to a size of  $1.12 \text{ m}^2$ . This is represented by active area B in figure 4.3.19.

Within this test, the margins were considered passive. However, this is not true as we have seen in the previous test: the margins contribute positively to the overall heat gain, while, at higher temperatures, the influence of the agrafes also increases and can contribute negatively. With well-insulating fastening, their influence can be minimized, and the overall contribution of the margins would probably be positive. So assuming the margins as passive is a conservative guess for the total heat gain.

Different glazed collectors were modeled with the previously described node model to compare heat gain curves of the differently structured modules. As all glazed collectors were insulated, this is valid according to the test “model comparison”. The model depicted in figure 4.3.4 with yellow, green and purple colored resistances was used.

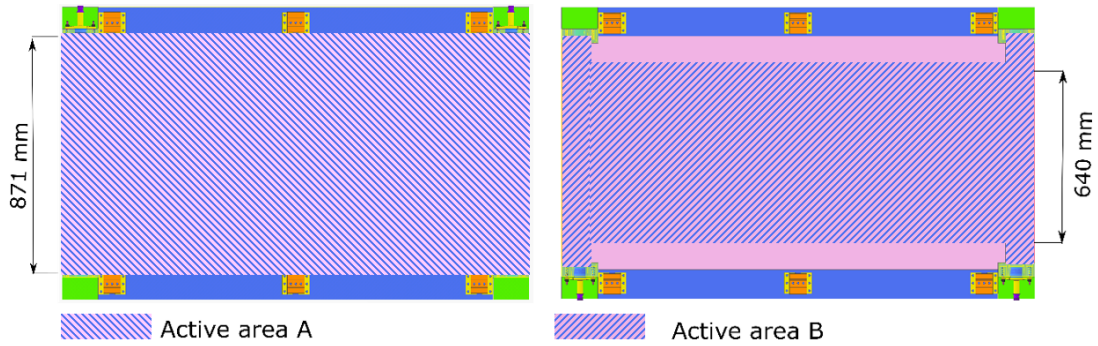


FIGURE 4.3.19. Schematic of different active areas within a UHPC collector of  $1.75 \text{ m}^2$ .

The heat transfer coefficient  $U_{abs,fluid}$  was determined for different channel distances with irradiances between  $500 \text{ W/m}^2$  and  $100 \text{ W/m}^2$ , two values for  $(\tau\alpha)_{eff}$  (0.71 and 0.89), fluid temperatures in the range between  $-15 \text{ }^\circ\text{C}$  to  $175 \text{ }^\circ\text{C}$ , and different values for  $U_{loss}$ . Almost all parameters had a negligible influence; only  $U_{loss}$  had an influence of up to 5% for large channel distances. The results are shown in figure 4.3.20.

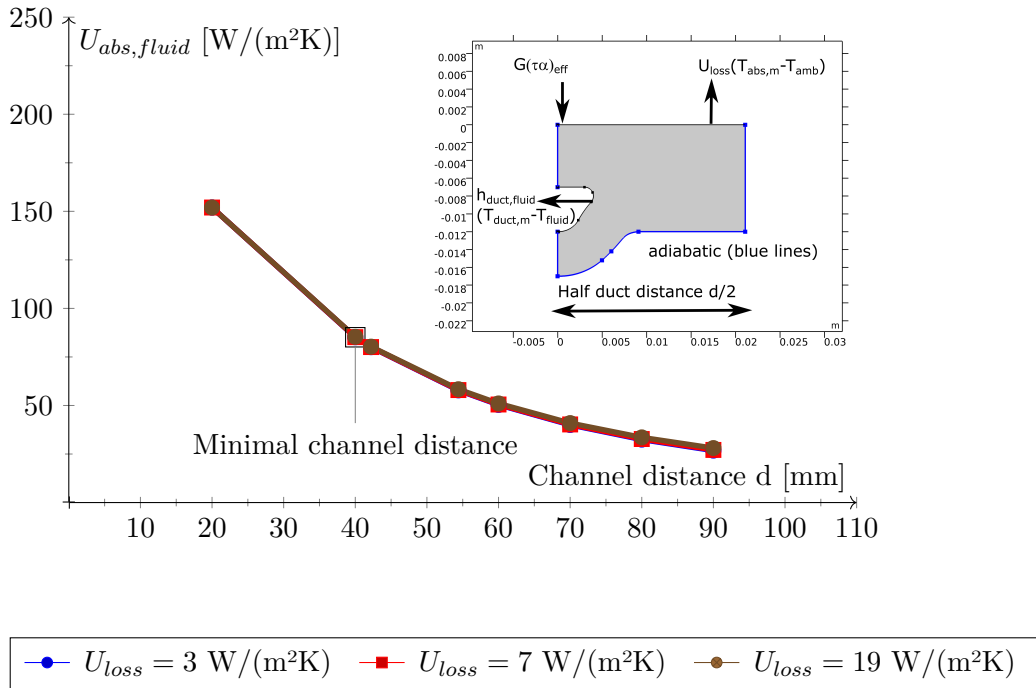


FIGURE 4.3.20.  $U_{abs,fluid}$  depending on the distance from center channels (center to center) for different  $U_{loss}$  calculated with FEM at  $\vartheta_{amb} = 25 \text{ }^\circ\text{C}$ .

The losses due to natural convection between absorber and glazing  $h_{conv,gap}$  is described with the Nusselt-Number  $Nu_L$ , the thermal conductivity of still gas for mean temperature with  $\lambda_{gas}$  and the characteristic dimension of the layer, the distance between glazing and absorber with  $L_{abs,glass}$  (3 cm for the simulation) in equation (4.3.31)

$$(4.3.31) \quad h_{conv,gap} = (Nu_L \cdot \lambda_{gas}) / L_{abs,glass}$$

Different empirical equations for natural convection in gas enclosures are summarized by Matuska [107]. Most of them are only valid for a specific range of tilt angles. Furthermore, the convection depends on the aspect ratio of the gap.

For the UHPC collector façade, the aspect ratio of the gap is unknown as frames horizontally separating the individual modules from each other are not foreseen.

Following ISO 9806 (2018) [36] collectors should be tested as provided by the manufacturer. So, façade collectors should be tested with a tilt angle  $\theta_t$  of 90°.

Testing data of the UHPC collectors or other façade collectors was unavailable and could not be compared to the different correlations to identify the best choice.

As the correlation of Hollands [79] (equation (4.3.33)), used by Lämmle [101] for the validation of a standard collector, is only valid up to a tilt angle of 60°, the Randall correlation [137] (equation (4.3.32)), valid in the occurring range of Rayleigh numbers from  $2.8 \cdot 10^3 < Ra < 2.2 \cdot 10^5$  for tilt angles between 45° and 90°, was compared to the correlation of Hollands at 60°.

This was done by calculating the heat gain curves for a glazed absorber with the two different correlations as shown in figure 4.3.21. The Randall correlation calculates lower values for the convective losses (higher heat gain curve), so it may underestimate the losses.

Even though the correlation of Hollands is not valid above 60°, they were anyway tested with at 80° (higher values for  $\theta_t$  produced errors).

The resulting heat gain curve lay between the heat gain curves calculated with the Randall correlation at 60° and 90°. But the convective losses were calculated with the correlation of Hollands at 80° to attain a conservative guess.

$$(4.3.32) \quad Nu_L = 0.118 \cdot (Ra \cdot \cos^2(\theta_t - 45))^{0.29}$$

$$(4.3.33) \quad Nu_L = 1 + 1.44 \cdot \left[ 1 - \frac{1708}{Ra \cdot \cos(\theta_t)} \right] \cdot \left( 1 - \frac{(\sin(1.8 \cdot \theta_t))^{1.6} \cdot 1708}{Ra \cdot \cos(\theta_t)} \right) + \left[ \left( \frac{Ra \cdot \cos(\theta_t)}{5830} \right)^{\frac{1}{3}} - 1 \right]$$

The heat transfer coefficients for glazing and insulation conductivity  $h_{cond,glass}$  and  $h_{cond,insul}$  were calculated according to equation (4.3.23) with thicknesses of 3.2 mm (glazing) and 50 mm (insulation) and conductivities of 1 W/(m K) (glazing) and 0.035 W/(m K) (insulation). The heat transfer coefficients for radiation between absorber and glazing  $h_{rad,gap}$  were calculated according to equation (4.3.22). Different types of glazing were analyzed. Their properties were measured at Fraunhofer ISE in the context of the project “PVTgen2” dealing with the development and pilot production of a covered PVT collector of the second generation with improved thermal performance [100]. The results are listed in table 4.3.3.

TABLE 4.3.3. Technical data of simulated glazing

Glazing	Transparency $\tau_{AM1.5}$	Emissivity $\varepsilon(100^\circ\text{C})$
K-GLASS	0.78	0.14
EuroWhite	0.862	0.186
ISE Low-E	0.79	0.1
AR Glas	0.94	0.84

## Results

In figure 4.3.21 (right) compares the heat gain curves of four collectors with an area of 1.75 m<sup>2</sup>. The “Center” curves refer to a hypothetical collector without margins. It can be seen that by increasing the channel distance from 40 mm to 54.4 mm with the resulting values for  $U_{abs,fluid}$  decreases the heat outcome only by around 11 W at irradiation of 750 W/m<sup>2</sup>.

Comparing the heat gain curves of the different active areas shows that the effect of the larger area clearly predominates the effect of the lower  $U_{abs,fluid}$ .

For better visualization and to evaluate the criterion for funding,  $Q_{coll,MAP}$  based on the annual gross collector output calculated according to equation (4.1.7) was determined with the tool ScenoCalc V4.06. The first three columns in figure 4.3.22 show  $Q_{coll,MAP}$  for hypothetical collectors without margins with different glazings. The commercially available K GLASS together with a gray-colored absorber does not achieve the criterion for funding of 525 kWh/m<sup>2</sup>, the same absorber with an improved emissivity based on

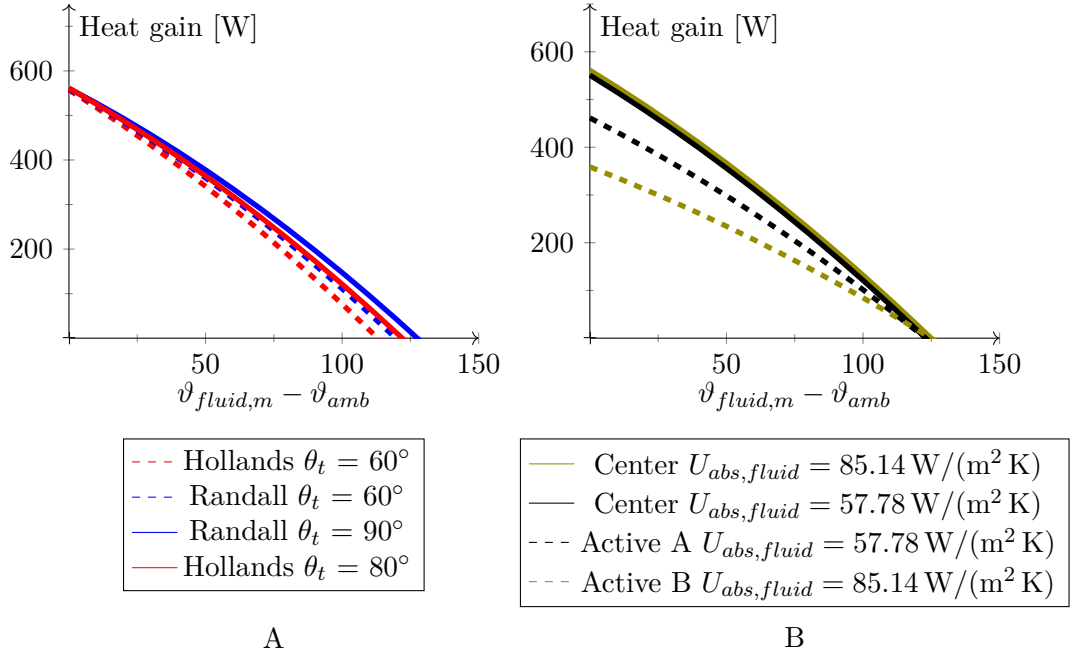


FIGURE 4.3.21. “A” shows a comparison of the heat gain curve of a gray-colored, insulated façade collector with EuroWhite glazing (properties see table 4.3.3) and  $U_{abs,fluid} = 85.14 \text{ W}/(\text{m}^2 \text{ K})$  calculated with the correlation of Randall (equation (4.3.32)) and Holland's (equation (4.3.33)) at different tilt angles  $\theta_t$ . “B” compares the heat gain curve of the same collector with the correlation of Holland's at  $80^\circ$  with different values for  $U_{abs,fluid}$ , and different active areas and their respective margins as described in figure 4.3.19. All heat gain curves are calculated at  $\vartheta_{amb} = 25^\circ \text{C}$ , irradiation  $G = 750 \text{ W}/\text{m}^2$ , wind velocity  $u_{wind} = 3 \text{ m}/\text{s}$ , sky view factor = 0.5.

a silver layer developed at Fraunhofer ISE almost reaches the criterion ( $524 \text{ kW h}/\text{m}^2$ ). The gray absorber only reaches the funding limit together with the EuroWhite glazing.

Calculating  $Q_{coll,MAP}$  for the different active areas reveals that with the assumed proportion of active area and margin, the collector with the gray absorber will probably never reach the funding limit, whereas the collector with black absorber almost touches the funding limit ( $499 \text{ kW h}/\text{m}^2$ ), meaning that with a slightly increased proportion of the active area the funding limit might be reached. An absorber with spectrally selective coating and anti-reflective glazing was also compared as a reference. This collector will probably reach the funding limit with the fully used activatable area “active A”. All results are based on modeling assumptions and do not replace measurements. The heat gain of the collectors was likely underestimated by neglecting the margins. Measurements



could therefore show higher outputs, and the eligible criterion of MAP might still be reached.

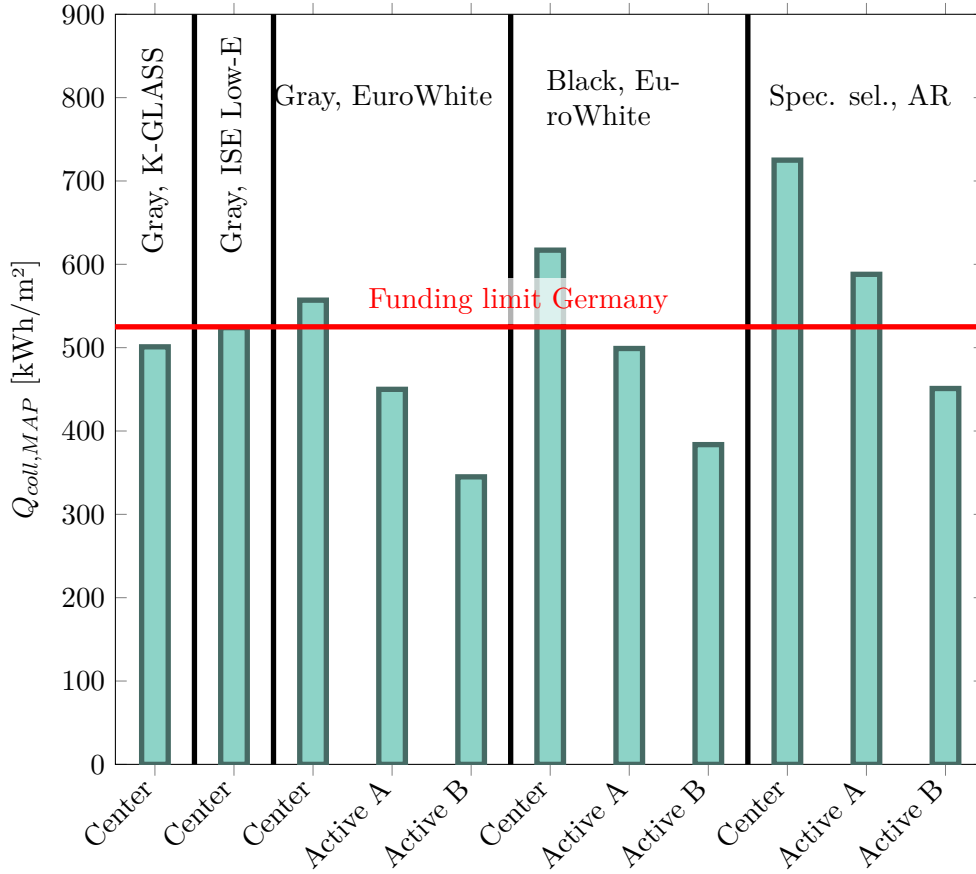


FIGURE 4.3.22.  $Q_{coll,MAP}$  for different UHPC collectors with an area of  $1.75 \text{ m}^2$ . “Center” refers to a hypothetical UHPC collector without margins and the minimal channel distance  $d = 40 \text{ mm}$ , “Active A” refers to a UHPC collector with a fully used activatable area and channel distance  $d = 54.4 \text{ mm}$ , and “Active B” refers to a UHPC collector with a partly used activatable area with the minimal channel distance  $d = 40 \text{ mm}$  as described in the setup of test “Active area vs. channel distance”.

#### 4.4. Summary and discussion of results

This chapter described the special features of UHPC collectors compared to other collectors. They affect system simulations based on characteristic curves, for example, due to increased thermal capacity. Observed vapor diffusion could mean that the collectors always have to be operated above 0 °C, which significantly impacts the system simulation.

FEM simulation of the UHPC absorber showed that a characteristic curve simulation based on a node model validated for insulated and glazed collectors does not adequately represent the characteristics of non-insulated UHPC collectors. The applied FEM simulation procedure solves the 2-D heat transfer equations for the geometry of the absorber with a set of boundary conditions that represent the heat transfer on the boundary and calculates the heat transferred to the heat carrier fluid. This is done for different operating points of the collector. The heat gain curve can then be determined via regression. The main difference to the mentioned simplified node model is that with this node model, the absorber's heat transfer coefficient is only simulated once at  $\vartheta_{amb} = \vartheta_{fluid,m}$  with the 2-D FEM model and adiabatic boundary conditions at the absorber backside, and is then assumed to be constant for other operating points. It could be shown that this simplification is only valid for insulated collectors; for collectors without back insulation, this approach leads to inaccuracies proportional to the temperature differences of the fluid and the ambient.

The developed FEM method was used to show the influence of rear ventilation on the façade and its orientation towards the sky. While the orientation towards the sky had very little influence on low-emissivity absorbers, the influence on the heat gain of a highly emitting absorber was about 50 W/m<sup>2</sup> to 60 W/m<sup>2</sup> at all operating points, which corresponds to about 11 % of the useful heat at  $\vartheta_{amb} = \vartheta_{fluid,m}$  with an irradiation of 750 W/m<sup>2</sup>. A closed gap behind the absorber led to higher achievable temperature levels but lower gains at operating temperatures below ambient temperature. The influence of fastenings and their space requirements and possible thermal bridges on the characteristic curve could also be estimated with the FEM model. It was found that their influence is significant at high temperature differences of the fluid and the ambient temperature. Characteristic curves were thus created for use in system simulations.

Furthermore, characteristic curves for glazed collectors with different active areas were created using a validated node model, based on a possible collector size with the production conditions of *TABSOLAR*<sup>®</sup> collectors. As a conservative guess, the margins were assumed as passive areas with no gains and losses as the focus was on the question of channel distance vs. area utilization. Here it was found that non-spectrally selective coated collectors of this size probably do not reach the eligibility criterion of the MAP

due to the large non-active edge areas. In reality, the margins are not passive; they only contribute less than the center area. The output of the center area serves as the upper limit. If a different area measurement were used as the basis for determining the characteristics, such collectors might be eligible without considering the contributions of the margins.

#### 4.5. Further research

The mentioned vapor diffusion of the UHPC collectors should be further investigated in long-term tests with water with and without antifreeze. The described FEM-simulation procedure is assumed to be more accurate for the uninsulated collector than the simulation with the node model. The influence of this inaccuracy on system simulation results has not yet been tested. Future investigations could quantify the influence. Validating the FEM simulation procedure with measurements would be the next step.

So far, only collectors made of UHPC have been investigated with the FEM method. It would be interesting to also determine the deviation of the FEM simulation procedure and the simulation using the described node model for absorbers without back insulation made from other materials with different thermal conductivities.

Strong simplifications were made in the simulation of the rear collector losses. Here, more precise knowledge about the prevailing conditions in the ventilation gap of the rear-ventilated façades could be transferred to the simulation model and thus improve the characteristic curve simulation. It could be investigated how to simplify the characteristic curve simulation by means of FEM simulation of the various operating points. With the knowledge gained about the margin influence, scientifically accompanied development efforts could be made towards smaller margins and smaller thermal bridges. As the FEM simulation procedure is not very fast and, in this work, the different steps were conducted by hand, ways to accelerate the generation of a heat gain curve with the same accuracy would be beneficial, for example, with a higher degree of automation.

With the described FEM setup, the temperature of the building wall can also be determined. The temperature drop or increase caused by collector operation below or above ambient temperature could be evaluated. It is assumed that within insulated rear-ventilated façade constructions with unglazed collectors, this influence is rather low. Hauer [65] investigated different façade setups with glazed collectors and found reductions of the heat demand of 6% with a direct coupling up to an increase of the heat demand to 5% with an air exchange rate of 100 between collector and wall. A low increase in cooling demand observed at low insulation thicknesses could be compensated with optimized building technology.

Existing correlations for convective losses in vertical columns were used for the simulation of the glazed collectors. However, these correlations depend on the aspect ratio. It should be investigated whether the assumed correlations also apply to the targeted aspect ratios or whether they would need to be adjusted. The margin losses and the thermal bridges in the glazed collectors could be assessed with the FEM approach and the heat gain curves adjusted. It is assumed that  $Q_{coll,MAP}$  would then be higher for “Active A” or “Active B”; the output for “Center” is assumed to be the upper limit. It is important to know whether the values would reach the eligibility criterion of the MAP.

## Solar thermal systems with UHPC collectors

This chapter deals with climate-compatible systems for the renovation of apartment buildings and the contribution that façade collectors made of UHPC can make. In an introduction, the basics of classical solar thermal systems are explained and why this thesis analyzes different combinations with heat pumps. The renovation approach is to design the renovation systems as close to the existing systems as possible and reuse existing components like radiators and storage tanks. Two types of UHPC façade collectors with different architectural flexibility and achievable temperature levels defined in chapter 4 are analyzed. Exemplary systems are designed, simulated, and compared with reference systems: for the economic benchmark, two systems with air-source heat pump, for the architectonic benchmark, a system with ground-source heat pump, and for the technical benchmark, a system with an unglazed, commercially available stainless steel collector. Tests show the influence of the area, the wind, the orientation, and a different control strategy of systems with UHPC façade collectors as single source for a heat pump and two systems with UHPC façade collectors operated with water as heat carrier in combination with an ice storage.

### 5.1. Fundamentals

#### 5.1.1. Solar thermal systems

Figure 4.1.2 in the previous chapter gives an overview of possible applications of solar thermal collector systems. The application “source for a heat pump” indicates the main heat provider, whereas “direct space heating” and “domestic hot water” can have other or – in very few cases – no energy co-providers. 100% solar thermal heat provision is only possible for systems whose heat demand optimally matches the solar supply or can be balanced sufficiently using storage.

Drinking water heating systems are the most widespread solar thermal systems: 56.6% of solar thermal systems installed in residential buildings in Germany deliver heat for drinking water only [29]. Solar thermal systems with heating support are also-called solar combi systems. They own a share of 45.4% of all solar thermal systems in residential buildings in Germany. The total share of residential buildings with solar thermal collectors in the country amounts to 14.4% (8.4% share with PV) [29].

In Germany, a certain amount of renewable energy is mandatory for new buildings and in some federal states even for replacing the heating system (Renewable Energies Heat Act of 2009 (EEWärmeG)). If a house owner wants to stay with gas as the main heat source, a small domestic solar thermal hot water system is one way to meet this obligation.

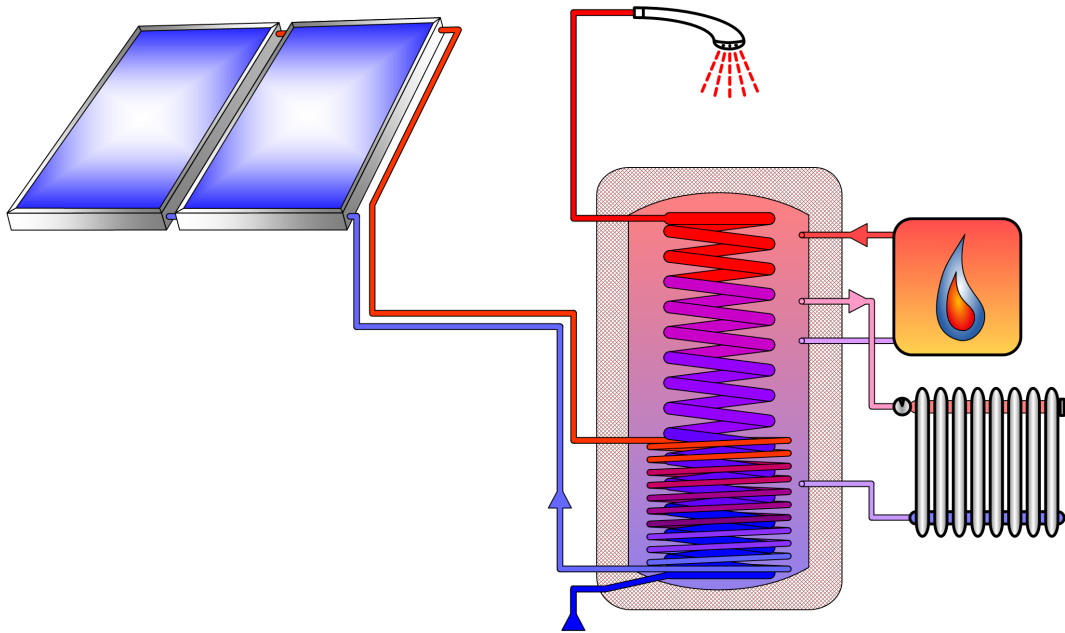


FIGURE 5.1.1. Typical solar combi system with combi storage. Source: Fraunhofer ISE

Figure 5.1.1 illustrates a solar combi system with combi storage. Solar systems are usually closed-loop systems. The solar fluid is equipped with antifreeze which must be professionally checked at certain intervals. A solution without antifreeze can be built with so-called drainback systems. Figure 5.1.2 illustrates the operational stages of such a drainback system. If the collector temperature drops below or rises above a limit temperature, the collector is drained. After each draining process, the collector loop has to be refilled, which requires a certain amount of additional pump power to overcome the static height. Drainback systems must be installed carefully as a constant inclination of the pipeline is indispensable for a proper draining process. In façade installations, this can be ensured more easily. As mentioned in section 4.2.2.2, drainback systems can be advantageous regarding costs: Philippen et al. showed that a water drainback system can save 18 % cost compared to a reference system [132].

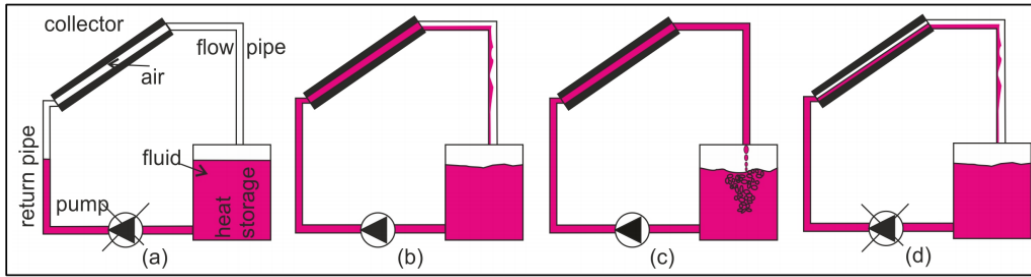


FIGURE 5.1.2. Operation stages of drainback systems: (a) not in operation, (b) filling process, (c) operation mode, (d) draining process [13].

The proportion of solar thermal energy to conventional energy can be described by the fractional energy savings  $f_{sav}$ . It describes the reduction of conventional energy by implementing a solar thermal system and can be expressed by equation (5.1.1).

$$(5.1.1) \quad f_{sav} = 1 - \frac{Q_{aux}}{Q_{conventional}}$$

$Q_{aux}$  describes the delivered auxiliary heat and  $Q_{conventional}$  the sum of the energy demand of the building and the losses of a conventional reference system. The fractional energy savings of solar thermal systems can vary immensely. In Germany, the most commonly mentioned achievable solar fraction for residential buildings is 60%, corresponding to an  $f_{sav}$  of 0.6. However, as a rule, only the hot water requirement is balanced, whereas the greater part of the heating requirement for the heating system is not included.

Solar combi systems are usually designed to provide 0.2 to 0.3 fractional energy savings. Buildings that provide more than 50% of their heating requirements by solar thermal means are called “Sonnenhaus” in Germany<sup>1</sup>. The Sonnenhaus-Institut offers an overview of built “Sonnenhäuser” in Germany, Austria, Switzerland, and Italy. On their website, 308 houses of this standard are referenced so far<sup>2</sup>. An important factor in achieving high fractional energy savings is the overall heat demand. If it is low and can be covered at low temperatures by underfloor heating or even concrete core activation, for example, this has a positive effect on the achievable fractional energy savings.

In the past, solar thermal energy in buildings has often been combined with gas. For a solar combi system with fractional energy savings of 0.3, this means that 30% of gas consumption can be saved. In other words, 70% of the CO<sub>2</sub> emissions of the gas remain.

<sup>1</sup>The term is defined by the Sonnenhaus-Institut ([www.sonnenhaus-institut.de](http://www.sonnenhaus-institut.de)) but not protected. Literal translation into English is solar house.

<sup>2</sup><https://www.sonnenhaus-institut.de/das-sonnenhaus/solarenergie-vorteile-gebaeudekonzept.html>

As a regenerative alternative to gas, biomass is occasionally used as a second heat source. However, looking at the global availability of biomass, it quickly becomes apparent that biomass cannot replace gas on a large scale [123, 84]. Additional alternatives to gas must be found for systems with low CO<sub>2</sub> emissions. One alternative often discussed is renewable hydrogen. It can be mixed with gas in existing networks to a certain extent. However, this admixture is currently limited to 10 Vol.-% in Germany. This limit might be lifted in the future, but if and when gas will be completely renewable in the future is an open question. Theoretically, a shift to 100 % hydrogen within the gas grid is possible, but all existing gas boilers would have to be replaced, which would lead to considerable costs. Renewable hydrogen as the sole source for the heating systems does not seem plausible either: the renewable energy amount to provide low-temperature heat with hydrogen is 500 to 600 % higher compared to the heat pump [57].

Infrared emitters operated with renewable electricity as heating systems are discussed, for example, by Heider et al. [69]. They provide a maximum of 1 kWh of heat with 1 kWh of electricity without losses. Compared to heat pumps that usually provide more than 3 kWh of heat per 1 kWh electricity, the thermal yield per 1 kWh electricity is rather low. So, this can only be a solution for very low heat demands or areas where water-driven heaters are hard to install, or installation costs are decisive.

### 5.1.2. Heat pump systems

Heat pumps combined with a renewable electricity mix become increasingly important for a climate-friendly heat provision for residential buildings with low to zero CO<sub>2</sub> emissions. Heat pumps usually use air, geothermal heat or groundwater as the heat source. Waste heat or solar thermal energy can also be used. They essentially increase the temperature of the source to a higher temperature level using energy. This can be thermal energy in the case of adsorption or absorption heat pumps, or electrical energy. Electrically driven heat pumps dominate the market and are the subject of this work. The cycle of an electrically driven heat pump is illustrated in figure 5.1.3.

The working fluid, a refrigerant, in its gaseous state is pressurized and circulated through the system by a compressor. In the first heat exchanger, the condenser, the hot and highly pressurized vapor condenses and cools down. The useful heat is delivered to the heating system. The still pressurized condensed fluid then passes an expansion vessel and evaporates in the next heat exchanger, the evaporator. It absorbs heat from the environment and enters the condenser again. Heat pumps that can change circulating direction are called reversible heat pumps.

The energy balance of an ideal heat pump without losses can be expressed by equation (5.1.2) with the heat flow through the condenser  $\dot{Q}_{con}$ , the heat flow in the evaporator  $\dot{Q}_{eva}$ , and the electrical power needed by the compressor of the heat pump  $P_{el,HP}$ .



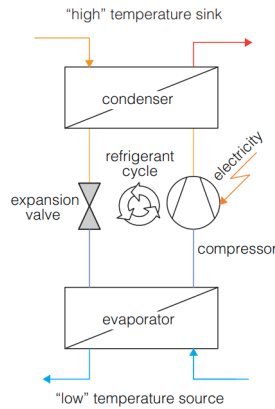


FIGURE 5.1.3. Schematic representation of the heat pump cycle [6]

$$(5.1.2) \quad \dot{Q}_{con} = \dot{Q}_{eva} + P_{el,HP}$$

The efficiency of a heat pump is expressed in terms of its delivered useful heat in relation to the electrical energy input to the compressor. It is also called the coefficient of performance (COP) and is defined as:

$$(5.1.3) \quad COP = \dot{Q}_{con} / P_{el,HP}$$

The theoretical limit of the COP is expressed by the reciprocal value of the Carnot efficiency:

$$(5.1.4) \quad COP_{lim} = \frac{1}{\eta_{Carnot}} = \frac{T_{sink}}{T_{sink} - T_{source}}$$

where the temperature of the sink and the source are to be entered in Kelvin. This illustrates that heat pumps work best with low temperature differences. So, high source and low sink temperatures are preferable. If the source temperature was not limited, and the temperature difference could be kept constantly small, higher sink temperatures would lead to higher  $COP_{lim}$  values.

It also indicates the dependency of the COP and the possible heat output  $Q_{con}$  from the sink and source temperature. Manufacturers usually provide a range with typical temperature combinations for both the COP values and the values for  $Q_{con}$ . If a single value is specified, usually the COP and  $Q_{con}$  at the nominal point are provided with the corresponding source and sink temperature. For ASHP this is (2 °C/35 °C); for GSHP, it is (0 °C/35 °C).

Heat pump systems can work monovalent, i.e. as the only heat source of a building, or bivalent when more heat providers in combination deliver the required heat for a building. A typical special case of a bivalent heat pump operation, namely the combination with a heating rod, is also called monoenergetic operation. The bivalence point  $\vartheta_{biv}$  describes the outdoor temperature up to which the heating load is completely taken over by the heat pump. At temperatures below the bivalence point, the second heat generator is switched on.

To describe the seasonal or the yearly performance of the heat pump, the seasonal performance factor ( $SPF_{HP}$ ) is defined as follows.

$$(5.1.5) \quad SPF_{HP} = \frac{\int \dot{Q}_{con} dt}{\int P_{el,HP} dt}$$

Figure 5.5.1 presents a visualization of the definitions of  $SPF_{HP}$  and other definitions for the SPF used in this thesis.

Haller et al. [6] give a general rule of thumb: a decrease of the temperature difference between the evaporation and the condensation by 1 K leads to about 2 % to 3 % increase of the COP under typical operating conditions.

The system performance can be described by including possible auxiliary heat and power for backup heaters, pumps, and other devices.

The energy flows provided are put in relation to the required energy flows. Depending on boundary conditions, it can be measured before ( $SPF_{SYS,1}$ ) or after ( $SPF_{SYS,2}$ ) the storages. The energy necessary for the provision of circulation is considered a necessary part of the DHW provision and is therefore included in the numerator of  $SPF_{SYS,1}$  and  $SPF_{SYS,2}$  even though it is a loss.

Following equation (5.1.6),  $SPF_{SYS,1}$  relates the energy flow from the condenser  $\dot{Q}_{con}$ , the auxiliary heat for the heating circuit  $\dot{Q}_{aux,HC}$  and for the domestic hot water  $\dot{Q}_{aux,DHW}$  that go into the storage to the energy required. In this definition, the loss of storage is handled as a necessary part of the heat provision.

For a fair comparison of different storage sizes,  $SPF_{SYS,2}$  with the definition following equation (5.1.7) with slightly lower resulting values should be used.

$$(5.1.6) \quad SPF_{SYS,1} = \frac{\int (\dot{Q}_{con} + \dot{Q}_{aux,HC} + \dot{Q}_{aux,DHW}) dt}{\int P_{el,tot} dt}$$

$$(5.1.7) \quad SPF_{SYS,2} = \frac{\int (\dot{Q}_{HC} + \dot{Q}_{DHW} + \dot{Q}_{circ}) dt}{\int P_{el,tot} dt}$$

with

$$(5.1.8) \quad P_{el,tot} = P_{el,HP} + P_{el,aux,HC} + P_{el,aux,DHW} + P_{el,pumps} + P_{el,aux,other}$$

The total energy required  $P_{el,tot}$  is the sum of the electrical energy needed for the heat pump  $P_{el,HP}$ , the auxiliary demand for the heating circuit  $P_{el,aux,HC}$  and for the domestic hot water circuit  $P_{el,aux,DHW}$ , the electrical energy needed for the pumps  $P_{el,pumps}$  and for other needed electrical devices such as control elements  $P_{el,aux,other}$ .  $P_{el,aux,HC}$  and  $P_{el,aux,DHW}$  correspond to  $\dot{Q}_{aux,HC}$  and  $\dot{Q}_{aux,DHW}$  if losses are neglected.

Miara et al. [114] report results from field tests conducted between 2007 and 2010 in Germany: the average annual performance factor for air-source heat pumps was  $SPF_{SYS,1,ASHP} = 2.9$ , whereas an average  $SPF_{SYS,1,GSHP} = 3.9$  has been measured for borehole heat sources. The deviation of the performance of a particular installation from the average of field test measurements can be quite substantial. A field test evaluation from 2018-2019 of single-family homes in stock shows a mean  $SPF_{SYS,1,ASHP}$  of 3.1 and  $SPF_{SYS,1,GSHP}$  of 4.1 [30].

Depending on their design, heat pumps have different restrictions on the temperature levels at source and sink. The upper limit for the condenser outlet  $T_{con,max}$  is around 65 °C for many heat pumps, but there are some that reach 70 °C or even higher temperatures. Higher temperatures are particularly advantageous for the provision of hot drinking water. For the evaporator, there is both a minimum and a maximum temperature. Air-source heat pumps usually cover the occurring spectrum of ambient air, whereas geothermal heat pumps cover a typical spectrum of occurring ground temperatures, which is smaller than the spectrum of ambient heat. If a ground-source heat pump is to be operated with collectors as the source, it must explicitly be ensured that these limits are respected. Otherwise, if temperatures are too low, very high pressures can occur, affecting the service life of the heat pump. If temperatures are too high, the viscosity of the compressor lubrication may no longer match the design and fail. In addition, the compressor outlet temperature – also-called hot gas temperature – must not become too high because it could otherwise cause damage. The respective temperature limits can be found in the manual of the heat pump.

### Market aspects of heat pumps

Groundwater or geothermal heat pumps are more efficient than air-source heat pumps due to the higher source temperatures and a higher heat transfer into the evaporator. But they are also more expensive and often cannot be used because of local conditions. Between the years 2000 and 2004, when annual sales numbers in Germany were steadily growing at a low level to almost 20.000, groundwater and geothermal heat pumps clearly

dominated the market. The sales numbers increased rapidly in 2005/2006 to around 65.000, then remained relatively steady until 2015 when they increased again to over 90.000 in 2017. Within the last 10 years, the share of air-source heat pumps increased steadily.

In 2017, 60% of all heat pumps sold were air-source heat pumps [19]. Acoustic and visual disadvantages due to the outside air unit seem to be acceptable regarding the advantage in investment cost.

The total share of heat pumps used in new buildings also increased significantly during the last years. In buildings built in 2019, this share reached 46% (33% in 2015) for single-apartment buildings, whereas only 24% (16% in 2015) of buildings with three or more apartments are equipped with a heat pump [145]. Multi-apartment buildings are usually situated in more densely populated urban areas. So, the lower shares of heat pumps in multi-apartment buildings may be caused by regulations concerning the distance of outside air units to other buildings and the space for boreholes. Other reasons could be the topographical conditions for boreholes, lower incentives, and higher investments for investors that do not benefit from their installation.

In the refurbishment sector, the share of heat pumps is significantly lower but has been growing over the last years (from 3.6% in 2014 to 5.5% in 2017) [19].

### 5.1.3. Solar-assisted heat pump systems

Solar thermal energy can be utilized to reduce the power consumption of heat pumps or simply to provide an alternative source. There are different approaches for the configuration of solar thermal systems and heat pumps. In the regenerative mode, solar thermal energy is used to warm or regenerate the main source, mostly the ground.

Sommerfeldt and Madani were able to show that around 50% or more of land used by boreholes could be saved with regenerating PVT collectors [143]. With serial configuration, solar thermal collectors are used as a direct source for the heat pump. In a survey conducted between 2011 and 2012, only 8 of 124 systems working in pure serial configurations were identified [63]. With this configuration, the solar collectors can raise the source temperature of the heat pump and improve its COP. If there is no irradiation, and the collector is the only source for the heat pump, the collector works as an ambient heat exchanger, and the source temperature drops below ambient temperature. Apart from that, the solar energy gained during daytime cannot be used if the heat pump is not working. However, the solar energy generated during the downtimes of the heat pump can be stored, for example, with latent storage such as ice storage. Depending on the size of the storage tank, the storage can also be seasonal, i. e., it gradually freezes to an almost solid state during the winter and is regenerated during the warmer period to be used as a sensitive storage tank. If the collector is a direct source for the heat

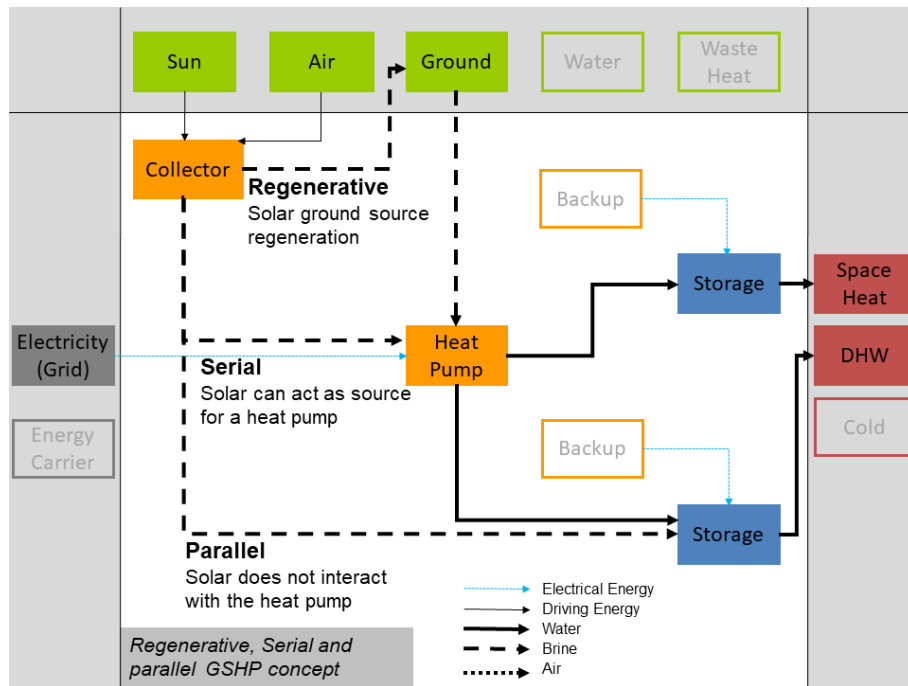


FIGURE 5.1.4. Representation of solar-assisted heat pump systems based on the visualization scheme developed by Frank et al. [53]

pump and can also provide direct heat for domestic hot water and/or heating as well as regenerate the ice storage, this configuration would be a combination of parallel, serial, and regenerative. Such a configuration can also be achieved by combining two types of collectors with different operating temperatures.

Most configurations with solar thermal and heat pumps found in the mentioned survey work only in a parallel setup, where both heat sources work separately. Any combination of regenerative, serial, and parallel configurations is possible, as well, and almost all of them were found in the market.

All mentioned configurations are illustrated in figure 5.1.4.

## 5.2. Modeling of solar thermal and reference systems

### 5.2.1. General remarks

System modeling is an important component of system design. The better a system represents reality, the better the statements about achievable system yields. Detailed models that illustrate the respective influence parameters are needed to understand the exact physical processes of a component and to optimize individual components. A physical model for generating characteristic curves for solar thermal collectors was presented in the previous chapter (section 4.3).

Characteristic curve models are often used for annual simulations of different components. Such characteristic curve models usually use measurement data or results of more detailed simulation models. Using characteristic curve models can offer considerable savings in computing time while usually maintaining sufficient prediction accuracy. Software environments such as TRNSYS, Modelica, and Polysun, for example, are available for detailed system simulations.

Even faster are rules of thumb. These consist of simple, rough calculations, result from experience with other systems or are derived from detailed modeling. They are particularly suitable for first rough designs. One example of a rule of thumb is an area calculation for a solar thermal drinking water system: [energieheld.de](http://energieheld.de)<sup>3</sup> proposes, for example, an area of 1.5 m<sup>2</sup> proposes, for example, an area of 1.5 m<sup>2</sup> flat plate collector per person. This system design leads to the typical “stamp” appearance on roofs often seen in Germany. The total area is about 4.5 m<sup>2</sup>-7.7 m<sup>2</sup> for a single-family home or less if vacuum tube collectors are used.

Rules of thumb are often valid for the most typical installations. In many cases, individual system installations are very similar and depend on one or only few parameters. In the case of solar thermal collectors, however, the influencing factors such as local solar radiation availability, storage, and configuration schemes differ so much that annual simulations are necessary. [energieheld.de](http://energieheld.de)'s rule of thumb is probably based on German weather conditions and a 45° tilted, unshaded roof with southern orientation. In other conditions, experience or more detailed yearly simulations are necessary.

### 5.2.2. Selection of reference systems

In this thesis, different system configurations with UHPC collectors are to be compared with reference systems based on the refurbishment of a standard apartment building. The reference systems should generally reflect the typical market environment. A comparison with gas systems or even oil systems would be representative in the current market environment. However, this work assumes that in the course of the transition towards a CO<sub>2</sub> neutral energy supply, systems with heat pumps and regenerative electricity will play a steadily growing role and represent the future market environment. Therefore two systems with air-source heat pumps (ASHP) and a system with a geothermal heat pump (GSHP) were selected as reference systems. The ASHP systems were used for the economic benchmark and the GSHP for the architectural benchmark defined in section 1.8. Additionally, a technical benchmark system with a commercially available

---

<sup>3</sup><https://www.energieheld.de/solaranlage/solarthermie/groesse-dimensionierung>

unglazed stainless steel absorber as the source for a heat pump was designed. All systems were designed according to current standards and then simulated.

### 5.2.3. Modeling environment and language

The systems were modeled using the Modelica modeling language. “The Modelica language is a non-proprietary, object-oriented, equation-based language to conveniently model complex physical systems containing, e. g., mechanical, electrical, electronic, hydraulic, thermal, control, electric power or process-oriented subcomponents” [116]. The Modelica Standard Library - Version 3.2.2 is used in this work. It contains a vast set of different models that can be developed further. Various modeling environments exist for simulation. In this work, the Dymola environment of Dassault Systèmes was used. Besides the Modelica Standard Library, components of other libraries such as the Buildings.lib, Version: 6.0.0, the IBPSA.lib, Version: 3.0.0, the Aixlib, Version: 0.7.4, and a project library of the project “LowEx im Bestand”<sup>4</sup> was used. The modeling of this thesis is based on a system model that Reher developed in his master’s thesis [138] as part of the project network “LowEx im Bestand”. Reher simulated a geothermal heat pump that supplies a multi-family home via a storage tank for domestic hot water and a heating tank. The basic scheme of this work (shown in appendix A, figure A.1) was retained but was fundamentally revised in terms of control, ground-source heat exchanger, building, domestic hot water provision, and circulation. The simulation time step was set to 200 s. The Dassel algorithm with a tolerance of 0.0001 was used for solving.

### 5.2.4. System configurations

In this work, two main systems with collectors as the source for a heat pump are compared to the reference systems. The first system uses the collector as the only source for a heat pump and is referred to as “Col-Dir”. The system scheme resembles that of the air-source (ASHP) and ground-source heat pump (GSHP) but has an additional auxiliary heater in case the collector outlet temperature is too low. The simplified system diagram for “Col-Dir”, ASHP, and GSHP is shown in figure 5.2.1. The “Col-Dir” system requires the use of antifreeze in the collector in all regions where outside temperatures below 0 °C occur, which is true for most of Central Europe. In the reference site investigated here, this is the case over a longer period of time in winter. As described in the previous chapter, the possibility of using antifreeze in the case of UHPC collectors has not yet been conclusively clarified. However, basic compatibility of the typical heat transfer fluid with UHPC could be clarified in the TABSOLAR I project. As a technical reference, a

---

<sup>4</sup>[www.lowex-bestand.de](http://www.lowex-bestand.de)

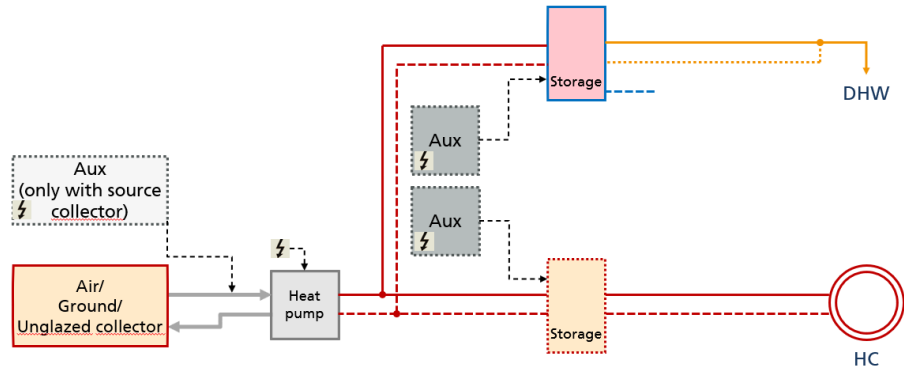


FIGURE 5.2.1. System scheme of monoenergetic systems (GSHP, ASHP, and Col-Dir) based on a schematic representation work developed in the project “LowEx im Bestand”.

“ColRef-Dir” system with a reference collector and the same system configurations as the “Col-Dir” was simulated.

As described at the beginning, it may make sense to store the solar energy. One possibility would be to store the solar energy on the warm side of the heat pump. To do so, one could, for example, increase the temperature in the storage tank when solar radiation is present. This control strategy was tested as a variant of the “Col-Dir” system.

Another possibility is to store the solar energy on the cold side. This can be done sensitively in water storage tanks or by concrete core activation, or latently in phase-change storage tanks. In this thesis, the basic suitability of systems with ice reservoirs is estimated and referred to as “Col-Ice”. Figure 5.2.2 shows a system schematic used for this purpose. In all systems, additional glazed collectors or the unglazed collectors used as a source could also be used directly to load the storage. This is indicated in figure 5.2.2 for domestic hot water. Investigations by Phillippen et al. [131],[27] showed that very high values for the seasonal performance factor SPF can be achieved with collectors delivering heat to a heat pump, to an ice storage, and to a hot storage for a single-family home. This work does not include the direct use of solar but considers it to be a promising option in the future.

The central storage system with an internal heat exchanger for the heat pump in the domestic hot water (DHW) tank has proven to be a widely used and cost-effective, robust system with low control engineering requirements [168]. At the beginning of this study, this system was to be used for the research work. However, as the internal heat



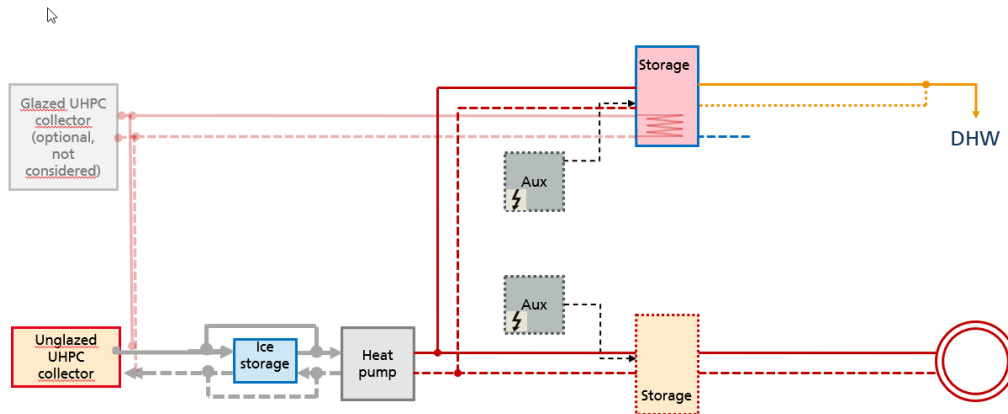


FIGURE 5.2.2. System schematic of bivalent systems (Col-Ice) based on a schematic representation work developed in the project “LowEx im Bestand”

exchanger of the DHW tank caused instability problems during simulations, the author decided to use a storage system without an internal heat exchanger but a freshwater station instead.

The number following “Col” is related to the collectors with the parameters given in table 4.3.2. So, the “Col1-Dir” system is the system with a gray, uninsulated UHPC collector as the only source for a heat pump, and “Col2-Ice” refers to a bivalent system with a spectrally selective, insulated UHPC collector.

### 5.3. Description and modeling of reference house

#### 5.3.1. Heating load

The renovation of multi-family homes (MFH) was identified as a promising application for UHPC collectors. The project network “LowEx-im-Bestand” analyzed the existing housing stock in Germany [42]. From this starting point, different standards for small, medium, and large multi-family homes with different construction age classes and energy standards in Germany were developed. Zones models were implemented in the simulation software TRNSYS 3- representing the different houses. Load files for the resulting heating load can be generated for each building type. The medium size multi-family home of construction class 1958–1978 was chosen for this study. This construction class has the largest share of total number of buildings (29%), total apartments (33%),

and of living area (32%) compared to all construction classes in Germany’s building stock until the year 2009 [35].

The aim of this study is a comparison of different renovation paths. A standard renovation of the selected building type fulfilling the requirements of EnEV 2016 was chosen. It is considered the minimum renovation level, with the residual heat demand being relatively high. A system that works for the comparison will also work for lower heat demands. The author generated the according load file with the building simulation setup in TRNSYS that was implemented in “LowEx-im-Bestand”. As the project network “LowEx-Bestand” is not yet completed, an intermediate status of the 3-zones model was used, which differs from the version that will be published later. The description of the building used can be found in table A.1. The specific yearly heating demand is  $68.4 \text{ kWh/m}^2$ , the total living area is  $581 \text{ m}^2$ .

A simplified, computing time-saving one-zone model is used for this work’s system simulation. The zone model is based on a resistor-capacitor model in compliance with the modeling standards of EN ISO 13790 with five thermal resistors and one capacitor [125]. The resistor-capacitor network of this model is shown in figure 5.3.1. The zone model was implemented and validated with field data as part of the dissertation by Wystrcil [167]. In this work, it was used and re-parametrized based on the geometrical and physical properties of the considered building described in table A.1. The zone’s thermal capacity was estimated to be  $165\,000 \text{ J/(K m}^2) \cdot A_f$ , which corresponds to a “medium” building according to DIN EN ISO 13790.

The resulting building heat load was compared and fitted to the load file generated in TRNSYS with the values given in table 5.3.1. A model with prescribed heat as shown in figure A.5 was used for the fit. Following abbreviations are used in figure 5.3.1:  $\vartheta_e$  = external air temperature,  $\vartheta_{air}$  = air temperature in the room,  $\vartheta_s$  = temperature of wall surface,  $\vartheta_{sup}$  = temperature of ventilation,  $H_{ve}$  = heat transfer coefficient of ventilation,  $H_{tr,w}$  = heat transfer coefficient of doors, windows, glazed walls, curtain façades,  $H_{tr,is}$  = heat transfer coefficient,  $H_{tr,ms}$  = coupling conductance to  $\vartheta_e$ ,  $H_{tr,em}$  = heat transfer coefficient of opaque construction elements,  $H_{tr,op}$  = resulting heat transfer coefficient of transmission through opaque construction elements,  $A_m$  = effective mass-related area,  $C_m$  = internal heat capacity,  $\phi_{HC,nd}$  = thermal capacity of heaters,  $\phi_{sol}$  = incoming solar heat,  $\phi_{int}$  = internal loads.

As the 3-zones model in TRNSYS is considered as reference, the focus was on meeting the same heat demand and not on a comparison of the two models. If the exact same input data had been used, the heating loads would differ more because of different levels of detail within the models.

The timeline, together with the ambient temperature and the integrated heating load of both models, can be found in figure 5.3.2.

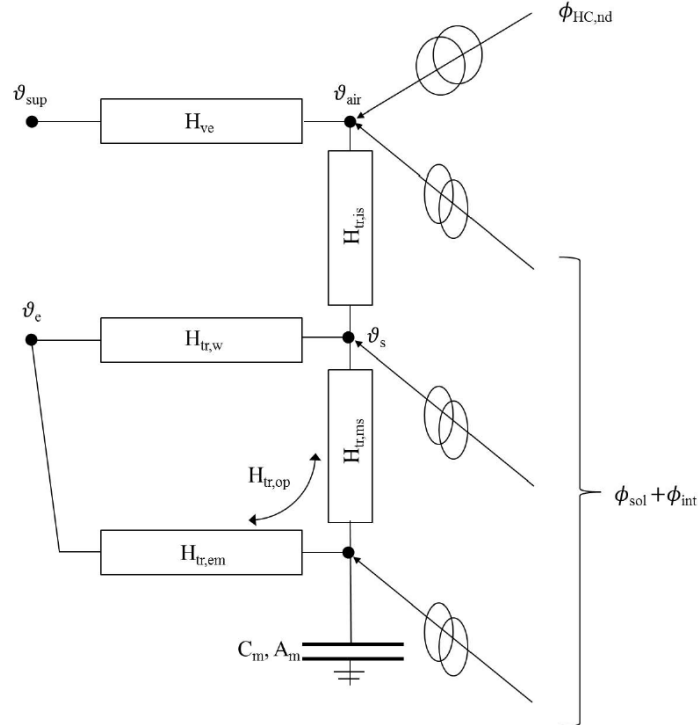


FIGURE 5.3.1. Resistor-capacitor network of zone model according to DIN EN ISO 13790:2008-09 [125]

TABLE 5.3.1. Fitted input data for zone model in Modelica according to DIN EN ISO 13790:2008-09 [125]

Category	Value	Unit
<b>General parameters</b>		
Heated net floor area $A_f$	581.07	[m <sup>2</sup> ]
Gross floor area	$1.1 \cdot A_f$	[m <sup>2</sup> ]
Gross volume of room	$1.1 \cdot 2.7 \text{ m} \cdot A_f$	[m <sup>3</sup> ]
Internal heat capacity of room	$165\,000 \text{ J}/(\text{K m}^2) \cdot A_f$	[J/K]

### Ventilation

TABLE 5.3.1. Fitted input data for zone model in Modelica according to DIN EN ISO 13790:2008-09 [125] - continued

Category	Value	Unit
Air exchange rate	0.5	[1/h]
<b>Transmission</b>		
U-value window	1.26	[W/(m <sup>2</sup> K)]
Gross area window north	24.38	[m <sup>2</sup> ]
Gross area window east	25.18	[m <sup>2</sup> ]
Gross area window south	31.5	[m <sup>2</sup> ]
Gross area window west	25.11	[m <sup>2</sup> ]
U-value opaque surface $U_{opaque}$	0.405	[W/(m <sup>2</sup> K)]
Area opaque surfaces	896	[m <sup>2</sup> ]
<b>Solar heat gains</b>		
Frame fraction of windows	0.3	[-]
Energy transmittance of glazings	0.709	[W/(m <sup>2</sup> K)]
Shading factor	0.5	[-]
Irradiation threshold for activating shading	1.0	[-]
Irradiation hysteresis for shading control	0.2	[-]
ground reflectance	0.2	[-]
<b>Internal heat gains</b>		
Internal heat gains without occupancy	$3\text{W/m}^2 \cdot A_f$	[W]

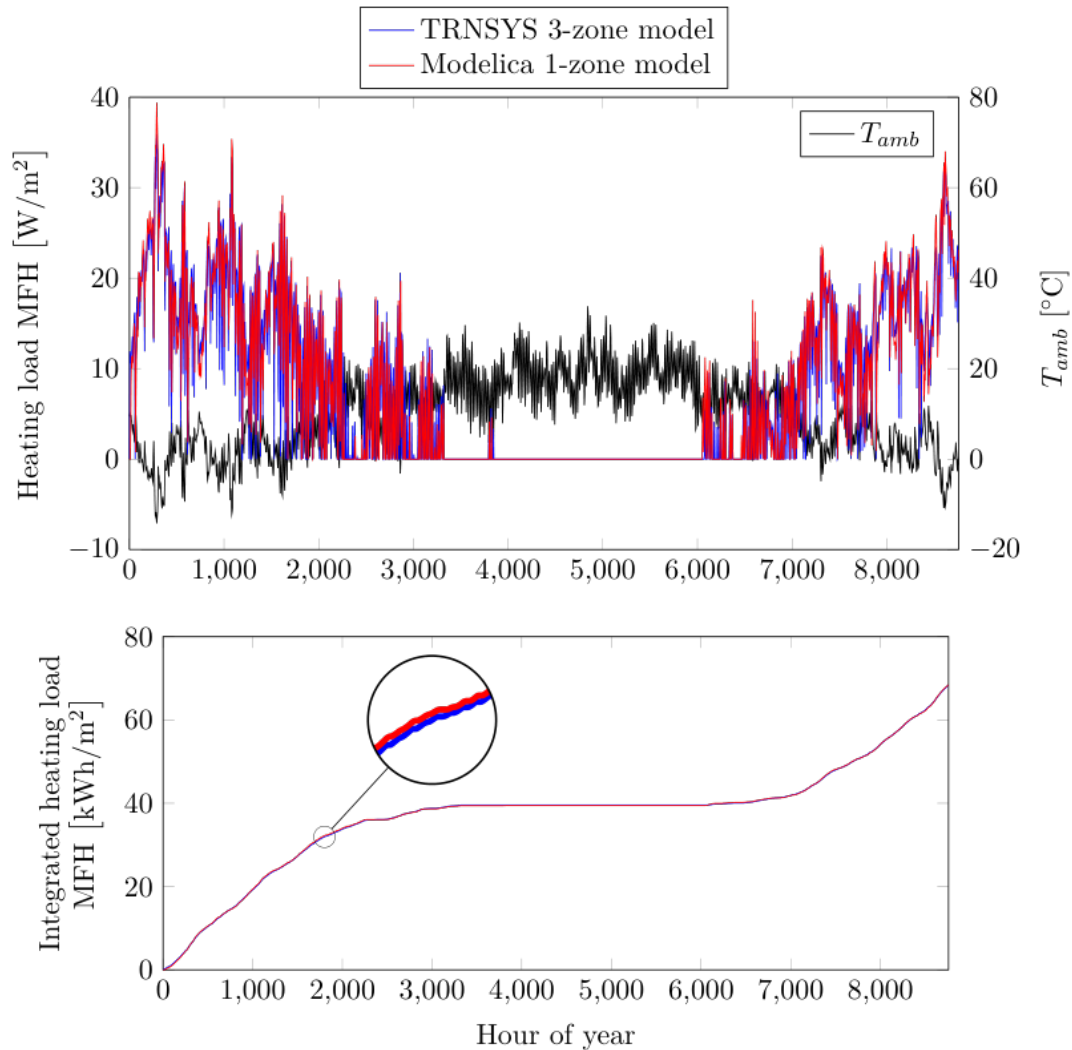


FIGURE 5.3.2. Heating load of the considered MFH in Potsdam modeled with the TRNSYS 3-zone model (blue) and with the Modelica 1-zone RC-model (red) with respect to net floor area  $A_f$  in the course of a year together with the ambient temperature (above) and integrated (below).

### 5.3.2. Site selection and weather data

This study focuses on the potential of UHPC collectors in Germany, and, following EnEV 2014<sup>5</sup>, therefore uses Potsdam, the reference location for Germany, as reference location. The weather data for both TRNSYS and Modelica simulations was generated

<sup>5</sup>Energieeinsparverordnung – EnEV 2014, Engl. Energy Saving Ordinance

with Meteonorm 7 version 7.3.3. Potsdam, weather station (52.4°N, 13.1°E, 81 m), Germany, was selected in the software. Further settings were: period radiation 1991–2010, period temperature 2000–2009, first random seed: 1.

The data for wind velocity is measured at a height of 10 m above ground to exclude local effects.

### 5.3.3. Domestic hot water and circulation

The hourly load profile for domestic hot water from the mentioned project network “LowEx im Bestand” was used for this work. It has been generated with the software Synpro<sup>6</sup>. Synpro uses a behavioral model to determine DHW tapplings. The software can generate synthetic load profiles by means of a stochastic model. The results were validated with measurements and compared to those of other tools such as DHWcalc [51]. The DHW load profile in this work uses the behavioral model of typical inhabitants of a multi-family home up to 10 residential units and omits vacation time.

The DHW demand side is connected to the storage via a freshwater station with an effectiveness of 0.9. The water flow rate on the consumer side of the freshwater station to the DHW taps is set to be calculated at each time step, according to the calculation of DHW heat demand:

$$(5.3.1) \quad \dot{m}_{DHW} = \frac{\dot{Q}_{DHW}}{c_p \cdot (\vartheta_{set,DHW} - \vartheta_{water,cold})}$$

The required DHW temperature  $\vartheta_{set,DHW}$  was set to 60 °C. For simplification, the cold water temperature  $\vartheta_{water,cold}$ , which changes throughout the year, was set to a constant value of 12 °C. Circulation following DIN 4701 [33] was implemented. The permissible cooling of the water in the circulation line between tank outlet and circulation line inlet is  $dT_{circ} = 5$  K. The circulation loss  $\dot{Q}_{loss,circ}$  can be calculated with equation (5.3.2).

$$(5.3.2) \quad \dot{Q}_{loss,circ} = \frac{1}{1000} \cdot U_{pipe,circ} \cdot z \cdot (L_V \cdot (\vartheta_{m,circ} - \vartheta_{m,V}) + L_S \cdot (\vartheta_{m,circ} - \vartheta_{m,S}))$$

with  $U_{pipe,circ}$  being the length-specific heat transfer coefficient of the circulation pipe, assumed with  $U_{pipe,circ} = 0.2$  W/(m K) and  $\vartheta_{m,circ}$  being the mean temperature of the pipe section.  $L_V$  stands for the pipe lengths in area V outside the thermal envelope, e. g. in a non-insulated basement with temperature  $\vartheta_{m,V}$ , and  $L_S$  is the pipe length in area S of the thermal envelope of the building with temperature  $\vartheta_{m,S}$ , which corresponds

<sup>6</sup><https://www.elink.tools/elink-tools/synpro>

to the room temperature. The values are determined with table 5.1-2 of DIN 4701 using the heated building area with equation (5.3.3).

$$(5.3.3) \quad L_V = 26.0 \text{ m} + 0.02 \text{ 1/m} \cdot A_f \quad \text{and} \quad L_S = 0.075 \text{ 1/m} \cdot A_f$$

In accordance with DIN 4701, period  $z$  per day during which the circulations pump is running was calculated with equation (5.3.4) to be 20.7 h.

$$(5.3.4) \quad z = 10 \text{ h/d} + \frac{1}{0.007 + \frac{50 \text{ m}^2}{A_f}} \text{ h/d}$$

The circulation mass flow can be calculated with equation (5.3.5).

$$(5.3.5) \quad \dot{m}_{circ} = \frac{\dot{Q}_{loss,circ}}{c_p \cdot dT_{circ}}$$

During times of DHW demand,  $\dot{m}_{circ}$  is reduced by the actually needed mass flow  $\dot{m}_{DHW}$ .

## 5.4. Components and dimensioning of heating systems

### 5.4.1. Solar collectors

The used Modelica model is based on the modeling principles of the Building Lib's collector model. The model was adapted by M. Lämmle to evaluate equation (4.1.4) described in section 4.1.3. The simulation in this work is based on the collector parameters of table 4.3.2.

### 5.4.2. Ice storage

Detailed modeling of an ice storage is quite complex: on the one hand, in liquid state, the reservoir should be able to represent internal stratification. On the other hand, icing and melting should be modeled as accurately as possible. The heat transfer varies depending on the thickness of the existing ice layer. The exact geometry of the internal heat exchanger plays a role in these processes. For example, two growing ice cylinders meet at parallel tube bundles after a certain time and can then no longer grow in this area. The heat transfer is reduced.

Ice storages are usually buried in the ground and have little or no insulation, which enables considerable additional gains from geothermal energy. The exact amount of heat that can be gained depends on the soil itself, the storage geometry, and the heat transfer coefficient of the storage walls to the surrounding soil. Depending on size and space

availability, ice storage units can also be accommodated inside the house, if necessary, with improved insulation.

D. Carbonell et al. describe a detailed model for an ice storage with an internal heat exchanger in the final report of project “Ice-Ex” [27]. It models both icing/deicing and the stratification in liquid stage in great detail. Comparisons with measurements showed very high accuracy. Unfortunately, this model is implemented for TRNSYS simulation software and is not yet available for Modelica. The implementation for TRNSYS is non-commercial and requires detailed knowledge to parametrize it correctly.

It would have been beyond the scope of this work to reproduce Carbonell’s very well elaborated model. Due to a lack of part effects data and because the focus of this work was not on ice storage, the author decided to exclude all of these effects. As a first approximation, a very basic and strongly simplified model was developed for this research project. It consists of two heat exchangers and a modified capacity model in which the specific enthalpy during the phase change of water is read via an external file, as shown in figure 5.4.1. This approach is based on a development used for PCM storage by H. Neumann [122]. It neglects losses in heat exchange caused by growing ice, stratification, and losses to the environment. The heat exchanger area is dimensioned according to the suggestions of the project “High Ice” by SPF Institute for Solar Technology in Rapperswil [131]:  $3 \text{ m}^2$  per  $1 \text{ kW}_{nom}$  of the heat pump.

The reduced model still shows the effect of limiting the evaporator inlet temperature. The simulated evaporator inlet temperature during operation with the ice storage as source serves as an upper limit. The actual inlet temperatures would be lower due to heat conduction through already grown ice layers.

The effect of stratification also influences the system’s behavior. Depending on the position of the outlet(s) related to the heat pump, the ice storage could, in principle, be loaded with higher temperatures than the upper limit temperature for the evaporator, as long as there remains sufficient volume that guarantees the upper limit temperature for the evaporator. This could be of particular importance during the transient times in spring and autumn. Higher temperatures in the upper regions of cold storage would also be available earlier in the loading process. The behavior of the used capacity model resembles concrete core activation in the summertime.

The additional gains through the walls can lead to lower required storage volumes. So dimensioning the simplified ice storage model only serves as an orientation and does not replace real dimensioning for a given ice storage at a given location. The results may differ significantly. If the storage is used as seasonal storage, the temperature at the end of the year should be the same as the initial temperature to ensure the energy balance



in the storage throughout the year. In the conducted simulations, this was ensured by iterations.

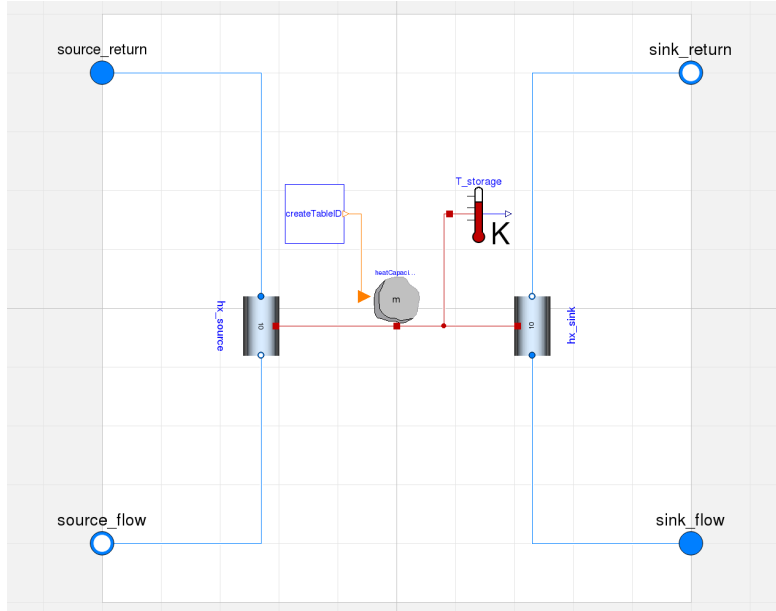


FIGURE 5.4.1. Implementation of simple adiabatic ice storage in Modelica

### 5.4.3. Heat pumps

The design of the heat pumps in the respective system was based on the heating load curve as proposed by VDI 4645 [156],[155]. First, the standard heating load for the chosen building was determined to be 21 kW, following DIN 12831 [37]. The heating temperature limit  $\vartheta_{limit,heating}$  was set to 15 °C. Together with the standard minimum outside temperature for Potsdam  $\vartheta_{stand,out}$  of  $-14$  °C [37] the heating load curve is defined as shown in figure 5.4.2. The system design is a bivalent, monoenergetic design. For the bivalent point, the design temperature for the heat pump was specified as  $\vartheta_{biv}$   $-5$ °. Below the bivalent point, backup heating supports the heat pump. The thermal capacity needed to cover heating demand  $\dot{Q}_{demand,biv,heat}$  is the intersection of the bivalent temperature and the standard heating load curve as shown in figure 5.4.2.

3.15 kW of additional capacity was assumed to provide domestic hot water. Together with  $\dot{Q}_{demand,biv,heat}$ , this results in  $\dot{Q}_{demand,biv,heat+DHW}$ , abbreviated with  $\dot{Q}_{demand,biv}$  in the following. In the considered building,  $\dot{Q}_{demand,biv}$  is 17.7 kW.

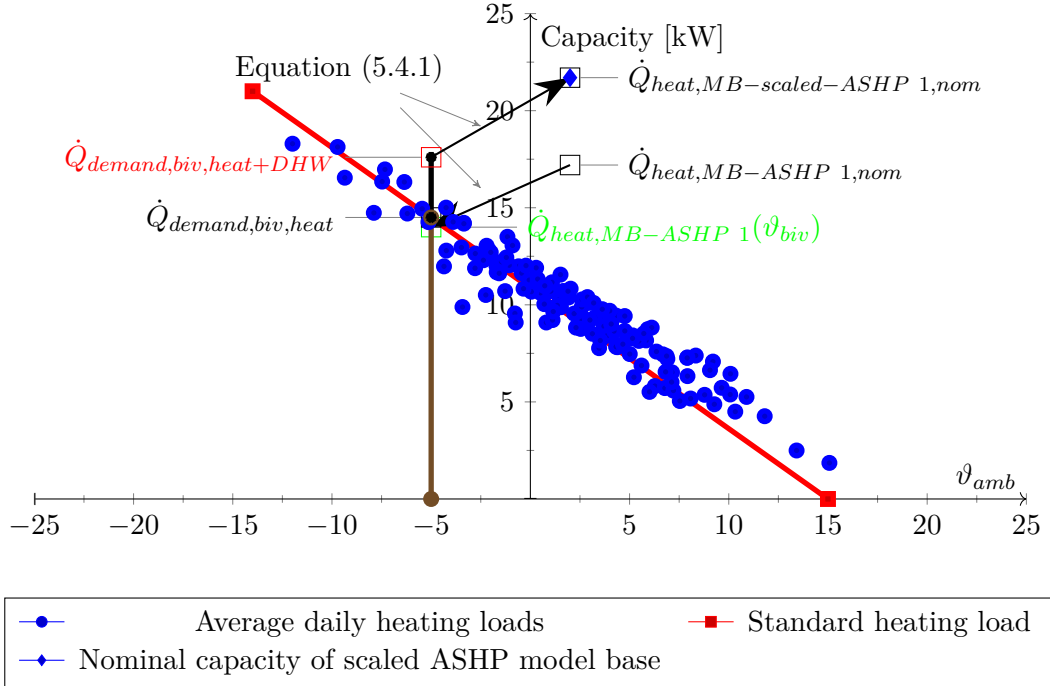


FIGURE 5.4.2. Standard heating load following DIN 12831 [37], which forms the basis for the design of the heat pump, and daily average of calculated heating load of MFH.

In the design process of a real system, a heat pump would be chosen that can at least cover this demand at  $\vartheta_{biv}$ . For the simulation, data fields of existing heat pumps can be scaled in a way that  $\dot{Q}_{demand,biv}$  fits exactly  $\dot{Q}_{heat,MB}(\vartheta_{biv})$ , assuming that the field gradients of smaller or larger heat pumps are similar.

The first step in this scaling procedure is determining the capacity of an ASHP or GSHP model base at the bivalent point  $\dot{Q}_{heat,MB}(\vartheta_{biv})$ . This can, for example, be done with a characteristic function of the model base heat pump. The scaling factor is the ratio of  $\dot{Q}_{demand,biv}$  and  $\dot{Q}_{heat,MB}(\vartheta_{biv})$ ; exemplified by the ASHP 1 model base and corresponding to the red and green square in figure 5.4.2. The resulting nominal capacity and the whole scaled data field used for the simulation can be obtained with this factor, for example, again with a characteristic function. The procedure is described in detail in the following.

To obtain the capacity of the model heat pump at the bivalent point  $\dot{Q}_{heat,MB}(\vartheta_{biv})$ , a characteristic function can be derived by regression from the data table given by the manufacturer. Equation (5.4.1) represents the resulting equation.

$$(5.4.1) \quad Q_{heat,MB} = a + b \cdot \vartheta_{con,out} + c \cdot \vartheta_{source} + d \cdot \vartheta_{con,out}^2 + e \cdot \vartheta_{source}^2 + f \cdot \vartheta_{con,out} \cdot \vartheta_{source}$$

Such a regression was done for an air-source heat pump (ASHP) and a ground-source heat pump (GSHP) with the data given in tables A.2 to A.7. The coefficients for the characteristic function given in equation (5.4.1) can be found in table A.8. Figures A.2 to A.4 visualize of the measurement data from the manufacturer and the corresponding points of the characteristic function.

With the temperatures for the given conditions at the bivalent point,  $\dot{Q}_{heat,MB}(\vartheta_{biv})$  can be calculated with equation (5.4.1), where  $\vartheta_{con,out}$  is the outlet temperature in the condenser, the heating supply temperature, and  $\vartheta_{source}$  is the entrance temperature in the evaporator, the source temperature. The following paragraphs describe the assumptions and calculation methods used for the required input temperatures.

For the ASHPs,  $\vartheta_{source}$  is equivalent to the bivalent temperature  $\vartheta_{biv}$  of  $-5^\circ\text{C}$ . For the GSHP, the typical source temperature at  $\vartheta_{biv}$  has to be identified. This work assumed a source temperature of  $\vartheta_{source} = 3.9^\circ\text{C}$  at  $\vartheta_{biv} = -5^\circ\text{C}$ . This temperature results from a fit of measurement data in previous projects.

The same model heat pump as for GSHP was chosen for the solar heat pump system, as the medium on the evaporator is also a liquid fluid. The source temperature at the bivalent point depends on the system configuration. If the solar and ambient heat collector was the only source, the source temperature was assumed to be ambient temperature  $\vartheta_{source} = \vartheta_{biv} = -5^\circ\text{C}$  for the conditions at night. If an ice storage was a second source, the source temperature was assumed to be  $\vartheta_{source} = \vartheta_{biv} = 0^\circ\text{C}$ .

$\vartheta_{con,out}$  was determined with the heating curve at  $\vartheta_{amb} = \vartheta_{biv}$  (equation (5.4.2)). The radiator exponent  $exp$  for the heating curve was assumed to be 1.2, the maximum supply temperature  $\vartheta_{HC,supply,max}$  to be  $45^\circ\text{C}$ . At  $\vartheta_{biv}$ , the supply temperature  $\vartheta_{con,out}$  was determined to be  $39.3^\circ\text{C}$ .

$$(5.4.2) \quad \vartheta_{con,out} = \vartheta_{room,set} + (\vartheta_{HC,supply,max} - \vartheta_{room}) \cdot \left( \frac{\vartheta_{room,set} - \vartheta_{amb}}{\vartheta_{room,set} - \vartheta_{stand,out}} \right)^{\frac{1}{exp}}$$

The so obtained temperatures  $\vartheta_{source}$  and  $\vartheta_{con,out}$  can be filled into equation (5.4.1) to obtain  $\dot{Q}_{heat,MB}(\vartheta_{biv})$ . According to equation (5.4.3) the scaling factor can then be calculated.

$$(5.4.3) \quad \text{Scaling Factor HP} = \frac{\dot{Q}_{demand,biv,heat+DHW}}{\dot{Q}_{heat,MB}(\vartheta_{biv})}$$

The nominal capacity for the different heat pumps can be obtained with the scaling factor and equation (5.4.1) filled in with the nominal temperatures. A nominal capacity of 16.5 kW at (0/35) was calculated for the ground-source heat pump, a nominal capacity of 21.7 kW at (2/35) for the air-source heat pump ASHP 1, and a nominal capacity of 22.0 kW at (2/35) and for the air-source heat pump ASHP 2. As for the ASHPs  $\vartheta_{source} = \vartheta_{amb}$  the resulting nominal capacity  $\dot{Q}_{heat,MB-scaled,nom}$  for the ASHP is illustrated in figure 5.4.2. The different nominal capacities result both from different nominal points and from different gradients of the characteristic curves. The gradients of the ASHP also differ. At the nominal point, both are almost equally efficient (ASHP 1: COP = 3.91, ASHP 2: COP = 3.86), but at 50 °C condenser temperature, ASHP 2 has a significantly worse efficiency (ASHP 1: COP = 2.79, ASHP 2: 2.44). For the solar system without ice storage a nominal capacity of 20.2 kW at (0/35) and with ice storage of 18.0 kW was calculated.

This design process for the heat pumps was used for a presentation during Berliner Energietage 2020 by Hess et al. [76] and then adapted for this thesis.

For the representation of the heat pumps in the system model, the model *HeatPumpDetailed* of AixLib V0.7.4 was chosen with a correction for high temperatures at the condenser, which can use data provided by manufacturers. Figure 5.4.3 shows the graphical representation of the ASHP in Dymola, figure 5.4.4 shows the one of GSHP, and figure 5.4.5 the one of a solar heat pump.

For the simulation in this work,  $\vartheta_{con,max}$  was set to 70 °C.

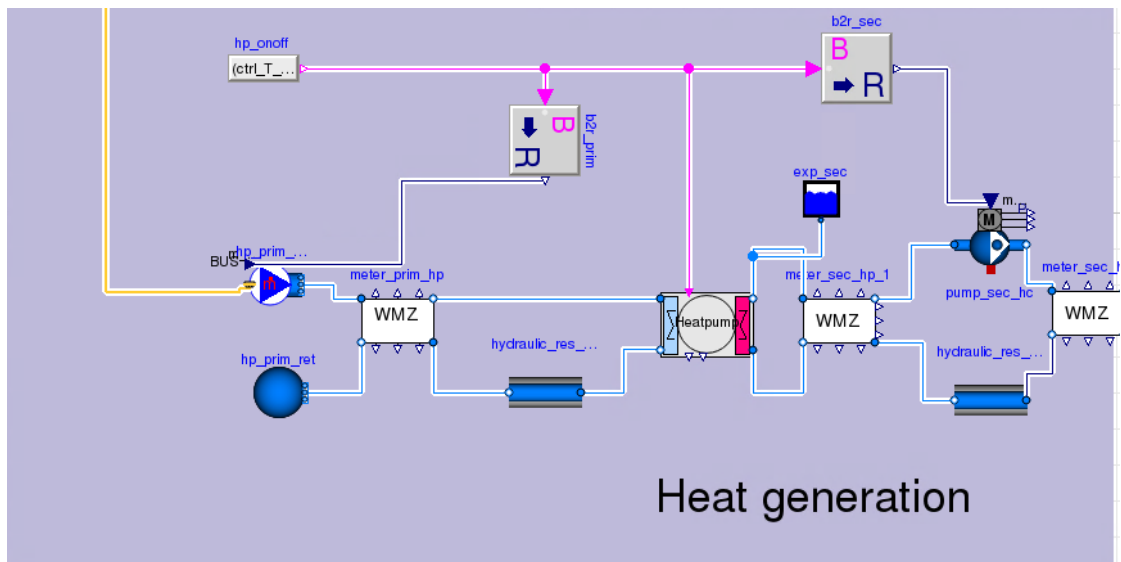


FIGURE 5.4.3. Implementation of ASHP in Dymola/Modelica

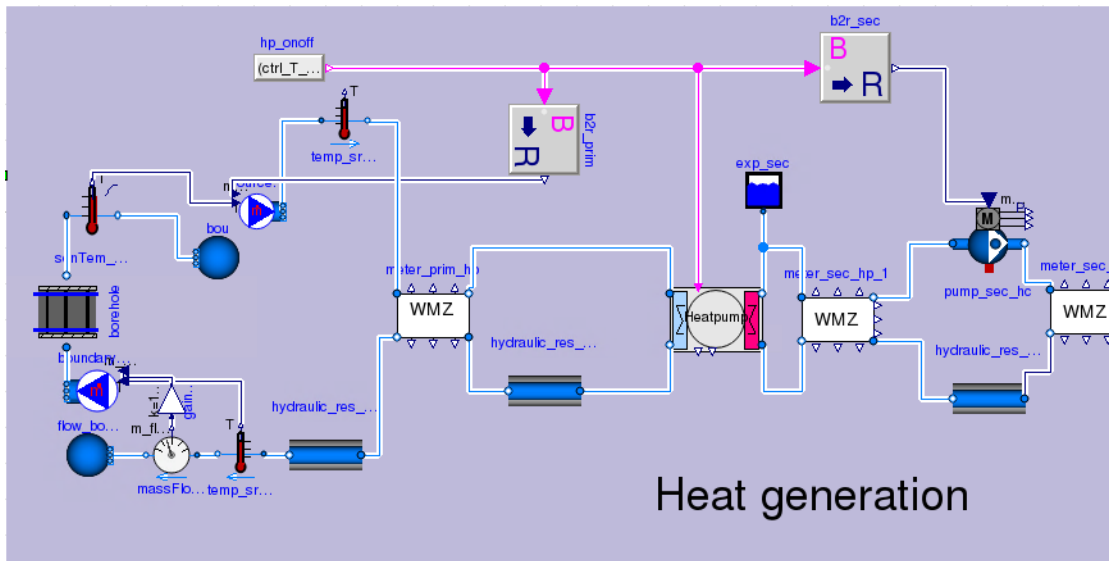


FIGURE 5.4.4. Implementation of GSHP in Dymola/Modelica

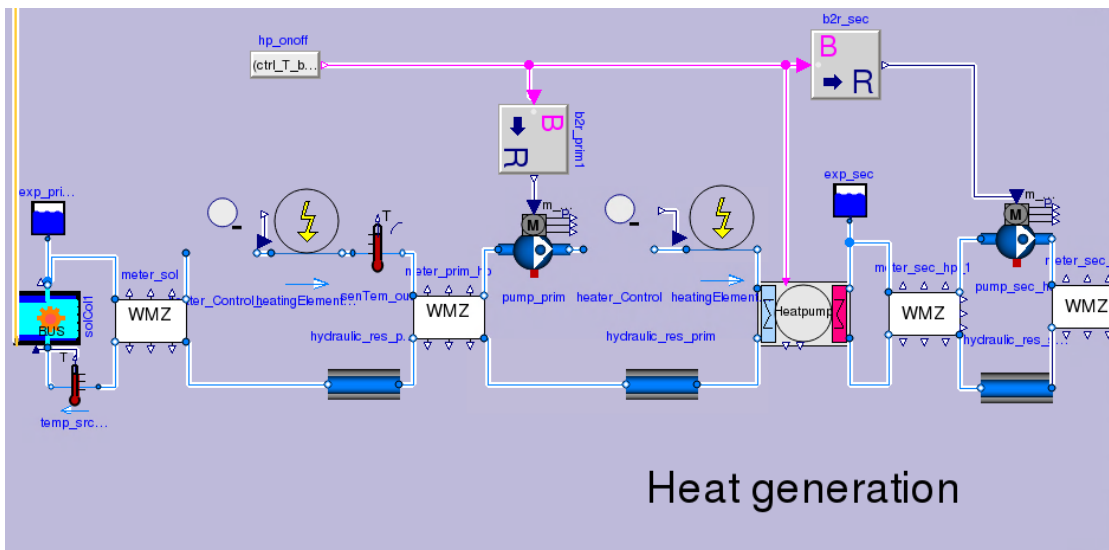


FIGURE 5.4.5. Implementation of solar direct system in Dymola/Modelica

#### 5.4.4. Borehole heat exchanger

The borehole heat exchanger is modeled with the *UTube* model of the *Buildings.lib*. The basis of this model approach is a scientific article by Bauer et al. in 2011 [7]. It is modeled as two double U pipes connected to a cylindrical ground model with the temperature of the undisturbed ground as the boundary condition. The heat transfer

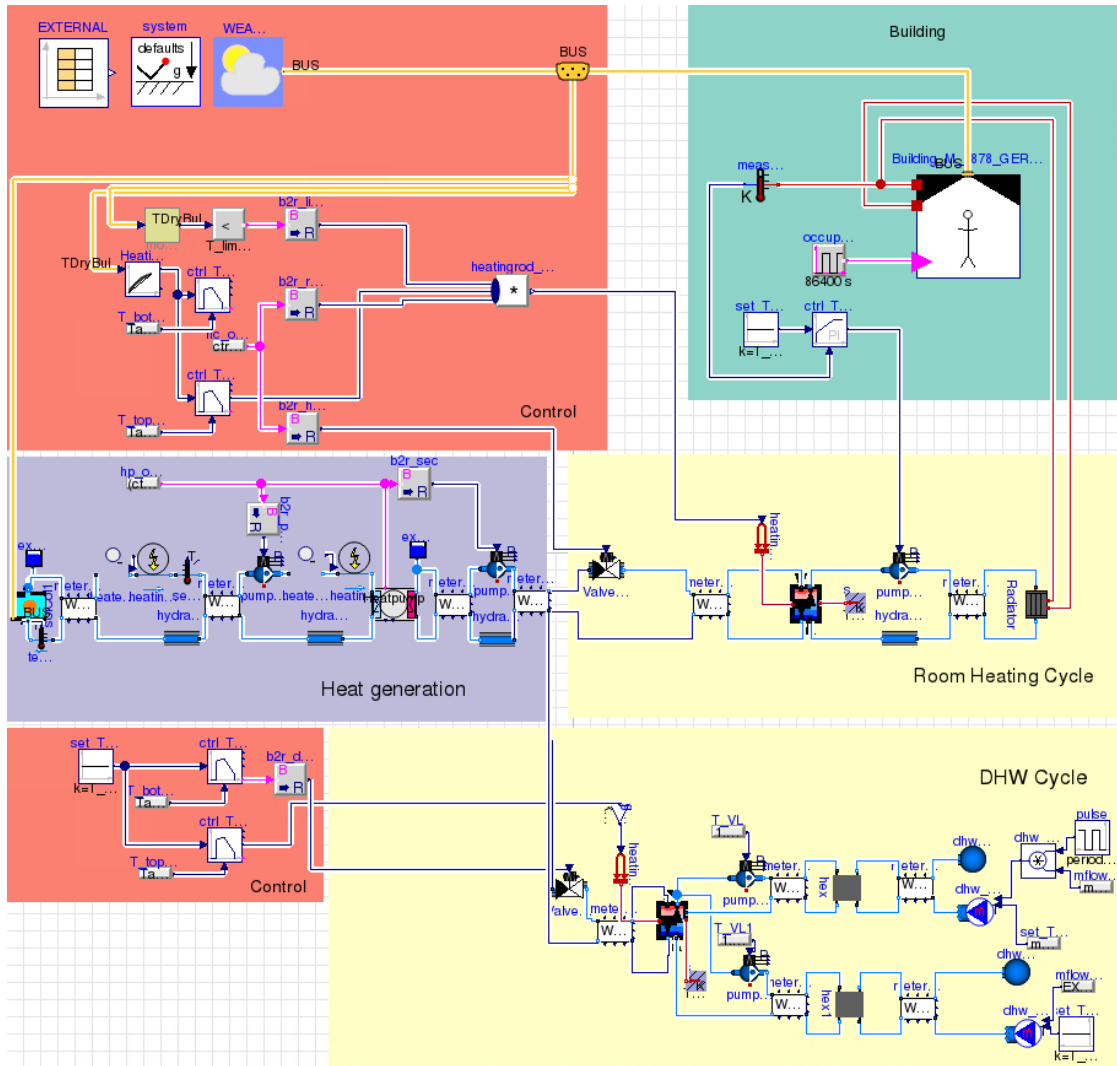


FIGURE 5.4.6. Implementation of a solar direct system (Col-Dir) in Dymola/Modelica

in the borehole is calculated using a convective heat transfer coefficient which depends on the flow velocity, the thermal resistance between the two pipes and the thermal resistance between the pipes, and the circumference of the borehole. In addition, the heat capacity of the fluid and the filling of the borehole is also taken into account. The initial far-field temperature  $\vartheta_{ext,start}$  at the outer radius of the cylindrical ground model  $r_{ext}$  is calculated as a function of depth  $z > 0$ . For the depth between 0 and  $z_0$ , the temperature is set to  $\vartheta_{ext,0,start}$ . For the temperature between  $z_0$  and the total depth of

the borehole  $h_{bor}$ , the following equation is applied:

$$(5.4.4) \quad \vartheta_{ext,start} = \vartheta_{ext,0,start} + (z_i - z_0) \cdot \Delta T/dz$$

with  $i \in \{1, \dots, n_{ver}\}$  and  $n_{ver}$  being the number of segments used for discretization in the vertical direction. The same equations apply to the backfill material. The gradient  $\Delta T/dz$  was set to 3 K per 100 m. The function *Buildings.Fluid.HeatExchangers.Ground.Boreholes.BaseClasses.temperatureDrop* is used to determine the temperature change. It calculates the temperature drop of the soil at the outer boundary of the cylinder and is based on the formula by Hart and Couvillion (1986).

The initial far-field temperature up to  $z_0 = 12$  m depth was set to 11 °C according to measurements for Potsdam by Potsdam Institute for Climate Impact Research<sup>7</sup> for the last five years. Older measurements show lower ground temperatures. The radius for the ground around the borehole  $r_{ext}$  was set to 4 m. The following properties were assumed for ground and fill material: density: 1.65 g/m<sup>3</sup>, specific heat capacity: 900 J K/kg, thermal conductivity: 2.35 W K/m.

The tube length was calculated with equation (5.4.5) according to VDI 4640 [157].

$$(5.4.5) \quad l_{probe} = \frac{\dot{Q}_{eva}}{n_{probe} \cdot P_{BHE}}$$

$$(5.4.6) \quad \dot{Q}_{eva} = \dot{Q}_{con} - P_{el}$$

The rated capacity of the evaporator  $\dot{Q}_{eva}$  was calculated to 12.7 kW with equation (5.4.6) and the specific heat extraction rate at turbulent flow  $P_{BHE}$  of the ground was assumed in accordance with VDI 4640 to 40 W/m. So, the required total borehole length was determined to be 317 m. This was divided into two probes with  $l_{probe} = 159$  m. The geometric parameters of the tubes were assumed as follows: radius of one tube 0.016 m, thermal conductivity of tube 0.4 W K/m, thickness of tube 0.003 m.

#### 5.4.5. Hot storages

Two hot storages are used in all configurations; one for space heating, one for domestic hot water.

The Buffer Storage Model with support for heating rods and two heating coils of the *AixLib* is used as is for the space heating storage (SH storage) and serves as the base model for the DHW storage.

The internal heat transfer was modeled with the function *AixLib.Fluid.Storage.BaseClasses.HeatTransferLambdaEffSmooth*, which models heat transfer with buoyancy and

<sup>7</sup><https://www.pik-potsdam.de/de/produkte/klima-wetter-potsdam/klimazeitreihen/bodentemperatur>

smoothing according to Viskanta et al. [159]. Both storages are equipped with a heating rod for peak loads and have no internal heat exchanger. The hot inlet from the heat pump and the outlet towards the radiator/freshwater station are situated on the top, and the cold inlet from the radiator/freshwater station and the outlet towards the heat pump at the bottom.

The DHW storage has an additional heat port for the circulation backflow.

According to Viessmann [158], the size of the storage tank for domestic hot water is determined based on the required domestic hot water during a reference period  $Q_{DHW,ref-period}$ . The data for  $Q_{DHW,ref-period}$  can be obtained from Viessmann [158] amongst others. For this work,  $Q_{DHW,ref-period}$  was assumed to be 24 kWh according to the upper range of the used load file for DHW. The design of the minimum storage tank size  $V_{stor,DHW,min}$  is based on the following formula with  $c_p$  being the specific heat capacity (1.36 Wh/(kg K) for water) and  $\vartheta_{water,cold}$  being the cold water inlet temperature (12°C was used). A supplement of 15% - 20% of the storage volume should be assumed for mixing-related non-usable storage. In the formula, this is considered by the factor 1.15.

$$(5.4.7) \quad V_{stor,DHW,min} = \frac{Q_{DHW,ref-period}}{c_p \cdot (\vartheta_{set} - \vartheta_{water,cold})} \cdot 1.15$$

The resulting  $V_{stor,DHW,min}$  of 494 l was rounded to 500 l for the simulations.

The size of the space heating storage can be dimensioned with a minimum volume  $v_{stor,HC,min}$  per kilowatt nominal capacity of the heat pump  $\dot{Q}_{HP,nom}$  according to equation (5.4.8).

$$(5.4.8) \quad V_{stor,HC} = \dot{Q}_{HP,nom} \cdot v_{stor,HC,min}$$

Viessmann recommends  $v_{stor,HC,min} = 201/\text{kW}$  for systems with radiators [158]. If there are mandatory off-times for the heat pump operation of about 2 h (for example required by a certain energy tariff), 601/kW is recommended. Considering the different sizes and types of heat pumps in this thesis, the storage volume was set to 1 m<sup>3</sup>. Variations with smaller SH storage sizes showed higher  $\text{SPF}_{HP,HC}$  but an increased need for auxiliary heat. This leads to lower values for  $\text{SPF}_{SYS}$ .

The settings for the relative heights of inlets and outlets, dimensioning of storage and heat exchanger area, insulation properties, and discretization of storage layers are summarized in table 5.4.1.



TABLE 5.4.1. Dimensions and parameter setting of hot storage tanks

Category	Unit	HC storage	DHW storage
Volume	[m <sup>3</sup> ]	1.0	0.5
Height	[m]	1.97	1.97
Diameter	[m]	0.8	0.8
Rel. height port inlet	[-]	1	1
Rel. height port outlet	[-]	0	0
Rel. height port circulation	[-]	0	0.5
Rel. height heating rod	[-]	0.8	0.8
Rel. height sensor top	[-]	0.8	0.8
Rel. height sensor bottom	[-]	0.2	0.2
Thickness insulation	[m]	0.12	0.12
Thermal conductivity insulation	[W/(m K)]	0.045	0.045
Number of tank segments	[-]	10	10

#### 5.4.6. Heat distribution

The heat from the space heating storage is transferred from the IBPSA library to the building model with a radiator model. The exponent for the heat transfer was set to 1.2.

#### 5.4.7. Control

##### 5.4.7.1. Room Temperature

The required supply temperature for the radiator is controlled with the Modelica components *PIDHysteresisTimer* in PI modus and *HotWaterTemperatureReset* of the *Buildings*-library. The component *HotWaterTemperatureReset* calculates the actual required supply temperature similar to the calculation of the heating curve in equation (5.4.2) dependent on the outside temperature  $\vartheta_{amb}$ , the heating exponent, the maximum supply temperature  $\vartheta_{HC, supply, max}$ , and the required room temperature  $\vartheta_{room}$ . This temperature is compared to the storage temperature at the bottom sensor. If necessary, the heat pump is activated via the PI controller with a hysteresis of  $\pm 1$  K. If the temperature at the top sensor cannot be met, the auxiliary heater is activated with a hysteresis of  $\pm 2.5$  K. The nominal and maximum supply temperature was set to 45 °C,

the nominal return temperature to 38 °C and the room temperature  $\vartheta_{room}$  to 20 °C. The heating period is active if the average of the last 72 h is below the heating limit temperature  $\vartheta_{limit,heating}$  of 15 °C.

#### 5.4.7.2. DHW Temperature

Drinking water systems in Germany have to be designed in accordance with the technical measures in working sheet W551 of DVGW<sup>8</sup> [31]. This rule was implemented as protection against the growth of Legionella. Legionella can be harmful to humans, and they grow most easily between 30 °C and 45 °C. In systems with circulation, the temperature at the top of the storage and at the outlet towards the circulation pipes has to be 60 °C or above, according to DVGW [31]. A PI controller ensures this temperature is between 60 °C and 62 °C. If the required temperature is not met, the auxiliary heater is activated until a temperature of 63 °C is reached.

The heat pump has a DHW priority, so the space heating storage is supplied only if no DHW demand occurs.

#### 5.4.7.3. Evaporator Inlet Temperature

As described in section 5.4.3 the temperature limits of the heat pump have to be respected. No special measures need to be taken for the reference systems.

In the case of solar systems, a distinction in control mechanisms must be made between systems with ice storage tanks and those without.

### Col-Dir systems

If there is no ice storage, the temperature at the evaporator inlet may be below the allowed temperature  $\vartheta_{min,eva}$  at low outdoor temperatures and with no or too little solar radiation. In this case, either the heat pump must be switched off or the collector outlet temperature must be preheated to such an extent that the permitted minimum temperature at the evaporator inlet is reached.

In her master's thesis [1], Alibas developed a control mechanism that ensures a minimum temperature via a heating element and heater control. Within the heater control, the enthalpy of a reference flow at  $\vartheta_{min,eva}$  is compared to the enthalpy of the actual flow. If the actual flows' enthalpy is lower than the enthalpy of the reference flow, the absolute difference is added to the flow by the downstream heating element. More detailed information about the functionality of the two control units can be found in Alibas' master's thesis [1].

---

<sup>8</sup>Deutscher Verein des Gas- und Wasserfaches e. V. (Engl.: German Association of the Gas and Water Industry)

Furthermore, Alibas [1] showed that preheating the evaporator inlet temperature is favorable compared to switching-off the heat pump. Her simulations showed that the auxiliary heat to ensure the required temperature in the storage exceeded the auxiliary heat needed for preheating. So, Alibas' control mechanism was also used for the simulation in this work. The minimum temperature,  $\vartheta_{min,eva}$ , was set to  $-10^{\circ}\text{C}$ .

The upper boundary temperature,  $\vartheta_{max,eva}$ , is set to  $20^{\circ}\text{C}$  for the heat pump evaporator. Alibas [1] implemented this via a mixing valve and a PID controller like it could be done in reality. For the simulation in this work, this implementation caused instability problems. Therefore, the control unit for preheating was adapted for cooling. If the collector output temperature exceeds  $\vartheta_{max,eva}$ , the absolute difference of the enthalpy flows is subtracted from the flow of the downstream cooling element. With this model, the excess energy above  $\vartheta_{max,eva}$  can be quantified, but not used. This cooling element model was used as a workaround for the unstable mixing valve with the PID controller to ensure the maximum evaporator inlet temperature  $\vartheta_{max,eva}$ .

If the collector output temperature was not limited in the simulations, the COP would be higher as the Modelica model extrapolates the heat pump's data. As the times of collector temperatures above  $\vartheta_{max,eva}$  occur mainly in summertime when the heat pump only serves domestic hot water, the simulation error of not limiting the evaporator inlet temperature was found to be very small in this case.

### Col-Ice systems

If there is an ice storage tank large enough to ensure a year-round minimum temperature at the evaporator of approximately  $0^{\circ}\text{C}$ , no measures need to be taken to ensure the minimum evaporator inlet temperature.

The ice storage is only loaded up to the maximum evaporator temperature. So, the heat pump uses the ice storage as a source if the collector output temperature is too high.

If the mean collector temperature is at least 4K above the temperature of the ice storage and the heat pump is not in operation, the ice storage is loaded.

## 5.5. Results of energy simulations and discussion

### 5.5.1. Performance figures

To be able to compare the different systems considered within this work, the system performance factors  $\text{SPF}_{SYS,1}$  or  $\text{SPF}_{SYS,2}$  can be used as explained at the beginning of this chapter. The definitions used in this thesis differ slightly from the initially given

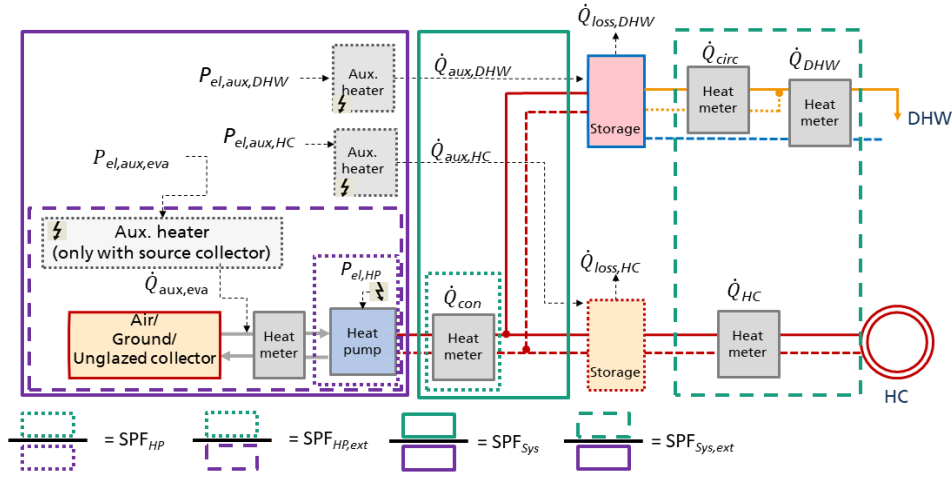


FIGURE 5.5.1. System schematic of monoenergetic systems (GSHP, ASHP, and Col-Dir) based on a schematic representation work developed in the project “LowEx im Bestand”. Frames indicate the calculation of the different seasonal performance factors following equations (5.1.5), (5.5.1), (5.5.3) and (5.5.5).

definitions as described in the following. A visualization of the used SPF values is given in figure 5.5.1

As the storage size is kept constant in this work, the system performance factor is defined according to the definition of  $SPF_{SYS,1}$  (see equation (5.1.6)) as follows:

$$(5.5.1) \quad SPF_{SYS} = \frac{\int (\dot{Q}_{con} + \dot{Q}_{aux,HC} + \dot{Q}_{aux,DHW}) dt}{\int P_{el,tot} dt}$$

with

$$(5.5.2) \quad P_{el,tot} = P_{el,HP} + P_{el,aux,HC} + P_{el,aux,DHW} + P_{el,aux,eva}$$

For means of comparability also a definition accounting for the storage losses according to equation (5.5.3) following the definition of  $SPF_{SYS,2}$  was used.

$$(5.5.3) \quad SPF_{SYS,ext} = \frac{\int (\dot{Q}_{HC} + \dot{Q}_{DHW} + \dot{Q}_{circ}) dt}{\int P_{el,tot} dt}$$

with

$$(5.5.4) \quad P_{el,tot} = P_{el,HP} + P_{el,aux,HC} + P_{el,aux,DHW} + P_{el,aux,eva}$$

A more accurate comparison would also include the necessary power for the different pumps and control devices. Usually, the power consumption of the pumps and control devices is low, and therefore the resulting error is relatively small if this energy is neglected. In the case of a drainback system, the required power can be higher. As explained in section 4.2.2.3, the pressure loss of *TABSOLAR*<sup>®</sup> collectors is not trivial to guess, and measurements do not yet exist. So, the uncertainty in calculating of the required pump power would be high.

As explained, the Col-Dir systems need additional auxiliary heating at the source side of the heat pump to meet the operational temperature limits of the heat pump. This additional power is considered necessary for the heat pump's operation. The  $SPF_{HP}$  was therefore extended to  $SPF_{HP,ext}$ , according to equation (5.5.5).

$$(5.5.5) \quad SPF_{HP,ext} = \frac{\int \dot{Q}_{con} dt}{\int P_{el,tot} dt}$$

with

$$(5.5.6) \quad P_{el,tot} = P_{el,HP} + P_{el,aux,eva}$$

Like explained in the beginning, the performance of the heat pumps depends very strongly on the source and sink temperatures. In order to compare different systems with each other, it is therefore helpful to compare the temperatures that occur in each case. For this purpose, the mean temperatures weighted with the condenser capacity were determined according to the following equation:

$$(5.5.7) \quad \vartheta_{av,w} = \frac{\int (\dot{Q}_{con} \cdot \vartheta) dt}{\int \dot{Q}_{con} dt}$$

### 5.5.2. Test solar direct systems “Col-Dir area and wind influence”

#### Setup

In a first step, the Col-Dir system was compared to the reference systems. To identify reasonable system sizes, variations of the collector area were assumed. The collector

area was referenced to  $\dot{Q}_{demand,biv}$ , which was 17.6 kW, so, the total area was varied from 34.6 m<sup>2</sup> to 156.6 m<sup>2</sup>. The first corresponds to 2 m<sup>2</sup>/kW, which was assumed as a lower limit; the latter corresponds to the total opaque area of the south façade where the collectors were positioned.

Two unglazed UHPC collector types and one unglazed, spectrally selective, uninsulated stainless steel reference collector were simulated. The first UHPC collector is a pure gray-colored absorber without insulation referred to as “Col1”. The second UHPC collector has a spectrally selective coating and back insulation and is referred to as “Col2”. The reference collector is referred to as “ColRef”. The used parameters are described in table 4.3.2.

As the collector’s efficiency is very sensitive to wind speed, a variety of wind speeds was conducted, too. The wind speed in the weather data is measured at the height of 10 m, but in urban environments, the wind speed might differ. It can be higher if local conditions concentrate the wind flow, but generally, wind speeds are lower. In wind-protected areas, wind speed can even tend to zero. So the area variation was conducted with the wind correction factors ( $wcf$ ) of 1, 0.5, and 0. The area variation for “ColRef” was only conducted for  $wcf = 0.5$ .

## Results

Figure 5.5.2 shows the results of  $SPF_{HP}$  (top, left),  $SPF_{HP,ext}$  (top, right),  $SPF_{SYS}$  (bottom, left), and  $SPF_{SYS,ext}$  (bottom, right) for direct solar systems in comparison to the reference systems. The respective results for the “ColRef” are shown in figure 5.5.8 for better clarity.

Considering only  $SPF_{HP}$ , it can be said that all Col-Dir systems have higher values than ASHP 1 and only some systems have lower values than ASHP 2 at low square meters. However, the GSHP is always better. Within the Col-Dir systems, the systems with the gray, uninsulated collector always perform better than the systems with the insulated collector with spectrally selective coating. Systems with the wind correction factor  $wcf$  of 1 perform better than systems with  $wcf$  of 0.5 or 0. However, in the consideration of  $SPF_{HP}$ , the difference between the Col-Dir systems are not significant. The differences between the spectrally selective collector without wind and the gray, uninsulated collector at full wind velocity lay between 0.16 and 0.24 points of  $SPF_{HP}$  or 4% to 7%.

Comparing  $SPF_{HP}$  and  $SPF_{HP,ext}$  highlights the considerable influence of the auxiliary heater that raises the collector outlet temperature to the permissible temperature

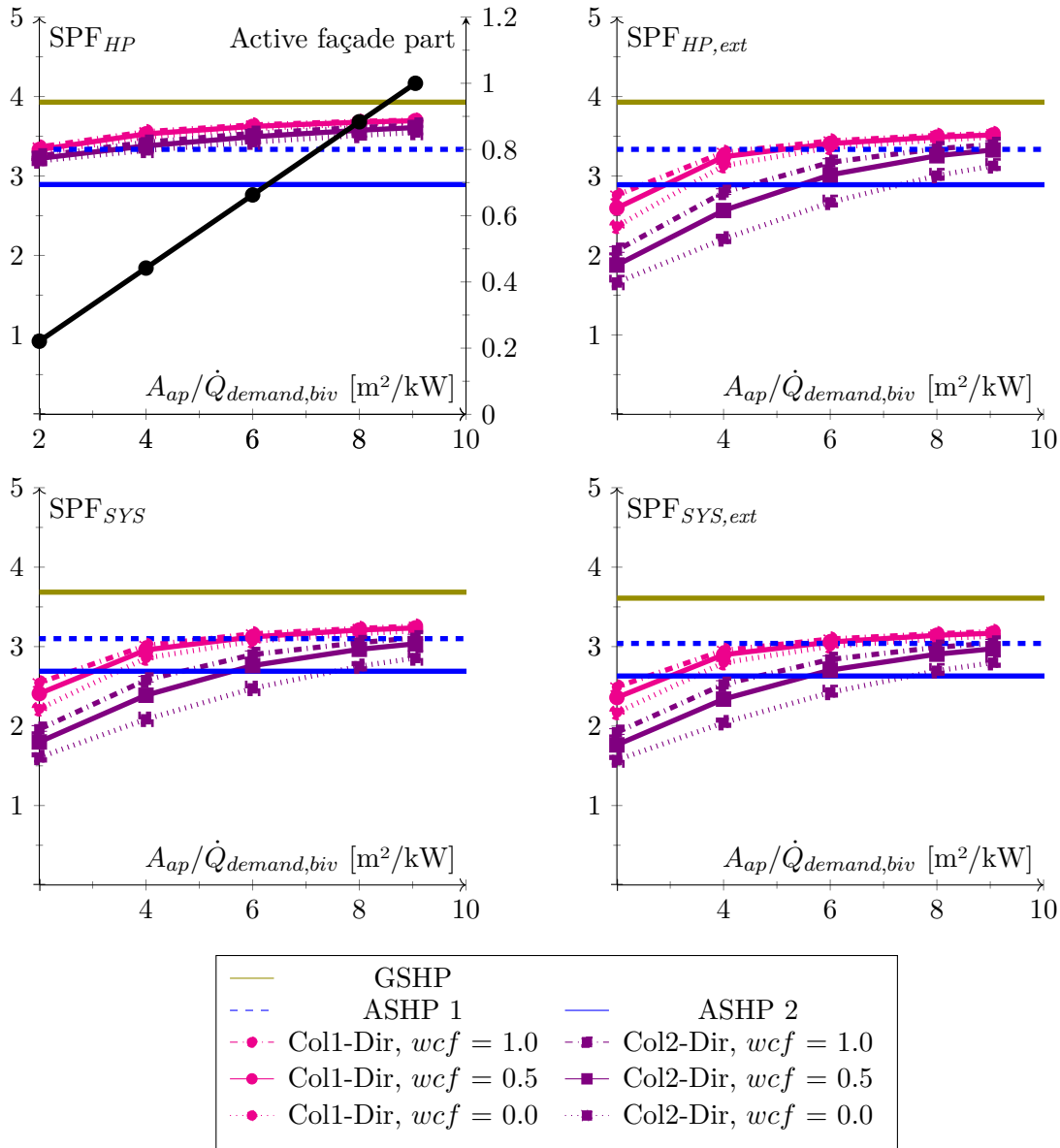


FIGURE 5.5.2. Seasonal performance factors  $SPF_{HP}$ ,  $SPF_{HP,ext}$ ,  $SPF_{SYS}$ , and  $SPF_{SYS,ext}$  of reference systems and direct solar systems for different aperture areas  $A_{ap}$  with respect to the heat demand for heating and hot water in bivalent point  $\dot{Q}_{demand,biv}$  and different wind correction factors ( $wcf$ ). The first plot shows the part of the south façade covered by the collector (black) on the right axis.

range: while the  $SPF_{HP}$  curves of the Col-Dir systems are still quite close together, the  $SPF_{HP,ext}$  curves spread out considerably further.

These large differences will disappear if the system is operated above the minimum evaporator inlet temperatures, for example, in climates with milder winters. For colder regions, heat pumps with a lower evaporator inlet temperature could be used.

The appearance of the  $SPF_{HP,ext}$  curves very much resembles the curves of  $SPF_{SYS}$  and  $SPF_{SYS,ext}$ . So, the auxiliary heat at the hot side of the heat pump and the storage losses have very little influence on the distances between the curves.

All  $SPF$  values of ColRef-Dir lie in between Col1-Dir and Col2-Dir; see figure 5.5.8. Due to the full-flow aperture area, the entire surface of ColRef can be used, and the margin losses are relatively small. ColRef has two corrugated plates on its backside, and thus the gains via the rear side in operation under ambient temperature are lower than those of Col1 but higher than those of the insulated Col2. The collector is, therefore, more efficient per aperture area than Col2. Thus, it is well explainable why this collector lies between Col1 and Col2.

The gains and losses were summarized to better understand the contribution of the different gains within the collector. The collector model calculates the energy according to equation (4.1.4) as explained in the beginning. Equation (5.5.8) points out only the evaluated terms. The respective terms of the convectional and solar gains and losses and the gains and losses due to capacitive effects are colored following the gain colors in figure 5.5.3.

$$(5.5.8) \quad \frac{\dot{Q}_{useful}}{A_{ap}} = \eta_0 \cdot (K_{\theta,b}(\theta) \cdot G_b + K_{\theta,d}(\theta) \cdot G_d) - c_6 \cdot u \cdot G - c_1 \cdot (\vartheta_{fluid,m} - \vartheta_{amb}) - c_3 \cdot u \cdot (\vartheta_{fluid,m} - \vartheta_{amb}) - c_5 \cdot \frac{dT_m}{dt}$$

This was done for the temperature difference  $\vartheta_{fluid,m} - \vartheta_{amb}$  in intervals of 2.5 K in figure 5.5.3.

This evaluation shows that the peak of the gains occurs when the collector temperature is 5 K to 2.5 K below the ambient temperature. The gains are dominated by the convectional gains (66%). The pure solar gains contribute only 3% within this interval. Throughout all intervals, convectional gains also dominate with a share of 48% of the total annual gains (357 kWh/m<sup>2</sup>). Solar gains contribute with an annual share of 18%, and capacitive effects have an annual share of 34%.

As the gains through capacity effects occur if the collector temperature is cooled down, at least the part to the right of the y-axis is due to solar radiation and could be added to the solar gains. On the left side of the y-axis, when the mean collector



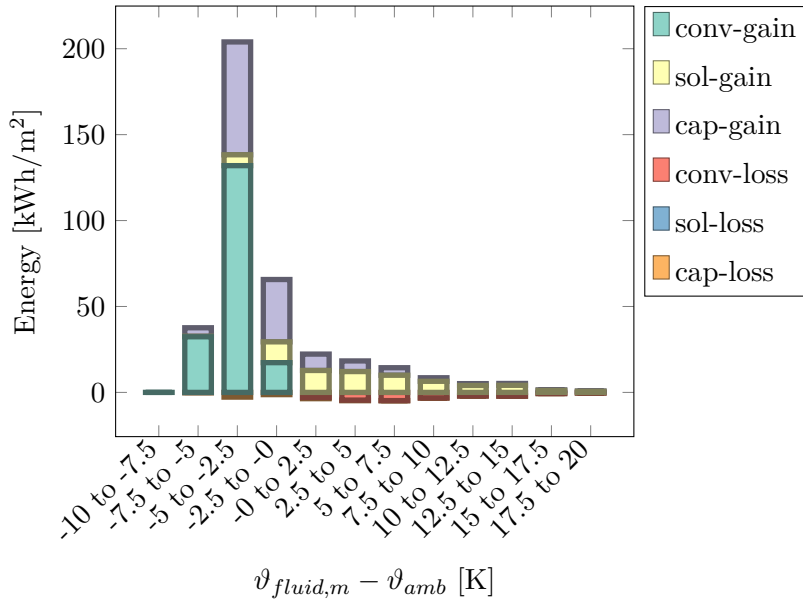


FIGURE 5.5.3. Proportions of different energy flows of the solar collectors (gray, NoInsu) with respect to the occurring temperature range  $\vartheta_{fluid,m} - \vartheta_{amb}$  within the operation of the Col-Dir system with  $A_{ap}/\dot{Q}_{demand,biv} = 6 \text{ m}^2/\text{kW}$  and  $wcf = 0.5$ .

temperature is below the ambient temperature, the gains from a solar-heated collector might still be present but cannot be separated from the heating through ambient.

Figure A.6, figure A.8 and figure A.7 in appendix A show the monthly and yearly average temperatures at the evaporator inlet and outlet and the condenser inlet and outlet of the reference systems. Figure A.9 in appendix A shows the same for a Col-Dir system with the gray, uninsulated collector ( $A_{ap}/\dot{Q}_{demand,biv} = 6 \text{ m}^2/\text{kW}$ ,  $wcf = 0.5$ ) and table A.10 reports all energy flows of these systems.

### 5.5.3. Test solar direct systems “Col-Dir north façade”

#### Motivation

As seen in figure 5.5.3, direct solar gains are relatively low compared to convective gains and gains from capacitive effects. This fact plays an important role when balancing system effectiveness and architectural design freedom. Conventional solar systems installed in the northern hemisphere deliver the highest gains when orientated towards the south with an optimal inclination depending on the latitude. However, if collectors serve

as ambient heat exchangers instead, orientation towards the sun becomes less critical and installations may even make sense on the north façade.

## Setup

The next test evaluates  $SPF_{SYS}$  of the gray, uninsulated collector installed on the north façade. For the test, solar irradiation was switched off completely, so even minor gains that might occur on the north façade were neglected. This is the same scenario as if the façade was fully shaded.

## Results

Figure 5.5.4 shows that the difference between the two façades is very small. The values of  $SPF_{SYS}$  differ only by about 0.1, or 2% to 3%.

Figure 5.5.5 shows the average monthly weighted evaporator inlet temperatures with  $A_{ap}/Q_{demand,biv} = 6 \text{ m}^2/\text{kW}$ . Mean temperatures are about 1 K lower on the north façade.

Following Haller et al. [6], a decrease of the temperature difference between the evaporation and the condensation by 1 K leads to about 2% to 3% COP increase under typical operating conditions. This corresponds very well with the outcome of this test.

The result clearly shows that collectors within such system configurations without any storage on the source side of the heat pump are mainly ambient-air heat exchangers and the improvements due to solar irradiation are almost negligible. From an architectural point of view, this extends possible installation areas to all building façades. The south façade can be used for PV or solar thermal collectors that work at higher operating temperatures and directly feed the hot storages.

### 5.5.4. Test solar direct systems “Col-Dir store-hot”

#### Motivation and setup

The previous test showed that the solar collectors without storage mostly work as ambient heat exchangers.

As said in the beginning, in principle, solar irradiation could increase the evaporator inlet temperature and thereby increase the efficiency of the heat pump.

One idea to increase solar gains could be to shift the operating time of the heat pump to times when irradiation occurs. Irradiation would increase the storage temperature and would, thus, lead to increased gains.

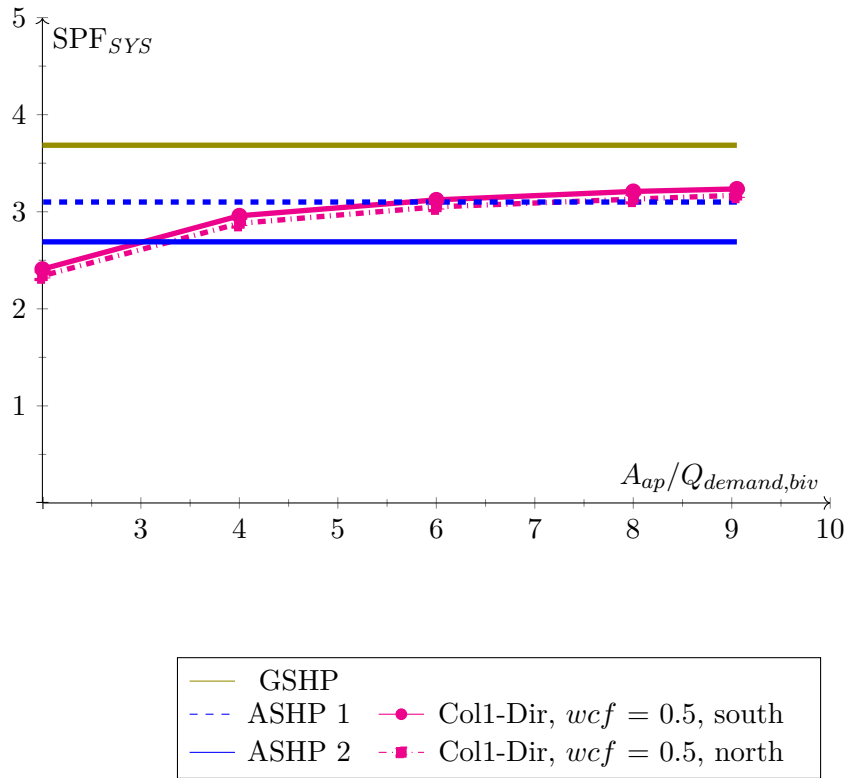


FIGURE 5.5.4. Seasonal performance factors  $SPF_{SYS}$  of reference systems and solar direct systems for different aperture areas  $A_{ap}$  with respect to the heat demand for heating and hot water in bivalent point  $Q_{demand,biv} = Q_{demand,biv,heating+DHW}$  and different wind correction factors ( $wcf$ ).

The following must still be considered: a shift in the condenser temperature causes decreases in the COP of the heat pump. If the condenser temperature is changed by 1 K, the evaporator temperature should be increased by 2 K to achieve a 2% to 3% increase of the COP under typical operating conditions.

Such a shift in operating hours could also be interesting from another point of view: related to the energy system and the fluctuating residual loads. The residual loads, which are still covered by fossil energy, are high in times of no irradiation and no wind. They could be reduced if the operating times of heat pump systems could be shifted to times with low residual loads. Shifting energy by means of heat pump systems was investigated by D. Fischer [50], amongst others. Fischer compared different shifting strategies such as switching off the heat pump until certain comfort criteria cannot be met anymore, forced on strategy, overheating the storage with the heat pump, and overheating the storage with the heat pump and the auxiliary heater. Based on a vast pool of different heat

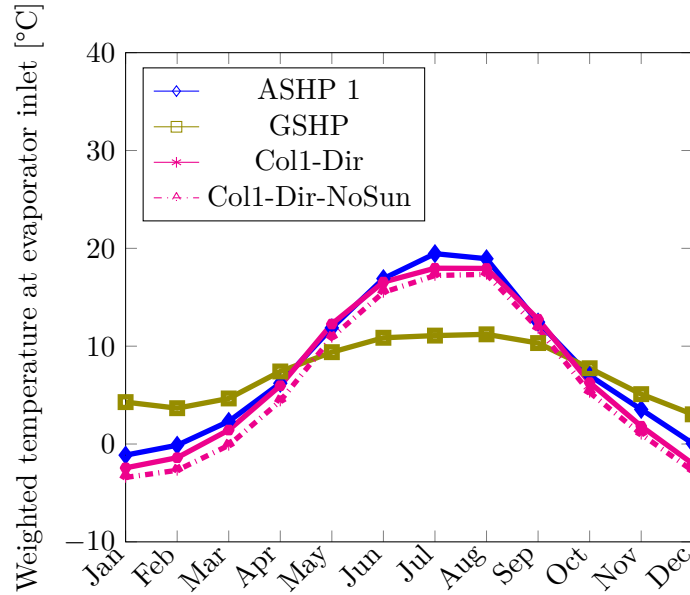


FIGURE 5.5.5. Temperature at evaporator inlet for the reference systems and the south and north installation ( $A_{ap}/\dot{Q}_{demand,biv} = 6 \text{ m}^2/\text{kW}$ ,  $wcf = 0.5$ ), monthly weighted averages.

pumps and buildings, he found that the absolute relationship between energy used by discharging and the energy required for charging was below one for all strategies except the switching off strategy. The more energy was shifted, the lower this relationship was. For the switching off strategy, this relationship was slightly above one for very short shifting times. Long shifting times ( $> 15 \text{ min}$ ) did not occur as the specified comfort criteria did not allow them.

Knotzer et al. [90] also investigated the energy flexibility of buildings and storage. They found that the final energy consumption increased due to the deviation from the “optimal” heating system operation and load shifting by around 2% to 5%. But due to different residual loads, in many cases, the  $\text{CO}_2$  emissions broken down to the consumption time was lower anyways.

Both the investigation by Fischer and by Knotzer show that with load shifting, a decrease in system efficiency seems inevitable for standard heat pump systems. But the investigation by Knotzer showed that it can still be advantageous in terms of  $\text{CO}_2$  emissions with the current electricity mix.

An additional advantage of shifting the operating hours is increasing the possible self-consumption of PV electricity. Ultimately, PV electricity (own or from the grid) is stored in the same way. So it could be useful to operate the heat pump during times

of high irradiation even if the  $SPF_{SYS}$  is lower if the  $CO_2$  emissions of the total energy used are lower.

For this test, the Col-Dir system control was changed to increase the specified heating storage temperature by 1 K when irradiation on the collector surface is above  $200 \text{ W/m}^2$  and the collector temperature above  $-5 \text{ }^\circ\text{C}$ .

## Results

Figure 5.5.6 compares  $SPF_{HP,ext}$  and  $SPF_{SYS}$ . Both are slightly lower with the “store-hot” strategy, which is consistent with the results of Fischer and Knotzer et al.. Future comparisons of load shifting with a Sol-Dir system to a system with an ASHP or GSHP can show if efficiency reductions are similar or lower.

Contrary to the assumption that the evaporator inlet temperature would increase, it slightly decreased on average (about 0.05 K decrease on a yearly average, figure 5.5.7, even if it increases in some months). This might be because of increased demand in times in which the heat pump would usually not operate. Further system variations should prove if this result is robust with other weather and load conditions. Nevertheless, even if there is no efficiency gain, this could be an optional control setting, and the overheating of the storage can even be higher to shift more load.

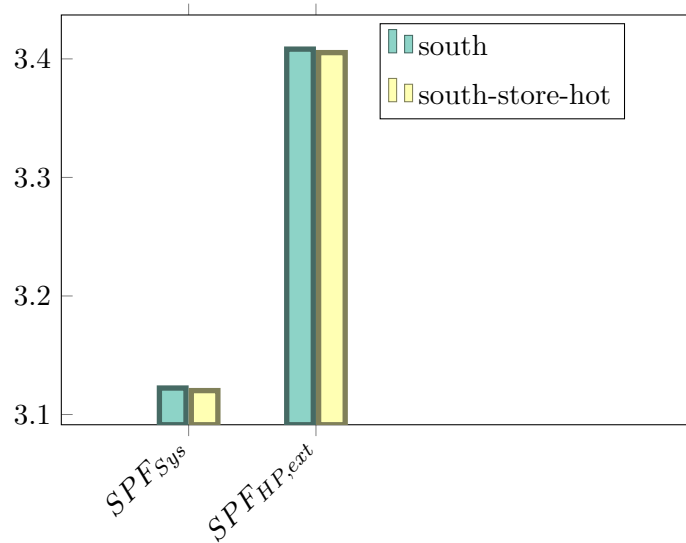


FIGURE 5.5.6. Comparison of an installation of the gray, uninsulated collector on the south façade with and without the store-hot condition ( $A_{ap}/\dot{Q}_{demand,biv} = 6 \text{ m}^2/\text{kW}$ ,  $wcf = 0.5$ )

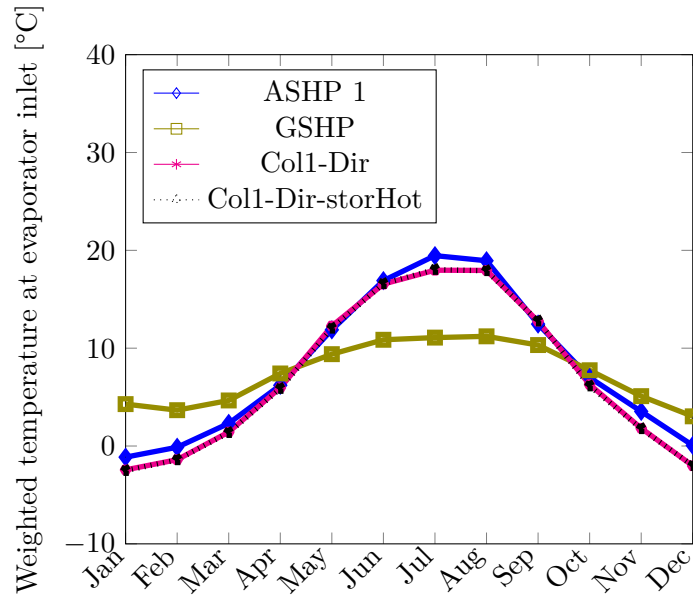


FIGURE 5.5.7. Temperature at evaporator inlet for the reference systems and the Col1-Dir system with and without the store-hot condition ( $A_{ap}/\dot{Q}_{demand,biv} = 6 \text{ m}^2/\text{kW}$ ,  $wcf = 0.5$ ), monthly weighted averages.

### 5.5.5. Test solar ice systems “Col-Ice south and north façade”

#### Motivation

Two factors lead to the system configuration of solar collectors with ice storage: On the one hand, there is a practical reason resulting from the UHPC collector design. As initially said, it has not been proven yet that the UHPC collector can be completely tight against the diffusion of antifreeze or water vapor. So, if the collectors were be operated without antifreeze, they could only be operated above  $0^\circ\text{C}$ . Besides these possible constructional reasons for water as a heat carrier, a decision for water can bring other benefits: costs for the heat carrier and its maintenance are lower, and recycling is far easier and not harmful to the environment. So, water as a heat carrier could be an interesting option independently of the collector type. If Col-Dir systems with water were be used, the auxiliary heat in times of ambient temperatures below  $0^\circ\text{C}$  would be immense. If solar energy can be stored, this energy can be used for feeding the heat pump in these times.

Another motivation is increased efficiency due to higher evaporator inlet temperatures. In times of solar irradiation, the ice storage can be regenerated. Solar energy generation can be shifted to times when it can be used.

If the storage on the cold side is connected to the soil, ground heat serves as a second source for the heat pump. This case was not considered in this work.

### Setup

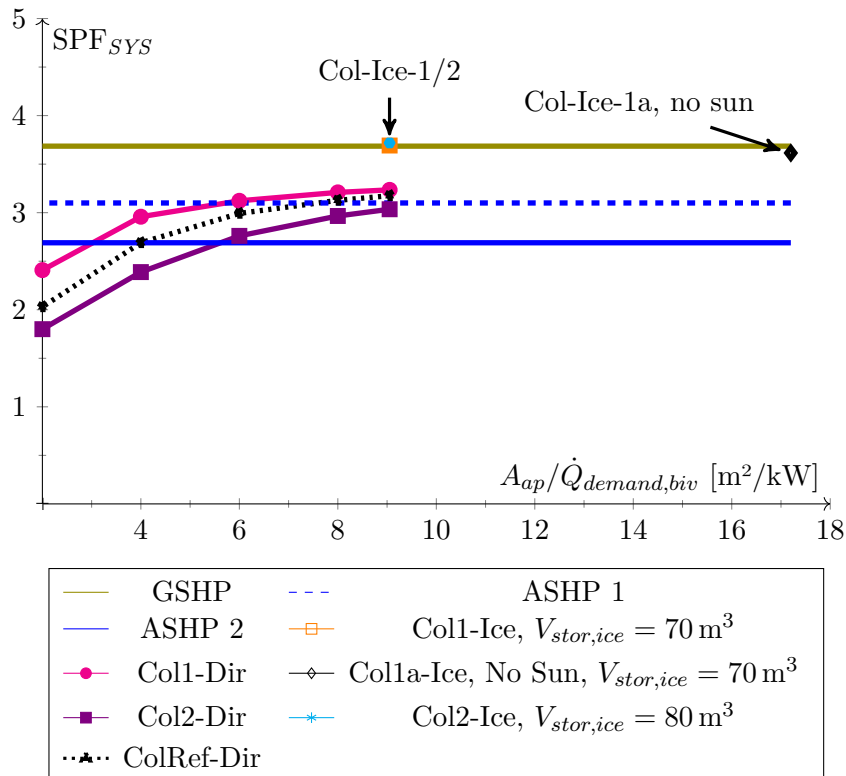


FIGURE 5.5.8. Seasonal performance factor  $SPF_{SYS}$  of reference systems, Col-Dir systems for different ratios  $A_{ap}/\dot{Q}_{demand,biv}$  ( $wcf = 0.5$ ) and different Col-Ice systems.

All Col-Ice systems are dimensioned for a minimum evaporator inlet temperature of  $0^{\circ}\text{C}$ . This means that the collectors can always be operated at temperatures above  $0^{\circ}\text{C}$ , and water without antifreeze can be used as heat transfer fluid in the collector. A particular safety distance in the temperature control should be considered so that the whole circuit does not fall below  $0^{\circ}\text{C}$ . If this configuration were built in an actual installation, an additional heat exchanger would be needed if the collectors were to be

used directly by the heat pump because a heat carrier with antifreeze is required in the heat pump circuit.

The condition of a minimum evaporator inlet temperature of  $0^{\circ}\text{C}$  requires a matching relation between the size of the ice storage and the collector area. The storage must never freeze completely. If long periods with air temperatures far below  $0^{\circ}\text{C}$  occur and only stored solar energy can be used for the heat pump, the storage must be large enough to remain in the latent storage phase. If the storage would be unloaded in a sensible mode below  $0^{\circ}\text{C}$ , the temperature can drop to temperatures below the minimum evaporator inlet temperature very quickly, and the heat pump would have to be switched off.

In the case considered here, the aperture area was set to the area of the whole south façade, and the sizes of the storages were derived in an iterative process to have the same ice storage temperature at the beginning and the end of the year. Smaller aperture areas are also possible but require larger ice storages to fulfill the condition of a minimum evaporator inlet temperature of  $0^{\circ}\text{C}$ . With Col1, a storage size of  $V_{stor,ice} = 70\text{ m}^3$  was found; with Col2, a slightly larger storage with  $V_{stor,ice} = 80\text{ m}^3$  was needed. It has to be kept in mind that the ice storage model was simulated adiabatically and no gains through the walls were considered. Actual storage sizes could be smaller depending on the amount of additional gains.

Another experiment was made to determine the minimum collector area installed on the north façade to guarantee a minimum evaporator temperature of  $0^{\circ}\text{C}$  with a storage volume of  $V_{stor,ice} = 70\text{ m}^3$ .

## Results

Figure 5.5.8 shows  $\text{SPF}_{SYS}$  of the reference systems, different Col-Dir systems, and three Col-Ice systems. The values of  $\text{SPF}_{SYS}$  compared to  $\text{SPF}_{HP}$ ,  $\text{SPF}_{HP,ext}$ , and  $\text{SPF}_{SYS,ext}$  can be seen in figure A.10.

The values for the Col2-Ice system with spectrally selective collector with back insulation are almost equal to the one with the gray, uninsulated collector. However, the systems differ in the volume of the storage. While the Col1-Ice system with the gray, uninsulated collector can guarantee a minimum evaporator temperature of  $0^{\circ}\text{C}$  with a storage volume of  $V_{stor,ice} = 70\text{ m}^3$ , the spectrally selective, insulated collector requires a volume of  $V_{stor,ice} = 80\text{ m}^3$  to fulfill the condition.

A Col1 installation on the north façade with  $V_{stor,ice} = 70\text{ m}^3$  leads to a significantly higher area: by increasing the area in steps of  $10\text{ m}^2$  an increase of 90% of the area was found necessary to fulfill this requirement.



Figure 5.5.9 depicts the weighted evaporator inlet temperature of both Col-Ice systems and the reference systems. Especially in transition periods, but also in wintertime, the evaporator inlet temperatures of the Col-Ice systems are higher than those of the ASHP systems. From March to November, they also exceed the evaporator inlet temperature in the GSHP system. The temperatures of the Col2-Ice80 system are higher than those of the Col1-Ice70 system in the transition periods. Both are higher than those of the GSHP system, which results in almost equal, but slightly higher  $SPF_{SYS}$  values.

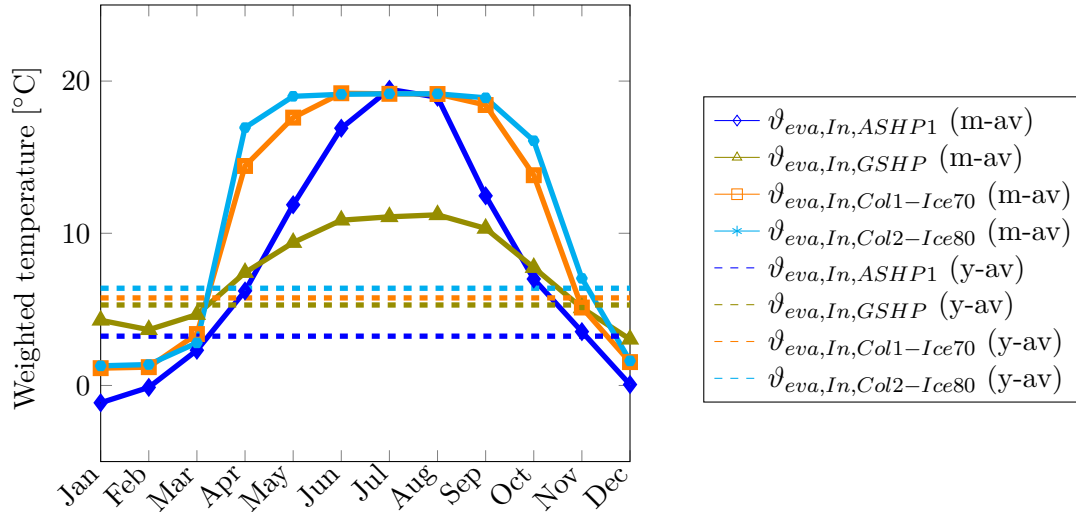


FIGURE 5.5.9. Temperature at evaporator inlet  $\vartheta_{eva,In}$  for reference systems and two Col-Ice systems: Col1-Ice70 has the gray, uninsulated collector, the Col2-Ice80 system is simulated with the spectrally selective, insulated collector ( $A_{ap}/\dot{Q}_{demand,biv} = 9.05$  and  $wcf = 0.5$ ), monthly (m-av) and yearly (y-av) averages.

Analyzing the different gains in the collector of the Col1-Ice70 system shows an entirely different picture compared to the Col-Dir system (figure 5.5.10). The peak is still in the same interval, and the distribution is more even. At 77%, the solar gains are the main contributor to the useful gain. Figure 5.5.11 illustrates the proportions of total useful energy flows for the Col1-Ice70 system. The highest share of useful energy is generated at collector temperatures below ambient temperatures.

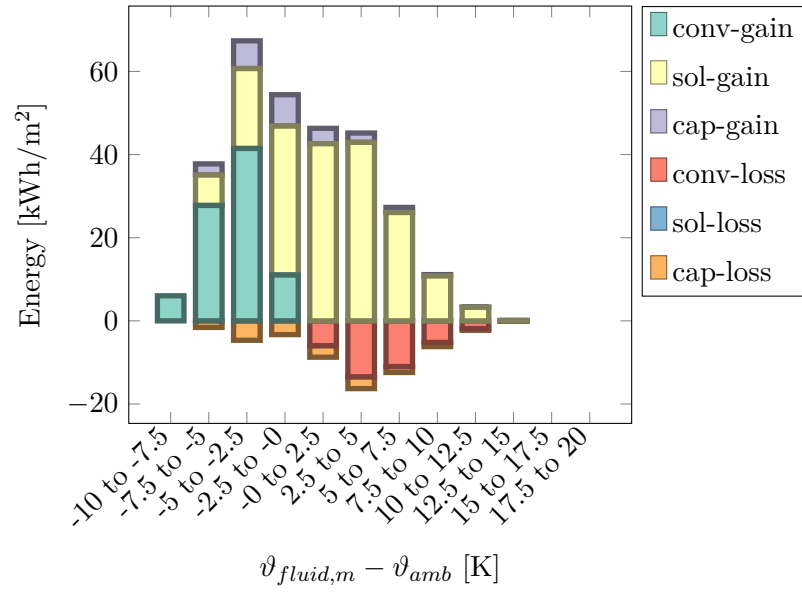


FIGURE 5.5.10. Proportions of different energy flows of the solar collectors (gray, NoInsu) with respect to the occurring temperature range  $\vartheta_{fluid,m} - \vartheta_{amb}$  in the operation of the Coll-Ice70 systems with  $A_{ap}/\dot{Q}_{demand,biv} = 9.05$  and  $wcf = 0.5$ .

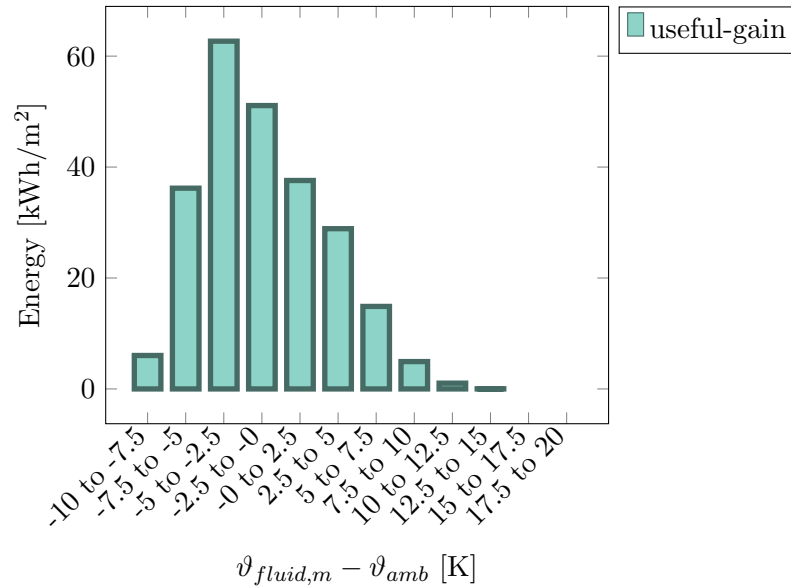


FIGURE 5.5.11. Proportions of total useful energy flows of the solar collectors (gray, NoInsu) with respect to the occurring temperature range  $\vartheta_{fluid,m} - \vartheta_{amb}$  in the operation of the Coll-Ice70 systems with  $A_{ap}/\dot{Q}_{demand,biv} = 9.05$  and  $wcf = 0.5$ .

### 5.6. Summary and discussion of results

In this chapter, two main system configurations with two unglazed variants of collectors made of ultra-high performance concrete (UHPC) for the renovation of a medium-size multi-family home in Potsdam were analyzed and compared to reference systems with air-source (ASHP) and ground-source (GSHP) heat pumps as well as to a technical reference with an unglazed, spectrally selective, stainless steel absorber as a source for a heat pump. In the Col-Dir and Col-Ice systems, the same heat pump was used as in the reference system with the GSHP. For the air source reference, two exemplary heat pumps with different performance data (ASHP 1 and ASHP 2) were selected and compared to indicate the wide variety of heat pump performance. A gray, uninsulated UHPC collector and a spectrally selective, insulated UHPC collector were compared in the simulations. Frost formation was not yet considered in this work.

Based on the assumptions made, the following results for the Col-Dir systems, the systems with collectors as the only source for the heat pump, can be summarized:

- Depending on the used area, Col-Dir systems can perform better than ASHP systems but do not reach the performance of the GSHP system. If the gray, uninsulated variant of the UHPC collector is used,  $SPF_{SYS}$  of the systems with  $6\text{ m}^2$  or more per  $1\text{ kW}$  of  $\dot{Q}_{demand,biv}$  exceeds the  $SPF_{SYS}$  of ASHP 1 and the system with  $4\text{ m}^2$  per  $1\text{ kW}$  of  $\dot{Q}_{demand,biv}$  still exceeds the  $SPF_{SYS}$  of ASHP 2. If spectrally selective, insulated collectors are used, only the system with  $9.05\text{ m}^2$  per  $1\text{ kW}$  of  $\dot{Q}_{demand,biv}$  (corresponding to the entire south façade of the considered building) and wind speeds as in  $10\text{ m}$  above ground (wind correction factor  $wcf=1$ ) exceeds the  $SPF_{SYS}$  of ASHP 1. The  $SPF_{SYS}$  of ASHP 2 can still be exceeded with  $4\text{ m}^2$  per  $1\text{ kW}$  of  $\dot{Q}_{demand,biv}$  and  $wcf$  1 and 0.5.
- Convective gains dominate the total gains. Increasing the collector's ability to use convective heat increases the performance of Col-Dir systems. Higher wind velocities increase convective heat transfer and lead to increased performance in Col-Dir systems.
- With the selected weather conditions of Potsdam and the chosen restrictions for the heat pump (minimum evaporator inlet temperature of  $-10^\circ\text{C}$ ), the auxiliary heat to meet the minimum evaporator temperature has a significant influence on system performance. Systems with lower convective gains need significantly more auxiliary heat on the source side.
- Solar gains are negligible in a Col-Dir system: an installation on the north façade shows only minor reductions in performance compared to an installation on the south façade.

- Increasing storage temperature in times of irradiation above  $200 \text{ W/m}^2$  does not increase efficiency in the considered case but can be used for load management.

The results of the simulations with the Col-Ice systems, the simplified ice storage that, together with UHPC façade collectors, serves as the source for a heat pump, can be summarized as follows:

- Both examined collectors in combination with an ice storage can reach the performance of GSHP.
- Except for July and August, evaporator inlet temperatures are significantly higher than those of the ASHP systems and exceed those of GSHP in the transitional periods and in the summertime.
- Large ice storages are needed to guarantee a minimum source temperature for the heat pump of  $0^\circ\text{C}$  throughout the year,. With the Col-Ice system with the gray, uninsulated collector,  $70 \text{ m}^3$  were needed if the entire south façade was covered with collectors. The Col-Ice system with the spectrally selective, insulated collector could reach this requirement only with a slightly larger storage volume of  $80 \text{ m}^3$  with the same aperture area. As the increment for the storage size variation was  $10 \text{ m}^3$ , this difference in required storage size does not reflect the absolute required difference. Both storage sizes were determined without considering possible gains of the soil through the walls of the ice storage.
- In Col-Ice systems, solar gains dominate the total gains of the collector.
- Without solar gains, Col-Ice systems need 90 %more area with a storage size of  $70 \text{ m}^3$  to guarantee a minimum evaporator inlet temperature of  $0^\circ\text{C}$  throughout the year.

As the simulation of the ice storage is very simple, and neither models gains through the surrounding earth nor simulates heat conduction through the already grown ice or any stratification, the size of the storage only indicates the necessary energy for the condition of  $0^\circ\text{C}$  minimum evaporator inlet temperature throughout the year.

### 5.7. Further research

The simulations in this chapter are based on simulated collector efficiency curves. As soon as measurements of the collectors are available, the simulations of the collector efficiency curves can be validated and refined. The system simulations can be redone with the measurement data.

As drainback systems promise a decrease in costs [132], the necessary pump power and its influence on system performance should be evaluated as soon as data for the pressure loss in the collectors is available.

If the collectors are operated below 0 °C, frost formation needs to be evaluated besides changes in system performance. Frost influences possible collector gains. Equations considering the frost formation should be included in the collector model. Haller et al. [64] also showed that the selectivity of unglazed selective collectors can be reduced or even disappear temporarily if humidity condensates on the absorber surface. This phenomenon should be tested for the newly developed spectrally selective coating of UHPC collectors and eventually be integrated into the collector model. If large areas of the collector are covered with frost, the danger from falling ice slabs may be severe, and a defrost operation must be considered.

The auxiliary heat to guarantee a minimum evaporator temperature influences the system performance considerably. New heat pumps with lower minimum inlet temperatures and higher maximum inlet temperatures at the evaporator should be investigated, as should be the influence on system efficiency. A sensitivity analysis with different types of heat pumps should be made to better understand the possible ranges of system efficiencies.

Further research related to system simulation would be to improve the ice storage model. The author's recommendation would either be trying to couple the validated TRNSYS model of Carbonell [27] into the Modelica environment or rebuilding the model completely in Modelica and validating the two. The latter would have the advantage of facilitating own changes as Modelica code is easier to program than TRNSYS code. A disadvantage would be that duplicated code would be more difficult to maintain. In addition to the ice storage model improvement, other phase change materials with higher phase change temperatures should be tested. They could raise the mean evaporator inlet temperature in winter and, thus, increase system efficiency. Combinations of direct use of solar heat in hot storage can be very promising. Different combinations of collectors and different control strategies should be investigated. As ice storage may involve high costs due to the necessary excavation work, solutions based on entire districts could be very interesting.

Regarding load management with overloading the building, for example, by means of a concrete core activation or floor heating system and/or the storage, Col-Dir and Col-Ice systems may show less loss in system performance than ground-source or maybe even air-source heat pumps: comparatively higher evaporator inlet temperatures may be achieved if the times of overloading correspond to times with higher irradiation. This could be investigated with detailed comparative system simulations. It should also be investigated whether gains in system performance can be achieved with load management in Col-Dir and Col-Ice systems.

Low temperatures are suitable for heat pumps as well as for solar collectors. Therefore, further investigation should be conducted related to floor heating systems or systems with concrete core activation as well as systems with low temperatures in the domestic hot water tank, for example, with ultrafiltration. Ultrafiltration is a relatively new and low standardized process for mechanical Legionella protection of DHW. According to one manufacturer [142], the temperatures in the DHW circuit can be reduced down to 45 °C. Based on system simulation in a multi-family home, Kropp et al. [99] showed an improvement of the yearly performance factor for DHW from 1.5 with a central DHW storage to 3.2 with ultrafiltration.

Especially if the examined variant of the spectrally selective, insulated collector is used both as a source for the heat pump/the ice storage, and for direct loading of the hot storages, the benefits of low temperatures in the domestic hot water tank could be immense: the longer the heat pump can be switched off completely in the summertime, the better the system performance can be. Combinations of different collectors for direct (direct feed in hot storages) and indirect use (source of heat pump) also contribute to better system efficiency, as was also shown by Arnold et al. [4].

Large parameter variations with the possible or conceivable collector properties and different systems configurations should be made to identify optimal collector-system combinations.

For southern regions or climate adaptations, an extension to cooling operations in the summertime could be investigated. The heat carrier could be pumped through the façade during nighttime and use the colder temperatures for cooling the building. This could be especially interesting if UHPC panels are installed with a high sky view factor, for example, on the roof, where the unglazed collectors face low sky temperatures and radiative heat transmission is high.

## CHAPTER 6

### Life cycle assessment of systems with UHPC collectors

This chapter comprises the description of all used inventories needed for the definition of the functional unit defined in chapter 3 with remarks on data collection, quality, and lifetime in section 6.1, the results of the life cycle impact assessment (LCIA) of the reference systems and the systems with UHPC collectors with the inputs from chapter 5 in section 6.2, and a discussion of the results with proposals for further research in sections 6.3 and 6.4.

#### 6.1. Inventory analysis

##### 6.1.1. Data collection and quality

As part of C. Pouloupoulos' master's thesis [134], the first basic field research was conducted on the materials and processes used in the manufacture of *TABSOLAR*<sup>®</sup> collectors. The thesis was supervised by the author. In the course of this work, the functional unit and the system boundary was changed and defined as described in section 3.5.2. In the subsequent project collaboration, further field research was carried out by the author, together with the project partners and external experts. The collected primary data was compiled in inventories, and the missing data was complemented with secondary data. In this work, the software Umberto<sup>®</sup> together with Ecoinvent database version 3.6 [164], was used for modeling.

An attempt was made to use the locally matching record, if available. The abbreviation [DE] stands for Germany, [GLO] for global, and [RoW] for rest of the world, since Ecoinvent version 3.2 corresponds to the data set for [GLO] [118]. [RER] stands for Europe.

All data is used as an “allocation cut-off”, i.e., recycling processes are allocated to the subsequent products, and no credit is issued corresponding to the approach used by Ecoinvent version 2 [54]. If there is market data (“market for ...”), it already includes standard transport routes and a typical production mix.

Transport is measured in metric tons · km, abbreviated as “tkm”.

This section presents all inventories used. The first subsection describes the different façade components. In the sense of the ILCD Handbook for LCA [46], this data can be called foreground data as specific instead of generic data is needed. So, all inventories

are based on primary data collected throughout this thesis. The following subsection presents the inventories used for the heating systems. These are based on collections from other authors and adapted to the purposes of this thesis. This data can also be called background data as it is not in the focus of this data compilation and is more generic. The last section describes the data for the use phase. It is also foreground data in the sense that the amount of energy used is the focus of the investigation. On the other hand, scenarios of different electricity mixes over the course of time or at different locations are not considered in the main part of this work. A short outlook is given for the period of 2020-2050 with the CO<sub>2</sub> emission factors assumed by Fritsche et al. [55] for this period. This work can be used to examine similar scenarios in the future.

The results of an LCA are only as good as the data it is based on. Since the process of data acquisition is quite lengthy and costly, the data in the databases is often old and very general. Typically, database updates are published annually. However, not all data is updated with each update, but only some records and all records that refer to these updated records. If the electricity mixes or production mixes of raw materials of a country change, this affects many other data sets. Technological components such as heat pumps are usually updated at much longer intervals. Innovations that involve material savings or material substitutions are often not included. For example, the data set for heat pumps used in this paper is 14 years old and reflects the market cross-section only very inaccurately.

Regarding the data used in this work, it can be said that the primary data on façade elements corresponds well to the technological, geographical, and temporal requirements. There are only a few inaccuracies, especially in the manufacturing process of the flow-through UHPC elements, as this has not yet been fully developed. As mentioned, the data for the system components are partly very old. In addition, the system components of the solar systems are not precisely designed and only represent an estimate. The data for the ice storage is based on primary data and therefore represents at least one variant of ice storage well. Philippen et al. [131] discuss the influence of different material substitutions in a sensitivity analysis and find only less than 10% change in PED and GWP if the ice storage casing is made of fiber reinforced plastic (FRP) or polypropylene (PP).

### 6.1.2. Lifetime

The lifetime of technical components is usually lower than that of construction elements. In their LCA report in 2007, Jungbluth and Stucki [87] assume a lifetime of 25 years for system components of a solar thermal system, Heck assumes a lifetime of 20 years for heat pumps [67] and 50 years for the bore hole heat exchanger. In 2012, Jungbluth and Stucki stick to the 25 years reported in 2007 [150]. In 2019, Hubbuch and



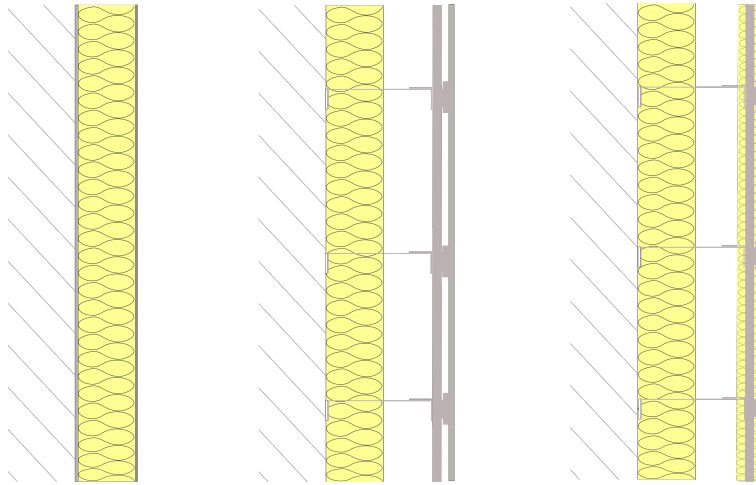


FIGURE 6.1.1. Different considered façade constructions. Left: External thermal insulation system (ETICS); center: uninsulated passive or active rear-ventilated façade with UHPC cladding; right: insulated active rear-ventilated façade with UHPC cladding.

Vecsei [80] publish a work on the life cycle cost of heat pumps with a broad statistical assessment of questionnaires filled in by heat pump owners in Switzerland. They find an expected lifetime of almost 27 years for ground-source and 20 years for air-source heat pumps. They find a Weibull distribution for both heat pump types. The lifetime of the ice storage is assumed with 50 years by Philippen et al. [131]. Hegger et al. [68] show a Gaussian distribution of damage frequency for construction elements: 50 % is damaged by 30 to 50 years, 90 % is damaged by 15 to 65 years. The lifetime is not only restricted by damage, but also by modernizing. A replacement of technical components can be economically or environmentally reasonable due to better efficiencies in newer components. Façades might be changed in consequence of a change in building use. In this study, it is assumed that all components last for at least 25 years. Only the heat carrier liquid in the solar components needs to be replaced every 10 years. Figure 6.2.6, figure 6.2.7, figure 6.2.8, and figure 6.2.9 depict the impact of all components over the course of time up to a lifetime of 50 years.

### 6.1.3. Façade components

The different considered façade constructions are depicted schematically in figure 6.1.1. A standard collector and an unglazed steel collector with spectrally selective coating (ColRef) were also modeled for comparison. A cross-section would resemble the picture on the right for the active, insulated UHPC collector with a thinner absorber held by a frame. The standard collector would be equipped with additional glazing.

### 6.1.3.1. *Standard flat plate collector*

Aiming for better assessment possibilities, many publications about new solar thermal collector concepts compare their results to a “standard collector”. This standard collector is defined by an efficiency curve, a price or other relevant properties and is claimed to be representative. In the case of life cycle assessment (LCA), all necessary steps for an LCA, as explained in section 3.3.2, should also be published for a standard collector. In literature, often, only parts of an entire LCA can be found, like a more or less precise life cycle inventory (LCI) or the results of the life cycle impact assessment (LCIA), for example, the global warming potential of a standard collector. These standard collectors are designed for a particular case and have a reasonably detailed description. Analyzing the diversity of all these “standard collectors” could be interesting, especially considering the course of time. But it is obvious that there is no “standard collector” for everything, but rather a considerable variety. Nevertheless, for comparability between different studies, it is very helpful to be able to refer to an “intermediate” or “normative” collector that is transparently published in detail with open access and, additionally, accepted in the community. This is especially important in the case of LCA: the results of LCA are far less intuitive even for experts than results of pure solar thermal system simulations, such as energy consumption, which can also be expressed monetarily. The pure figures of the saved CO<sub>2</sub> amount are difficult to put into context. If less common impact categories such as eutrophication measured in kg nitrogen equivalent are evaluated, non-experts are even more helpless.

In 2007, Jungbluth [87] built a detailed inventory for solar thermal systems, including a flat plate collector with a copper absorber. The elaborated data is accessible via Ecoinvent, one of the most important databases for LCA. In 2012, Jungbluth and Stucki published an update report [150] that included a flat plate collector with an aluminum-copper absorber. In a market overview of 2017 [113], only 13 % of the presented flat plate collectors have a copper absorber, which means that this update seems still reasonable. This report allows LCA practitioners to manually model this collector with Ecoinvent 2.2 data. Meanwhile, new versions of Ecoinvent with updated data came on the market, and some major changes in data were introduced. In this work, the inventory of the collector with aluminum-copper absorber for Ecoinvent 2.2 [150] was transferred to Ecoinvent 3.6.

This transfer proved to be non-trivial. The corresponding adjustments are described below. As an example, one can see that the selection and availability of data can strongly influence the result of an LCA. The used inventory can be found in table A.11.

As already described in Stucki and Jungbluth’s report, copper and aluminum have a dominant impact in most categories. Data uncertainty is most critical for the two metals. In Ecoinvent 2.2, regional consumption mixes were defined that do not

exist anymore in Ecoinvent 3.6. On the personal advice of the author of the collector study, an attempt was made to transfer the originally modeled data set, which works with a European production mix, and not to work with the global data set. This data set was compared with an environmental product declaration (EPD) for copper pipes issued in 2015 [83]. It was explicitly stated that this type of copper pipe is the one also used for collectors. Within this EPD, a recycling rate of 65 % was declared.

Therefore, the updated consumption mix with increased recycling percentage was used for the updated collector model. The inventory is presented in table A.13 in appendix A, followed by the inventory used for aluminum in table A.14. The differences in global warming potential and cumulated energy of the different data sets are presented in figure 6.1.2. It can be seen that the global data set has a significantly higher global warming potential and also higher primary energy use. So the environmental impact depends strongly on where the copper is extracted. The differences can be manifold; for example, caused by different raw material extraction techniques, different standards, different geological conditions, and, of course, different transport routes and means of transport. This example of the vast differences of the different data sets for a single material also displays the considerable uncertainties remaining in the field of LCA.

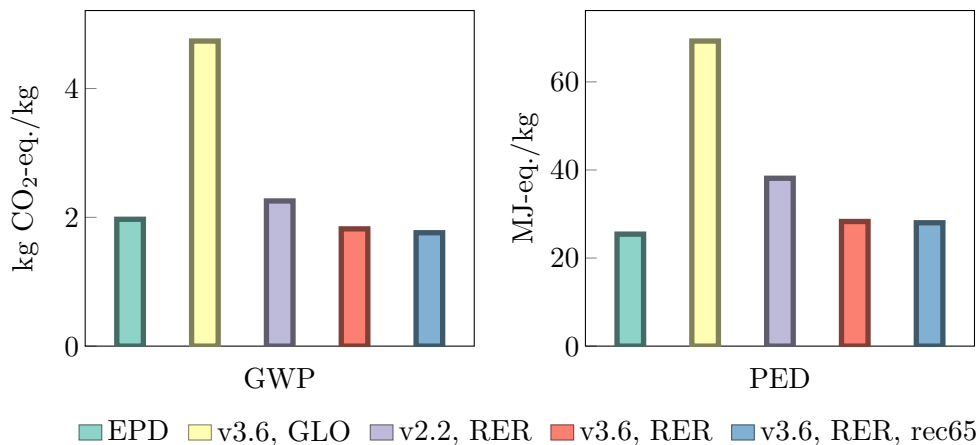


FIGURE 6.1.2. Global warming potential (GWP) and primary energy demand (PED) of differently modeled copper pipes: the environmental product declaration “EPD” [83] is compared to copper pipes modeled with copper data for the global market (“v3.6, GLO”) and for a European production mix “copper, at regional storage [RER]”. “V2.2, RER” represents the original consumption mix [2] in Ecoinvent v2.2, “v3.6, RER” represents the original mix transferred to Ecoinvent v3.6, and “v3.6, RER, rec65” corresponds to the updated inventory with increased recycling input shown in table A.13.

### 6.1.3.2. Reference steel collector

In the work of Philippen et al., an inventory for the unglazed steel absorber with spectrally selective coating was modeled and published [131].

Following their work, it was also modeled in this work; the inventory used is given in table A.12.

### 6.1.3.3. External thermal insulation system (ETICS)

As described in section 3.5.2, the most economical solution for the insulation of a façade would be with an external thermal insulation system (ETICS). A possible standard setup for renovations of a wall with an initial U-value of  $1.13 \text{ W}/(\text{m}^2 \text{ K})$  to the required, resulting U-value of  $0.23 \text{ W}/(\text{m}^2 \text{ K})$  was assembled together with an expert from the industry (table 6.1.1). The bonding with adhesive mortar does not occur over the entire surface; it is assumed that 40 % of the façade area is covered with layers of 15 mm. The amounts of adhesive mortar with an average thickness of 7 mm accommodate for additional material needed to level out uneven surfaces. Mineral wool with a thickness of 120 mm was selected for the insulation.

TABLE 6.1.1. Inventory of  $1 \text{ m}^2$  external thermal insulation system (ETICS) with mineral wool with a U-value of the wall of  $0.28 \text{ W}/(\text{m}^2 \text{ K})$  for renovation based on datasheets [21, 24, 22, 23] and [38]

Category	Material/Process	Value	Unit
Adhesive mortar, 7 mm	market for adhesive mortar [GLO]	10.5	[kg]
Stone wool, 120 mm	market for stone wool, packed [GLO]	14.4	[kg]
Base plaster, 4 mm	market for base plaster [GLO]	6	[kg]
Reinforcement mesh	market for glass fiber reinforced plastic, polyamide, injection molded [GLO]	0.1815	[kg]
Mineral cover plaster, 2 mm	market for cover plaster, mineral [GLO]	2.9	[kg]

TABLE 6.1.1. Inventory of 1 m<sup>2</sup> external thermal insulation system (ET-ICS) with mineral wool with a U-value of 0.28 W/(m<sup>2</sup> K) for renovation based on datasheets [21, 24, 22, 23] and [38]. - continued

Category	Material/Process	Value	Unit
Production	market for plaster mixing [GLO]	19.4	[kg]
End-of-life	treatment of waste cement in concrete and mortar, collection for final disposal [Europe without Switzerland]	16.5	[kg]
	treatment of waste mineral wool, collection for final disposal [Europe without Switzerland]	14.4	[kg]
	treatment of waste mineral plaster, collection for final disposal [RoW]	2.9	[kg]
	treatment of waste plastic, mixture, municipal incineration [RoW]	0.1815	[kg]

#### 6.1.3.4. UHPC collectors

The core of the *TABSOLAR*<sup>®</sup> elements are the deep-drawn UHPC elements. The integrated fluid channels of the UHPC elements are connected to the integrated header duct. Different UHPC elements can be connected to each other via fluid connectors, as shown in figure 4.2.4. A coating can be applied on the surface of the panel. The detailed construction depends on the type of façade. Table 6.1.2 lists the inventory for the pure UHPC absorber (*TABSOLAR*<sup>®</sup> *Design*) installed as a rear ventilated, insulated façade with the optional materials and processes for insulated, coated and/or glazed UHPC collectors (*TABSOLAR*<sup>®</sup> *Economy* and *Premium*). The transport distance of the UHPC absorber to the installation location was assumed to be 100 km.

TABLE 6.1.2. Inventory of 1 m<sup>2</sup> *TABSOLAR*<sup>®</sup> collectors. The basic inventory accounts for the variant *Design*, other parts accounting for different variants are labeled “optional”.

Category	Material/Process	Value	Unit
Material	UHPC, mixed, custom	28.12	[kg]
	market for glass fiber [GLO]	0.29	[kg]
	fluid connectors, custom	3.4	[unit]
	substructure, custom	1	[m <sup>2</sup> ]
Insulation house	market for stone wool, packed [GLO]	14.4	[kg]
Selective Coating (optional)	selective coating of UHPC, custom	1	[m <sup>2</sup> ]
Non-selective coating (optional)	alkyd paint production, white, water-based, product in 60 % solution state [RER]	1	[m <sup>2</sup> ]
Insulation (optional)	market for stone wool, packed [GLO]	6	[kg]
Glazing (optional)	solar glass production, low-iron [RER]	8.27	[kg]
	tempering, flat glass [RER]	8.27	[kg]
	transport, freight train, electricity [Europe without Switzerland]	12.57	[tkm]
Heat carrier liquid for 10 years (optional)	propylene glycol production, liquid [RER]	0.524	[kg]
	water production, completely softened, from decarbonized water, at user [RER]	0.786	[kg]
Production	deep-drawing UHPC, custom	1	[m <sup>2</sup> ]

TABLE 6.1.2. Inventory of 1 m<sup>2</sup> *TABSOLAR*<sup>®</sup> collectors. The basic inventory accounts for the variant *Design*, other parts accounting for different variants are labeled “optional”.- continued

Category	Material/Process	Value	Unit
Installation (100 km transport) End-of-life	transport, freight, lorry >32 metric ton, EURO5 [RER]	3.38	[tkm]
UHPC	treatment of waste concrete, inert material landfill [Europe without Switzerland]	28.12	[kg]
Insulation house			
Insulation (optional)	market for waste mineral wool [Europe without Switzerland]	6	[kg]
Glazing (optional)	treatment of waste glass sheet, collection for final disposal [Europe without Switzerland]	8.27	[kg]
Heat carrier liquid for 10 years (optional)	treatment of heat carrier liquid, 40 % C3H8O2, capacity 1.1E10 l/year [CH]	0.524	[kg]
	treatment of wastewater, from residence, capacity 1.1E10 l/year [RoW]	0.786	[kg]

### Ultra-high performance concrete (UHPC)

The particularity of UHPC lies in its composition. Regionally available aggregates are combined with various fillers of different size to produce a very high packing density. Besides silica (quartz) sand, silica sand flour and microsilica are used. Silica sand flour is silica (quartz) sand, with the difference that the particles of the flour sand are very finely ground. Usually, the grain size ranges between  $5\ \mu\text{m}$  -  $40\ \mu\text{m}$  with a maximum particle size of  $100\ \mu\text{m}$  [128]. Microsilica or silica fume is a by-product of the manufacture of silicon or ferrosilicon alloy, which rises from the furnaces as an oxidized vapor [98]. With extremely fine particles (average diameter of about  $0.1\ \mu\text{m}$  -  $0.3\ \mu\text{m}$ ), its main application is as a micro-filler in cementitious mixtures.

The dense packaging results in much smaller spaces between the individual constituents. Low water-cement ratios can be achieved, which, in turn, leads to higher strength. But superplasticizer is needed to keep the concrete with low water content flowable. Standard cements can be used for high-performance concretes. The cement contents required for high-strength concretes are higher than those for normal-strength concretes. However, due to the higher strength, the amount of material that can be saved overall means that, ultimately, less cement is needed for a component.

The recipe for the UHPC used in *TABSOLAR*<sup>®</sup> projects, developed by G.tecz Engineering for precast concrete manufacturer Spürgin, is not published. In personal communication with T. Sablotny from G.tecz Engineering, a recipe published by Fehling et al. [49] was agreed to be a good approximation of the used mixture. However, the presented inventory represents the recipe M1Q omitting the steel fiber contained in the report of Fehling et al. [49]. The electric energy for mixing was assumed to be comparable to the mixing energy for normal concrete, which, however, must be verified in actual production. It was assumed that a 110 kW mixing plant needs 6 min for  $1\ \text{m}^3$  of concrete. The transport distances for sand and cement were taken from the distances of the typical suppliers of Spürgin to their plant. The values were determined using the tool *reiseplanung.de*. The standard distance suggested by Borken-Kleefeld and Weidema [12] were applied for unknown supplier distances.

The regular sand and the silica sand flour were modeled with the same data set in Ecoinvent. For the current UHPC mix, a polycarboxylate-ether based (PCE) superplasticizer was used. A report by Stengel and Schießl [153] and personal communication between C. P. and the authors during the work on [134] were used as a source of the



modeling data of the superplasticizer. In their study, the authors carry out a life cycle assessment on some key materials for the production of UHPC. Among others, it provides information about the production of PCE superplasticizers.

The modeled recipe can be found in table 6.1.3. The contained superplasticizer was modeled as described in table 6.1.4.

TABLE 6.1.3. Inventory of 1 m<sup>3</sup> ultra-high performance concrete (UHPC), mixed (“UHPC, mixed, custom”) based on Fehling et al. [49]

Category	Material/Process	Value	Unit
PCE superplasticizer	superplasticizer production, custom	28.6	[kg]
Microsilica	market for silica fume, densified [GLO]	230	[kg]
Silica sand flour	silica sand production [DE]	183	[kg]
Water	tap water production, conventional treatment [Europe without Switzerland]	161	[kg]
Portland cement (CEM I)	cement production, Portland [Europe without Switzerland]	733	[kg]
Silica sand	silica sand production [DE]	1008	[kg]
Mixing	market for electricity, low voltage [DE]	11	[kWh]
Transport to plant	market for transport, freight, lorry 16-32 metric ton, EURO5 [RoW]	605.362	[tkm]

TABLE 6.1.4. Inventory of 1 kg “superplasticizer production, custom” based on Stengel and Schießl [153].

Category	Material/Process	Value	Unit
maleic acid	maleic anhydride production by direct oxidation of n-butane [RER]	0.1	[kg]
ethylene glycol	ethylene glycol production [RER]	0.2	[kg]

TABLE 6.1.4. Inventory of 1 kg “superplasticizer production, custom”. - continued

Category	Material/Process	Value	Unit
biocides	triazine-compound production, unspecified [RER]	0.01	[kg]
sodium hydroxide	chlor-alkali electrolysis, diaphragm cell [RER]	0.11	[kg]
water	water production, deionized, from tap water, at user [RoW]	0.45	[kg]
hydrogen peroxide	hydrogen peroxide production, product in 50 % solution state [RER]	0.03	[kg]
acrylic acid	acrylic acid production [RER]	0.1	[kg]
energy for polymerization	market for electricity, medium voltage [DE]	0.0405	[kWh]

### Deep-drawing process

The deep-drawing process of the UHPC absorber is under development and no data about the energy and material requirements of the final process was available yet. The used inventory (see table 6.1.5) accounts for the membrane and the energy for a folding pallet, a machine type also used in the precast concrete industry for the production of double walls. A folding pallet comprises two tables, placed side-by-side. One of the tables can be hydraulically moved and turned 180° over the other table. Both tables can be brought together, so that the concrete elements can be joined. The total energy needed was assumed to be 1.2 kWh. This amount of energy probably overestimates the necessary power for the folding of the *TABSOLAR*<sup>®</sup> elements, which are far lighter than a precast wall, and the uncertainty is rather high. The amount of energy needed for the evacuation pump was assumed to be small, and because of lacking data it was omitted. The membrane was assumed with 200 g/m<sup>2</sup>. It is further assumed to be used twice on the base of experience during laboratory work. Additional material might be needed depending on the re-usability of casting elements. The aim is to reuse the needed material as often as possible in final production process.

TABLE 6.1.5. Inventory of deep-drawing of 1 m<sup>2</sup> *TABSOLAR*<sup>®</sup> element, custom process, based on experience during the production development (“deep-drawing UHPC, custom”)

Category	Material/Process	Value	Unit
Membrane (used for 2 elements)	market for acrylonitrile-butadiene-styrene copolymer [GLO]	0.1	[kg]
Energy for folding pallet	market for electricity, low voltage [DE]	1.2	[kWh]

## Substructure

The inventory of the substructure listed in table 6.1.6 was based on considerations by Priedemann Facade-Lab and the drawing shown in figure 6.1.3. Agrafes, distance pieces, traverse profiles, vertical L-profiles and mounts were considered. The aluminum data modeled in table A.14 was used. The element size shown is slightly smaller (1.06 m<sup>2</sup>) than the element size considered during this work (1.16 m<sup>2</sup>), but this is considered negligible. The same substructure was used for the rear-ventilated façade with the standard collector.

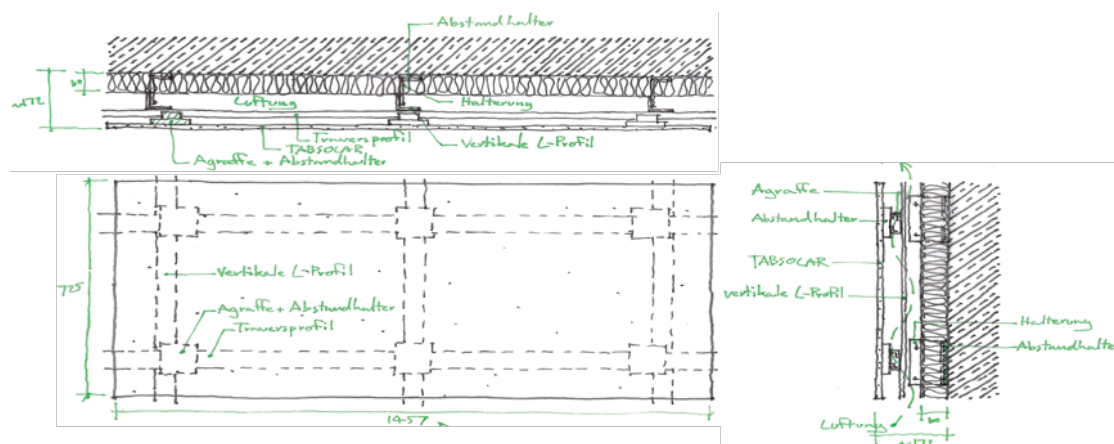


FIGURE 6.1.3. Drawing of a substructure for *TABSOLAR*<sup>®</sup> collectors during the planning process. Source: Priedemann Facade-Lab.

TABLE 6.1.6. Inventory of the substructure for 1 m<sup>2</sup> of a UHPC cladding (active or passive) (“substructure, custom”)

Category	Material/Process	Value	Unit
Aluminum for agrafes, distance pieces, travers profiles, vertical L-profiles, mounts	aluminum, production mix, wrought alloy, at plant [RER] (custom)	4.82	[kg]
Production	section bar extrusion, aluminum [RER]	4.82	[kg]

### Spectrally selective coating

Table 6.1.7 presents the inventory used for the spectrally selective coating of UHPC. An attempt to estimate the data from the laboratory sputtering machine at Fraunhofer ISE resulted in far higher global warming potentials and primary energy demands than the one of the current data set for spectrally selective coating in Ecoinvent, which were taken from industrial sputter plants and should be more accurate for serial production. Therefore, it was decided to take the Ecoinvent data set as a basis and only add aluminum and titanium dioxide, which are part of the spectrally selective coating used for UHPC. Additionally, the amount of electricity was doubled to account for a longer evacuation time in the sputtering machine. A pre-drying process with the inventory in table 6.1.8 was established to lower the evacuation time. The data was derived from laboratory practice and had to be revised for the final process.

TABLE 6.1.7. Inventory of 1 m<sup>2</sup> spectrally selective coating of UHPC. This dataset is based on “selective coating, copper sheet, sputtering [DE]”. The electricity value was doubled to account for the long operating time of the vacuum pump. Furthermore, aluminum and titanium dioxide were added to account for the used layers (“selective coating of UHPC, custom”).

Category	Material/Process	Value	Unit
Material of original data set	argon, liquid	0.00328	[kg]

TABLE 6.1.7. Inventory of 1 m<sup>2</sup> spectrally selective coating of UHPC. This dataset is based on “selective coating, copper sheet, sputtering [DE]”. The electricity value was doubled to account for the long operating time of the vacuum pump. Furthermore, aluminum and titanium dioxide were added to account for the used layers (“selective coating of UHPC, custom”). - continued

Category	Material/Process	Value	Unit
	chromium	0.0074	[kg]
	copper	0.0818	[kg]
	corrugated board box	0.0177	[kg]
	diesel, burned in building machine	0.225	[kg]
	kraft paper, bleached	0.000555	[kg]
	light fuel oil	0.0062	[kg]
	lubricating oil	0.000773	[kg]
	metal coating facility	0.000000333	[unit]
	nitrogen, liquid	0.00182	[kg]
	oxygen, liquid	0.000909	[kg]
	polyethylene, low density, granulate	0.000518	[kg]
	tap water	7.236	[kg]
	tin	0.00862	[kg]
Added material	aluminum, primary, ingot	0.0004065	[kg]
Added material	titanium dioxide	0.000114	[kg]
Electricity demand doubled	electricity, medium voltage	6.94	[kWh]

TABLE 6.1.8. Inventory of pre-drying of 1 m<sup>2</sup> TABSOLAR panel, according to laboratory tests at Fraunhofer ISE. This process has to be revised as soon as the necessary drying parameters are better known.

Category	Material/Process	Value	Unit
Pre-Drying	market for electricity, low voltage [DE]	14.8	[kWh]

### Fluid connectors

The fluid connectors are modeled according to the state of development at the time of the LCA preparation. The inventory is presented in table 6.1.9.

TABLE 6.1.9. Inventory of one of four fluid connectors for a TABSOLAR design panel (“fluid connectors, custom”)

Category	Material/Process	Value	Unit
Material	market for steel, chromium steel 18/8 [GLO]	0.1523	[kg]
Production	drawing of pipe, steel [RER]	0.0033	[kg]
	market for metal working, average for steel product manufacturing [GLO]	0.149	[kg]
Sealing	market for silicone product [RoW]	0.004	[kg]

### 6.1.4. System components

#### 6.1.4.1. Heat pumps

The inventory used for the heat pumps was based on the dataset “heat pump production, brine-water, 10 kW [CH]” generated by Heck in 2007 [67]. Heck suggested to scale the data according to the capacity of the heat pump; a procedure that was followed here.

In Ecoinvent, no data set is available for the outdoor air unit of an air-source heat pump. In the report for the data description of heat pump systems [67], the existing data set for a 10 kW ground-source heat pump is scaled by a factor of 1.6 due to increased material and refrigerant use to generate the data for the air-source heat pump. This procedure was also followed here.

For the borehole, the data set “Borehole heat exchanger, 150 m for 10 kW heat pump” was used and scaled according to the length of the borehole calculated in section 5.4.4.

As mentioned in section 6.1.3.1, the transfer to newer versions of Ecoinvent is not always easy. As in the case of the flat plate collector, the mixture shown in table A.13 was used for copper instead of the global mixture in the input data of the dataset “heat pump production, brine-water, 10 kW [CH]”.

Regarding the accuracy of this data, it should be noted that the underlying report by Heck [67] is from 2007, and heat pumps have undergone many developmental changes since. In particular, there are various alternatives for heat transfer fluids that differ greatly in their toxicity and global warming potential. In this dataset, the heat carrier tetrafluoroethene (R134a) was used. It would be very helpful if Ecoinvent updated one or more of the relevant data sets.

#### 6.1.4.2. *Solar system*

The data in the solar systems reports by Jungbluth [87] and Stucki and Jungbluth [150] were used and adapted for modeling the necessary additional system parts for the systems with collectors (heat carrier liquid in case of Col-Dir systems, membrane expansion vessel, pump, piping, transport, packaging). No detailed dimensioning was conducted. The Col-Dir systems account for the additional requirement of an electrical heater to preheat the collector output temperature and heat carrier liquid in the system. The Col-Ice systems use water.

#### 6.1.4.3. *Ice storage*

The ice storage was modeled according to the data from Philippen et al. [131]. The inventory used for an ice storage of 20 m<sup>3</sup> is shown in table A.15. The data “unreinforced concrete production, with cement CEM II/B, custom” was adapted according to the proposed mixture by Philippen et al. [131]. A cuboid shape with an end face of 7.5 m<sup>2</sup> was assumed for larger storages, and the length was scaled accordingly. The impact of the casing was scaled according to the resulting surface of the casing. Philippen et al. [131] assumed 8 heat exchangers with an area of 2.1 m<sup>2</sup> for the 20 m<sup>3</sup> ice storage. In this work, the number of heat exchangers with the according piping was adapted according to the storage volume of larger storages. In the work of Philippen et al. [131], the heat exchanger was filled with heat carrier liquid, and the same heat exchanger was used for loading and unloading. In this work, the ice storages serve as a seasonal backup for temperatures below 0 °C. The collectors can be operated with water, and the incoming water will always have a temperature above the melting point. However, temperatures below 0 °C occur during unloading, which is why a second heat exchanger is needed that can be operated with heat carrier liquid. So, the number of heat exchangers in this work

is 0.8 per 10 m<sup>3</sup> of ice storage. The piping to the collectors remains the same for all ice storage sizes. The amount of heat carrier liquid is assumed to be the same as for an external air unit of 10 kW.

The simulation section of this work assumes adiabatic ice storage to exclude the unknown influence from the soil. This neglects gains through the typically uninsulated side and bottom walls when the storage temperature is below the soil temperature. This assumption, together with the requirement of a minimum collector and storage temperature of 0°C, also leads to larger ice storages than in reality. In an LCA, the adiabatic boundary condition could theoretically be approximated with a very effective insulation. In reality, however, many commercial ice storages only have insulation on the top. The side and bottom walls are uninsulated. As mentioned, this allows for additional gains from the soil in winter when the soil temperature is above the storage temperature of 0°C and reduces storage losses when storage temperatures are higher. The described ice storage by Philippen et al. [131] is also only equipped with topside insulation. To represent existing ice storage, the inventory for calculating of the global warming potential and the primary energy demand includes topside insulation but no side and bottom insulation. The storage size was taken from the simulations.

#### 6.1.5. Use phase

The electricity required was modeled using the static data set “market for electricity, low voltage [DE]” in the main part of this work. As this work is based on Ecoinvent V 3.6 from 2019 and the data update of the database takes time, this data set is based on the rather old IEA data from 2014. To assess the influence of the changing CO<sub>2</sub> emission factor, the global warming potential was also evaluated with time-dependent emission factors as a side evaluation. The basis for the development of the CO<sub>2</sub> emission factor was a short study by the International Institute for Sustainability Analysis and Strategies (IINAS) [55]. This study assumes a 95 % emission reduction by 2050 compared to 1990. Figure 6.1.4 shows the assumed development and the reference CO<sub>2</sub> emission factor of 2014. The total energy needed per year ( $W_{el,tot}$ ) of the investigated systems is documented in tables A.9 and A.10.

## 6.2. Life cycle impact assessment (LCIA) and discussion

### 6.2.1. LCIA of components

Figure 6.2.1 compares the primary energy consumption for different variants of the UHPC collectors based on the *TABSOLAR*<sup>®</sup> concept, an unglazed, spectrally selective steel absorber, a standard collector with a spectrally selective aluminum-copper absorber and passive UHPC cladding, each as a rear-ventilated façade next to an external thermal



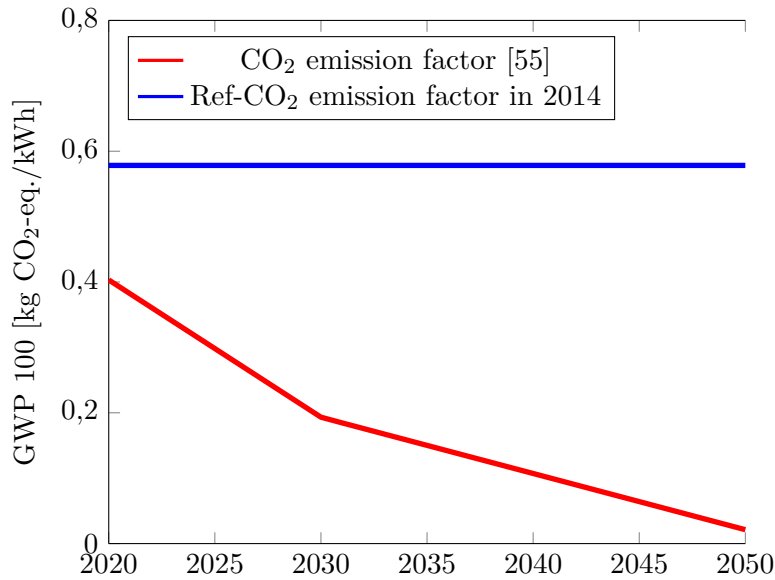


FIGURE 6.1.4. Specific CO<sub>2</sub> emission factor for the years 2020 to 2050 following Fritsche et al. [55] and the reference CO<sub>2</sub> emission factor in 2014, both of German electricity mix.

insulation system (ETICS) with mineral wool. The *TABSOLAR*<sup>®</sup> variants *Design* with and without insulation and spectrally selective coating (Col1 and Col2), *Economy* (Col3), and *Premium* (Col4) with a variant in which the coating is carried out in an existing commercial piecework coating plant in Mikkeli (Finland)<sup>1</sup> were presented for the UHPC collectors. Compared to the standard collector, the proportion of spectrally selective coating of the UHPC collectors is very large. This is due to the pre-drying required for UHPC and the increased pump energy for evacuation. However, this additional amount can probably be greatly reduced by improving the drying processes. In addition, the age of the concrete plays an important role; the UHPC elements should cure for several weeks before they are coated. Furthermore, the large proportion of the collector frame in the standard collector is noticeable compared to the primary energy expenditure. It should be noted here that a cover strip probably required between the collectors and at the edge of the field was not yet considered for the UHPC collectors due to lack of data. In addition, the standard collector was modeled with an aluminum frame. If this was constructed of wood in the façade, this proportion would be significantly reduced.

<sup>1</sup>To the knowledge of the author, the coating plant in Mikkeli, Finland, is the only commercial coating plant that offers piecework coating with a sputter process. Other coating plants work with coils and run-through processes.

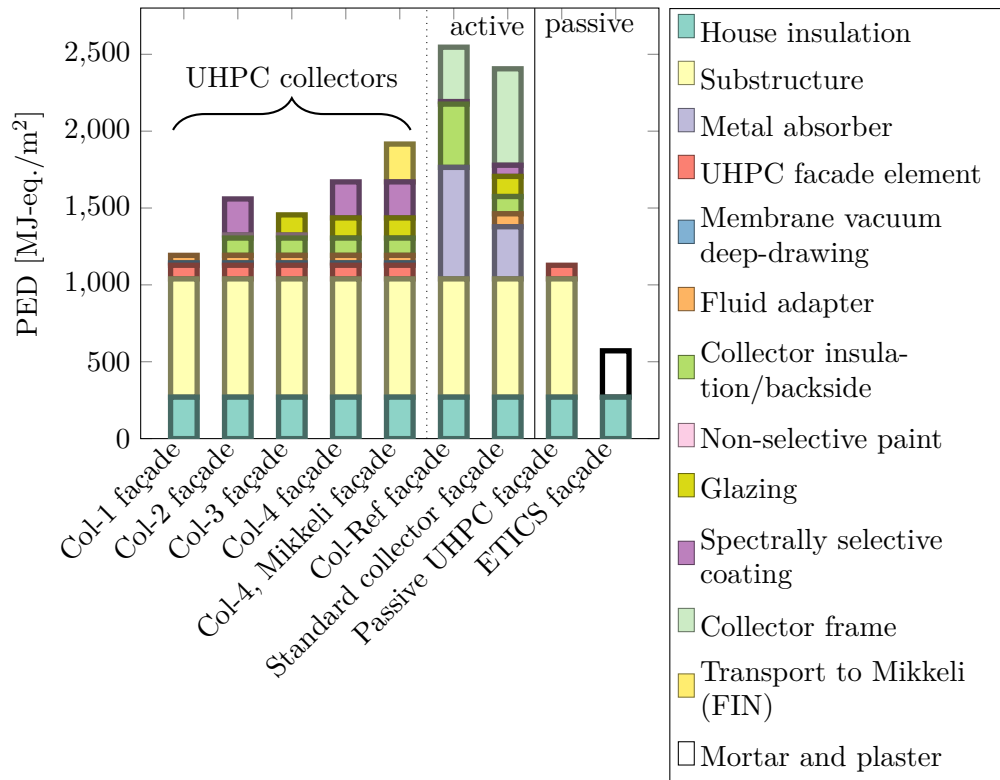


FIGURE 6.2.1. Primary energy demand of different active and passive façades. All UHPC collectors are based on the *TABSOLAR*<sup>®</sup> concept. Col1 represents the gray *Design* variant without insulation, Col2 the *Design* variant with insulation and spectrally selective coating. Col3 stands for the variant *Economy*, Col4 for *Premium*. ColRef is an unglazed steel collector. The standard collector is equipped with an absorber made of an aluminum sheet with copper pipes.

Looking at the reference collector ColRef, the commercial collector “Solardach AS” by Energie Solaire SA, both the impact of the stainless steel absorber and of the collector backside consisting of two corrugated, fiber-reinforced plastic (FRP) sheets are considerably higher than the corresponding parts in standard or UHPC collectors. The corrugated sheets are not equivalent to insulation; they serve as draining, water-tight roof elements. They are needed in the case of a roof construction, but if used for a rear ventilated façade, the FRP backside might not be required. The “Solardach AS” construction is shown in figure A.11. It is possible that the impact ratio of stainless steel absorbers and UHPC absorbers could change in favor of stainless steel absorbers in the future due to the generally excellent recycling possibilities of stainless steel. Nevertheless, the recycling possibility of *TABSOLAR*<sup>®</sup> absorbers might not be restricted to fillers

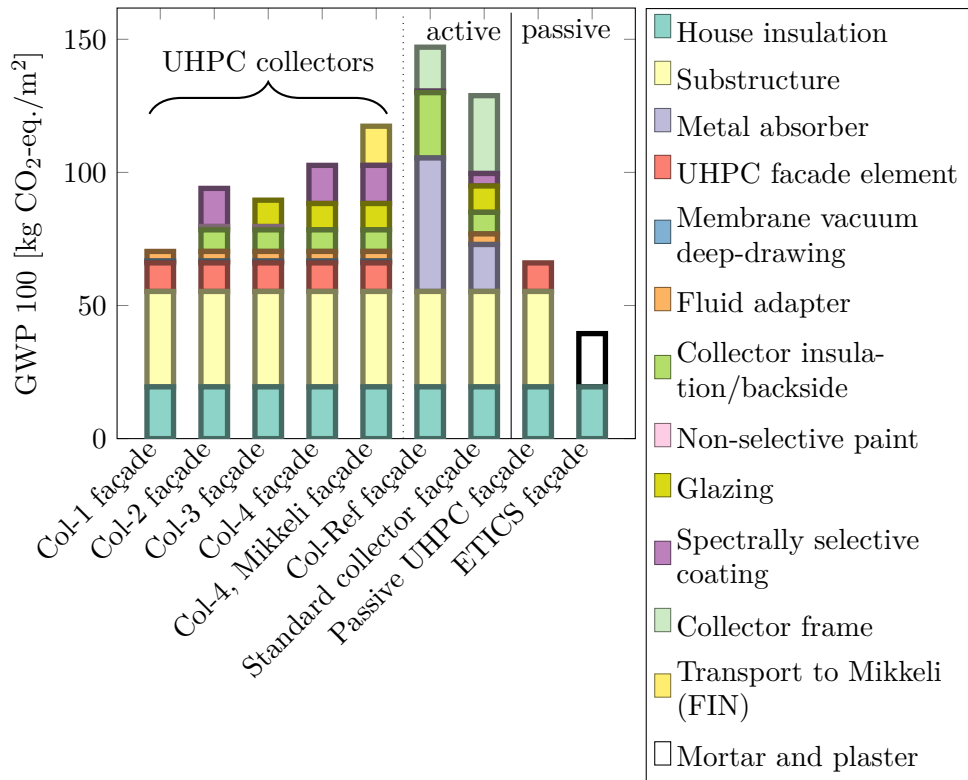


FIGURE 6.2.2. Global warming potential of different active and passive façade components. All UHPC collectors are based on the *TABSOLAR*<sup>®</sup> concept. The variant Col1 represents the gray *Design* variant without insulation, Col2 the *Design* variant with insulation and spectrally selective coating. Col3 stands for the variant *Economy*, Col4 for *Premium*. ColRef is an unglazed steel collector. The standard collector is equipped with an absorber made of an aluminum sheet with copper pipes.

in street construction or similar: the whole rather than crushed elements may also find a second life as pavement, for example.

The ETICS has the lowest overall primary energy consumption in production, but just like the passive UHPC cladding, it cannot be used for energy generation. Therefore, the savings in the utilization phase must be offset for a fair comparison. The same statements apply to the global warming potential (figure 6.2.2); the shares of the respective processes and materials differ only slightly. Figure 6.2.3 shows the primary energy demand and the global warming potential of the considered systems. They all comprise the south façade and heating systems without storage and heat distribution.

In total, there are four reference systems shown: the ground-source heat pump with UHPC cladding (GSHP + UHPC façade) represents an architectonic benchmark,

whereas the air-source heat pumps together with ETICS (ASHP 1/2 + ETICS) represent the economic benchmarks. In the system simulation, two different types of air-source heat pumps were simulated to show the range in the market. The same inventory was used as a basis for both air-source heat pumps. The ASHP 2 is slightly larger (22 kW instead of 21.7 kW, ASHP 1), but this is hardly relevant in this context. The use phase is more relevant for the PED and the GWP and differs for both ASHP types, as presented in the following paragraph in figure 6.2.4 and figure 6.2.5. Depending on the difference in investment costs of both types, the energy price and the lifetime, the economic benchmark would be one or the other. The technical benchmark is represented with the ColRef-Dir system. The system components are the same as in the Col-Dir system, and only the façade component, more accurately the collector, differs.

The façade has the largest share ( $> 50\%$ ) of primary energy demand in almost all systems. The façade has lower shares (47%) only in the Col1-Ice system with the 70 m<sup>3</sup> ice storage. In terms of global warming potential, the shares of the façade on total emissions are similar but slightly lower. The ice storage systems are both below 50%.

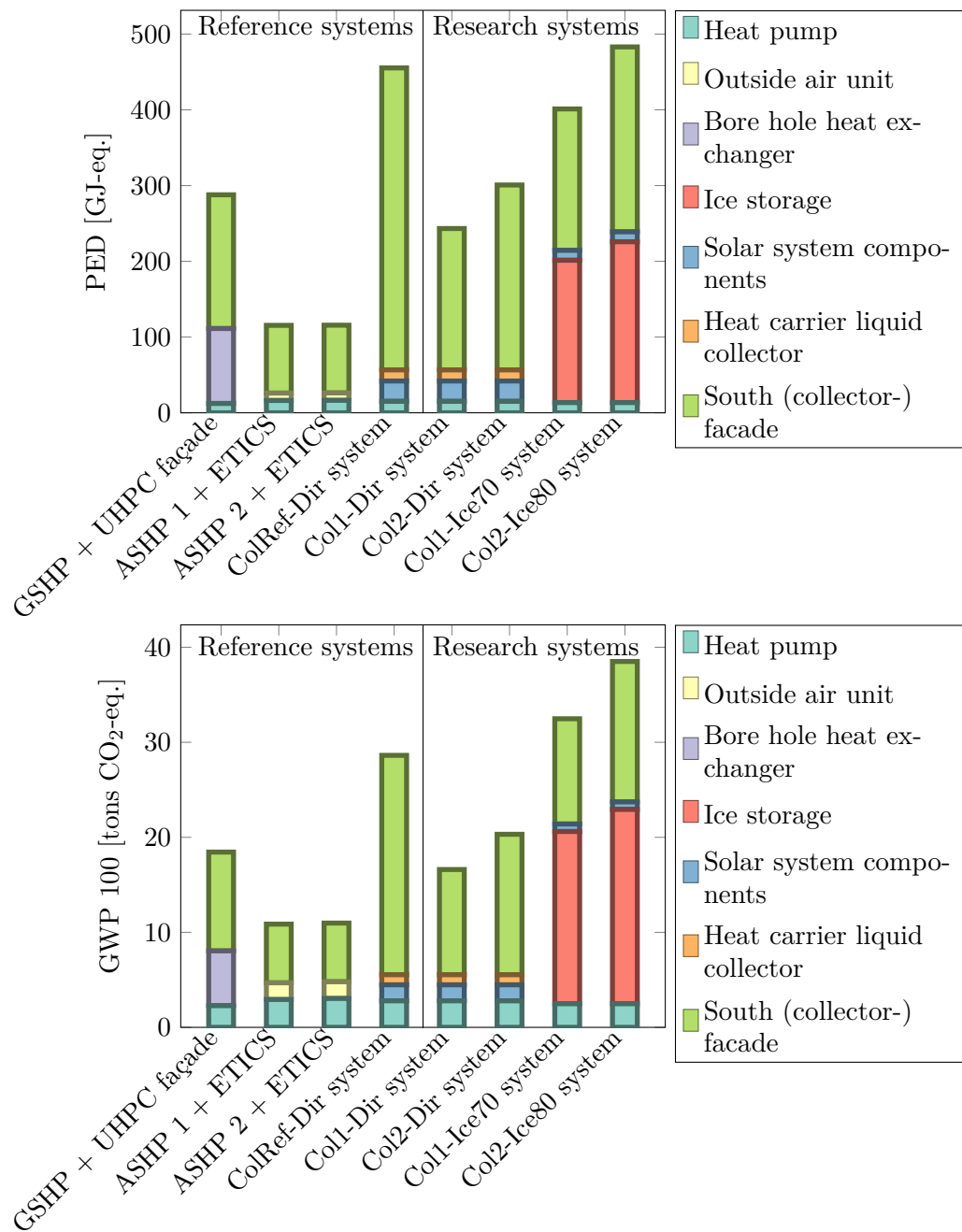


FIGURE 6.2.3. Primary energy demand (above) and global warming potential (below) of the system components.

### 6.2.2. LCIA of life cycle

The fix CO<sub>2</sub> factor of the year 2014 in Germany was used for the main evaluation of the use phase, and a further evaluation shows the influence of changing CO<sub>2</sub> factors. Considering the use phase of the system with an operating time of 25 years, figure 6.2.4 and figure 6.2.5 clearly show its dominating role. In these plots, the yearly emissions are shown per square meter of floor area. For each system, the percentage of the system components on the total impact is depicted in blue. The Col2-Ice80 system has the highest share of the system components regarding the entire life cycle (12% considering PED, 16% when considering GWP 100).

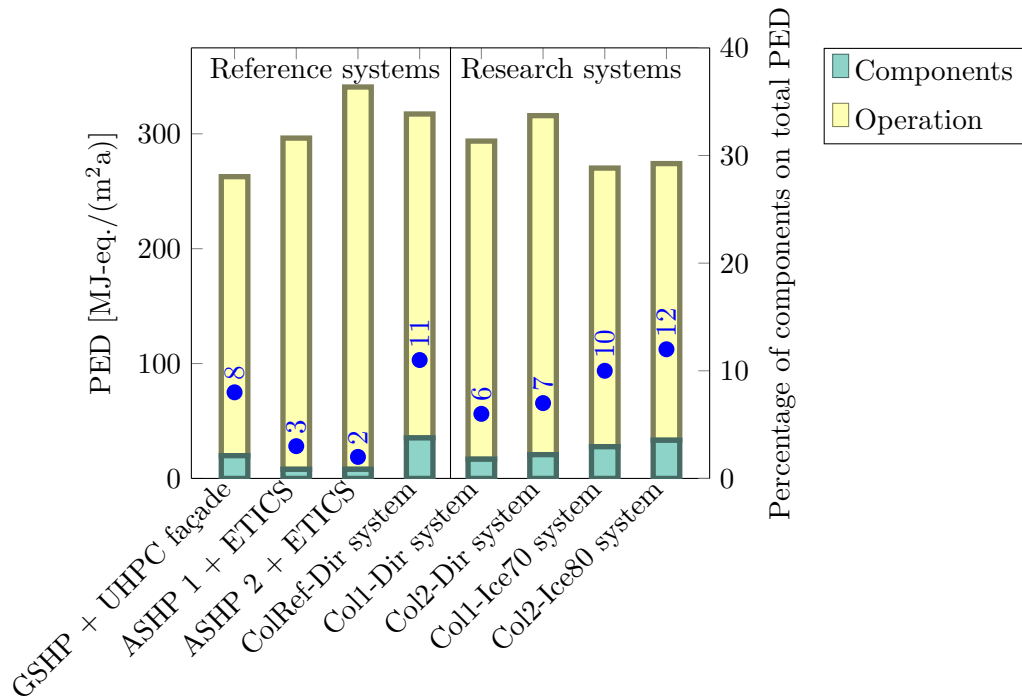


FIGURE 6.2.4. Yearly primary energy demand of the system components and the operation per floor area based on 25 years of operation.

As stated in the beginning, it is assumed that all components would last at least 25 years. Only the heat carrier liquid in the solar components needs to be replaced every ten years. Figure 6.2.6, figure 6.2.7, figure 6.2.8, and figure 6.2.9 depict the impact over time up to a lifetime of 50 years of all components. The end-of-life impacts and the impact of the heat carrier liquid changed during lifetime are included in the components' impact. The y-axis intercept represents this impact. Zooming in on the first ten years of operation is shown below the respective plot to better see the time of amortization

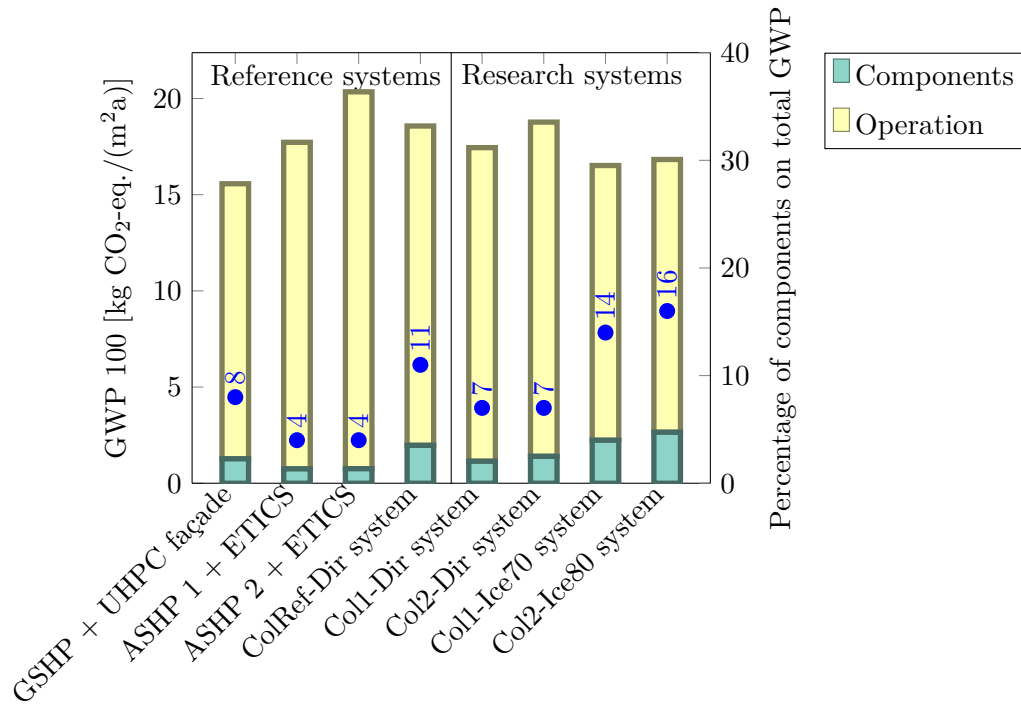


FIGURE 6.2.5. Yearly global warming potential of the system components and the operation per floor area  $A_f$  based on 25 years of operation.

of the Col-Dir and Col-Ice systems with respect to the ASHP reference systems. The respective savings of the Col1-Dir and Col1-Ice system compared to the ASHP 1 and ASHP 2 system are also depicted as a function of time in the graphic. For 25 years, it ranges from 1 % (2 %) to 14 % (14 %) for the Col1-Dir system and from 9 % (7 %) to 21 % (19 %) for PED (GWP). The GSHP system performs best up to a lifetime of 50 years. The Col-Ice systems have slightly lower emissions during their lifetime, but the difference is so small that the higher emissions of the components cannot be compensated within a reasonable time.

This static modeling of the electricity mix does not incorporate changes in the electricity mix throughout the use phase. This does not correspond to reality since Germany aims for climate neutrality by 2045 [15], and the electricity mix has already changed towards more renewable energies since 2014. However, since only the amount of electricity required in the use phase is compared, considering a dynamic evolution of the electricity mix would result in an absolute difference between the individual systems for the utilization phase and longer times of amortization. If systems using oil or gas, for example,

were included in the comparison, the difference in primary energy and global warming potential in the use phase would shift in favor of the electricity-powered systems.

In the overall evaluation of the systems in this work, systems with low CO<sub>2</sub> emissions of the components would perform proportionally better with a dynamic calculation of the CO<sub>2</sub> impact, since the current electricity mix of the production would be considered for the components, but there would be increasingly less impact per kilowatt-hour in the use phase. Depending on the assumed lifetime of the components, in some cases, this could mean, that systems with high energy consumption in the use phase would score better than those with lower consumption.

To illustrate the described influence of a dynamic evolution of the CO<sub>2</sub> emission factor, the global warming potential was evaluated according to Fritsche et al. [55] in figures A.14 and A.15 for the period 2020 to 2050. Figure A.13 shows the proportion of the use phase with these assumptions.

As described, the times of amortization are significantly longer, or amortization cannot be reached at all within a period of 30 years. The proportions of the respective components on the total emissions increase to values from 11 % for the ASHP 2 system with ETICS to 36 % for the Col2-Ice80 system.

Hess et al. [77] investigated techno-economic and ecologic perspectives for air-source and ground-source heat pumps in multi-family homes in Germany using the dynamic evolution of the CO<sub>2</sub> emission factor proposed by Fritsche et al. [55]. They come to the conclusion that 50 % of the CO<sub>2</sub> emissions can be saved with the investigated heat pump systems compared to a system with a condensing boiler.

This illustrates the strong influence of the change from a gas heating system to a heat pump system.



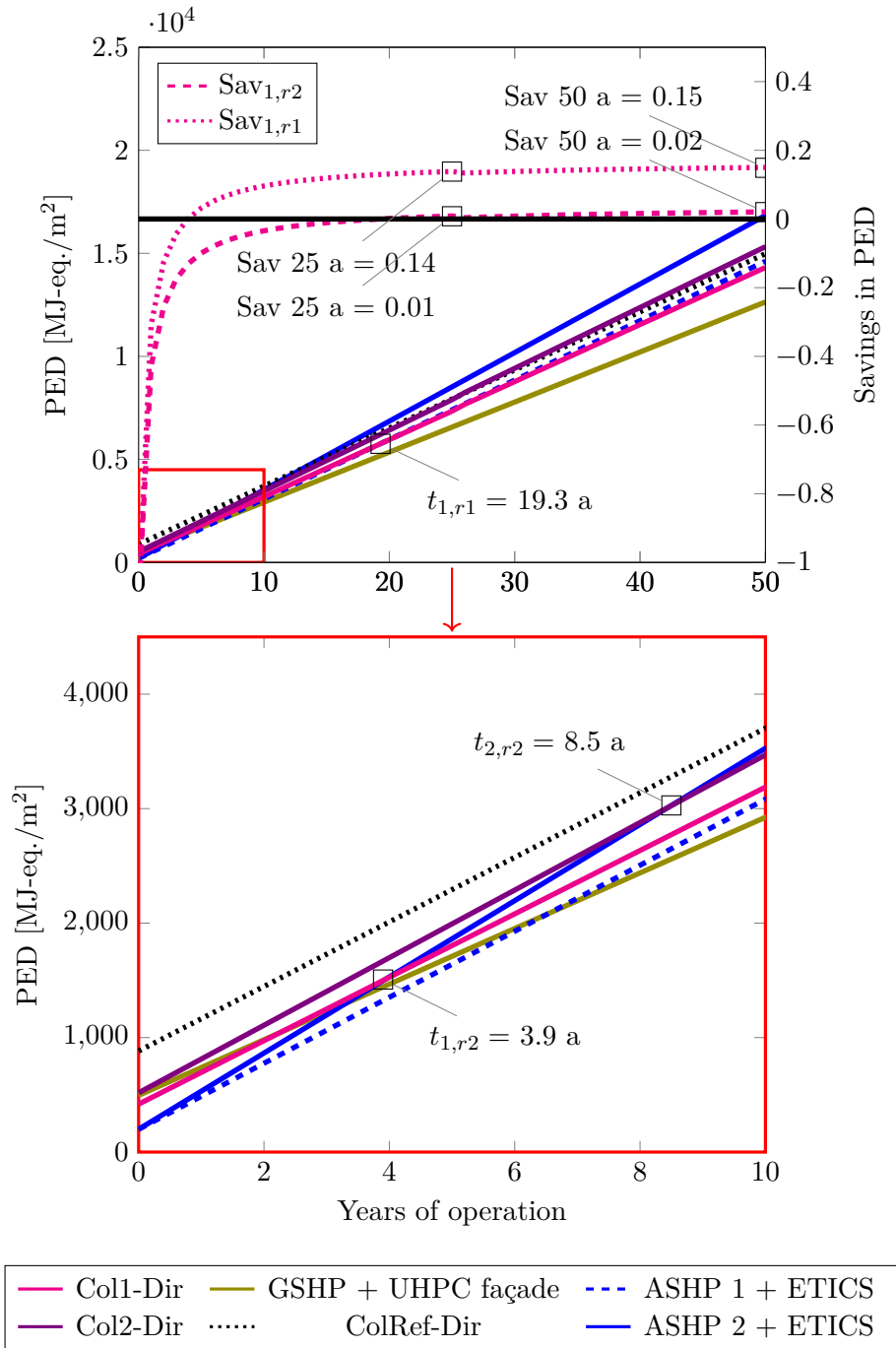


FIGURE 6.2.6. Primary energy demand in the course of operating time. The time of amortization of primary energy of the Col-Dir systems referred to the ASHP systems is indicated with  $t_{x,ry}$ , exemplary savings on the right axis with  $Sav_{x,y}$ . The first index refers to Col1-Dir (1) or Col2-Dir (2), the second index refers to ASHP 1 + ETICS (r1) or ASHP 2 + ETICS (r2).

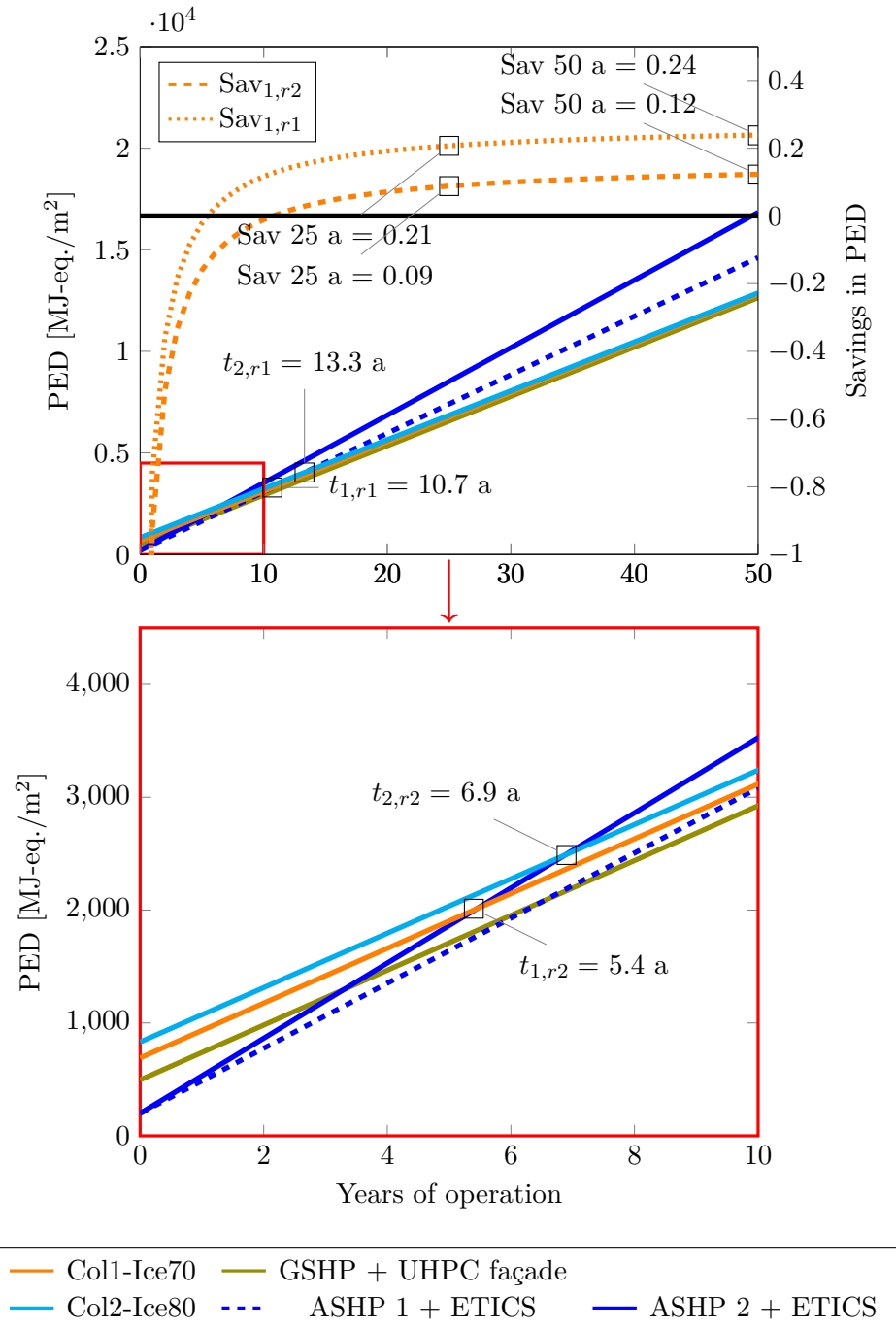


FIGURE 6.2.7. Primary energy demand in the course of operating time. The time of amortization of primary energy of the Col-Ice systems referred to the ASHP systems is indicated with  $t_{x,ry}$ , exemplary savings on the right axis with  $Sav_{x,y}$ . The first index refers to Col1-Ice70 (1) or Col2-Ice80 (2), the second index refers to ASHP 1 + ETICS (r1) or ASHP 2 + ETICS (r2).

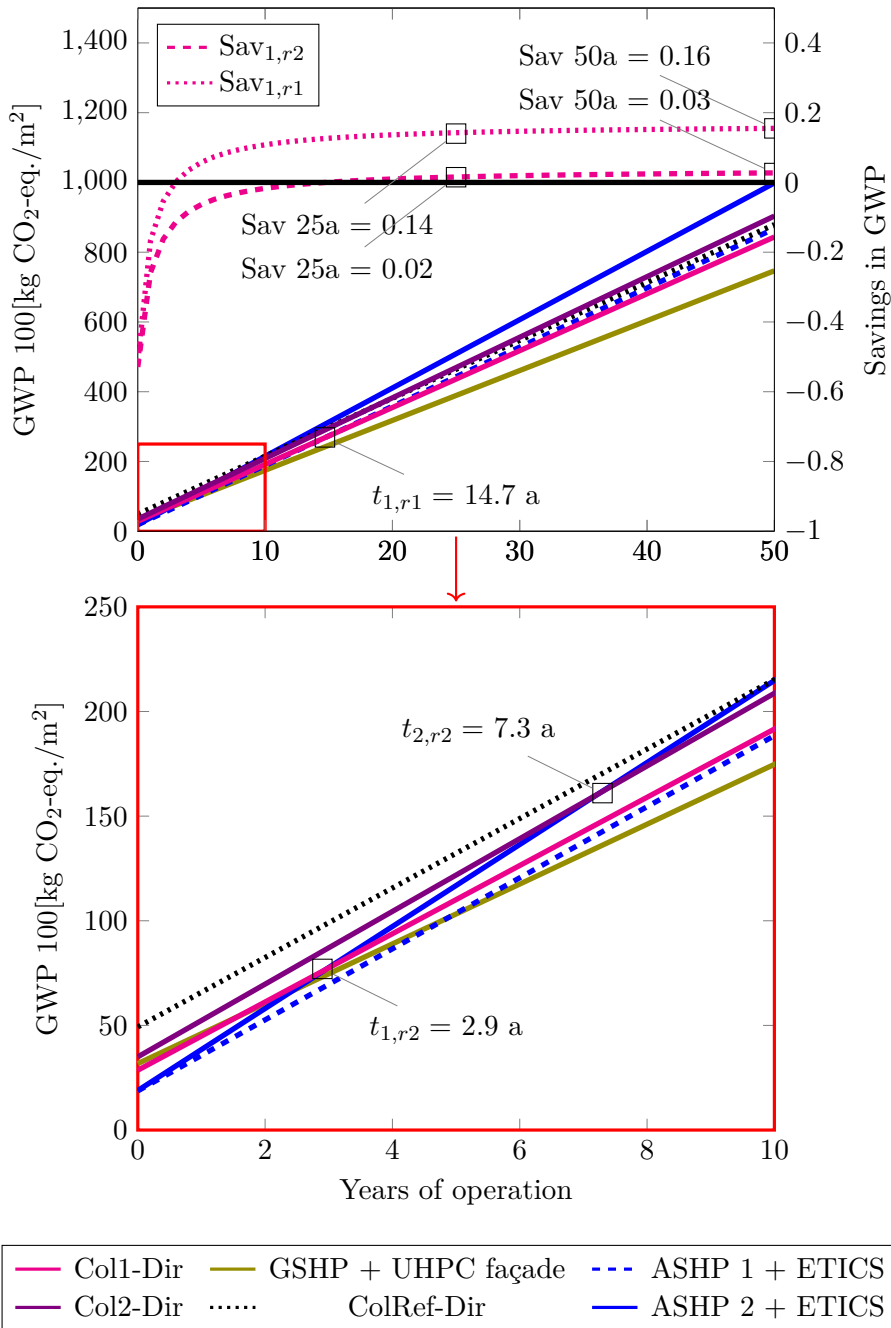


FIGURE 6.2.8. Global warming potential in the course of operating time. The time of amortization of global warming potential of the Col-Dir systems referred to the ASHP systems is indicated with  $t_{x,ry}$ , exemplary savings on the right axis with  $Sav_{x,y}$ . The first index refers to Col1-Dir (1) or Col2-Dir (2), the second index refers to ASHP 1 + ETICS (r1) or ASHP 2 + ETICS (r2).

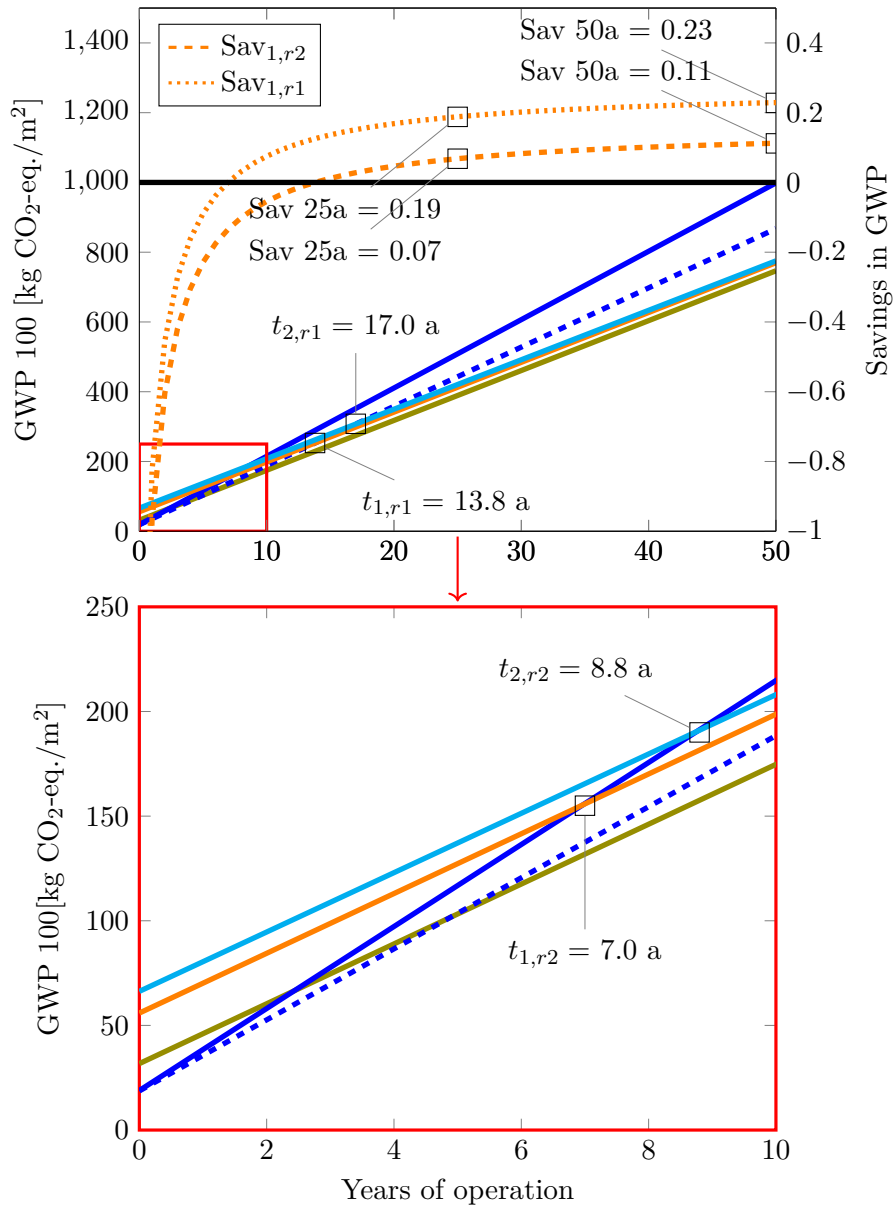


FIGURE 6.2.9. Global warming potential in the course of operating time. The time of amortization of global warming potential of the Col-Ice systems referred to the ASHP systems is indicated with  $t_{x,ry}$ , exemplary savings on the right axis with  $Sav_{x,y}$ . The first index refers to Col1-Ice70 (1) or Col2-Ice80 (2), the second index refers to ASHP 1 + ETICS (r1) or ASHP 2 + ETICS (r2).

### 6.3. Summary and discussion of results

#### Components

Based on the described data and considering the limitations mentioned in section 6.1.1, the evaluation results of the façade elements can at least dispel the doubts that UHPC elements could have an even greater influence than metal elements on the PED and GWP of buildings. Aspects of the circular economy are not yet considered in detail here. Production mixes were used that also include secondary metal. Whereas currently, metals are easier to recycle, more and more efforts are underway to recycle cement-bound materials. And recycling metals requires a lot of energy because of the high temperatures needed in the process. The rear-ventilated façade needs a substructure that is assumed to be made of aluminum. A wooden substructure could possibly compensate for its higher emissions in GWP and PED with respect to ETICS.

The high contribution of the façade to the total emissions of the system boundaries considered here, which includes only the south façade, highlights that an improvement there has a significant impact on the total emissions of a building.

#### Use phase

The use phase is the most important contributor to the life cycle of all considered systems. With the fixed CO<sub>2</sub> emission factor determined in 2014, their contribution clearly dominates (96 to 84% in 25 years in GWP), with a decreasing CO<sub>2</sub> emission factor of only 89% to 64% of total GWP occurring in the use phase. This emphasizes the importance of good system design and supports further investigation to improve system efficiencies.

The lower CO<sub>2</sub> loads per kilowatt-hour in the dynamic consideration could lead to the assumption that this consumption would then be acceptable. This assumption, in turn, leads to one of the rebound effects that slow down the energy transition to the point of making it impossible.

So, in the author's opinion, the pure consideration of the dynamic CO<sub>2</sub> emission factor as shown is of little purpose for the intention of this work. True dynamic consideration should also assess the manufacturing of the components dynamically and would need to assess system efficiency differently. This is quite complex, and further investigations could be interesting in the future.

The author recommends using a fixed CO<sub>2</sub> emission factor for a fair comparison of the systems.

### Life cycle

Considering the assumptions made, the hypothesis could be supported that renovations of multi-family homes in Germany with rear-ventilated façade systems with unglazed *TABSOLAR*<sup>®</sup> collectors as cladding that, alone or in combination with an ice storage serve as a source for a heat pump, can be advantageous to passive ETICS façade systems with air heat pump with respect to primary energy and CO<sub>2</sub> demand during lifetime.

The unglazed, uninsulated UHPC collector Col1 is advantageous for both ASHP systems regarding primary energy demand and CO<sub>2</sub> emissions in a direct system (single source for a heat pump) and a system combined with ice storage. The amortization of PED is 3.9 years for ASHP 2 and 19.3 years for ASHP 1 in a direct system. In a system combined with ice storage, 5.4 years for ASHP 2 and 10.7 years for ASHP 1 were achieved. The amortization of GWP is 2.9 years for ASHP 2 and 14.7 years for ASHP 1 in a direct system. In a system combined with ice storage, 7.0 years for ASHP 2 and 13.8 years for ASHP 1 were achieved.

The system with ice storage has longer times of amortization, but considering a lifetime of 50 years, significantly more savings can be obtained.

In a direct system, the insulated, spectrally selective collector Col2 is not advantageous for the ASHP 1 system (5% increase in PED, 4% increase in GWP over 50 years of operation). For ASHP 2, it is still advantageous. The amortization time is 8.5 years, and the decrease in PED over 50 years of operation is 9%. For GWP, the time of amortization is 7.3 years and the decrease over 50 years of operation is 9%. In systems that work with ice storage, both collectors perform very similarly.

The lower simulated savings of Col2-Dir compared to Col1-Dir do not imply that Col2 is not recommendable in Col-Dir systems: on the one hand, the main differences are caused by the electrical backup on the source side of the heat pump needed to meet the minimum required temperature. This can change if A) the occurring ambient temperatures are higher and/or B) if the heat pump allows for lower temperatures. On the other hand, Col2 has a higher potential to contribute directly to the hot storages of the building and, by that, reduce the total energy demand of the building. This needs to be further investigated in the future.

#### 6.4. Further research

Data refinement can be done for the UHPC collectors as soon as better data is available. This holds true for both the processes and materials and for the heat gain curve modeling and its influence on system modeling and simulated required energy in the use phase.

Further investigations on system design as explained in section 5.7 should be made, and possible improvements should be assessed.

The high CO<sub>2</sub> emissions of cement are well known and can only partly be eliminated with the current production technology. New cement production technologies could help to further reduce the GWP impact. Ellis [44] describes an electrolyser-based process where highly pure CO<sub>2</sub> can be separated and used. With 5.2 MJ to 7.1 MJ, the described procedure consumes more electric energy than conventional production with coal which consumes 4.6 MJ. If sufficient renewable electricity was available, this could be a viable option.

Further reduction potential of CO<sub>2</sub> emissions may be found in the recipe of the UHPC. It would be interesting to investigate how far the cement ratio could be reduced.

Better assumptions for the required system components and the energy consumption in the use phase could be gained from demonstration installations. To effectively use LCA results, LCA assessment should be integrated into Building Information Modeling (BIM) to see the LCA impact of design decisions in an early stage of the building design process. In a survey of Bruce-Hyrkäs et al. [14] 86.5% of the respondents would conduct an LCA if it was integrated into BIM.





## CHAPTER 7

### Life cycle cost assessment of systems with UHPC collectors

As part of a sustainability assessment as described in chapter 3 this chapter describes the approach and the results for the life cycle cost assessment of systems with UHPC collectors, draws a conclusion, and offers indicators for further research.

#### 7.1. Methodology

As described in chapter 3, life cycle costing is used to assess the relevant costs for a product or a process during its lifetime compared to the respective alternatives. In other contexts, this is also referred to as total cost of ownership (TCO) or full cost assessment. All these methods can vary in detail, like considering or neglecting certain types of costs, but they have the same goal: assessing all (relevant) costs of a product across its entire life cycle.

Life cycle cost assessment in the context of this work includes the necessary investment costs for the respective type of façade and the investment costs for the system components. Operational costs cover the price for the respective amount of electricity plus maintenance costs. Possibly, there might be differences in rental income for the system of research and the architectonic benchmark on the one hand and the economic benchmark on the other hand. So, these costs are also considered part of the operational costs. In this work, an effort was made to estimate the costs of the different types of façade. Rough calculations were made to estimate whether the Col-Dir or Col-Ice systems presented in this work would be profitable in terms of energy costs compared to the economic benchmark. Rental income was not assessed due to a lack of data. A comparison to standard collector installations is presented for the glazed collector variant *TABSOLAR<sup>®</sup> Premium*.

#### 7.2. Cost assumptions of façade components

Together with the project partners of TABSOLAR II, the author estimated costs for the two UHPC collectors *TABSOLAR<sup>®</sup> Design* and *Premium*, and published the outcome in the final project report [75]. For this chapter, the underlying assumptions are translated, summarized, and extended by the cost of ETICS and building insulation.

The calculations for both collector variants take into account plant costs (including mixer and silo) of two million euros with a depreciation period of 5 years, an imputed interest rate of 5%, and an annual production of initially 30 000 m<sup>2</sup>. Also included are material costs for UHPC (initially 10.50 €/m<sup>2</sup> due to small quantity acceptance, potential: approx. 5 €/m<sup>2</sup> from 375.000 m<sup>2</sup> per year), anchoring (12 €/m<sup>2</sup>) and fluid connections (24 €/m<sup>2</sup>), labor costs (10 €/m<sup>2</sup>), rental costs for buildings (5 €/m<sup>2</sup>), and a protective coating (8 €/m<sup>2</sup>). For the *TABSOLAR® Premium* variant, additional cost assumptions are included for thermal insulation and glazing (30 €/m<sup>2</sup> [25]+10 €/m<sup>2</sup> additional cost for more elaborate glass holder) and for a spectrally selective coating (10 €/m<sup>2</sup>).

The mean costs for the installed substructure are assumed with (87.5 €/m<sup>2</sup>), the mean margin of the façade constructors with (0.55 €/m<sup>2</sup>), and additional costs for increased installations work of *TABSOLAR®* was assumed with (12.5 €/m<sup>2</sup>).

This work compares different renovation pathways, which include façade insulation. The economic façade reference in this work consists of an External Thermal Insulation Composite System (ETICS). The BMVBS<sup>1</sup> [78] published a study based on DENA<sup>2</sup> data from 2010 about 531 energetic renovation projects. They all were examined, and the total costs were derived. The average cost for a 15 cm insulation was 123 €/m<sup>2</sup>. The basic cost was 87 €/m<sup>2</sup>, and the cost dependent on the thickness of the insulation was 2.43 €/cm/m<sup>2</sup> [78]. The coefficient of determination of this correlation was  $R^2 \approx 0.16$ , which means that higher insulation thickness does not have to lead directly to higher costs as there is a strong scatter. In the case of 12 cm, the cost ranges from 85 to 150 €/m<sup>2</sup>. These costs include varying extra work, for example, for window and balcony framing and other edging work. Nevertheless, following T. Nürnberger's estimation from DAW SE [129] these prices can be considered a valid range for today's ETICS without extra work as prices for wage and material increased. Therefore, this range is given in figure 7.3.2. T. Nürnberger estimated the price difference of ETICS and building insulation in a rear-ventilated façade to be 20 €/m<sup>2</sup> for a 12 cm mineral wool insulation as the mineral wool prices for the different façade applications vary: the plaster needed for the application in an ETICS façade can be omitted in the case of a rear-ventilated façade. In addition, shorter installation work time is needed for the building insulation in a rear-ventilated façade. For the comparison in figure 7.3.2, the cost for the 12 cm building insulation was assumed to have a mean value of 100 €/m<sup>2</sup> according to the suggestions of T. Nürnberger.

<sup>1</sup>Bundesministerium für Verkehr, Bau und Stadtentwicklung, Engl.: Federal Ministry of Traffic, Construction and City Development

<sup>2</sup>Deutsche Energie Agentur, Engl.: German energy agency

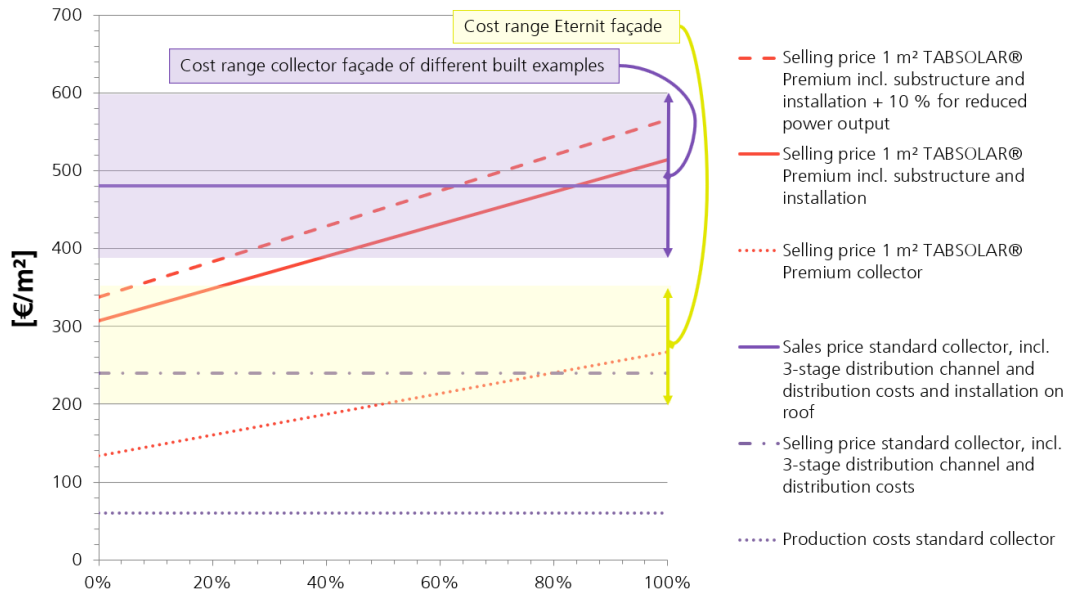


FIGURE 7.3.1. Profit margin as a percentage of the manufacturing price for 1 m<sup>2</sup> *TABSOLAR® Premium* element. Costs for standard collector and cost ranges for built façade collectors are based on Cappel et al. [25]. Source for cost ranges for Eternit: Priedemann Facade-Lab. Source for cost range ETICS: BMVBS [78].

### 7.3. Results and discussion

#### 7.3.1. Glazed UHPC collector

Figure 7.3.1 shows average cost estimates per square meter as a function of the profit margin as a percentage of the manufacturing price for the variant *TABSOLAR® Premium*.

When comparing this variant with standard collectors, it must be taken into account that *TABSOLAR® Premium* has reduced performance. According to old simulations of a single-family home (SFH) in Würzburg, Germany, during the project *TABSOLAR* [74] (figure A.12), the fractional energy savings  $f_{sav}$  of a 15 m<sup>2</sup> façade installation is reduced by approximately 7.5% when comparing *TABSOLAR® Premium* (case 2 figure A.12) to the selected high-performance reference collector (0.309 instead of 0.334). This can be compensated for in certain areas by an increased collector area and thus higher costs. In the above-mentioned simulation study, for example,  $f_{sav}$  of 0.348 could be achieved with 20 m<sup>2</sup> of *TABSOLAR® Premium*. However, it must be noted that these initial

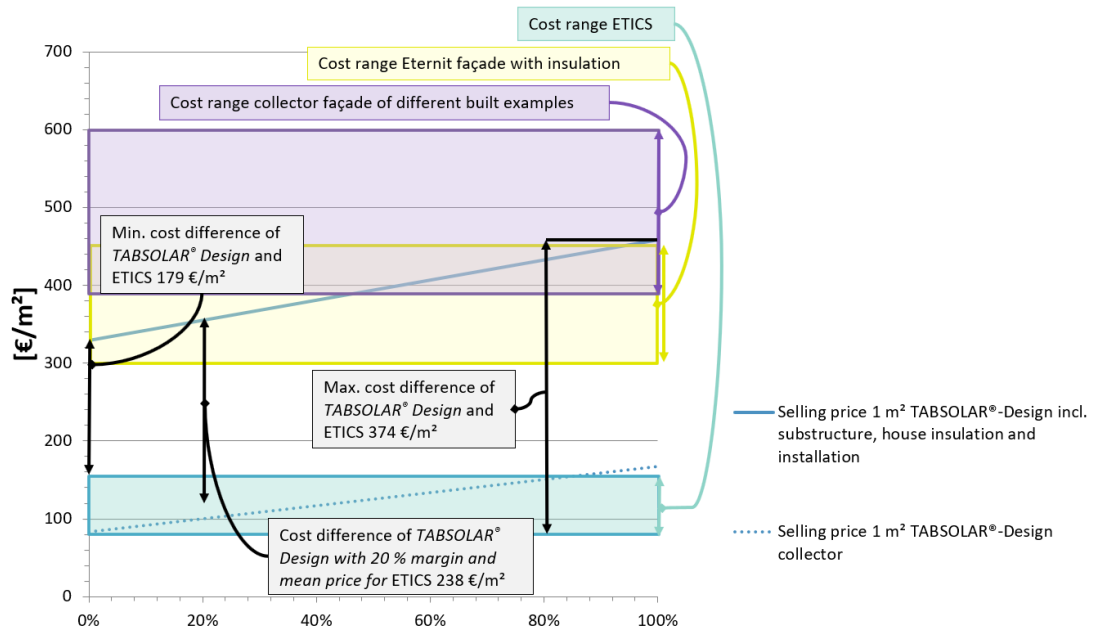


FIGURE 7.3.2. Profit margin as a percentage of the manufacturing price for  $1 \text{ m}^2$  *TABSOLAR® Design* element. Source for cost ranges for Eternit: Priedemann Facade-Lab, façade insulation BMVBS [78]. Source for cost range ETICS: BMVBS [78].

simulation calculations were based on an old channel design. Due to the slightly larger channel spacing and the smaller channel cross-section in the current design, the pressure loss of the absorber to the fluid increases somewhat, and the yield turns out to be slightly lower. Taking into account the losses on a low active margin, the gain per area decreases again. Still, the general achievable temperature limit would only slightly decrease, as can be seen in the simulation of heat gain curves for an insulated, unglazed UHPC collector in figure 4.3.16.

However, this correction is not expected to change the general conclusions: in the comparison in figure 7.3.1, *TABSOLAR® Premium*, including costs for the substructure, the installation, and additional costs to compensate for the larger areas required, lies in the range of built façade collector installations. A significant advantage of *TABSOLAR®* collectors is also seen in the fact that the typical 3-stage distribution channel with installer and intermediary can be replaced by a 1-stage distribution channel.

### 7.3.2. Unglazed UHPC collector

As presented in the previous two sections, *TABSOLAR<sup>®</sup> Design* requires other system concepts. Therefore, the costs of the respective façade must be compared together with the appropriate system.

Since ice storage systems are not mass-produced and oversized systems, in particular, are often custom-made, for the time being, the proposed renovation path with Col1-Ice70 or Col2-Ice80 will not pay off economically over a period of 25 years compared to the economic benchmark of ASHP 1 or 2 with an ETICS façade. However, the added architectural and acoustic value has not yet been priced in. If this was done, it might shift the economics in favor of the Col-Ice systems. The question here is how much the customer is willing to pay for this added value.

As mentioned in the previous chapters, the ice storage is larger than needed in reality, as additional gains from the soil through the storage walls were not considered. These additional gains depend very much on the soil conditions and the construction and size of the ice storage and could not be determined in this work. Which means that the exact size needed could not be determined, either.

By optimizing the system, for example, by using heat transfer fluids that can be used below 0 °C, the size of the ice storage can probably be reduced further. In addition, the ice storage itself still offers savings potential, for example, through a change of material in the shell from regular concrete to UHPC, series production or increased degree of prefabrication. It is thus conceivable that the *TABSOLAR<sup>®</sup> Design* with ice storage system will pay off economically in the future.

Whether a Col-Dir system is economically worthwhile depends on many details. For example, a range is given for both ETICS and *TABSOLAR<sup>®</sup> Design*, and depending on where exactly one is located within this range, the cost differences between the two types of façade range from 179 € to 374 € euros (compare figure 7.3.2). For a façade area of 156.6 m<sup>2</sup>, the opaque south façade of the multi-family home (MFH) considered in this work results in a cost difference of 28 000 € to 58 600 €. The minimum cost difference can only be achieved with a 0 % margin for the production of the UHPC collectors and a maximum price for ETICS. Assuming a small margin of 20 % and average costs for ETICS, the cost difference for the whole south façade would be about 37 300 €.

Both economic reference systems are ASHP systems, but as they differ in efficiency and slightly in size (ASHP 1: 21.7 kW, ASHP 2: 22.0 kW), they probably also differ in investment costs. The heat pump used in the Col-Dir system is a GSHP type and with 20.2 kW is still slightly smaller than the ASHP 1. Probably they are in the same cost range as the ASHPs, including their outside air unit, as the difference in costs of

ASHP and GSHP are mainly caused by the borehole heat exchanger, which is very cost-intensive and not needed in the case of a Col-Dir system. Assuming the investment costs of the three types of heat pump were the same, the costs for the additionally needed solar system components would also need to be accounted in the Col-Dir system. This can also only be guessed very roughly.

Future electricity prices would need to be known to determine operating costs. It is very difficult to estimate how electricity prices will develop in the future. This would require detailed knowledge of the development of electricity production costs, grid charges, taxes, the CO<sub>2</sub> price, and possible social compensation measures for fair financing of the energy transition. The author lacks the knowledge of whether an increase or a decrease in the electricity price is more likely over the next 25 years. Nor can she make any statements about possible rates of reduction or increase. An indication for the price development can be found in a short study by the Institute of Energy Economics in Cologne (EWI) and RWTH Aachen University commissioned by E.ON Energy Research Center [160]. They estimated the price for electricity and gas depending on two different scenarios for the development of the CO<sub>2</sub> price until the year 2050. The first results in a price of 180 €/t CO<sub>2</sub>-equivalent (COP1), the second in 260 €/t CO<sub>2</sub>-equivalent in 2050 (COP2). The price of electricity decreases from 0.298 €/kWh in 2017 to 0.243 €/kWh in 2030 and slightly increases to 0.251 €/kWh or 0.252 €/kWh depending on the scenario in 2050, while the price for gas more than doubles within timeframe (from 0.066 €/kWh in 2017 to 0.147 €/kWh or 0.166 €/kWh in 2050). The purchase price for heat pump electricity can be assumed lower than the normal household tariff [17].

This work only determined that a Col-Dir system saves electricity compared to an ASHP system when the south façade is fully covered with collectors. The amount of saved electricity depends on the reference system (ASHP 1 or ASHP 2) and on the considered operating time. Table A.9 and table A.10 list the total electricity needed per year for each reference system and the Col-Dir and Col-Ice systems with a fully covered south façade. Regarding ASHP 2, the Col-Dir system can save 82.000 kWh over 25 years. With the current electricity price of 0.28 €/kWh, this would result in about 23 100 €. This is considered the upper limit of cost savings as neither a decrease in electricity price nor a reduced price for a heat pump tariff is considered. These saved operational costs must be balanced with the additional façade costs of 37 300 € and the solar system components and its imputed interests.

Figure 7.3.3 shows the estimated invest costs without imputed interests of reference façade systems and collectors façade systems without the investment costs and its imputed interests of system components like for example the ice storage, piping and pumps and the operating costs over 25 years of operation with an assumed electricity price of

0.28 €/kWh. The costs for the passive UHPC façade elements were assumed to be the mean price of the Eternit elements whose cost range is shown in figure 7.3.2. The real cost figures can differ greatly from the values shown in figure 7.3.3.

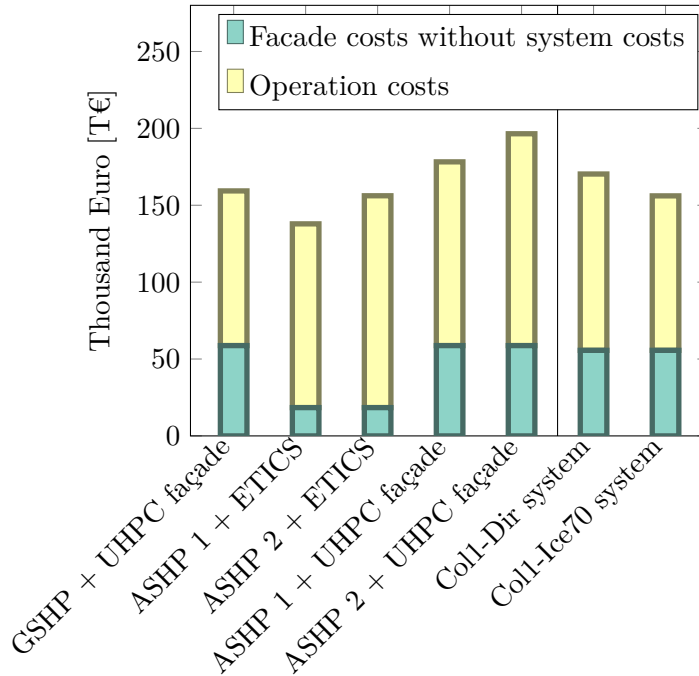


FIGURE 7.3.3. Estimated investment costs of façade without imputed interests and costs of 25 years of operation for reference systems, Coll-Dir and Coll-Ice70 systems with an electricity price of 0.28 €/kWh. The price for the passive UHPC façade elements was assumed to be similar to Eternit façade elements. Investment costs of system components like ice storage with their imputed interests are not shown.

It quickly becomes clear that a Col-Dir system is probably not economically favorable compared to an ASHP reference system with an ETICS façade if, according to the predictions [160], electricity prices do not rise significantly and differences in rental incomes are not considered or do not exist. Nevertheless, the Coll-Dir system, with its lower energy costs and higher investment costs, might be in the same life cycle cost range as the ASHP 1 with ETICS. It might thus prove a real alternative with the advantage of a high-quality rear-ventilated UHPC façade. If the reference system would consist of an ASHP with a passive UHPC façade, the Col-Dir system could possibly be profitable.

Hess et al. [77] investigated techno-economic and ecologic perspectives for air-source and ground-source heat pumps in multi-family homes in Germany. Their research was

based on the dynamic evolution of the CO<sub>2</sub> price proposed by the Institute of Energy Economics in Cologne (EWI) and RWTH Aachen University commissioned by E.ON Energy Research Center [160] and own calculations (COP1). They conclude that with subsidies (investment grants), the HP systems investigated have lower heat production costs than the gas condensing boiler in the period under consideration (2020-2045). And as cited in chapter 6, these heat pump systems save 50 % of the CO<sub>2</sub> emissions compared to a system with a condensing boiler.

This result underlines the importance of incentives and the need to reduce investment costs.

## Conclusion

The calculations show that *TABSOLAR*<sup>®</sup> elements can achieve attractive prices as a façade for energy generation. A façade that is comparable to *TABSOLAR*<sup>®</sup> elements in terms of architectural design such as Eternit, for example, costs approximately 200 to 350 €/m<sup>2</sup> (depending on the pattern, color, sizes, and fastening system) and approximately 300 to 450 €/m<sup>2</sup> with insulation. For energy façades, reduced distribution costs due to bypassing a three-stage distribution channel are an essential factor for attractive prices. Concerning the overall systems, ice storage systems still represent a high-cost factor in the current state of the art, which can have a significant impact on economic efficiency. Large ice storage tanks are required (1.13 m<sup>3</sup> to 1.32 m<sup>3</sup> of ice storage per MWh of heating demand in the simulations presented) if the collector is operated only with water and only at temperatures above 0 °C<sup>3</sup>. However, only small or no ice storage tanks are required if the collector can be operated with heat transfer fluids with antifreeze protection and, therefore, at temperatures below 0 °C during the winter months. In this case, there may be slightly higher maintenance costs and slightly higher component costs due to the heat transfer fluid.

Simplified calculations showed that a Col-Dir system would probably not save costs compared to the economic benchmark of an ASHP with an ETICS façade. Nevertheless, it would probably not much more expensive and could prove an alternative if a high-quality façade is desired or an ASHP cannot be installed.

Overall, therefore, low-cost ice storage concepts or concepts that can completely dispense with ice storage are of great importance.

---

<sup>3</sup>As explained in section 4.2.2.2 tests showed that *TABSOLAR*<sup>®</sup> elements might not be completely water vapor-tight. Water without antifreeze can be used to strictly avoid leakage of a possibly toxicologic heat carrier.



#### 7.4. Further research

Only strongly simplified estimations regarding investment and operational cost could be made in the result and discussion section. Demonstration plants could be the next step to refine the cost estimation. The installation involves different trades: a façade builder typically installs a rear-ventilated façade, while an installer installs the collectors. It should be examined whether the proposed façade collectors could be fitted with a plug-and-play connection so that a trained façade builder could take over this task. In this case, the installer would only be needed to connect the collectors to the heat pump. This process must be tested, monitored, and scientifically accompanied.

In this work, the collectors only serve as a heat pump source. A spectrally selective, insulated collector could also be used directly for the preparation of hot water or heating. The energy savings might be higher, which would lead to more cost savings. Another possibility would be combining different UHPC collectors types for low and high temperature levels. This as well as the propositions for further research in system design in section 5.7, should be evaluated in the future.



## CHAPTER 8

### Discussion of results, conclusion, and further research

This chapter presents the overall summary, discussion, and conclusion of this work with regard to further research. It also recalls the respective detailed sections of chapter 4 (collector description and modeling), chapter 5 (system description and modeling), chapter 6 (LCA data presentation), and chapter 7 (life cycle costs).

#### 8.1. Summary and discussion of results

Based on the assumption of a necessary heat transition, chapter 2, “Architecture and solar thermal”, analyzes literature and examples on the relationship between architecture, and façades in particular, and components that convert solar radiation into energy. Several theses are derived from this analysis, representing the basic assumptions of this work. Based on the fact that façades have a symbolic value, the thesis that collectors with higher freedom of design and a broader range of options would better meet the requirements of façades is a main motivation for this work. Since collectors made of UHPC are assumed to offer higher freedom of design than most state-of-the-art collectors and could therefore extend the palette of existing collectors, they are the subject of this research. Qualitative evaluation factors for BIST collectors are collected and presented in a diagram.

Chapter 3 outlines why sustainability assessments of BIST can be helpful, what should be looked at, and how this assessment can be done. As this work deals with the contribution of solar thermal façade collectors made of UHPC to the urban heat transition, the functional unit comprises the renovation of a multi-family home. This is the most relevant building size regarding the number of apartments in the German building stock, especially in urban environments. The renovation comprises a new façade and a new heating system. An economic benchmark (ASHP+ETICS), an architectonic benchmark (GSHP+passive UHPC cladding), and a technical reference (unglazed steel collector as a direct source for a heat pump) are defined. The developed workflow to determine the primary energy and the CO<sub>2</sub> emissions of all systems is described in a diagram.

Chapter 4 describes the considered UHPC collectors and outlines questions that arise when modeling unglazed collectors with a direct coupling on the façade. An FEM

modeling approach for generating heat gain curves from different operation points is presented and applied. The FEM modeling approach is compared to a validated node model for the generation of heat gain curves and its limits for collectors without back-insulation is discussed. Two heat gain curves that also consider margin and thermal bridge effects for a gray, uninsulated, unglazed UHPC collector (Col1) and a spectrally selective, insulated, unglazed UHPC collector (Col2) are presented for further use in system simulations. For a set of glazed collectors with different active areas, the criterion for MAP funding was calculated. As a conservative guess, the margins were assumed as passive areas with no gains and losses as the focus was on channel distance vs. area utilization. Here it was found that non-spectrally selectively coated collectors with Low-E glazing of the considered size might not reach the current funding limit in Germany (MAP). Only the spectrally selective UHPC collector with glazing and insulation reaches the funding limit. As the possible heat gain contribution of the margins was neglected, real heat gain curves might be higher. Measurements need to show if non-spectrally selectively coated collectors with Low-E glazing reach the funding limit of MAP.

Chapter 5 explains the design of the systems of research and the defined reference systems and presents the results. Different tests were conducted with UHPC collectors as a direct source for a heat pump (Col-Dir systems) and in combination with an ice storage (Col-Ice systems).

In the first test of the Col-Dir systems, the collector area and the wind exposure were varied. It was found that Col-Dir systems can be advantageous over ASHP systems. Depending on the selected ASHP, Col1-Dir systems would have similar  $SPF_{sys}$  values at  $6 \text{ m}^2$  per Kilowatt of  $Q_{demand,biv}$  (ASHP 1) or  $3 \text{ m}^2$  per Kilowatt of  $Q_{demand,biv}$  (ASHP 2). Col2-Dir could only reach similar  $SPF_{sys}$  values as ASHP 2 with full wind exposure. At half of the wind exposure at 1 m altitude, Col2-Dir matched the value of ASHP 2 with about  $5 \text{ m}^2$  per Kilowatt of  $Q_{demand,biv}$ . The higher the wind exposure of the collectors, the better the system efficiencies as convective gains dominate the collector gains at operating temperatures of  $-5 \text{ K}$  to  $-2.5 \text{ K}$  below ambient temperature. Solar gains play a minor role, which was shown in a test on the north façade: the values of  $SPF_{sys}$  of the Col1-Dir system are only slightly lower than on the south façade. An increase of storage temperature in times of solar irradiation above  $200 \text{ W/m}^2$  did lead to lower values of  $SPF_{sys}$ . So, this can be a measure for load management, but at the cost of higher energy demand.

The Col-Ice systems were dimensioned under the condition that the collector would only operate at temperatures above  $0 \text{ }^\circ\text{C}$ . Another condition was that storage assumed adiabatic should never be fully frozen. This resulted in storage sizes of  $1.51 \text{ m}^3$  to  $1.32 \text{ m}^3$  of ice storage per MWh of total heating energy delivered ( $Q_{delivered,tot}$ ). The Col-Ice

systems reached about the same  $SPF_{sys}$  value as the GSHP. In the Col-Ice system, the solar gains dominated the total gains of the collector with 77 %. An installation on the north façade showed that an area increase of 90 % would be required with the same ice storage size under the conditions that the ice storage never freezes and the collector operating temperature remains above 0 °C.

Chapter 6 describes the primary energy and CO<sub>2</sub> emissions of the reference and the research systems. A comparison is conducted, including only the Col-Dir and Col-Ice systems with the whole south façade covered with collectors exposed to half of the wind velocities at 10 m of altitude. The yearly impacts of operation and components with a lifetime of 25 years show the dominating role of the use phase: the Col-Ice systems have the highest percentage of components on the total impact with 10 % to 12 % of PED (same as ColRef) and 14 % to 16 % of GWP. However, the respective savings are oriented on the results of the system simulations. The amortization times of the Col-Dir and Col-Ice systems are calculated with respect to the two ASHP systems. They range from 3.9 years (amortization of GWP of Col1-Dir with respect to ASHP 2) to 19.3 years (amortization of PED of Col1-Dir with respect to ASHP 1). The considered Col2-Dir system does not amortize compared to ASHP 1, only compared to ASHP 2 after 8.5 years. The GSHP system performs in the range of the Col-Ice systems, which performs almost equally well with both considered collector types.

Depending on the type of ASHP, savings over 25 years of operation range from 1 % to 14 % in PED and 2 % to 14 % in GWP for the Col1-Dir system. For the Col1-Ice70 system, savings range from 9 % to 21 % in PED and 7 % to 19 % in GWP. If longer lifetimes of up to 50 years can be reached, savings range from 2 % to 15 % in PED and 3 % to 16 % in GWP for the Col1-Dir system. For the Col1-Ice70 system with a lifetime of 50 years, savings range from 12 % to 24 % in PED and 11 % to 23 % in GWP.

Chapter 7 shows that *TABSOLAR*<sup>®</sup> elements can achieve attractive prices as a façade for energy generation. But neither a Col-Ice nor a Col-Dir system can be more profitable than the economic benchmark of an ASHP system with an ETICS façade. Nevertheless, the cost difference between an ETICS façade and a rear-ventilated façade could be reduced by the energy costs saved and, thus, make high-quality rear-ventilated façades more attractive. If a passive rear-ventilated façade with an ASHP 2 system would be used as the reference, the Col-Dir system might pay off. The Col-Ice systems are more efficient and thus save more energy costs than an ASHP system. However, since ice storage systems are not mass-produced yet, and oversized systems are often custom-made, the proposed renovation path with Col1-Ice or Col2-Ice will, for the time being, not pay off economically over a period of 25 years compared to the economic benchmark of ASHP 1 or 2 with an ETICS façade.

## 8.2. Conclusion

To answer the initial research question, it was broken up into multiple questions. The original general research question was “Can a renovation with a rear-ventilated façade system with unglazed UHPC collectors as cladding elements that serve as a source for a heat pump be an economically competitive and sustainable restructuring plan for existing multi-family homes in Germany?” In this part, the answers to the single questions given in this work are briefly summarized and a general conclusion is drawn. Each chapter corresponds to a more specific research question.

(1) **Chapter 2: what are the qualitative parameters of solar thermal for good architectural integration?**

Basic qualitative parameters of solar thermal are availability and functional evaluation parameters described by the standards for solar thermal. Other parameters are important for the installation and maintenance process. Special attention in the evaluation and development of BIST require life cycle costs, life cycle impact and aesthetics.

(2) **Chapter 3: what is the functional unit and the reference system to fairly assess architecturally integrated, technical renovation plans?**

The functional unit of architecturally integrated, technical renovation plans should comprise the components of the façade or building envelope system and the heating system and the energy needed during the considered lifetime.

(3) **Chapter 4: how can UHPC collectors be simulated depending on the existence of a back insulation and glazings and what is their heat output?**

A validated node model for the simulation of characteristic curves of insulated and glazed collectors was tested for the simulation of UHPC collectors. This was done by comparing it with an FEM simulation model presented in this work. It could be shown that the simplification in the mentioned node model is valid for insulated, unglazed UHPC collectors as well as for insulated glazed UHPC collectors. It does not adequately represent the characteristics of non-insulated UHPC collectors. For collectors without back insulation, the approach of the node model leads to inaccuracies proportional to the temperature differences of the fluid and the ambient. The FEM model presented in this thesis avoids these inaccuracies, but needs to be validated with experimental data.

The FEM model can also be used to determine margin losses, thermal bridges or influence of back ventilation. The heat output of uninsulated, unglazed

collectors is low at operating temperature above ambient temperature and high at operating temperatures below ambient temperature.

For the determination of the heat output of glazed façade collectors, the respective correlations for convective losses in vertical columns should be used and further studied.

The current funding limit in Germany (MAP) is oriented on the heat output at temperatures in the relevant range for direct heat provision for heating or DHW. This limit is relevant for glazed collectors. It could be shown that non-spectrally selectively coated UHPC collectors with Low-E glazing do not meet the MAP criterion in the case considered. A spectrally selective UHPC collector with glazing and insulation reaches this limit.

(4) **Chapter 5: how can systems with unglazed UHPC collectors be designed and which energy demand do they have?**

Unglazed UHPC collectors without back insulation have low heat output at operating temperatures above ambient temperature and therefore are not able to provide direct heat for heating or DHW. As their heat output at temperatures below ambient is high, these collectors are well suited to provide heat at the source side of a heat pump (Col-Dir system). In the case, that the temperature level is below the allowed temperature range for the heat pump, an auxiliary heater on the source side of the heat pump should be installed. If an ice storage is installed as well, no auxiliary heater on the source side is needed as long as the ice storage is large enough to not entirely freeze during wintertime (Col-Ice system). Insulated, unglazed UHPC collectors with spectrally selective coating have the option of direct heat provision during the summer. Compared to an ASHP system, Col-Dir and Col-Ice systems can save energy. The amount of saved energy depends on the collector area, the type of AHPS and the type of collector. Col-Dir systems can not save energy compared to an GSHP system. Col-Ice systems are in the same range as GSHP systems regarding their energy demand.

(5) **Chapter 6: what is the primary energy demand and the CO<sub>2</sub> emissions for materials, processing, transport, use phase, and end-of-life of the architecturally integrated, technical systems considered?**

The primary energy demand and the CO<sub>2</sub> emissions of a rear-ventilated façade is generally higher than that of an ETICS façade. This is due to the substructure needed which was made of aluminum in the case considered here. Compared to a passive UHPC façade cladding, the unglazed UHPC collector without back insulation has only slightly higher primary energy demand and the

CO<sub>2</sub> emissions. Both claddings still have fewer than a third of the emissions of the substructure and house insulation together. Applying spectrally selective coating and glazing leads to primary energy demand and the CO<sub>2</sub> emissions almost in the range of the substructure and house insulation together.

Regarding the system components, the ice storage has comparatively high primary energy demand and the CO<sub>2</sub> emissions. Neglecting the façade components, this leads to a doubling or more of the primary energy demand and CO<sub>2</sub> emissions of the total system of the Col-Ice systems compared to all other systems.

Looking at an operation time of 25 years, the primary energy demand and the CO<sub>2</sub> emissions of the operation clearly dominate. System components play a minor role.

**(6) Chapter 7: what are the life cycle costs of the architecturally integrated, technical systems considered?**

The additional costs of a Col-Dir system (rear-ventilated façade with unglazed, uninsulated collector cladding as a source for a heat pump) compared to an economic benchmark system (ETICS with ASHP) are higher than the saved energy costs in 25 years. This means that despite its ecological advantages a Col-Dir system is not economically competitive to the most economic benchmark system. If the Col-Dir system is compared to a system with similar façade structure and ASHP the Col-Dir system can be ecologically and economically competitive. Col-Ice systems have even higher additional investment costs due to the large ice storage. So, despite that the energy costs savings compared to an ASHP system are higher than those of the Col-Dir system, the total costs of the Col-Ice system are also higher than the economic benchmark.

Generally speaking, the data derived from the modeling procedure presented in this work supports the initial hypothesis that renovations of multi-family homes (MFH) in Germany with rear-ventilated façade systems and unglazed UHPC collectors can have lower primary energy demand and CO<sub>2</sub> emissions during lifetime than an economic benchmark. This is based on the condition that the unglazed UHPC collectors are installed as cladding and serve as a source for a heat pump in combination with an ice storage (Col-Ice) or alone (Col-Dir). They are compared to the economic benchmark, a passive ETICS façade system with an air-source heat pump (ASHP).

Compared to a renovation with the architectonic benchmark, which was defined as a ground-source heat pump (GSHP) with a passive rear-ventilated UHPC façade, Col-Dir and Col-Ice systems are not advantageous concerning primary energy and CO<sub>2</sub> emissions during lifetime. The considered Col-Ice systems do perform slightly better energetically



than the GSHP system. Still, the difference is very low and cannot compensate for the slightly higher emissions of the components.

A simplified calculation of the life cycle costs (LCC) revealed that the savings in energy costs would not compensate for the higher investment costs of the façade and the system. Nevertheless, the total additional costs of the Col-Dir system compared to the economic benchmark are lower than the total additional costs of a passive rear-ventilated façade with ASHP system compared to the economic benchmark. This supports the initially posed hypothesis that these architecturally integrated system combinations without a need of a visible outside air unit can increase attractiveness of rear-ventilated high-quality façade systems and, at the same time, lead to CO<sub>2</sub> savings.

The exact savings depend on the actual additional systems costs of the Col-Dir system for installation, ducting, etc., the energy price, and the type of ASHP used in the benchmark.

The Col-Ice systems have higher energy cost savings compared to the economic benchmark, but investment costs are rather high and hard to estimate: ice storages are still a niche product, and especially large storages are often custom-made and cost-intensive. So, the considered Col-Ice system will not pay off within a reasonable time.

Besides the savings in energy and the resulting lower energy costs, the architectonic-technical combinations of Col-Dir and Col-Ice systems do not need a visible outside air unit with the inherent acoustic emissions. Especially in narrow urban environments with high noise pollution, systems that take up as little exterior space as possible and emit minimum noise can provide additional benefit. Slightly higher costs might be acceptable.

The presented systems could also promote heat pump systems in cases where regional conditions do not allow for the use of geothermal heat, and an air-source heat pump is no alternative because of distance regulations to the noise-emitting outside air unit or other reasons. In this case, the presented system would most likely replace an oil or gas heating system and could lead to significant CO<sub>2</sub> savings compared to that reference.

Two types of unglazed UHPC collectors were investigated in the Col-Dir and Col-Ice systems: a gray, uninsulated collector (Col1) and a collector with back insulation and spectrally selective coating (Col2). Col1 with its gray, ceramic-like surface is expected to have higher potential for architectonic integration than Col2 with its dark blue surface behind which the UHPC material disappears. Nevertheless, with regard to the flexibility in surface texture, both collector types extend the existing palette of thermally active cladding elements. Shape and size can be varied, as well as the jointing. In the considered system configurations, the largest share of useful energy was gained with collector temperatures below ambient temperatures. For maximum gain from the ambient, the collector should have a large area exposed to the ambient and should not have back

insulation. Amongst Col-Dir systems without storage of gained solar energy, Col1 performed better than Col2 as the solar energy could hardly be used. A minimum aperture area of approximately  $4\text{ m}^2$  to  $6\text{ m}^2$  per kW of the heat demand at the bivalent point  $\dot{Q}_{demand,biv}$  should be provided for. This corresponds to 44 % to 66 % of the opaque part of the south façade of the considered MFH.

If solar energy can be stored, both collector types perform very similarly. As soon as the energy is used directly, back insulation and a spectrally selective coating are needed to achieve the required system temperatures. So, systems with Col2 are advantageous as Col1 is hardly able to provide temperature levels for direct use. Combinations with glazed UHPC collectors could be beneficial, as well. Regarding architectural flexibility, insulated, gray UHPC collectors with Low-E coated glazing can be an option.

### 8.3. Further research

All ideas for further research are detailed in the respective chapters; please refer to sections 4.5, 5.7, 6.4 and 7.4.

Demonstration plants are needed to validate and refine simulation models and to learn from design, production, installation, and monitoring.

For economic competitiveness, an emphasis should be made on low additional investment costs for the solar active façade and related system components. This can be achieved by a high degree of prefabrication, standardization, and simplification of interfaces, automation in the design and installation process, high automation in the manufacturing process of the UHPC façade collectors as well as high capacity utilization of production lines by producing co-products, such as heating and cooling elements and passive UHPC cladding elements.

Further improvements in the system design should be investigated to lower the remaining energy demand. Improvements could be achieved with new types of heat pumps with extended operational limits, other latent storage concepts with higher phase-change temperature, district concepts with central storage, combinations of different collector types and direct use of solar heat, lower temperatures at the demand side by concrete core activation or underfloor heating, and other concepts for domestic hot water such as ultrafiltration. Extending the application to cooling in the summertime by using colder night temperatures might be interesting for southern regions or climate adaptations.

## Bibliography

- [1] Şirin Alibaş. “Simulation of PVT Collectors as Heat Source to Heat Pumps in Multi Family Houses”. Master’s Thesis. Freiburg im Breisgau: Albert-Ludwigs-Universität, 2019-11-26. (Visited on 12/11/2019).
- [2] Hans-Joerg Althaus et al. *Life Cycle Inventories of Metals: Data v2.1 (2009): ecoinvent v2.1 report No. 10*. Dübendorf, CH, 2009. (Visited on 01/22/2019).
- [3] Evan Stuart Andrews et al. *Guidelines for Social Life Cycle Assessment of Products: Social and socio-economic LCA guidelines complementing environmental LCA and Life Cycle Costing, contributing to the full assessment of goods and services within the context of sustainable development*. Belgium: Druk in de weer, 2009. ISBN: 978-92-807-3021-0. (Visited on 08/10/2018).
- [4] Oliver Arnold et al. “Efficiency Analysis of Solar Assisted Heat Supply Systems in Multi-Family Houses”. In: *EuroSun 2016 Conference Proceedings*. Ed. by Víctor Martínez and José González. Freiburg im Breisgau: International Solar Energy Society (ISES), 2017, pp. 1–13. ISBN: 978-3-9814659-6-9. DOI: 10.18086/eurosun.2016.04.21. (Visited on 04/04/2018).
- [5] Asa Wahlström. *Procedures for environmental performance assessment for solar thermal systems: Report in WP 4.9 of NEGST - New generation of solar thermal systems*. 2007. URL: [http://www.swt-technologie.de/WP4-D2.8.b-final\\_report.pdf](http://www.swt-technologie.de/WP4-D2.8.b-final_report.pdf) (visited on 11/18/2015).
- [6] Andreas K. Athienitis, Liam O’Brien, and Jean-Christophe Hadorn, eds. *Modeling, design, and optimization of net-zero energy buildings*. Solar heating and cooling. Berlin: Ernst & Sohn, 2015. (Visited on 10/27/2020).
- [7] D. Bauer et al. “Thermal resistance and capacity models for borehole heat exchangers”. In: *International Journal of Energy Research* 35.4 (2011), pp. 312–320. ISSN: 0363907X. DOI: 10.1002/er.1689. (Visited on 10/21/2020).
- [8] Gerd Becker et al. *Gebäudeintegrierte Solartechnik: Architektur gestalten mit Photovoltaik und Solarthermie*. 1. Auflage. DETAIL Green Books. München: Institut für internationale Architektur-Dokumentation, 2016. ISBN: 978-3-95553-325-0.

- [9] Irene Bergmann and Werner Weiss. *Fassadenintegration von thermischen Sonnenkollektoren ohne Hinterlüftung: Systemtechnische und bauphysikalische Grundlagen für die Fassadenintegration von thermischen Sonnenkollektoren ohne Hinterlüftung*. Ed. by AEE Intec. Gleisdorf, 2002. (Visited on 05/02/2018).
- [10] Gian Andrea Blengini and Tiziana Di Carlo. “The changing role of life cycle phases, subsystems and materials in the LCA of low energy buildings”. In: *Energy and Buildings* 42.6 (2010), pp. 869–880. ISSN: 03787788. DOI: 10.1016/j.enbuild.2009.12.009. (Visited on 01/07/2019).
- [11] Paolo Bonato et al. *State-of-the-art and SWOT analysis of building integrated solar envelope systems*. 2019. DOI: 10.18777/ieashc-task56-2019-0001. (Visited on 11/12/2020).
- [12] Borken-Kleefeld J., Weidema B P. “Global default data for freight transport per product group”. In: *International Journal of Life Cycle Assessment* Manuscript for specialecoinvent 3.0 issue (2013).
- [13] Ruslan Botpaev. “Experimental investigations of water filled drainback systems”. Dissertation. Kassel: University of Kassel, 2017-03-30. URL: <https://kobra.uni-kassel.de/handle/123456789/2017081653257> (visited on 11/17/2020).
- [14] Tytti Bruce-Hyrkäs, Panu Pasanen, and Rodrigo Castro. “Overview of Whole Building Life-Cycle Assessment for Green Building Certification and Ecodesign through Industry Surveys and Interviews”. In: *Procedia CIRP* 69 (2018), pp. 178–183. ISSN: 22128271. DOI: 10.1016/j.procir.2017.11.127. (Visited on 05/14/2018).
- [15] Bundesministerium der Justiz und für Verbraucherschutz. *Bundesklimaschutzgesetz: KSG*. 12.12.2019/18.8.2021. URL: <https://www.gesetze-im-internet.de/ksg/KSG.pdf>.
- [16] Bundesministerium für Wirtschaft und Energie. *Richtlinie zur Förderung von Maßnahmen zur Nutzung erneuerbarer Energien im Wärmemarkt: Fassung vom 30.Dezember 2019*. 2019.
- [17] Bundesnetzagentur and Bundeskartellamt. *Monitoringbericht 2019*. Ed. by Bundesnetzagentur and Bundeskartellamt. Bonn, 2019. URL: [www.bundesnetzagentur.de/SharedDocs/Mediathek/Berichte/2019/Monitoringbericht\\_Energie2019.pdf?\\_\\_blob=publicationFile&v=5](http://www.bundesnetzagentur.de/SharedDocs/Mediathek/Berichte/2019/Monitoringbericht_Energie2019.pdf?__blob=publicationFile&v=5). (visited on 11/18/2021).
- [18] Bundesverband Solarwirtschaft e.V. *Statistische Zahlen der deutschen Solarwärmebranche (Solarthermie)*. Ed. by Bundesverband Solarwirtschaft e.V. Feb. 2018. (Visited on 09/10/2018).

- [19] Bundesverband Wärmepumpen e. V. and Bundesverband der Deutschen Heizungsindustrie BDH. *Branchenstudie 2018: Marktanalyse - Szenarien - Handlungsempfehlungen*. Ed. by Bundesverband Wärmepumpen e. V. Dec. 4, 2018. (Visited on 04/30/2021).
- [20] Bundeszentrale für politische Bildung zusammen mit dem Statistischen Bundesamt, dem Wissenschaftszentrum Berlin und dem Sozio-oekonomischen Panel des Deutschen Instituts für Wirtschaftsforschung. *Datenreport 2016: Ein Sozialbericht für die Bundesrepublik Deutschland*. Bonn: Bundeszentrale für politische Bildung, 2016. (Visited on 12/18/2020).
- [21] Caparol Farben Lacke Bautenschutz GmbH. *Capatect Klebe- und Armierungsmasse 186M - Technische Information Nr. 186: Mineralischer Wektrockenmörtel zum Kleben und Armieren von Dämmplatten. Optimiert für den Maschineneinsatz*. Ed. by CAPAROL. Ober-Ramstadt, Sept. 2017. (Visited on 03/28/2019).
- [22] Caparol Farben Lacke Bautenschutz GmbH. *Capatect Mineralputz - Technische information Nr. 146: Mineralischer Werkrockenmörtel nach EN 998-1, Oberputz für außen und innen*. Ed. by Caparol Farben Lacke Bautenschutz GmbH. Ober-Ramstadt, May 2017. (Visited on 03/28/2019).
- [23] Caparol Farben Lacke Bautenschutz GmbH. *Capatect MW-Fassaden-Dämmplatte 149 WHITE WLZ 035 - Technische Information Nr.149*. Ed. by Caparol Farben Lacke Bautenschutz GmbH. Ober-Ramstadt, Mar. 2019. (Visited on 04/23/2019).
- [24] Caparol Farben Lacke Bautenschutz GmbH. *Capatect-Gewebe 650/110 - Technische Information Nr. 650/110: Speziell ausgerüstetes, schiebefestes Glasfasergewebe*. Ed. by Caparol Farben Lacke Bautenschutz GmbH. Mar. 2011. (Visited on 03/28/2019).
- [25] Christoph Cappel et al. *AKTIFAS - Fassadenintegrierte Solarthermie: Bestandsaufnahme und Entwicklung zukunftsfähiger Konzepte: Schlussbericht*. Ed. by Fraunhofer Institut für solare Energiesysteme ISE. 2015. (Visited on 06/19/2018).
- [26] Christoph Cappel et al. “Barriers to the Market Penetration of Façade-integrated Solar Thermal Systems”. In: *Energy Procedia* 48 (2014), pp. 1336–1344. ISSN: 18766102. DOI: 10.1016/j.egypro.2014.02.151.
- [27] D. Carbonell et al. *Ice-Ex Heat exchanger analyses for ice storages in solar and Heat pump applications: Untersuchung von Eisspeicher-Wärmeübertragern für Solar-Wärmepumpen-Heizungen: Final Report*. Nov. 7, 2017. (Visited on 11/24/2020).
- [28] Christina Chatzipoulka et al. “Sky view factor as predictor of solar availability on building façades”. In: *Solar Energy* 170 (2018), pp. 1026–1038. ISSN: 0038092X. DOI: 10.1016/j.solener.2018.06.028. (Visited on 11/13/2020).
- [29] Holger Cischinsky and Nikolaus Diefenbach. *Datenerhebung Wohngebäudebestand 2016: Datenerhebung zu den energetischen Merkmalen und Modernisierungsraten im deutschen und hessischen Wohngebäudebestand*. Darmstadt, Apr. 17, 2018.

- [30] Danny Günther, Jeannette Wapler, Robert Langner, Sebastian Helmling, Dr.-Ing. Marek Miara, Dr.-Ing. David Fischer, Dirk Zimmermann, Tobias Wolf, Dr.-Ing. Bernhard Wille-Hausmann. *Wärmepumpen in Bestandsgebäuden: Ergebnisse aus dem Forschungsprojekt "WPsmart im Bestand" (Abschlussbericht): Abschlussbericht*. Ed. by Fraunhofer Institut für solare Energiesysteme ISE. July 23, 2020. (Visited on 03/18/2021).
- [31] Deutscher Verein des Gas- und Wasserfaches e. V. DVGW. *Bemessung von Zirkulationssystemen in zentralen Trinkwassererwärmungsanlagen: DVWG-Arbeitsblatt W553*. Bonn, 1998-12-01. (Visited on 10/29/2020).
- [32] Deutsches Institut für Gütesicherung und Kennzeichnung e. V. *Solarenergieanlagen Gütesicherung RAL-GZ 966: Ausgabe 2008*. Stankt Augustin, 2008. URL: [https://www.dgs.de/fileadmin/files/RAL\\_Solar/RAL-GZ\\_966-Endversion.pdf](https://www.dgs.de/fileadmin/files/RAL_Solar/RAL-GZ_966-Endversion.pdf) (visited on 12/14/2020).
- [33] Deutsches Institut für Normung e. V. *Energetische Bewertung heiz- und raumlufttechnischer Anlagen: Teil 10: Heizung, Trinkwassererwärmung, Lüftung*. Berlin, 2001-02-01. (Visited on 08/18/2020).
- [34] DGNB. *DGNB System: Kriterienkatalog Gebäude Neubau: Neu Version 2018*. Ed. by Deutsche Gesellschaft für Nachhaltiges Bauen - DGNB e. V., Tübinger Straße 43, Stuttgart. 2018. (Visited on 05/29/2018).
- [35] Nikolaus Diefenbach. *Basisdaten für Hochrechnungen mit der Deutschen Gebäudetypologie des IWU: Neufassung Oktober 2013*. Ed. by Institut Wohnen und Umwelt. Darmstadt, Oct. 9, 2013. (Visited on 05/03/2021).
- [36] DIN Deutsches Institut für Normung. *Solar energy - Solar thermal collectors - Test methods (ISO 9806:2017); German version ENISO 9806:2017*. Berlin, 2018-04-01. (Visited on 09/23/2020).
- [37] DIN-Normenausschuss Heiz- und Raumluftechnik sowie deren Sicherheit and DIN-Normenausschuss Bauwesen. *Energetische Bewertung von Gebäuden - Verfahren zur Berechnung der Norm-Heizlast; Deutsche Fassung EN 12831-1:2017: Teil 1: Raumheizlast, Modul M3-3*. Berlin, 2017-09-01. (Visited on 08/04/2020).
- [38] Dr. Thomas Loewenstein, Caparol Farben Lacke Bautenschutz GmbH. *Composition of external thermal insulation systems for renovation: E-mail*. In collab. with Lotta Koch. 2019-04-24.
- [39] T. Drössler. *Innovative Application of UHPC in Germany: Ultra-High Performance Concretes for fair-faced Facades and Custom Elements with glued Connections*. Ed. by Kassel University Press. Kassel, 2016.
- [40] J. A. Duffie and W. A. Beckman. *Solar engineering of thermal processes*. 3rd ed. Hoboken N.J.: Wiley, 2006. ISBN: 9780471698678.

- [41] P. Dupeyrat. “Experimental development and simulation investigation of a photovoltaic-thermal hybrid solar collector”. Dissertation. Lyon, France: Lyon, INSA, 2011-07-01.
- [42] Bernd Ebert. *LowEx-Bestand Analyse Abschlussbericht zu AP 1.1: Systematische Analyse von Mehrfamilien-Bestandsgebäuden*. Ed. by Karlsruher Institut für Technologie. June 13, 2018. (Visited on 11/25/2019).
- [43] Björn Ehrismann. *Technical study report on solar thermal technology LCIA methods and LCC models*. Ed. by United Nations Environment Programme. 2015. (Visited on 04/25/2018).
- [44] Leah D. Ellis et al. “Toward electrochemical synthesis of cement—An electrolyzer-based process for decarbonating CaCO<sub>3</sub> while producing useful gas streams”. In: *Proceedings of the National Academy of Sciences of the United States of America* (2019). DOI: 10.1073/pnas.1821673116. (Visited on 09/25/2019).
- [45] Energie Solaire SA. *Solardach AS: Das Produkt und seine Anwendungen*. Ed. by Energie Solaire SA. Dec. 2012. URL: [https://ec7cbcf3-ecd1-4dfe-9621-ef4be7ea9a79.filesusr.com/ugd/8d1d54\\_83d93b1278574216adf38ab238dfdc1b.pdf](https://ec7cbcf3-ecd1-4dfe-9621-ef4be7ea9a79.filesusr.com/ugd/8d1d54_83d93b1278574216adf38ab238dfdc1b.pdf) (visited on 10/16/2021).
- [46] European Commission - Joint Research Centre - Institute for Environment and Sustainability. *International Reference Life Cycle Data System (ILCD) Handbook - General guide on LCA - Detailed guidance*. First edition. Printed in Italy: Luxembourg: Publications Office of the European Union, 2010. ISBN: 978-92-79-19092-6. DOI: 10.2788/38479. URL: <http://europa.eu/> (visited on 12/07/2017).
- [47] European Parliament, Council of the European Union. *Directive 2010/31/EU of the European Parliament and of the Council of 19 May 2010 on the energy performance of buildings*. 2010-05-19. (Visited on 04/20/2018).
- [48] K. Farkas and M. Horvat. “Report T.41.A.1 Building Integration of Solar Thermal and Photovoltaics - Barriers, Needs and Strategies”. In: (2012). (Visited on 11/13/2020).
- [49] Ekkehard Fehling, Michael Schmidh, and Simone Stürwald, eds. *Proceedings of the Second International Symposium on Ultra High Performance Concrete*. Schriftenreihe Baustoffe und Massivbau, Structural Materials and Engineering Series. Kassel: kassel university press, 2008. ISBN: 978-3-89958-376-2.
- [50] David Fischer. “Integrating Heat Pumps into Smart Grid: A study on system design, controls and operation”. Dissertation. Stockholm, Schweden: Royal institut of Technology, KTH, 2017. (Visited on 11/15/2021).
- [51] David Fischer et al. “A stochastic bottom-up model for space heating and domestic hot water load profiles for German households”. In: *Energy and Buildings* 124

- (2016), pp. 120–128. ISSN: 0378-7788. DOI: 10.1016/j.enbuild.2016.04.069. (Visited on 03/10/2021).
- [52] Stefan Fortuin and Lotta Koch. *Grafic based on Kapitel 4 – Leitfaden Solarthermische Anlagen*. Ed. by DGS LV Berlin Brandenburg e.V. und LV Hamburg/Schleswig-Holstein e.V. Frankfurt am Main, 2008. (Visited on 09/15/2020).
- [53] Elimar Frank et al. “Systematic Classification of Combined Solar Thermal and Heat Pump Systems”. In: *Proceeding of the EuroSun 2010*. Ed. by ISES EuroSun Conference. 2010. (Visited on 05/05/2021).
- [54] R. Frischknecht et al. “The ecoinvent database: Overview and methodological framework”. In: *International Journal of Life Cycle Assessment* 10 (2005), pp. 3–9. DOI: 10.1065/1ca2004.10.181.1. (Visited on 06/18/2021).
- [55] Uwe R. Fritsche and Hans-Werner Greß. *Der nichterneuerbare kumulierte Energieverbrauch und THG-Emissionen des deutschen Strommix im Jahr 2017 sowie Ausblicke auf 2020 bis 2050: Bericht für die HEA - Fachgemeinschaft für effiziente Energieanwendung e. V.* Ed. by Internationales Institut für Nachhaltigkeitsanalysen und -strategien GmbH. Darmstadt, Nov. 2018. URL: [http://iinas.org/tl\\_files/iinas/downloads/GEMIS/2018\\_KEV\\_THG\\_Strom-2017\\_2020-2050.pdf](http://iinas.org/tl_files/iinas/downloads/GEMIS/2018_KEV_THG_Strom-2017_2020-2050.pdf) (visited on 10/26/2021).
- [56] Matthias Fuchs. “Nachhaltigkeitsorientierte Architekturwettbewerbe Kriterien und Indikatoren zur Integration von Nachhaltigkeitsanforderungen in Wettbewerbsverfahren sowie Empfehlungen und Werkzeuge für die praktische Durchführung”. Doctoral Thesis. tuprints and E-Publishing-Service der TU Darmstadt: Darmstadt, Technischen Universität, 2012.
- [57] N. Gerhardt et al. *Wasserstoff im zukünftigen Energiesystem: Fokus Gebäudewärme: Studie zum Einsatz von H2 im zukünftigen Energiesystem unter besonderer Berücksichtigung der Gebäudewärmeversorgung*. Ed. by Fraunhofer-Institut für Energiewirtschaft und Energiesystemtechnik IEE. Hannover, May 2020. (Visited on 05/07/2021).
- [58] GfK SE. “Consumer Index Juli 2017: ‘BIO’ kommt im Mainstream an”. In: *GfK Consumer Index x 2017* (2017). (Visited on 02/26/2019).
- [59] Volker Gnielinski. “G1 Heat Transfer in Pipe Flow”. In: *VDI Heat Atlas*. Berlin, Heidelberg: Springer Berlin Heidelberg, 2010, pp. 691–700. ISBN: 978-3-540-77877-6. DOI: 10.1007/978-3-540-77877-6\_34.
- [60] Rainer Griebhammer et al. *EcoTopTen - Innovationen für einen nachhaltigen Konsum: Pilot-Phase*. Ed. by Oeko-Institut Institute for Applied Ecology. Freiburg, 2004.
- [61] Rainer Griebhammer et al. *PROSA - Product Sustainability Assessment: Guideline*. Ed. by Oeko-Institut Institute for Applied Ecology. Freiburg.



- [62] Rainer Griebhammer et al. *PROSA-Product Sustainability Assessment. Beschreibung der Methode (Hauptbericht)*. Ed. by Oeko-Institut Institute for Applied Ecology. Freiburg, 2007. (Visited on 12/14/2017).
- [63] Jean-Christophe Hadorn, ed. *Solar and heat pump systems for residential buildings*. Solar heating and cooling. Berlin: Ernst & Sohn, 2015. ISBN: 978-3-433-03040-0. (Visited on 11/27/2020).
- [64] M. Haller et al. *SOL-HEAP. Solar and Heat Pump Combisystems: Final report*. 2014. (Visited on 09/02/2021).
- [65] Martin Hauer and Wolfgang Streicher. “Gebäudegekoppelte Simulation fassadenintegrierter Kollektoren mit TRNSYS”. In: *23. Symposium Thermische Solarenergie*. Ed. by Ostbayerisches Technologie-Transfer-Institut e. V. 24.-26. April 2013. (Visited on 09/02/2021).
- [66] Björn Haugland and Jorgen Randers. *Future of spaceship earth: The Sustainable Development Goals - Business Frontiers*. 2016. URL: <https://www.dnvgl.com> (visited on 01/12/2018).
- [67] Thomas Heck. “Wärmepumpen: Teil X, Data v2.0 (2007)”. In: *Life Cycle Inventories of Energy Systems: Results for Current Systems in Switzerland and other UCTE Countries*. Ed. by Paul Scherrer Institut Villingen, Swiss Centre for Life Cycle Inventories. Dübendorf, CH, 2007. (Visited on 03/07/2019).
- [68] Manfred Hegger et al. *Energie Atlas: Nachhaltige Architektur: Edition Detail*. erste Auflage. München: Institut für internationale Architektur-Dokumentation GmbH & Co. KG, 2007.
- [69] Jan Heider et al. *Potenzial von Infrarot-Heizsystemen für hocheffiziente Wohngebäude: Forschungsprojekt ”IR-Bau”*. Ed. by Fraunhofer IRB Verlag. Stuttgart, 2020. (Visited on 05/14/2021).
- [70] Hans-Martin Henning and Andreas Palzer. *Was kostet die Energiewende? Wege zur Transformation des deutschen Energiesystems bis 2050: Die modellbasierte Studie untersucht sektor- und energieträgerübergreifend die System- und Kostentwicklung einer klimaschutzkompatiblen Transformation des deutschen Energiesystems*. Ed. by Fraunhofer Institut für solare Energiesysteme ISE. Freiburg, 2015. URL: <https://www.ise.fraunhofer.de/de/daten-zu-erneuerbaren-energien.html> (visited on 10/24/2017).
- [71] Michael Hermann. “Bionische Ansätze zur Entwicklung energieeffizienter Fluidsysteme für den Wärmetransport”. Dissertation. Karlsruhe: Universität Karlsruhe, 2005.
- [72] Michael Hermann. *Final report of EU-project BIONICOL, Development of a bionic solar collector with aluminium roll-bond absorber*. 2011.

- [73] Michael Hermann et al. “New Absorber Manufacturing and Materials - Challenges for Absorber Design and Evaluation”. In: *Proceedings of ISES Solar World Congress 2011*. Ed. by International Solar Energy Society ISES. 2011, pp. 1–12. DOI: 10.18086/swc.2011.19.17. URL: <http://proceedings.ises.org/?mode=list&conference=swc2011>.
- [74] Michael Hermann et al. *TABSOLAR - Solarabsorber und andere thermisch aktive Bauteile aus Ultrahochleistungsbeton (UHPC): Schlussbericht*. Ed. by Fraunhofer-Institut für Solare Energiesysteme ISE. May 2015. (Visited on 05/18/2018).
- [75] Michael Hermann et al. *TABSOLAR II - Solarabsorber und anderer thermisch aktive Bauteile aus Ultrahochleistungsbeton (UHPC): Schlussbericht*. Ed. by Fraunhofer-Institut für Solare Energiesysteme ISE. Feb. 2020. (Visited on 09/29/2020).
- [76] S. Hess, C. Bongs, and J. Wapler. *Einsparung von CO<sub>2</sub>-Emissionen und Betriebskosten durch Wärmepumpen in Mehrfamilienhäusern*. Digitaler Sommer der Energiewende, 2020-06-04. URL: [https://www.energietaege.de/fileadmin/user\\_upload/2020/Vortraege/5.05\\_Hess\\_LowEx-Bestand.pdf](https://www.energietaege.de/fileadmin/user_upload/2020/Vortraege/5.05_Hess_LowEx-Bestand.pdf).
- [77] S. Hess et al. “Techno-ökonomische und ökologische Perspektiven für Wärmepumpen im Mehrfamilienhaus-Bestand”. In: *Deutsche Kälte- und Klimatagung 2021*. Ed. by Deutscher Kälte- und Klimatechnischer Verein. 2021. (Visited on 11/23/2021).
- [78] Eberhard Hinz. *Kosten energierelevanter Bau- und Anlagenteile bei der energetischen Modernisierung von Wohngebäuden*. Ed. by Bundesministerium für Verkehr, Bau und Stadtentwicklung. Online-Publikation, 2012. (Visited on 08/11/2021).
- [79] Hollands, K. G. T. et al. “Free Convective Heat Transfer Across Inclined Air Layers”. In: *Journal of Heat Transfer-Transactions of the Asme* 98.2 (1976), pp. 189–193. ISSN: 0022-1481. DOI: 10.1115/1.3450517.
- [80] Markus Hubbuch and Pascal M. Vecsei. *Lebenszykluskosten von Wärmepumpen: Kurzfassung*. Ed. by Zürcher Hochschule für Angewandte Wissenschaften. 2019. (Visited on 10/13/2021).
- [81] M.A.J. Huijbregts et al. *ReCiPe 2016 v1.1: A harmonized life cycle impact assessment method at midpoint and endpoint level Report I: Characterization*. Ed. by National Institute for Public Health and the Environment. 2016. (Visited on 12/18/2020).
- [82] IEA SHC Task 51. *Innovative Solar Products for Building Integration - Webpage. Website startet by Task 41 in 2013*. 2016.
- [83] Institut für Bauen und Umwelt e. V. *Umwelt-Produktdeklaration nach ISO 14025 und EN 15804: Blanke Kupfer - Hausinstallationsrohre KME Germany GmbH & Co. KG*. Ed. by Institut für Bauen und Umwelt e. V. Apr. 2, 2015. (Visited on 12/19/2018).

- [84] Almut Jering et al. *Globale Landflächen und Biomasse - nachhaltig und ressourcenschonend nutzen*. Ed. by Umweltbundesamt: 2013. URL: <https://www.umweltbundesamt.de/publikationen/globale-landflaechen-biomasse> (visited on 10/19/2021).
- [85] C. Jugel et al. *Abschlussbericht dena-Projekt Urbane Energiewende*. Ed. by Deutsche Energie-Agentur. 2019. (Visited on 11/24/2021).
- [86] N. Jungbluth. *Life cycle inventory of solar thermal collector, data for copper and aluminum: E-mail*. In collab. with Lotta Koch. 2017-11-30.
- [87] Niels Jungbluth. *Sachbilanzen von Energiesystemen: Grundlagen für den ökologischen Vergleich von Energiesystemen und den Einbezug von Energiesystemen in Ökobilanzen für die Schweiz. Teil XI, Datenbestand V2.0: Sonnenkollektoranlagen*. Ed. by R. et al. Dones. Dübendorf, CH, 2007.
- [88] M. Kaltschmitt, W. Streicher, and A. Wiese, eds. *Erneuerbare Energien: Systemtechnik, Wirtschaftlichkeit, Umweltaspekte*. 5. Auflage. Springer Vieweg, 2012. (Visited on 11/10/2017).
- [89] Alexandro Kleine. *Operationalisierung einer Nachhaltigkeitsstrategie - Ökologie, Ökonomie und Soziales integrieren*. Wiesbaden: Gabler, 2009.
- [90] A. Knotzer et al. *IEA Energie in Gebäuden und Kommunen (EBC) Annex 67: Energie-flexible Gebäude: Arbeitsperiode 2015 - 2019*. Ed. by Bundesministerium Verkehr, Innovation und Technologie. Wien, 2019. (Visited on 05/06/2021).
- [91] Lotta Koch. *Bewertung multifunktionaler Kollektoren unter Nachhaltigkeitsaspekten*. Berlin, 2013. URL: <http://www.solarthermietechologie.de/konferenz/>.
- [92] Lotta Koch, Michael Hermann, and Maximilian Bauch. "Investigation of new integrated solar thermal absorbers by means of a 2-D model". In: *Geimer, K.* Ed. by B. Franković and J.-O. Dalenback. Croatian Solar Energy Association, International Solar Energy Society (ISES), 2012. ISBN: 978-953-6886-20-3.
- [93] Lotta Koch et al. "Entwicklung von Solarabsorbern aus Stahl auf Basis partiell plattierter Hybridhalbzeuge". In: *21. Symposium Thermische Solarenergie*. Ed. by Ostbayerisches Technologie-Transfer-Institut e. V. 11.-13- Mai 2011.
- [94] Lotta Koch et al. "Erfahrungen und Ergebnisse aus der Entwicklung von Stahlabsorbern". In: *22. Symposium Thermische Solarenergie*. Ed. by Ostbayerisches Technologie-Transfer-Institut e. V. 2012. (Visited on 05/18/2018).
- [95] Lotta Koch et al. *SAPRES Herstellung von Solarabsorbern im Hohlpräge-Streckziehverfahren: Schlussbericht*. Ed. by Fraunhofer-Institut für Solare Energiesysteme ISE. 2015.
- [96] Lotta Koch et al. "Steelabsorbers in Mass Production - Challenges, Opportunities and Produced Samples". In: *Conference proceedings / EuroSun 2014, International Conference on Solar Energy and Buildings, Aix-les-Bains, France, 16-19*

- September*. Ed. by Elimar Frank and Philippe Papillion. Freiburg: International Solar Energy Society, 2015, pp. 1–10. ISBN: 978-3-9814659-3-8. DOI: 10.18086/eurosun.2014.16.12. (Visited on 05/03/2018).
- [97] Lotta Koch et al. “Vom Heizkörper zum Solarabsorber – Erste Schritte zur Herstellung von Stahl- und Aluminiumabsorbern im Hohlpräge- Streckziehverfahren”. In: *23. Symposium Thermische Solarenergie*. Ed. by Ostbayrisches Technologie-Transfer-Institut e. V. 24.-26. April 2013.
- [98] Steven H. Kosmatka, Beatrix Kerkhoff, and William C. Panarese. *Design and Control of Concrete Mixtures*. Ed. by Portland Cement Association. Skokie, Illinois, USA, 2002. (Visited on 07/15/2021).
- [99] Michael Kropp et al. “Einfluss der Trinkwarmwasser-Systemvariante auf die Performance von Wärmepumpen in Mehrfamilienhäusern”. In: *Deutsche Kälte- und Klimatagung 2020 online*. Hannover: Deutscher Kälte- und Klimatechnischer Verein e.V. DKV, 2021. ISBN: 9783932715532. (Visited on 10/18/2021).
- [100] Manuel Lämmle. “PVTgen2 - Entwicklung und Pilotfertigung eines abgedeckten photovoltaisch - thermischen Hybrid-Kollektors der zweiten Generation mit verbesserter thermischer Leistungsfähigkeit: Abschlussbericht”. In: (2017). (Visited on 04/20/2021).
- [101] Manuel Lämmle. “Thermal management of PVT collectors: Development and modelling of highly efficient glazed, flat plate PVT collectors with low-emissivity coatings and overheating protection”. Dissertation. Freiburg im Breisgau: Albert-Ludwigs-Universität, 2018. (Visited on 09/06/2018).
- [102] Chr. Lamnatou et al. “Building-integrated solar thermal system with/without phase change material: Life cycle assessment based on ReCiPe, USEtox and ecological footprint”. In: *Journal of Cleaner Production* (2018). ISSN: 09596526. DOI: 10.1016/j.jclepro.2018.05.032. (Visited on 05/22/2018).
- [103] Chr. Lamnatou et al. “Life cycle analysis of a building-integrated solar thermal collector, based on embodied energy and embodied carbon methodologies”. In: *Energy and Buildings* 84 (2014), pp. 378–387. ISSN: 03787788. DOI: 10.1016/j.enbuild.2014.08.011. (Visited on 05/25/2018).
- [104] Chr. Lamnatou et al. “Review and perspectives on Life Cycle Analysis of solar technologies with emphasis on building-integrated solar thermal systems”. In: *Renewable Energy* 75 (2015), pp. 833–846. ISSN: 09601481. DOI: 10.1016/j.renene.2014.09.057. (Visited on 04/20/2018).

- [105] Chr. Lamnatou et al. “The environmental performance of a building-integrated solar thermal collector, based on multiple approaches and life-cycle impact assessment methodologies”. In: *Building and Environment* 87 (2015), pp. 45–58. ISSN: 03601323. DOI: 10.1016/j.buildenv.2015.01.011. (Visited on 05/28/2018).
- [106] Katrin Lenz et al. “LCA of energy generating components for facade integration in existing high-rise buildings”. In: *International Journal of Sustainable Building Technology and Urban Development* Vol. 3, No. 3 (2012), pp. 168–176. (Visited on 05/29/2018).
- [107] Tomas Matuska, J. Metzger, and Vladimir Zmrhal. “Design tool KOLEKTOR 2.2 for virtual prototyping of solar flat-plate collectors”. In: (visited on 09/07/2020).
- [108] Tomas Matuska and Vladimir Zmrhal. *A mathematical model and design tool KOLEKTOR 2.2: reference handbook (3rd draf, 01-2009)*. 2009.
- [109] Christoph Maurer, Christoph Cappel, and Tilmann E. Kuhn. “Methodology and First Results of an R&D Road Map for Façade-integrated Solar Thermal Systems”. In: *Energy Procedia* 70 (2015), pp. 704–708. ISSN: 18766102. DOI: 10.1016/j.egypro.2015.02.179. (Visited on 07/03/2018).
- [110] Christoph Maurer, Christoph Cappel, and Tilmann E. Kuhn. “Progress in building-integrated solar thermal systems”. In: *Solar Energy* 154 (2017), pp. 158–186. DOI: 10.1016/j.solener.2017.05.065. (Visited on 04/25/2018).
- [111] Christoph Maurer et al. *Report on Barriers for New Solar Envelope Systems*. 2018. DOI: 10.18777/ieashc-task56-2018-0001. (Visited on 11/12/2020).
- [112] W. H. McAdams. *Heat Transmission: 3rd edition, pp. 249*. New York: McGraw-Hill, 1954.
- [113] J.-P. Meyer. “Leistungsstark, sicher, schick: Marktübersicht Kollektoren”. In: *Sonne Wind & Wärme* 2017.10/2017 (2017-10-01), pp. 20–23. ISSN: 1861-2741 H 2607. (Visited on 11/28/2018).
- [114] M. Miara et al. *Wärmepumpen Effizienz: Messtechnische Untersuchung von Wärmepumpenanlagen zur Analyse und Bewertung der Effizienz im realen Betrieb*. Freiburg im Breisgau, 2011. (Visited on 10/28/2020).
- [115] Michaela Meir, Inaventa Solar AS, Norway. *Solar Energy Harvesting Systems, Product gallery*. Ed. by task56.iea-shc.org.
- [116] Modelica Association Project. *Modelica Language*. CC BY-SA 4.0. 1998-2020. URL: <http://modelica.org/modelicalanguage.html>.
- [117] Philipp Molter. “Technikintegration von offenen Fassadensystemen: Entwicklung einer mehrfachfunktionalen Fassadenmoduls mit dem Schwerpunkt der exemplarischen Bewertung eines Bausteins im ganzheitlichen Kontext”. Dissertation. München: Technische Universität München, 2016. (Visited on 05/02/2018).

- [118] Emilia Moreno Ruiz et al. *Documentation of changes implemented inecoinvent database 3.2*. Ed. by Ecoinvent Centre. Zürich, Switzerland, 2015. (Visited on 06/18/2021).
- [119] Munari Probst, M. C. and C. Roecker. *Architectural integration and design of solar thermal systems*. Architecture and Urbanism. Lausanne and Suisse: Eapl Press, 2011. ISBN: 9780415667913.
- [120] Munari Probst, M. C. and C. Roecker. “Integration and formal development of solar thermal collectors”. In: *PLEA2005 - The 22nd conference on passive and low energy architecture*. Ed. by Passive and Low Energy Architecture. 2005. (Visited on 11/27/2020).
- [121] Munari Probst, M. C. and C. Roecker. “Towards an improved architectural quality of building integrated solar thermal systems (BIST)”. In: *Solar Energy* 81.9 (2007), pp. 1104–1116. ISSN: 0038092X. DOI: 10.1016/j.solener.2007.02.009.
- [122] Hannah Neumann. “Untersuchung eines Latentwärmespeichers für Prozesswärmeanwendungen”. Dissertation. Freiburg im Breisgau: Albert-Ludwigs-Universität, 2020-01-10. (Visited on 12/04/2020).
- [123] Joachim Nitsch et al. *Langfristszenarien und Strategien für den Ausbau der erneuerbaren Energien in Deutschland bei Berücksichtigung der Entwicklung in Europa und global: Schlussbericht BMU - FKZ 03MAP146*. Ed. by DLR and IFNE IWES. 2012. (Visited on 10/19/2021).
- [124] Norm prEN ISO 9806:2012. *Solarenergie – Thermische Sonnenkollektoren – Prüfverfahren, Ausgabe 2012-03*.
- [125] Normenausschuss Bauwesen (NABau), Normenausschuss Heiz- und Raumlufttechnik. *Energieeffizienz von Gebäuden - Berechnung des Energiebedarfs für Heizung und Kühlung (ISO 13790:2008) Deutsche Fassung EN ISO 13790:2008*. Berlin, 2008-09-01. (Visited on 08/03/2020).
- [126] Normenausschuss Grundlagen des Umweltschutzes (NAGUS) im DIN. *DIN EN ISO 14040 Umweltmanagement - Ökobilanz - Grundsätze und Rahmenbedingungen (ISO 14040:2006); Deutsche und Englische Fassung EN ISO 14040:2006*. Berlin, November 2009. (Visited on 12/07/2017).
- [127] Normenausschuss Grundlagen des Umweltschutzes (NAGUS) im DIN. *Umweltmanagement - Ökobilanz - Anforderungen und Anleitungen (ISO 14044:2006); Deutsche und Englische Fassung EN ISO 14044:2006*. Berlin, 2006-10-01. (Visited on 12/07/2017).

- [128] NTP National Toxicology Program. “Chemical Information Review Document for Silica Flour (Micronized alpha-Quartz) [CAS No. 14808-60-7]: Supporting Nomination for Toxicological Evaluation by the National Toxicology Program”. In: (2009). URL: <http://ntp.niehs.nih.gov/> (visited on 07/15/2021).
- [129] T. DAW SE Nürnberger. *Costs of ETICS and rear-ventilated facade systems: oral*. In collab. with L. Koch. 2021-11-25.
- [130] Philip Sterchele et al. *Studie: Wege zu einem klimaneutralen Energiesystem - Die deutsche Energiewende im Kontext gesellschaftlicher Verhaltensweisen*. Ed. by Fraunhofer Institute for Solar Energy Systems. Feb. 2020. (Visited on 11/30/2020).
- [131] D. Philippen et al. *High-Ice - System development for high solar thermal gains with ice storage and heat pump: Final Report*. Ed. by Eidgenössisches Departement für Umwelt, Verkehr, Energie und Kommunikation UVEK, Bundesamt für Energie BFE. July 22, 2015. (Visited on 12/06/2020).
- [132] Daniel Philippen and Calfisch, M., Brunold, S, Haller, M. “Kosten der Solarthermie in Mehrfamilienhäusern erfolgreich senken.” In: *Symposium Solarthermie 2018*. 2018.
- [133] Werner Platzer, Mervyn Smyth, and David Kennedy, eds. *COST Action TU1205 - Overview of BIST state of the art, models and applications*. 2015. (Visited on 06/27/2018).
- [134] Christoforos Pouloupoulos. “Life Cycle Assessment of a Multifunctional Solar Thermal Facade System and a Reference Model”. Master thesis. Freiburg: University of Freiburg, 2015-01-08.
- [135] Alejandro Prieto et al. “Solar façades - Main barriers for widespread façade integration of solar technologies: Journal of Facade Design and Engineering, Vol 5, No 1 (2017): Special Issue PowerSkin / Journal of Facade Design and Engineering, Vol 5, No 1 (2017): Special Issue PowerSkin”. In: (2017). DOI: 10.7480/JFDE.2017.1.1398. (Visited on 11/12/2020).
- [136] Thorsten Raabe. “Herausforderungen an die Konsumforschung: Perspektiven einer kulturwissenschaftlichen Orientierung: Schwerpunkt: Nachhaltigkeits-Marketing”. In: *Ökologisches Wirtschaften* 2005.3 (2005), pp. 18–20. (Visited on 12/06/2017).
- [137] K. R. Randall, J. W. Mitchell, and M. M. El-Wakil. “Natural Convection Heat Transfer Characteristics of Flat Plate Enclosures”. In: *Journal of Heat Transfer-Transactions of the Asme* 101.1 (1979), pp. 120–125. ISSN: 0022-1481. DOI: 10.1115/1.3450901.
- [138] Philipp Reher. “Simulationsstudie zu Trinkwassererwärmungskonzepten mit Wärmepumpen in Mehrfamilien-bestandesgebäuden mit Dymola/Modelica: Simulation

- Study on Domestic Water Heating Systems using Heat Pumps in Existing Apartment Buildings with Dymola/Modelica”. Master’s thesis. Aachen: RWTH Aachen, 2019-02-01. (Visited on 11/27/2020).
- [139] Mathieu Saurat and Michael Ritthoff. *Overview of existing sustainability assessment methods and tools, and of relevant standards: SAMT - Sustainability assessment methods and tools to support decision-making in the process industries - Deliverable 1.1*. June 1, 2015. URL: <https://www.spire2030.eu/samt> (visited on 12/14/2017).
- [140] Michael Schmidt, ed. *Ultra high performance concrete: (UHPC) ; 10 years of research and development at the University of Kassel*. Vol. H. 7. Structural materials and engineering series. Kassel: Kassel Univ. Press, 2007. ISBN: 978-3-89958-347-2. (Visited on 10/08/2020).
- [141] Michael Schmidt, Ekkehard Fehling, and Susanne Fröhlich, eds. *Nachhaltiges Bauen mit Ultrahochfestem Beton: Ergebnisse des Schwerpunktprogrammes 1182 gefördert durch die Deutsche Forschungsgemeinschaft (DFG)*. Vol. 22. Baustoffe und Massivbau. Kassel: kassel university press, 2014. ISBN: 3862194809.
- [142] Solvis GmbH. *SolvisClean: Energieeffiziente Trinkwasserhygiene: Legionellendesinfektion durch Ultrafiltration*. Ed. by Solvis GmbH. Braunschweig, Mar. 2016. URL: <https://s3.eu-central-1.amazonaws.com/solvis-files/downloads/broschueren/solvisclean-produktbroschuere.pdf> (visited on 10/18/2021).
- [143] Nelson Sommerfeldt and Hatem Madani. “In-depth techno-economic analysis of PV/Thermal plus ground source heat pump systems for multi-family houses in a heating dominated climate”. In: *Solar Energy* 190 (2019), pp. 44–62. ISSN: 0038092X. DOI: 10.1016/j.solener.2019.07.080. (Visited on 10/28/2020).
- [144] Rapperswil SPF. *Datenblatt Solardach AS, Registration No. 011-7S677 F: Unglazed collector, unabgedeckter Kollektor, capteur sans vitrage*. Ed. by D. CERTCOIN. TÜV Rheinland. Feb. 6, 2009. (Visited on 01/15/2020).
- [145] Statistisches Bundesamt, ed. *Baufertigstellungen neuer Gebäude: Deutschland, Jahre, Gebäudeart, Energieverwendung, Energieart: 31121-0004*. 2020. URL: <https://www-genesis.destatis.de/genesis/online>.
- [146] Frank Steinbach et al. *Entwicklung von Solarabsorbern in Stahlbauweise auf Basis partiell plattierter Hybridhalbzeuge IGF-Nr. 339 ZN = Processing of solar absorbers in steel design based on partially roll bonded hybrid semi-finished parts*. Forschungsvereinigung Stahlanwendung. 2015. ISBN: 978-3-942541-63-3.
- [147] Immanuel Stieß et al. *Handlungsmotive, -hemmnisse und Zielgruppen für eine energetische Gebäudesanierung: Ergebnisse einer standardisierten Befragung von*



- Eigenheimsanierern: Hypothesen zur Sanierungsentscheidung*. Frankfurt am Main, 2010. (Visited on 12/05/2017).
- [148] Thomas F. Stocker, ed. *Climate change 2013: The physical science basis ; summary for policymakers, a report of Working Group I of the IPCC, technical summary, a report accepted by Working Group I of the IPCC but not approved in detail and frequently asked questions ; part of the Working Group I contribution to the fifth assessment report of the Intergovernmental Panel on Climate Change*. New York: Intergovernmental Panel on Climate Change, 2013. (Visited on 12/18/2020).
- [149] Gerhard Stryi-Hipp et al. *GroSol - Studie zu großen Solarwärmeeanlagen*. 2007. DOI: 10.13140/2.1.1702.6245. (Visited on 12/14/2020).
- [150] Matthias Stucki and Niels Jungbluth. *Update of the Life Cycle Inventories of Solar Collectors*. Ed. by ESU-services Ltd. Uster, Schweiz, Aug. 7, 2012.
- [151] W. C. Swinbank. "Long-wave radiation from clear skies". In: *Quarterly Journal of the Royal Meteorological Society* 1963.89 (1963), pp. 339–348. DOI: 10.1002/qj.49708938105. (Visited on 09/07/2020).
- [152] Inc. TESLA. *Solar Roof*. 2018.
- [153] Thorsten Stengel and Peter Schiebl. "Sustainable Construction with UHPC - from Life Cycle Inventory Data Collection to Environmental Impact Assessment". In: *Proceedings of the Second International Symposium on Ultra High Performance Concrete*. Ed. by Ekkehard Fehling, Michael Schmidh, and Simone Stürwald. Schriftenreihe Baustoffe und Massivbau, Structural Materials and Engineering Series. Kassel: kassel university press, 2008. ISBN: 978-3-89958-376-2. (Visited on 10/17/2017).
- [154] Tyforop Chemie GmbH, ed. *Safety data sheet Tyfocor L: Version: 3.5, ID-No.: 2400-01\_EN\_EN*. Hamburg, Apr. 1, 2022. (Visited on 09/19/2022).
- [155] Verein Deutscher Ingenieure VDI. *Berichtigung zur Richtlinie DI 4645:2018-03 Corrigendum concerning standard VDI 4645:2018-03: VDI 4645 - Berichtigung Corrigendum*. Berlin, 2018-08-01. (Visited on 03/18/2021).
- [156] Verein Deutscher Ingenieure VDI. *Heizungsanlagen mit Wärmepumpen in Ein- und Mehrfamilienhäusern Planung, Errichtung, Betrieb Heating plants with heat pumps in single-family and multi-family houses Planning, Construction, Operation: VDI 4645*. Berlin, 2018-03-01. (Visited on 03/18/2021).
- [157] Verein Deutscher Ingenieure VDI. *Thermische Nutzung des Untergrunds: Erdgekoppelte Wärmepumpenanlagen*. Berlin, 2015. (Visited on 09/09/2020).
- [158] Viessmann Deutschland GmbH. "Planungshandbuch Wärmepumpen". In: (2011). (Visited on 01/15/2021).

- [159] R. Viskanta and A. Karalds. “Interferometric observations of the temperature structure in water cooled or heated from above”. In: *Advances in Water Resources* 1977. Volume 1 (1977), pp. 57–69. (Visited on 01/08/2021).
- [160] Johannes Wagner et al. *Auswirkungen von CO<sub>2</sub>-Preisen auf den Gebäude-, Verkehrs- und Energiesektor: Im Auftrag der E.ON SE: Kurzstudie*. Ed. by E.ON Energy Research Center, RWTH Aachen, Energiewirtschaftliches Institut der Universität zu Köln gGmbH. 2019. URL: [https://www.ewi.uni-koeln.de/cms/wp-content/uploads/2019/11/Auswirkungen-von-CO2-Preisen\\_Executive-Summary.pdf](https://www.ewi.uni-koeln.de/cms/wp-content/uploads/2019/11/Auswirkungen-von-CO2-Preisen_Executive-Summary.pdf) (visited on 10/26/2021).
- [161] Wagner & Co. *Solar-Roof Kollektordach / Fassadenkollektor: Technische Information*. Ed. by Wagner & Co. Cölbe/Marburg, 2007.
- [162] Jens Wehenkel. *B+L Outlook Fassade DE: Confidential*. Ed. by B+L Marktdaten GmbH. 2018. (Visited on 09/05/2018).
- [163] Werner Weiss and Monika Spörk-Dür. *Solar Heat Worldwide: Global Market Development and Trends in 2020, Detailed Market Figures 2019*. Ed. by AEE INTEC AEE - Institute for Sustainable Technologies Federal Ministry Republic of Austria. 2021. (Visited on 08/17/2021).
- [164] G. Wernet et al. “The ecoinvent database version 3 (part I): overview and methodology.” In: *The International Journal of Life Cycle Assessment* 2016 (2016), pp. 1218–1230. URL: <http://link.springer.com/10.1007/s11367-016-1087-8>.
- [165] Wikipedia. *Ökobilanzdatenbank*. 10. February 2018.
- [166] Bettina Wolf geb. Volz. “Glasprofile in der Fassade: Entwicklung einer solar optimierten Systemfassade”. Dissertation. Universität Stuttgart, 2006-06-21. (Visited on 06/26/2018).
- [167] Dominik Wystreil. “Ein Beitrag zur thermo-hydraulischen Optimierung niederenergetischer Wärme- und Kälteversorgungssysteme”. Dissertation. Freiburg im Breisgau: Albert-Ludwigs-Universität, 2016. (Visited on 08/10/2020).
- [168] Jürgen Zeisberger. “Beitrag zur energieeffizienten Trinkwassererwärmung: Messtechnische Untersuchungen zu Bewertung und Optimierung von Trinkwasserwärmungssystemen”. Dissertation. München: Technische Universität München, 2017-06-01. URL: <https://mediatum.ub.tum.de/doc/1356343/file.pdf> (visited on 10/24/2020).

APPENDIX A

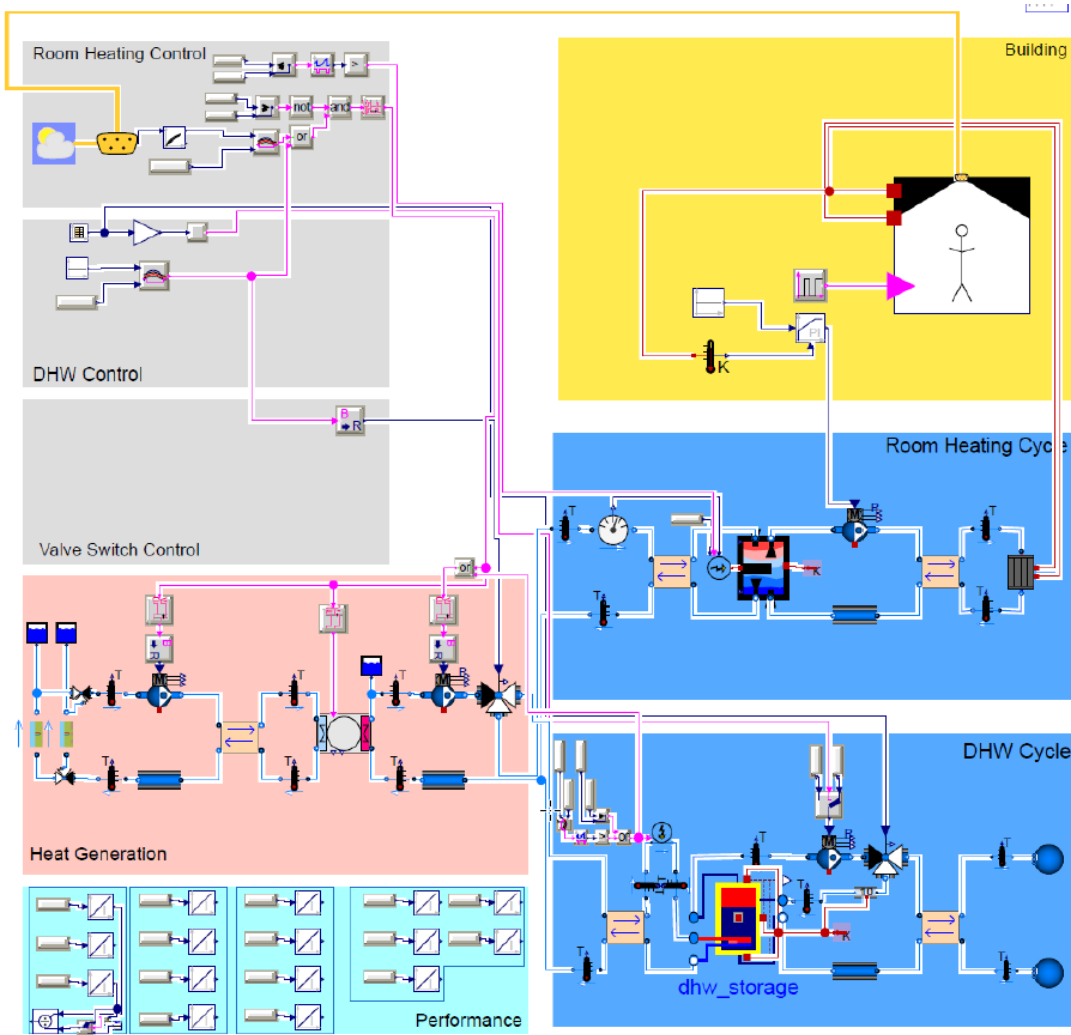


FIGURE A.1. Basic scheme of Reher's Modelica system model on Dymola [138]

TABLE A.1. Technical data of simulated building for TRNSYS simulation

Category	Value	Unit
<b>General description</b>		
Number of stories	3	[-]
Number of apartments	9	[-]
Number of stairwells	1	[-]
Basement	existent, non-heated	[-]
Roof	saddle roof, non-heated	[-]
Number of inhabitants	13	[-]
Orientation of building	East-West	[-]
<b>Volumes and areas of building</b>		
Gross floor area (sum of all usable floor areas on all the floors according to DIN 277: $A_f \cdot 1.1$ )	639	[m <sup>2</sup> ]
Net floor area $A_f$	581	[m <sup>2</sup> ]
Heated gross building volume $A_f \cdot 1.1 \cdot 2.7$ m	1725.8	[m <sup>3</sup> ]
Heated living space volume $A_f \cdot 2.5$ m	1452.7	[m <sup>3</sup> ]
Net floor area per apartment	64.6	[m <sup>2</sup> ]
Area of top floor ceiling to the unheated attic $A_{ceiling}$	232.2	[m <sup>2</sup> ]
Area of ground to unheated basement $A_{bottom}$	232.2	[m <sup>2</sup> ]
Building width	10	[m]
Building length	23.2	[m]
Story height (external dimension)	2.7	[m]

TABLE A.1. Technical data of simulated building for TRNSYS simulation - continued

Category	Value	Unit
Story height (inner dimension)	2.5	[m]
Volume of attic	335.2	[m <sup>3</sup> ]
Volume of living space	1452.7	[m <sup>3</sup> ]
Volume of basement	580.6	[m <sup>3</sup> ]
Area of façade north	188.1	[m <sup>2</sup> ]
Area of façade east	81	[m <sup>2</sup> ]
Area of façade south	188.1	[m <sup>2</sup> ]
Area of façade west	81	[m <sup>2</sup> ]
Total gross area of windows	106.2	[m <sup>2</sup> ]
Gross area window north	24.4	[m <sup>2</sup> ]
Gross area window east	25.2	[m <sup>2</sup> ]
Gross area window south	31.5	[m <sup>2</sup> ]
Gross area window west	25.1	[m <sup>2</sup> ]
Frame fraction of windows	0.3	[-]
Total area of wall to exterior $A_{wall}$	430	[m <sup>2</sup> ]
Area of wall to exterior north	161.7	[m <sup>2</sup> ]
Area of wall to exterior east	55.8	[m <sup>2</sup> ]
Area of wall to exterior south	156.6	[m <sup>2</sup> ]
Area of wall to exterior west	55.9	[m <sup>2</sup> ]
<b>Specification of building parts</b>		
Solar heat gain coefficient windows (g-value)	0.709	[-]
U-value windows	1.26	[W/(m <sup>2</sup> K)]
U-value exterior wall $U_{wall}$	0.23	[W/(m <sup>2</sup> K)]

TABLE A.1. Technical data of simulated building for TRNSYS simulation - continued

Category	Value	Unit
U-value top floor ceiling $U_{ceiling}$	1.87	[W/(m <sup>2</sup> K)]
U-value roof $U_{roof}$	0.187	[W/(m <sup>2</sup> K)]
U-value bottom plate $U_{bottom}$	0.278	[W/(m <sup>2</sup> K)]
Supplement for thermal bridges $U_{supplement}$	0.1	[W/(m <sup>2</sup> K)]
ground reflectance	0.2	[-]
shading factor	0.4	[-]
<b>Data of appartements</b>		
Room temperature	20	[°C]
Internal gains	3	[W/m <sup>2</sup> ]
Heating limit temperature for heating control	15	[°C]
Air exchange rate	0.4	[1/h]
Infiltration	0.1	[1/h]
<b>Simulated heating demand</b>		
Total heating demand	39.74	[MWh/a ]
Specific heating demand	68.4	[kWh/m <sup>2</sup> a]

TABLE A.2. Characteristic curve for  $\dot{Q}_{con}$  of air-source heat pump model “Ochsner GMLW 19” in [W], referred to as “ASHP 2”

		$\vartheta_{source}$		
		-10 °C	2 °C	7 °C
$\vartheta_{con}$	35 °C	11600	17000	20200

---

50 °C   10200   15600   18800

---

TABLE A.3. Characteristic curve for  $P_{el}$  of air-source heat pump model “Ochsner GMLW 19” in [W], referred to as “ASHP 2”

		$\vartheta_{source}$		
		−10 °C	2 °C	7 °C
$\vartheta_{con}$	35 °C	4300	4400	4600
	50 °C	6300	6400	6600

---

TABLE A.4. Characteristic curve for  $\dot{Q}_{con}$  of air-source heat pump model “Ochsner GMLW 19 plus” in [W], referred to as “ASHP 1”

		$\vartheta_{source}$		
		−10 °C	2 °C	7 °C
$\vartheta_{Con}$	35 °C	12600	16800	19800
	50 °C	11700	15900	18900
	60 °C	11400	15600	18600

---

TABLE A.5. Characteristic curve for  $P_{el}$  of air-source heat pump model “Ochsner GMLW 19 plus” in [W], referred to as “ASHP 1”

		$\vartheta_{source}$		
		−10 °C	2 °C	7 °C
$\vartheta_{con}$	35 °C	4100	4300	4400
	50 °C	5500	5700	5800
	60 °C	6300	6500	6600

---

TABLE A.6. Characteristic curve for  $\dot{Q}_{con}$  of ground-source heat pump model “Waterkotte Ecotouch DS 5056.5T” in [W]

		$\vartheta_{source}$					
		$-5^{\circ}\text{C}$	$0^{\circ}\text{C}$	$5^{\circ}\text{C}$	$10^{\circ}\text{C}$	$15^{\circ}\text{C}$	$20^{\circ}\text{C}$
$\vartheta_{con}$	$30^{\circ}\text{C}$	37800	43300	49200	55700	62700	70300
	$35^{\circ}\text{C}$	37100	42400	48200	54500	61300	68700
	$40^{\circ}\text{C}$	36500	41600	47200	53300	59900	67000
	$45^{\circ}\text{C}$	35800	40800	46100	52000	58400	65300
	$50^{\circ}\text{C}$	35200	39900	45100	50700	56900	63500
	$55^{\circ}\text{C}$	34500	39000	44000	49400	55300	61700
	$60^{\circ}\text{C}$	33800	38100	42900	48000	53700	59800

TABLE A.7. Characteristic curve for  $P_{el}$  of ground-source heat pump model “Waterkotte Ecotouch DS 5056.5T” in [W]

		$\vartheta_{source}$					
		$-5^{\circ}\text{C}$	$0^{\circ}\text{C}$	$5^{\circ}\text{C}$	$10^{\circ}\text{C}$	$15^{\circ}\text{C}$	$20^{\circ}\text{C}$
$\vartheta_{con}$	$30^{\circ}\text{C}$	8100	8300	8400	8600	8700	8800
	$35^{\circ}\text{C}$	9000	9200	9300	9500	9600	9800
	$40^{\circ}\text{C}$	9900	10100	10300	10500	10700	10800
	$45^{\circ}\text{C}$	10900	11100	11400	11600	11800	12000
	$50^{\circ}\text{C}$	12000	12300	12600	12800	13100	13300
	$55^{\circ}\text{C}$	13200	13500	13900	14200	14500	14700
	$60^{\circ}\text{C}$	14500	14900	15300	15700	16000	16300



TABLE A.8. Fit parameters for heat pumps

Heat pump	a	b	c	d	e	f
ASHP 1	999.3	454.5	-791.8	-0.1	3.1	-1.5
ASHP 2	34.5	-37.6	-252.4	-1.8	-1.0	4.1
GSHP	546.8	562.6	-1069.5	-0.7	4.4	-1.3

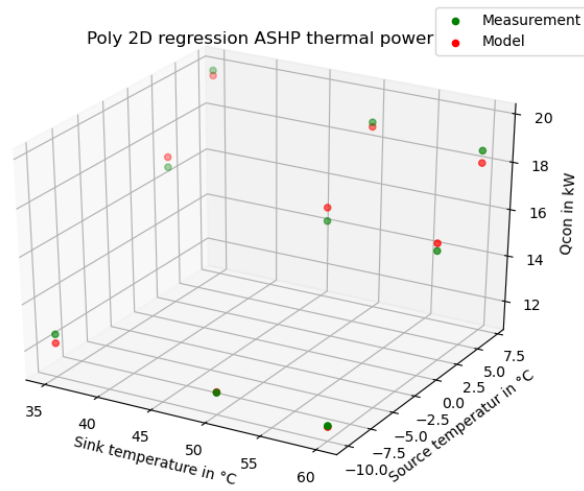


FIGURE A.2. Comparison of measured data and 2D regression model of ASHP 1

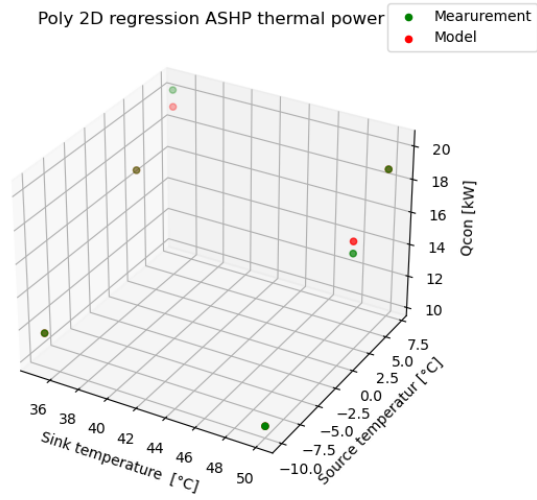


FIGURE A.3. Comparison of measured data and 2D regression model of ASHP 2

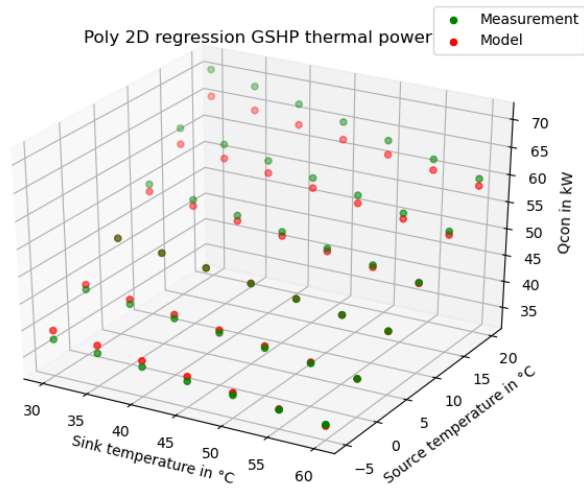


FIGURE A.4. Comparison of measured data and 2D regression model of GSHP

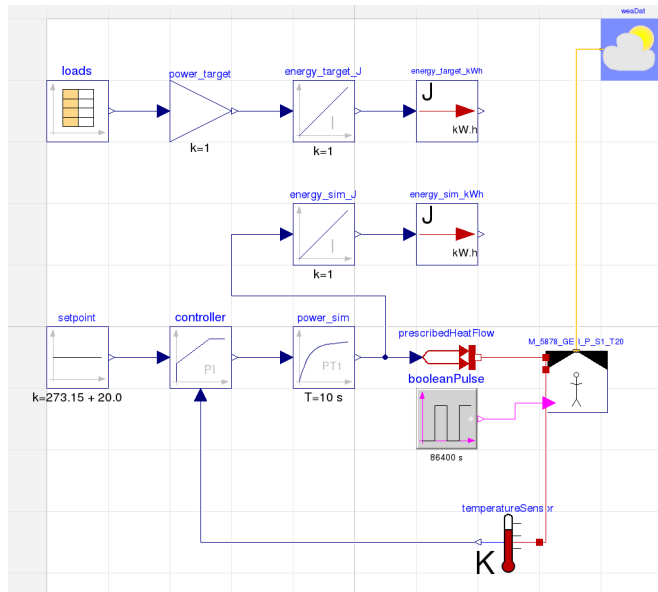


FIGURE A.5. Implementation of fit model with prescribed heat in Mod-  
elica

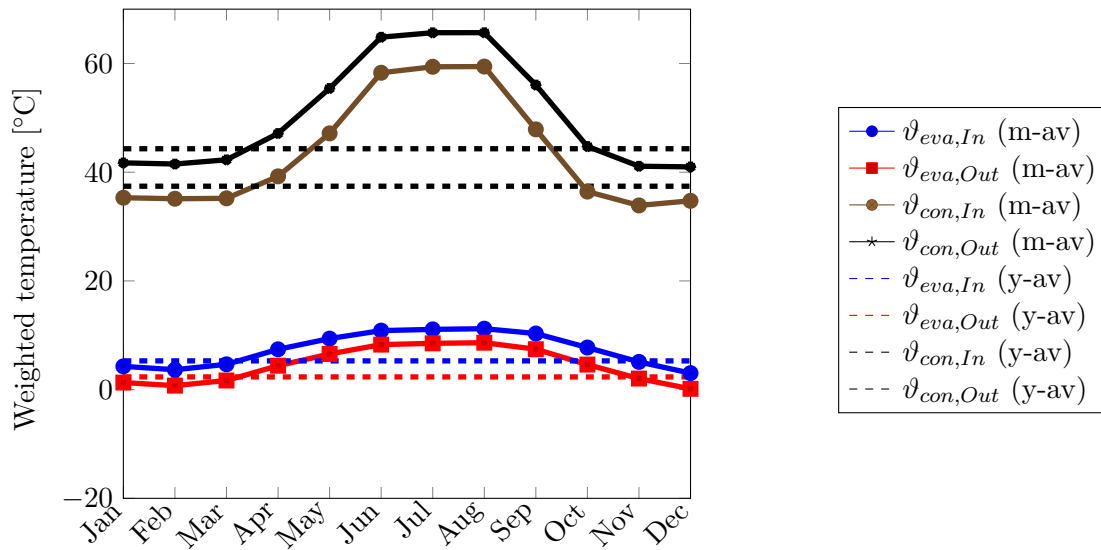


FIGURE A.6. Temperatures weighted with  $Q_{con}$  at the evaporator inlet and outlet and condenser inlet and outlet for GSHP, monthly (m-av) and yearly (y-av) averages.

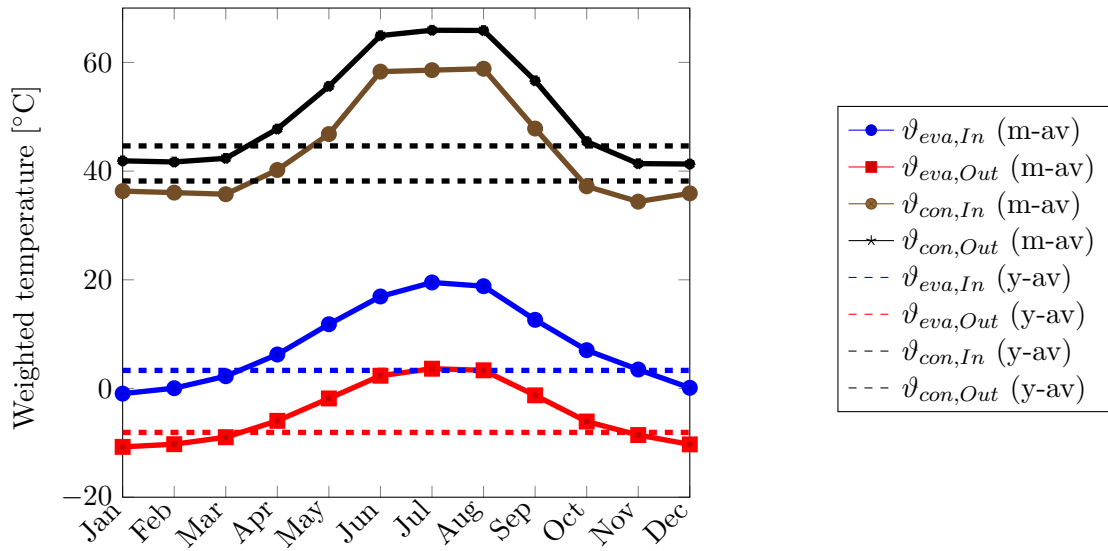


FIGURE A.7. Temperatures weighted with  $Q_{con}$  at the evaporator inlet and outlet and condenser inlet and outlet for ASHP 2, monthly (m-av) and yearly (y-av) averages.

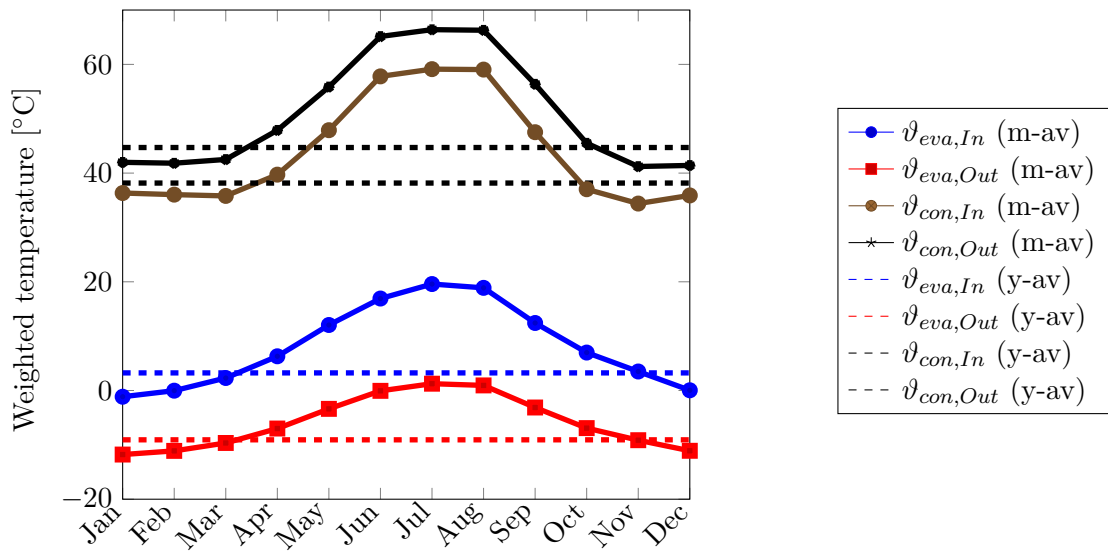


FIGURE A.8. Temperatures weighted with  $Q_{con}$  at the evaporator inlet and outlet and condenser inlet and outlet for ASHP 1, monthly (m-av) and yearly (y-av) averages.

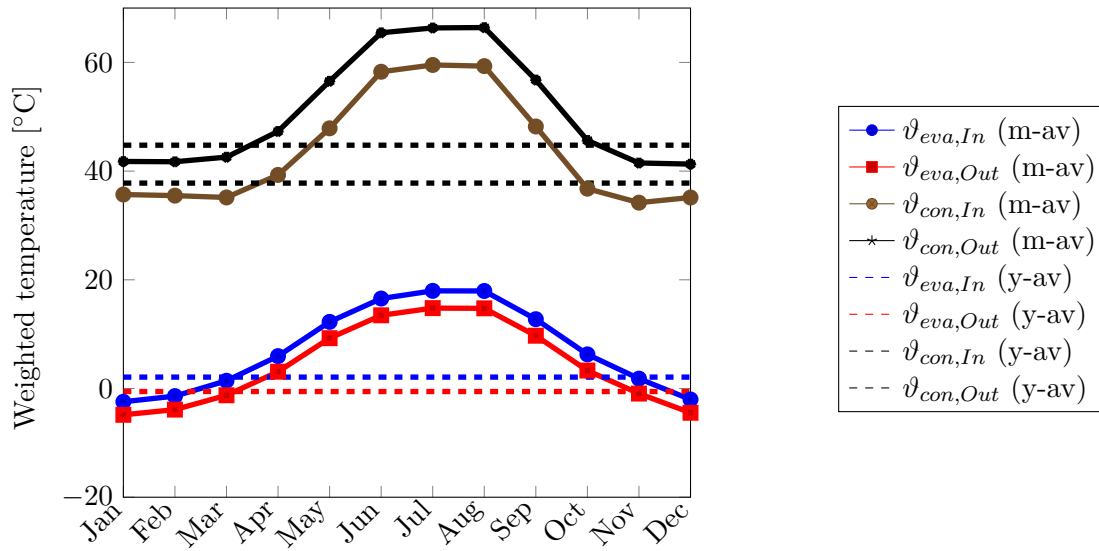


FIGURE A.9. Temperatures weighted with  $Q_{con}$  at the evaporator inlet and outlet and condenser inlet and outlet for the Col-Dir system with  $wcf=0.5$  and  $A_{ap}$  of  $6\text{ m}^2$  per  $\dot{Q}_{demand,biv}$  ( $17.3\text{ kW}$ ), monthly (m-av) and yearly (y-av) averages.

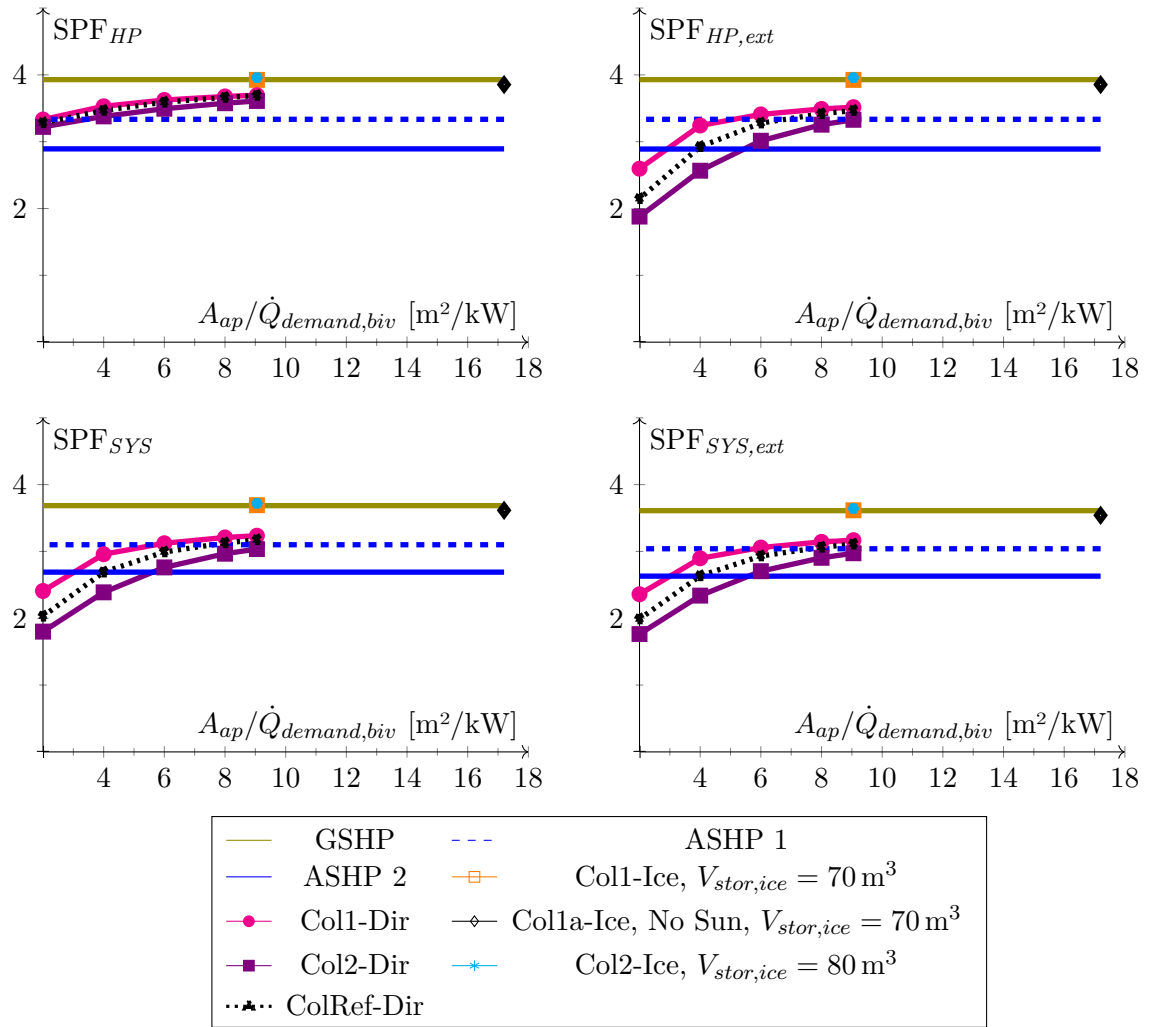


FIGURE A.10. Seasonal performance factors  $SPF_{HP}$ ,  $SPF_{HP,ext}$ ,  $SPF_{SYS}$  and  $SPF_{SYS,ext}$  of reference systems, Col-Dir systems for different ratios  $A_{ap}/\dot{Q}_{demand,biv}$  ( $wcf = 0.5$ ) and different Col-Ice systems.

TABLE A.9. Annual energy flows of the Col1-Dir/Col1-Ice70 with Gray, uninsulated collector and Col2-Dir/Col2-Ice80 with spectrally selective coating and back insulation. Both Col-Dir and Col-Ice systems with  $A_{ap}/\dot{Q}_{demand,biv} = 9 \text{ m}^2/\text{kW}$  and  $wcf = 0.5$ .

Category	Unit	Col1-Dir	Col2-Dir	Col1-Ice70	Col2-Ice80
<b>HP</b>					
$Q_{con}$	[MWh]	51.15	50.79	51.82	51.81
$Q_{eva}$	[MWh]	37.32	36.72	38.62	38.73
$W_{el,HP}$	[MWh]	13.84	14.07	13.2	13.09
$SPF_{HP,tot}$	[-]	3.7	3.61	3.92	3.96
<b>Aux</b>					
$Q_{aux,SH}$	[MWh]	1.36	1.7	0.83	0.85
$Q_{aux,DHW}$	[MWh]	0.47	0.5	0.32	0.31
$Q_{aux,eva}$	[MWh]	0.71	1.19	0	0
<b>Delivery</b>					
$Q_{HC}$	[MWh]	40.65	40.65	40.6	40.6
$Q_{HC,tank}$	[MWh]	39.64	39.31	40.14	40.11
$Q_{DHW}$	[MWh]	6.86	6.86	6.88	6.89
$Q_{DHW,tank}$	[MWh]	11.51	11.48	11.69	11.7
$Q_{circ}$	[MWh]	4.38	4.38	4.38	4.38
<b>Losses</b>					
$Q_{loss,SH}$	[MWh]	-0.38	-0.38	-0.38	-0.38
$Q_{loss,DHW}$	[MWh]	-0.74	-0.73	-0.74	-0.74
<b>Total</b>					
$Q_{delivered,tot}$	[MWh]	52.98	52.99	52.98	52.12
$W_{el,tot}$	[MWh]	16.38	17.46	14.35	14.24
$SPF_{SYS}$	[-]	3.23	3.03	3.69	3.72
Part of aux, wo. $Q_{aux,eva}$	[-]	0.11	0.13	0.08	0.08
Part of aux, incl. $Q_{aux,eva}$	[-]	0.16	0.19	0.08	0.08

TABLE A.10. Annual energy flows of systems with both ASHPs, GSHP, and the collector reference system ColRef-Dir. The shown ColRef-Dir-system was simulated with the entire south façade ( $A_{ap}/\dot{Q}_{demand,biv} = 9 \text{ m}^2/\text{kW}$ ) and  $wcf = 0.5$ .

Category	Unit	ASHP 2	ASHP 1	GSHP	ColDirRef
<b>HP</b>					
$Q_{con}$	[MWh]	50.67	51.21	51.75	50.97
$Q_{eva}$	[MWh]	33.21	35.85	38.58	37.17
$W_{el,HP}$	[MWh]	17.47	15.35	13.17	13.81
$SPF_{HP,tot}$	[-]	2.9	3.34	3.93	3.69
<b>Aux</b>					
$Q_{aux,HC}$	[MWh]	1.39	0.98	0.92	1.5
$Q_{aux,DHW}$	[MWh]	0.82	0.73	0.27	0.47
$Q_{aux,eva}$	[MWh]	0	0	0	0.9
<b>Delivery</b>					
$Q_{HC}$	[MWh]	40.63	40.63	40.63	40.61
$Q_{HC,tank}$	[MWh]	39.6	40.02	40.05	39.47
$Q_{DHW}$	[MWh]	6.78	6.81	6.85	6.86
$Q_{DHW,tank}$	[MWh]	11.07	11.19	11.69	11.51
$Q_{circ}$	[MWh]	4.38	4.38	4.38	4.38
<b>Losses</b>					
$Q_{loss,SH}$	[MWh]	-0.38	-0.38	-0.37	-0.38
$Q_{loss,DHW}$	[MWh]	-0.73	-0.73	-0.73	-0.74
<b>Total</b>					
$Q_{delivered,tot}$	[MWh]	52.89	52.92	52.94	52.95
$W_{el,tot}$	[MWh]	19.68	17.07	14.37	16.68
$SPF_{SYS}$	[-]	2.69	3.1	3.69	3.17
Part of aux, wo. $Q_{aux,eva}$	[-]	0.11	0.1	0.08	0.12
Part of aux, incl. $Q_{aux,eva}$	[-]	0.11	0.1	0.08	0.17



TABLE A.11. Inventory of 1 m<sup>2</sup> flat plate collector with aluminum-copper absorber following Stucki and Jungbluth [150] and updated to Ecoinvent 3.6. Copper was modeled following table A.13, aluminum following table A.14.

Category	Material/Process	Value	Unit
Absorber	aluminum, production mix, wrought alloy, at plant [RER] - updated	1.41	[kg]
	brazing solder production, cadmium free [RER]	0.00368	[kg]
	copper, at regional storage [RER] - updated, adapted	1.73	[kg]
	drawing of pipe, steel [RER]	1.73	[kg]
	sheet rolling, aluminum [RER]	1.41	[kg]
	soft solder, Sn97Cu3 [RER]	0.0588	[kg]
	selective coat, aluminum sheet, nickel pigmented aluminum oxide [SK]	1	[m <sup>2</sup> ]
	steel, chromium steel 18/8, hot rolled [RER]	0.0771	[kg]
Frame	section bar extrusion, aluminum [RER]	3.93	[kg]
	aluminum, production mix, wrought alloy, at plant [RER] - updated	3.39	[kg]
Glazing	solar glass, production, low-iron [RER]	8.27	[kg]
	tempering, flat glass [RER]	8.27	[kg]
Insulation	stone wool, packed [CH]	1.59	[kg]
Other	solar collector factory construction [RER]	0.0000002	[unit]
	synthetic rubber production [RER]	0.857	[kg]
	silicone product production [RER]	0.0857	[kg]
	market for tap water [CH]	9.4	[kg]
	market for electricity, medium voltage [CH]	1.16	[kWh]
	EUR-flat pallet production [RER]	0.0451	[unit]

TABLE A.11. Inventory of 1 m<sup>2</sup> flat plate collector with aluminum-copper absorber following Stucki and Jungbluth [150] and updated to Ecoinvent 3.6. Copper was modeled following table A.13, aluminum following table A.14.- continued

Category	Material/Process	Value	Unit
	polyethylene production, high density, granulate [RER]	0.00857	[kg]
	transport, freight train, electricity [Europe without Switzerland]	7.12	[tkm]
	transport, freight, lorry 16–32 metric ton, EURO5 [RER]	14.37	[tkm]
Use-Phase	propylene glycol production, liquid [RER]	1.02	[kg]
	water production, completely softened, from decarbonized water, at user [RER]	1.74	[kg]
End-of-life	treatment of heat carrier liquid, 40 % C <sub>3</sub> H <sub>8</sub> O <sub>2</sub> , capacity 1.1E10l/year [CH]	0.00276	[m <sup>3</sup> ]
	treatment of wastewater, from residence, capacity 1.1E10l/year [CH]	0.0094	[m <sup>3</sup> ]
	treatment of waste glass sheet, collection for final disposal [Europe without Switzerland]	8.27	[kg]
	market for waste mineral wool [Europe without Switzerland]	1.59	[kg]
	treatment of waste wood, untreated, sanitary landfill [Europe without Switzerland]	0.857	[kg]
	market for waste plastic, mixture [Europe without Switzerland]	0.942	[kg]

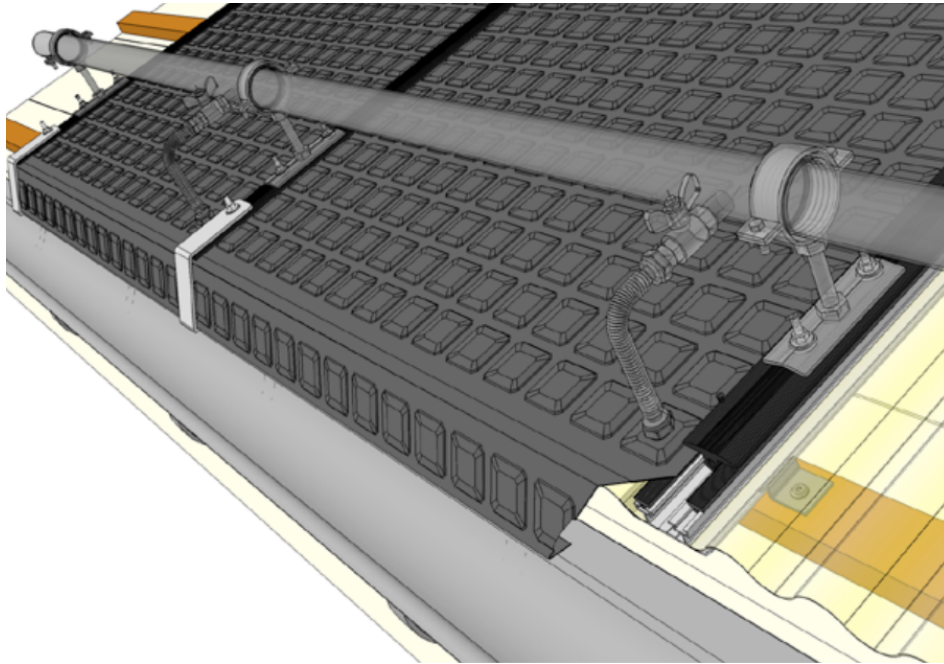


FIGURE A.11. Drawing of Solardach AS (ColRef), excerpt of handbook of Energie Solaire SA [45].

TABLE A.12. Inventory of 1 m<sup>2</sup> unglazed flat plate collector with steel absorber Philippen et al. [131]. Aluminum was modeled following table A.14.

Category	Material/Process	Value	Unit
Absorber	steel, chromium steel 18/8	19.9	[kg]
	sheet rolling, chromium steel	19.9	[kg]
	welding, arc, steel	6.4	[m]
	selective coat, stainless steel sheet, black chrome	2.03	[m <sup>2</sup> ]
Frame	aluminum, production mix, custom	4.5	[kg]
	section bar extrusion, aluminum	4.5	[kg]
Insulation	glass fiber reinforced plastic, polyamide, injection molded	5.8	[kg]
Use-Phase	propylene glycol, liquid	1.9	[kg]

TABLE A.12. Inventory of 1 m<sup>2</sup> unglazed flat plate collector with steel absorber Philippen et al. [131]. Aluminum was modeled following table A.14.- continued

Category	Material/Process	Value	Unit
	water, completely softened	3.7	[kg]
End-of-life	treatment of heat carrier liquid, 40 % C <sub>3</sub> H <sub>8</sub> O <sub>2</sub> , capacity 1.1E10l/year [CH]	0.0019	[m <sup>3</sup> ]
	market for waste plastic, mixture [Europe without Switzerland]	2.4	[kg]

TABLE A.13. Inventory of 1 kg copper pipe based on the copper production mix “copper, at regional storage [RER]” from Ecoinvent v2 [2] with increased percentage of secondary copper (from 44 % to 65 %) following the description in the EPD of a representative manufacturer of copper pipes [83]. The original data set was transferred and adapted to Ecoinvent v3.3.

Category	Material/Process	Value	Unit
copper production mix, custom [RER]	market for transport, freight, sea, transoceanic ship [GLO]	8.53	[tkm]
	market for transport, freight train [Europe without Switzerland]	0.72	[tkm]
	treatment of copper scrap by electrolytic refining [RER]	0.43	[kg]
	market for copper concentrate, sulfide ore [GLO]	0.52	[kg]
	sorting and pressing of iron scrap [RER]	0.22	[kg]
	copper production, primary [RER]	0.15	[kg]

TABLE A.13. Inventory of 1 kg copper pipe based on the copper production mix “copper, at regional storage [RER]” from Ecoinvent v2 [2] with increased percentage of secondary copper (from 44 % to 65 %) following the description in the EPD of a representative manufacturer of copper pipes [83]. The original data set was transferred and adapted to Ecoinvent v3.3. - continued

Category	Material/Process	Value	Unit
production of pipes	copper production, primary [RLA]	0.12	[tkm]
	transport, freight, inland waterways, barge tanker [RER]	0.11	[tkm]
	transport, freight, lorry 16-32 metric ton, EURO6 [RER]	0.099073	[kg]
	drawing of pipe, steel [RER]	1	[kg]

TABLE A.14. Inventory for 1 kg of aluminum (“aluminum, production mix, wrought alloy, at plant [RER] (custom)”)

Category	Material/Process	Value	Unit
New aluminum	aluminum production, primary, ingot [IAI Area, EU27 and EFTA]	0.9	[kg]
Recycled aluminum	market for aluminum scrap, new [RER]	0.1	[kg]

TABLE A.15. Inventory for an ice storage of 20 m<sup>3</sup>

Category	Material/Process	Value	Unit
Casing	aluminum, production mix, custom	7.6	[kg]

TABLE A.15. Inventory for an ice storage of 20 m<sup>3</sup> - continued

Category	Material/Process	Value	Unit
	unreinforced concrete production, with cement CEM II/B, custom	8.8	[m <sup>3</sup> ]
	excavation, skid-steer loader	172	[m <sup>3</sup> ]
	market for polystyrene, extruded	135	[kg]
	reinforcing steel production	684	[kg]
	market for steel, chromium steel 18/8	8.2	[kg]
	market for transport, freight, lorry >32 metric ton, EURO6	1 293.00	[tkm]
Heat exchanger (8 · 2.1 m <sup>2</sup> )	extrusion, plastic pipes	5	[kg]
	polypropylene, granulate	5	[kg]
	section bar rolling, steel	4.8	[kg]
	sheet rolling, chromium steel	82.4	[kg]
	steel, chromium steel 18/8	114.8	[kg]
	water, deionized, from tap water, at user	99.4	[kg]
	welding, arc, steel	43.2	[m]
	refrigerant R134a production [RER]	1.85	[kg]
	wastewater, from residence	0.0994	[m <sup>3</sup> ]
	waste polypropylene	5	[kg]
Piping	chromium steel pipe	3.35	[kg]
	polyethylene, high density, granulate	0.4	[kg]
	polyurethane, flexible foam	4.5	[kg]
	water, completely softened, from decarbonized water, at user	19.05	[kg]
	wastewater, from residence	0.02	[m <sup>3</sup> ]

TABLE A.15. Inventory for an ice storage of 20 m<sup>3</sup> - continued

Category	Material/Process	Value	Unit
	waste polyethylene/polypropylene product	0.4	[kg]
	waste polyurethane	4.5	[kg]

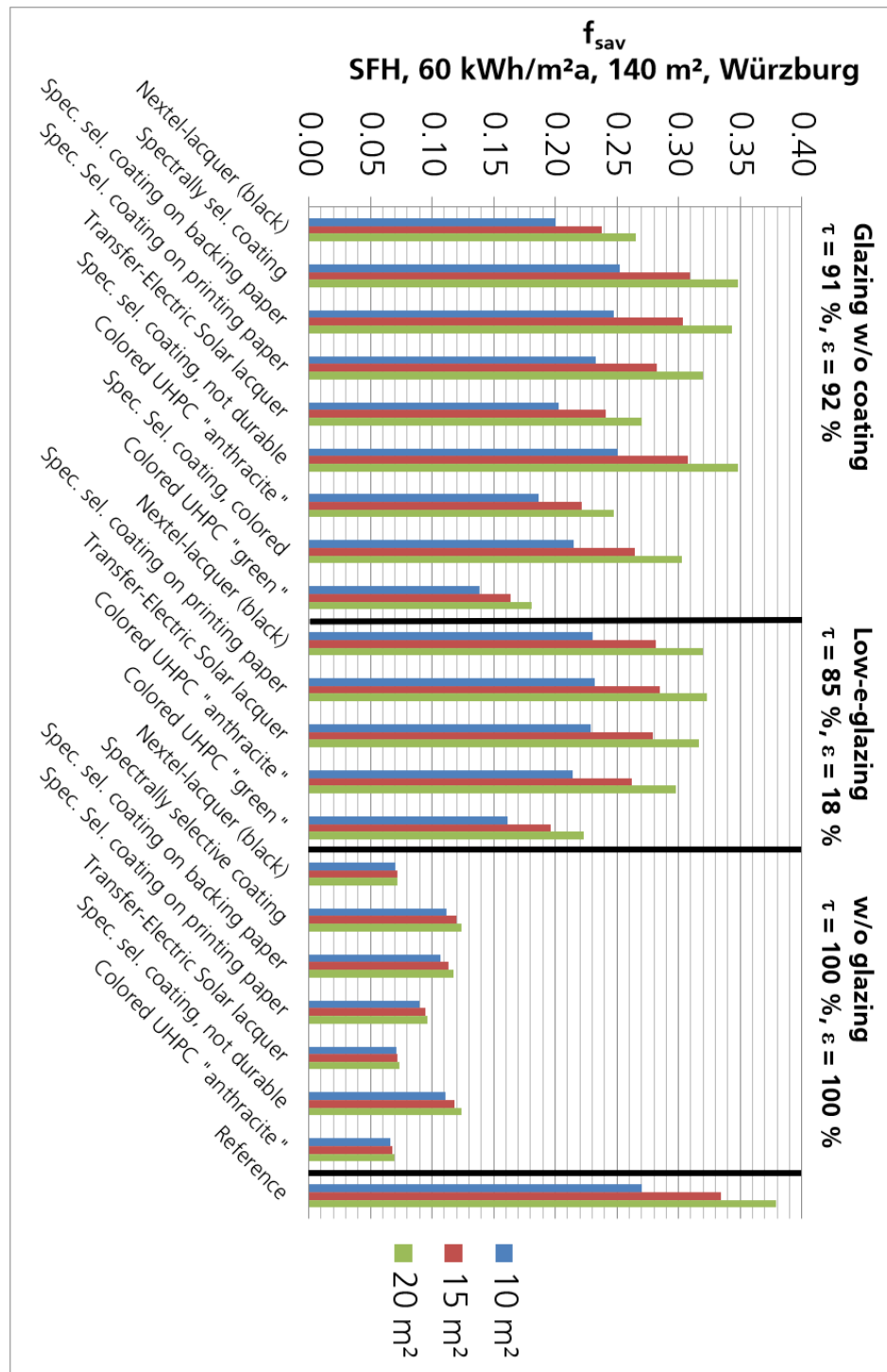


FIGURE A.12. Results of TABSOLAR system simulation during the first TABSOLAR project [74]



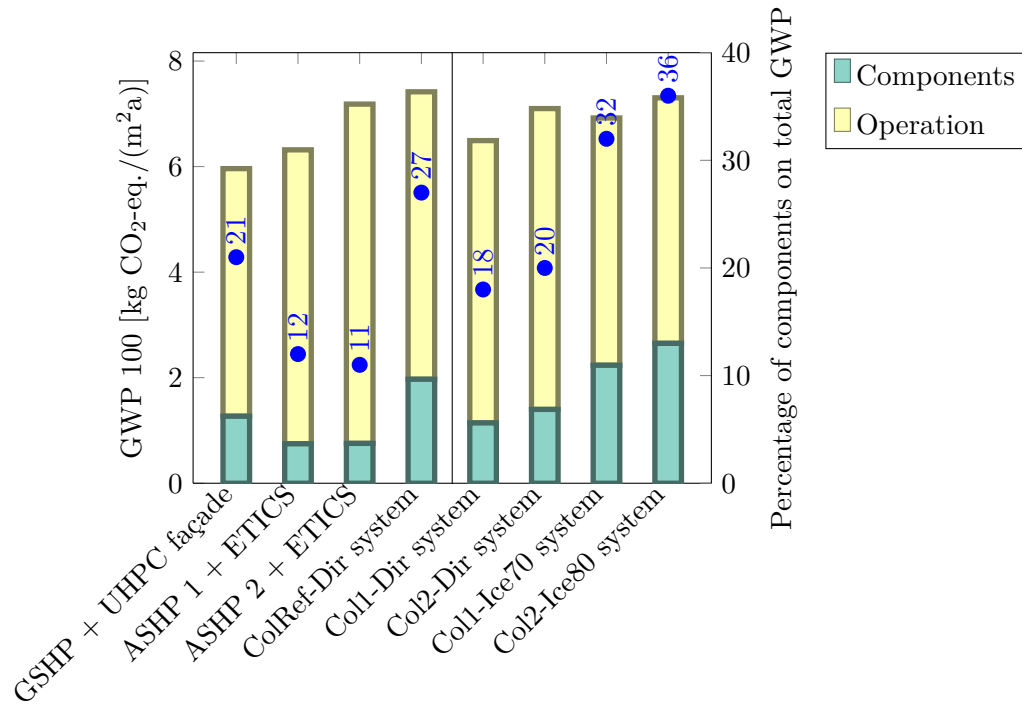


FIGURE A.13. Yearly global warming potential of the system components and the operation per floor area  $A_f$  on the base of 25 years of operation with CO<sub>2</sub> emissions factors following [55].

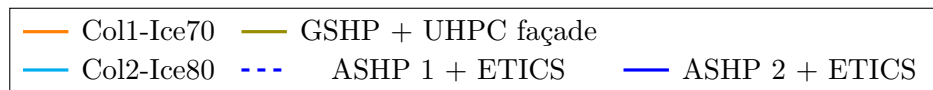
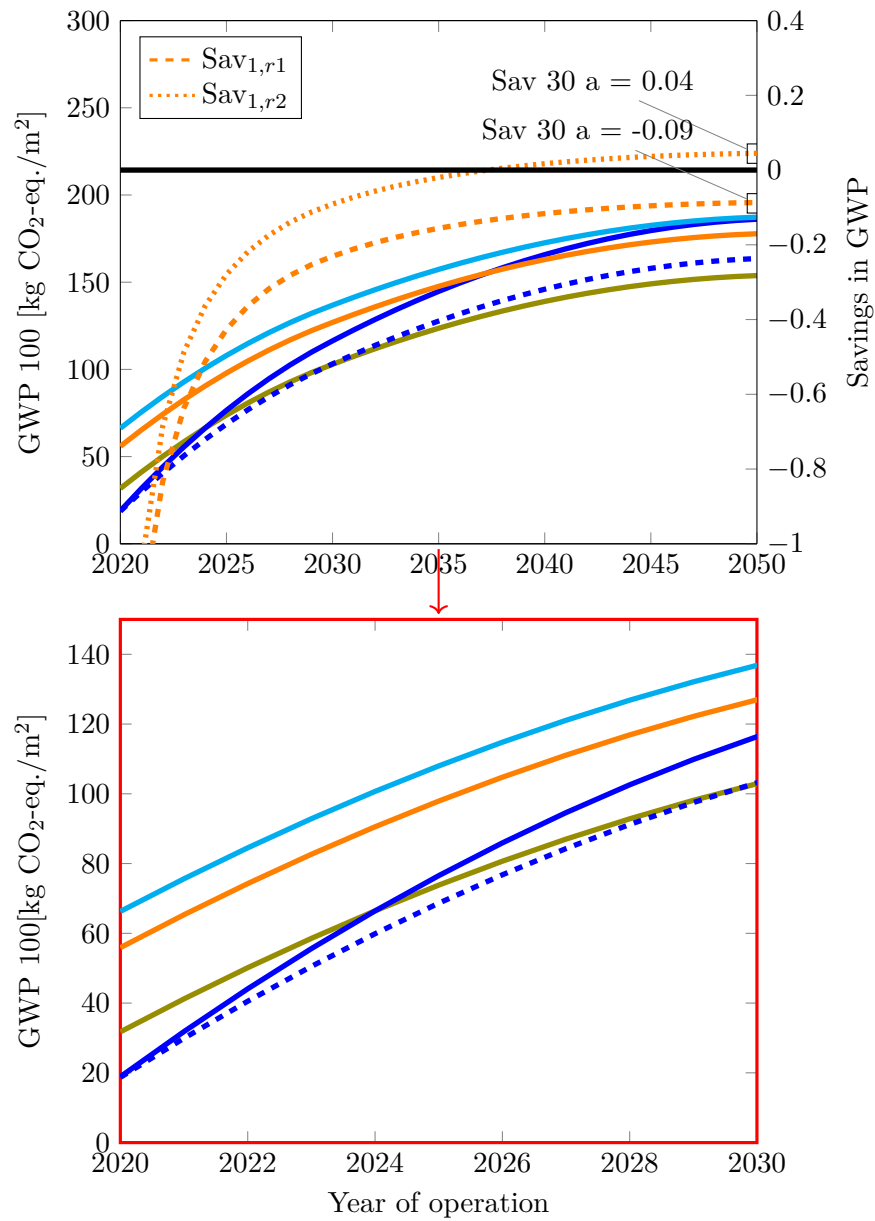


FIGURE A.14. Global warming potential in the course of operating time. The time of amortization of global warming potential of the Col-Ice systems referred to the ASHP systems is indicated with  $t_{x,ry}$ , exemplary savings on the right axis with  $Sav_{x,y}$ . The first index refers to Col1-Ice70 (1) or Col2-Ice80 (2), the second index refers to ASHP 1 + ETICS (r1) or ASHP 2 + ETICS (r2).

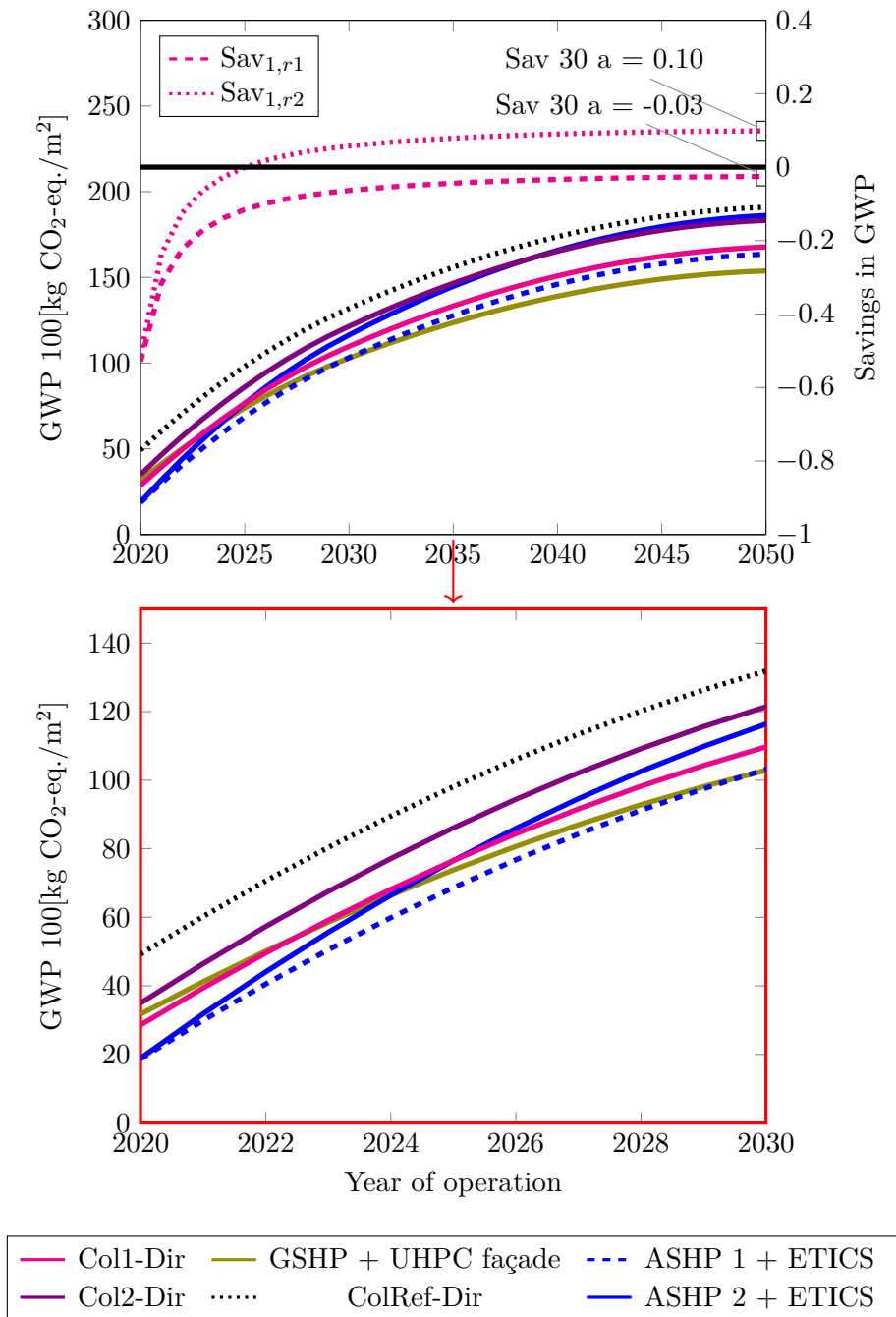


FIGURE A.15. Global warming potential in the course of operating time. The time of amortization of global warming potential of the Col-Dir systems referred to the ASHP systems is indicated with  $t_{x,ry}$ , exemplary savings on the right axis with  $Sav_{x,y}$ . The first index refers to Col1-Dir (1) or Col2-Dir (2), the second index refers to ASHP 1 + ETICS (r1) or ASHP 2 + ETICS (r2).



## List of Figures

Figure 1.2.1	Impression of trade fair BAU 2019: (A, left) <i>TABSOLAR</i> <sup>®</sup> <i>Premium</i> with spectrally selective coating and (A, right) <i>TABSOLAR</i> <sup>®</sup> <i>Design</i> unglazed in two colors. (B) The little cutout demonstrates a possible surface structure. Depending on the point of view the contrast of the pattern varies. (C) Backside of the collector with cutout of the back insulation (Source: Fraunhofer ISE). . . . .	3
Figure 1.2.2	<i>TABSOLAR</i> <sup>®</sup> concept. Left: impression of trade fair BAU 2019 (Source: Fraunhofer ISE). Center: schematic of possible system configuration (Source: Priedemann Facade-Lab GmbH). Right: thermographic image of small a <i>TABSOLAR</i> <sup>®</sup> sample (Source: Fraunhofer ISE). . . . .	4
Figure 1.8.1	Visualization of a representative multi-family home with a <i>TABSOLAR</i> <sup>®</sup> /ice storage system (left) and the economic benchmark with air heat pump and ETICS façade (right), schematically . . . .	9
Figure 1.9.1	Overview of thesis chapter organization . . . . .	11
Figure 2.1.1	Development of the installed capacity of solar thermal energy plants for the provision of low temperature heat in individual buildings (decentralized), in connection with heating networks, and in trade and industrial processes [70]. . . . .	14
Figure 2.1.2	Exemplary loadfile for the demand of space heating of a single-family home (SFH) with 140 m <sup>2</sup> according to Task 32 SFH 60 (60 kWh/(m <sup>2</sup> a)) and the demand for domestic hot water according to DHWcalc, location Würzburg (Germany). . . . .	16
Figure 2.1.3	Global Irradiation on tilted surface per square meter (0°, 45°, 75° and 90°), monthly averages, orientation: south, location Würzburg (Germany). . . . .	17
Figure 2.1.4	Visualization of actual markets of solar thermal and façades in Germany with intersecting set BIST façades. Each market is	

	represented with a circular area representing the size of the market. As the façade market (blue) is far larger than the solar thermal market (yellow) only a cutout of its representing circular area is shown. The graphic is based on a graphic developed during FDays®.	19
Figure 2.1.5	Possible Scenarios for the development of solar thermal and façade markets shown in figure 2.1.4. Scenario A: possible future intersecting set of markets of solar thermal and façades if markets merge together and sizes stagnate; Scenario B: Visualization of needed market growth up to 2050 following figure 2.1.1. The graphic is based on a graphic developed during FDays®.	20
Figure 2.2.1	Examples for BIST, BIPV and glazed materials. (A) Villanova (Spain) [119], (B) Solarsiedlung Köln-Bocklemünd (Germany) [119], (C) left: Multi-family atrium house in Oslo (Norway), right: Bjørkelangen school (Norway) [115], (D) Copenhagen-International-School-Nordhavn (Denmark), Adam Mørk, (E) Haus der Bauern (Freiburg, Germany), Joergens.mi/Wikipedia, (F) Cambridge Water Company Headquarters (England), Pilkington.	23
Figure 2.2.2	Three approaches to active solar thermal energy generation in context of sustainable buildings with different possible scores in “Baukultur and design quality” and “Sustainable development goals”, in this graphic’s context referred to decarbonization (Yellow = mediocre, green = good, light green = good with small restrictions).	25
Figure 2.2.3	SOLARroof of Wagner & Co, excerpt of technical information from 2007 [161].	26
Figure 2.2.4	Planned Solar roof of Tesla, Inc. [152]	27
Figure 2.2.5	Mock-up of semitransparent BIST element [166]	27
Figure 2.5.1	Evaluation parameters for BIST, first level based on Maurer et al. [109], second level “Aesthetics” based on Munari Probst and Roecker [119].	33
Figure 3.1.1	Left: theory of an integrated sustainability model, visualized following [89], right: exemplary application to solar thermal collectors following [91]	36
Figure 3.2.1	Various LCA goals related to energy-producing building envelope elements (e.g., solar thermal collectors) with associated system boundaries.	39

Figure 3.3.1	Basic structure of PROSA – product sustainability assessment [61]	40
Figure 3.3.2	Exemplary life cycle stages of a solar thermal collector . . . . .	42
Figure 3.3.3	Framework of Life cycle assessment (LCA) [126]. The numbering indicates the order within the iterative process. . . . .	42
Figure 3.3.4	Framework of Social Life Cycle, assessment system from categories to unit of measurement. [3], p. 45. . . . .	45
Figure 3.3.5	Evaluation of sustainability of three examples in a spiderweb chart. “A” could represent the evaluation of BIST conducted by the “engineer’s approach”, “B” the one of the “architect’s approach”, and “C” could represent the “interdisciplinary approach” in figure 2.2.2, of which the sum of all sustainability numbers is the highest. . . .	46
Figure 3.5.1	Above: residential buildings in building size classes (BSC) of 1, 2, 3-6 and more than 7 apartments in percent; below: shares of apartments in BSC. Evaluation for city-states (Hamburg, Bremen, Berlin) in Germany and all of Germany in 2011, own graphic based on [20].	50
Figure 3.5.2	Visualization of an apartment building of the building age class 1958–1978. South side, east side in section, without heat generation system. . . . .	51
Figure 3.5.3	Visualizations of economic benchmark, architectural benchmark, and the solar systems . . . . .	52
Figure 3.5.4	Overview and workflow of used methods within this work using the example of solar systems. . . . .	54
Figure 4.1.1	Indicative overview of solar thermal applications (based on output temperature) with a rough classification of solar thermal technologies. Grayed applications and collector concepts are not explicitly treated within this work. PVT stands for Photovoltaic thermal collectors [52]. . . . .	56
Figure 4.1.2	Cross-sections of different collectors: air collector (top, left), unglazed absorber (top, right), vacuum tube collector (bottom left) and flat plat collector (bottom, right) [52]. . . . .	56
Figure 4.1.3	Absorption and emission factors for various absorber coatings [52].	57
Figure 4.1.4	Different channel designs of classical absorbers: (A) harp, (B) double harp, (C) meander, (D) meander designed for drainback systems [52], cutout of unglazed pillow absorber, source: <a href="http://www.energie-solaire.com">www.energie-solaire.com</a>	

	(E), uncoated triangular sample with FracTherm <sup>®</sup> design built within the European project BIONICOL (F) [72] . . . . .	58
Figure 4.1.5	Schematic sketches of fin/sheet-and-tube absorber (left) and integrated absorber (right) [73] . . . . .	59
Figure 4.1.6	Typical instantaneous efficiency curves of various flat plate collector types with and without glazing and with and without spectrally selective coating (left). For two of the shown four collector types, the heat gain curve is given for two values of irradiation: $G = 750 \text{ W/m}^2$ and $G = 250 \text{ W/m}^2$ (right). Significant differences from actual collectors may occur ( $\eta$ = instantaneous thermal efficiency, $\vartheta_{fluid,m}$ = medium collector temperature, $\vartheta_{amb}$ = ambient temperature, $G$ = Irradiation). Values based on the aperture area of the collector. Values are based on measurement at $G = 1000 \text{ W/m}^2$ and a wind velocity of $u_{wind} = 3 \text{ m/s}$ . . . . .	63
Figure 4.2.1	Impressions of TAKTL <sup>®</sup> elements (left, center left, source: <a href="http://www.taktl-llc.com">www.taktl-llc.com</a> ); Volksbank in Krefeld, Germany, with white UHPC cladding [39] (center right); ESTP - Cachan, Architect: Architecture Studio, source: <a href="https://fehrgroup.com">https://fehrgroup.com</a> (left) . . . . .	64
Figure 4.2.2	Exhibit of TABSOLAR <sup>®</sup> Premium, Economy and Design (left), Exhibit of TABSOLAR <sup>®</sup> Premium and Design on trade fair BAU 2019 in Munich (center, top), UHPC sample with spectrally selective coating (right), design of a planned mobile demonstration building, source: Priedemann Facade-Lab . . . . .	65
Figure 4.2.3	Different façade systems with fluid-carrying UHPC elements for renovation and new buildings: External thermal insulation composite system (ETICS) (left), rear-ventilated façade (center), sandwich wall (right) [75]. . . . .	66
Figure 4.2.4	Schematic of UHPC element of current design (left). Principle possibilities to mount a UHPC element, piping structure adapted to vertical orientation (center). Schematic of two hydraulically connected UHPC elements with agrafes for fastening on traverse; view from the backside (left). Source: Fraunhofer ISE. . . . .	67
Figure 4.2.5	Variants of glazing for TABSOLAR <sup>®</sup> Premium and Economy. Variant (B) and (D) are depicted with sealing rubber and silicone (black). Source: Priedemann Facade-Lab. . . . .	68



Figure 4.2.6	Production of <i>TABSOLAR</i> <sup>®</sup> elements with channels by membrane vacuum deep-drawing. . . . .	69
Figure 4.2.7	<i>TABSOLAR</i> <sup>®</sup> element with channels . . . . .	70
Figure 4.3.1	Heat loss mechanisms in a glazed solar thermal collector [52]. . . . .	73
Figure 4.3.2	Thermal resistance network of the overall collector heat loss coefficient $1/U_{loss}$ of a glazed collector. The dashed line between $h_{rad,Cover}$ and $\vartheta_{amb}$ indicates the differentiation between sky and ambient temperature. Graphic adapted from Lämmle [101]. . . . .	75
Figure 4.3.3	Equivalent thermal resistance network of the internal heat transfer coefficient $U_{abs,fluid}$ . Graphic adapted from Lämmle [101]. . . . .	77
Figure 4.3.4	Thermal resistance network of the overall collector heat loss coefficient $1/U_{loss}$ of a glazed façade collector. Green and yellow colored resistances were used for test “Model comparison”. For glazed collectors within test “Active area vs. channel distance” also the purple colored resistances were used. Graphic adapted from Lämmle [101]. . . . .	79
Figure 4.3.5	Geometry, boundary conditions, and temperature distribution to determine the heat transfer coefficient $U_{Abs,Fluid,fix}$ with $\varepsilon = 0.95$ , $\vartheta_{amb} = \vartheta_{fluid,m} = 25^\circ\text{C}$ , $G = 750\text{ W/m}^2$ and $u_{wind} = 3\text{ m/s}$ . Adiabatic boundary conditions are shown in blue. . . . .	80
Figure 4.3.6	Cross-section of UHPC element, cutout with two channels . . . . .	80
Figure 4.3.7	Geometry and boundary conditions for FEM simulation of partition Centre. Adiabatic boundary conditions are shown in blue. . . . .	81
Figure 4.3.8	Calculated temperature distribution of FEM simulation in Kelvin for partition Center for $\varepsilon = 0.95$ , $\vartheta_{amb} = \vartheta_{fluid,m} = 25^\circ\text{C}$ , $G = 750\text{ W/m}^2$ and $u_{wind} = 3\text{ m/s}$ . Arrows indicate heat flow. . . . .	84
Figure 4.3.9	Comparison of heat gain curves simulated with different models for an unglazed UHPC absorber with $G = 750\text{ W/m}^2$ , $u_{wind} = 3\text{ m/s}$ and radiation towards $\vartheta_{amb}$ . Right: $\varepsilon = 0.95$ , left: $\varepsilon = 0.2$ , above without back insulation, below with back insulation. Heat gain calculated for an aperture area = $1.16\text{ m}^2$ with an active area of $0.98\text{ m}^2$ . . . . .	85
Figure 4.3.10	Comparison of heat gain curves simulated with different boundary conditions for an unglazed UHPC absorber with $G = 750\text{ W/m}^2$ , $u_{wind} = 3\text{ m/s}$ and $\vartheta_{amb} = 25^\circ\text{C}$ . Right: $\varepsilon = 0.95$ ,	

	left: $\varepsilon = 0.2$ , Heat gain calculated for aperture area $=1\text{ m}^2$ without margin effects. . . . .	87
Figure 4.3.11	Areas of different efficiencies of UHPC collector, marked in colors. . . . .	89
Figure 4.3.12	Boundary conditions for FEM calculation of margins L and geometry of margin S. . . . .	89
Figure 4.3.13	Boundary condition for margins with agrafe and part of the center area. . . . .	90
Figure 4.3.14	Comparison of heat gain curves simulated with different geometries for an unglazed UHPC absorber with $G = 750\text{ W/m}^2$ , $u_{wind} = 3\text{ m/s}$ and radiation towards $\vartheta_{amb} = 25\text{ }^\circ\text{C}$ . Right: $\varepsilon = 0.95$ , left: $\varepsilon = 0.2$ , heat gain calculated for aperture area $A_{ap} = 1\text{ m}^2$ . . . . .	91
Figure 4.3.15	Temperature distribution for margin with agrafe (total and excerpt) calculated with $\varepsilon = 0.2$ , $\vartheta_{amb} = 25\text{ }^\circ\text{C}$ , $\vartheta_{fluid,m} = 15\text{ }^\circ\text{C}$ , $G = 750\text{ W/m}^2$ and $u_{wind} = 3\text{ m/s}$ . Arrows indicate normed total heat flux. . . . .	92
Figure 4.3.16	Comparison of heat gain curves simulated with different geometries for an unglazed UHPC absorber with $G = 750\text{ W/m}^2$ and sky view factor $SVF = 0.5$ . Right: Insulated, $\varepsilon = 0.1$ , $u_{wind} = 0\text{ m/s}$ , left: uninsulated, $u_{wind} = 3\text{ m/s}$ , $\varepsilon = 0.95$ , heat gain calculated for aperture area $= 1\text{ m}^2$ . . . . .	93
Figure 4.3.17	Temperature distribution for insulated margin with agrafe. The unit of temperature scale is $^\circ\text{C}$ . It is calculated with radiation toward $\vartheta_{amb}$ , ventilated, $\vartheta_{amb} = 25\text{ }^\circ\text{C}$ , $\varepsilon = 0.1$ , $u_{wind} = 0\text{ m/s}$ , $G = 750\text{ W/m}^2$ . Arrows indicate heat flow and are sized proportionally to the heat flux. . . . .	94
Figure 4.3.18	Influence of different margins on the total heat output of an unglazed UHPC absorber with an area of $A = 1.16\text{ m}^2$ . The uppermost line would be the heat gain curve if the element had no margins. Heat output calculated for $G = 750\text{ W/m}^2$ and sky view factor $SVF = 0.5$ . . . . .	95
Figure 4.3.19	Schematic of different active areas within a UHPC collector of $1.75\text{ m}^2$ . . . . .	99
Figure 4.3.20	$U_{abs,fluid}$ depending on the distance from center channels (center to center) for different $U_{loss}$ calculated with FEM at $\vartheta_{amb} = 25\text{ }^\circ\text{C}$ . . .	99

- Figure 4.3.21 “A” shows a comparison of the heat gain curve of a gray-colored, insulated façade collector with EuroWhite glazing (properties see table 4.3.3) and  $U_{abs,fluid} = 85.14 \text{ W}/(\text{m}^2 \text{ K})$  calculated with the correlation of Randall (equation (4.3.32)) and Hollands (equation (4.3.33)) at different tilt angles  $\theta_t$ . “B” compares the heat gain curve of the same collector with the correlation of Hollands at  $80^\circ$  with different values for  $U_{abs,fluid}$ , and different active areas and their respective margins as described in figure 4.3.19. All heat gain curves are calculated at  $\vartheta_{amb} = 25^\circ\text{C}$ , irradiation  $G = 750 \text{ W}/\text{m}^2$ , wind velocity  $u_{wind} = 3 \text{ m}/\text{s}$ , sky view factor = 0.5. . . . . 102
- Figure 4.3.22  $Q_{coll,MAP}$  for different UHPC collectors with an area of  $1.75 \text{ m}^2$ . “Center” refers to a hypothetical UHPC collector without margins and the minimal channel distance  $d = 40 \text{ mm}$ , “Active A” refers to a UHPC collector with a fully used activatable area and channel distance  $d = 54.4 \text{ mm}$ , and “Active B” refers to a UHPC collector with a partly used activatable area with the minimal channel distance  $d = 40 \text{ mm}$  as described in the setup of test “Active area vs. channel distance”. . . . . 103
- Figure 5.1.1 Typical solar combi system with combi storage. Source: Fraunhofer ISE . . . . . 108
- Figure 5.1.2 Operation stages of drainback systems: (a) not in operation, (b) filling process, (c) operation mode, (d) draining process [13]. . . . . 109
- Figure 5.1.3 Schematic representation of the heat pump cycle [6]. . . . . 111
- Figure 5.1.4 Representation of solar-assisted heat pump systems based on the visualization scheme developed by Frank et al. [53] . . . . . 115
- Figure 5.2.1 System scheme of monoenergetic systems (GSHP, ASHP, and Col-Dir) based on a schematic representation work developed in the project “LowEx im Bestand”. . . . . 118
- Figure 5.2.2 System schematic of bivalent systems (Col-Ice) based on a schematic representation work developed in the project “LowEx im Bestand” 119
- Figure 5.3.1 Resistor-capacitor network of zone model according to DIN EN ISO 13790:2008-09 [125] . . . . . 121
- Figure 5.3.2 Heating load of the considered MFH in Potsdam modeled with the TRNSYS 3-zone model (blue) and with the Modelica 1-zone RC-model (red) with respect to net floor area  $A_f$  in the course of a

	year together with the ambient temperature (above) and integrated (below). . . . .	123
Figure 5.4.1	Implementation of simple adiabatic ice storage in Modelica . . . . .	127
Figure 5.4.2	Standard heating load following DIN 12831 [37], which forms the basis for the design of the heat pump, and daily average of calculated heating load of MFH. . . . .	128
Figure 5.4.3	Implementation of ASHP in Dymola/Modelica . . . . .	130
Figure 5.4.4	Implementation of GSHP in Dymola/Modelica . . . . .	131
Figure 5.4.5	Implementation of solar direct system in Dymola/Modelica . . . . .	131
Figure 5.4.6	Implementation of a solar direct system (Col-Dir) in Dymola/Modelica	132
Figure 5.5.1	System schematic of monoenergetic systems (GSHP, ASHP, and Col-Dir) based on a schematic representation work developed in the project “LowEx im Bestand”. Frames indicate the calculation of the different seasonal performance factors following equations (5.1.5), (5.5.1), (5.5.3) and (5.5.5). . . . .	138
Figure 5.5.2	Seasonal performance factors $SPF_{HP}$ , $SPF_{HP,ext}$ , $SPF_{SYS}$ , and $SPF_{SYS,ext}$ of reference systems and direct solar systems for different aperture areas $A_{ap}$ with respect to the heat demand for heating and hot water in bivalent point $\dot{Q}_{demand,biv}$ and different wind correction factors ( $wcf$ ). The first plot shows the part of the south façade covered by the collector (black) on the right axis. . . . .	141
Figure 5.5.3	Proportions of different energy flows of the solar collectors (gray, NoInsu) with respect to the occurring temperature range $\vartheta_{fluid,m} - \vartheta_{amb}$ within the operation of the Col-Dir system with $A_{ap}/\dot{Q}_{demand,biv} = 6 \text{ m}^2/\text{kW}$ and $wcf = 0.5$ . . . . .	143
Figure 5.5.4	Seasonal performance factors $SPF_{SYS}$ of reference systems and solar direct systems for different aperture areas $A_{ap}$ with respect to the heat demand for heating and hot water in bivalent point $\dot{Q}_{demand,biv} = Q_{demand,biv,heating} + DHW$ and different wind correction factors ( $wcf$ ). . . . .	145
Figure 5.5.5	Temperature at evaporator inlet for the reference systems and the south and north installation ( $A_{ap}/\dot{Q}_{demand,biv} = 6 \text{ m}^2/\text{kW}$ , $wcf = 0.5$ ), monthly weighted averages. . . . .	146

Figure 5.5.6	Comparison of an installation of the gray, uninsulated collector on the south façade with and without the store-hot condition ( $A_{ap}/\dot{Q}_{demand,biv} = 6 \text{ m}^2/\text{kW}$ , $wcf = 0.5$ ) . . . . .	147
Figure 5.5.7	Temperature at evaporator inlet for the reference systems and the Col1-Dir system with and without the store-hot condition ( $A_{ap}/\dot{Q}_{demand,biv} = 6 \text{ m}^2/\text{kW}$ , $wcf = 0.5$ ), monthly weighted averages. . . . .	148
Figure 5.5.8	Seasonal performance factor $\text{SPF}_{SYS}$ of reference systems, Col-Dir systems for different ratios $A_{ap}/\dot{Q}_{demand,biv}$ ( $wcf = 0.5$ ) and different Col-Ice systems. . . . .	149
Figure 5.5.9	Temperature at evaporator inlet $\vartheta_{eva,In}$ for reference systems and two Col-Ice systems: Col1-Ice70 has the gray, uninsulated collector, the Col2-Ice80 system is simulated with the spectrally selective, insulated collector ( $A_{ap}/\dot{Q}_{demand,biv} = 9.05$ and $wcf = 0.5$ ), monthly (m-av) and yearly (y-av) averages. . . . .	151
Figure 5.5.10	Proportions of different energy flows of the solar collectors (gray, NoInsu) with respect to the occurring temperature range $\vartheta_{fluid,m} - \vartheta_{amb}$ in the operation of the Col1-Ice70 systems with $A_{ap}/\dot{Q}_{demand,biv} = 9.05$ and $wcf = 0.5$ . . . . .	152
Figure 5.5.11	Proportions of total useful energy flows of the solar collectors (gray, NoInsu) with respect to the occurring temperature range $\vartheta_{fluid,m} - \vartheta_{amb}$ in the operation of the Col1-Ice70 systems with $A_{ap}/\dot{Q}_{demand,biv} = 9.05$ and $wcf = 0.5$ . . . . .	152
Figure 6.1.1	Different considered façade constructions. Left: External thermal insulation system (ETICS); center: uninsulated passive or active rear-ventilated façade with UHPC cladding; right: insulated active rear-ventilated façade with UHPC cladding. . . . .	159
Figure 6.1.2	Global warming potential (GWP) and primary energy demand (PED) of differently modeled copper pipes: the environmental product declaration “EPD” [83] is compared to copper pipes modeled with copper data for the global market (“v3.6, GLO”) and for a European production mix “copper, at regional storage [RER]”. “V2.2, RER” represents the original consumption mix [2] in Ecoinvent v2.2, “v3.6, RER” represents the original mix transferred to Ecoinvent v3.6, and “v3.6, RER, rec65” corresponds to the updated inventory with increased recycling input shown in table A.13. . . . .	161

Figure 6.1.3	Drawing of a substructure for <i>TABSOLAR</i> <sup>®</sup> collectors during the planning process. Source: Priedemann Facade-Lab. . . . .	169
Figure 6.1.4	Specific CO <sub>2</sub> emission factor for the years 2020 to 2050 following Fritsche et al. [55] and the reference CO <sub>2</sub> emission factor in 2014, both of German electricity mix. . . . .	175
Figure 6.2.1	Primary energy demand of different active and passive façades. All UHPC collectors are based on the <i>TABSOLAR</i> <sup>®</sup> concept. Col1 represents the gray <i>Design</i> variant without insulation, Col2 the <i>Design</i> variant with insulation and spectrally selective coating. Col3 stands for the variant <i>Economy</i> , Col4 for <i>Premium</i> . ColRef is an unglazed steel collector. The standard collector is equipped with an absorber made of an aluminum sheet with copper pipes. . . . .	176
Figure 6.2.2	Global warming potential of different active and passive façade components. All UHPC collectors are based on the <i>TABSOLAR</i> <sup>®</sup> concept. The variant Col1 represents the gray <i>Design</i> variant without insulation, Col2 the <i>Design</i> variant with insulation and spectrally selective coating. Col3 stands for the variant <i>Economy</i> , Col4 for <i>Premium</i> . ColRef is an unglazed steel collector. The standard collector is equipped with an absorber made of an aluminum sheet with copper pipes. . . . .	177
Figure 6.2.3	Primary energy demand (above) and global warming potential (below) of the system components. . . . .	179
Figure 6.2.4	Yearly primary energy demand of the system components and the operation per floor area based on 25 years of operation. . . . .	180
Figure 6.2.5	Yearly global warming potential of the system components and the operation per floor area $A_f$ based on 25 years of operation. . . . .	181
Figure 6.2.6	Primary energy demand in the course of operating time. The time of amortization of primary energy of the Col-Dir systems referred to the ASHP systems is indicated with $t_{x,ry}$ , exemplary savings on the right axis with $Sav_{x,y}$ . The first index refers to Col1-Dir (1) or Col2-Dir (2), the second index refers to ASHP 1 + ETICS (r1) or ASHP 2 + ETICS (r2). . . . .	183
Figure 6.2.7	Primary energy demand in the course of operating time. The time of amortization of primary energy of the Col-Ice systems referred to the ASHP systems is indicated with $t_{x,ry}$ , exemplary savings on the right axis with $Sav_{x,y}$ . The first index refers to Col1-Ice70 (1) or	

	Col2-Ice80 (2), the second index refers to ASHP 1 + ETICS (r1) or ASHP 2 + ETICS (r2). . . . .	184
Figure 6.2.8	Global warming potential in the course of operating time. The time of amortization of global warming potential of the Col-Dir systems referred to the ASHP systems is indicated with $t_{x,ry}$ , exemplary savings on the right axis with $Sav_{x,y}$ . The first index refers to Col1-Dir (1) or Col2-Dir (2), the second index refers to ASHP 1 + ETICS (r1) or ASHP 2 + ETICS (r2). . . . .	185
Figure 6.2.9	Global warming potential in the course of operating time. The time of amortization of global warming potential of the Col-Ice systems referred to the ASHP systems is indicated with $t_{x,ry}$ , exemplary savings on the right axis with $Sav_{x,y}$ . The first index refers to Col1-Ice70 (1) or Col2-Ice80 (2), the second index refers to ASHP 1 + ETICS (r1) or ASHP 2 + ETICS (r2). . . . .	186
Figure 7.3.1	Profit margin as a percentage of the manufacturing price for 1 m <sup>2</sup> <i>TABSOLAR</i> <sup>®</sup> <i>Premium</i> element. Costs for the standard collector and cost ranges for built façade collectors are based on Cappel et al. [25]. Source for cost ranges for Eternit: Priedemann Facade-Lab. Source for cost range ETICS: BMVBS [78] . . . . .	193
Figure 7.3.2	Profit margin as a percentage of the manufacturing price for 1 m <sup>2</sup> <i>TABSOLAR</i> <sup>®</sup> <i>Design</i> element. Cost ranges for built façade collectors are based on Cappel et al. [25]. Source for cost ranges for Eternit: Priedemann Facade-Lab, façade insulation BMVBS [78]. Source for cost range ETICS: BMVBS [78] . . . . .	194
Figure 7.3.3	Estimated investment costs of façade without imputed interests and costs of 25 years of operation for reference systems, Col1-Dir and Col1-Ice70 systems with an electricity price of 0.28 €/kWh. The price for the passive UHPC façade elements was assumed to be similar to Eternit façade elements. Investment costs of system components like ice storage with their imputed interests are not shown. . . . .	197
Figure A.1	Basic scheme of Reher's Modelica system model on Dymola [138] .	225
Figure A.2	Comparison of measured data and 2D regression model of ASHP 1	231
Figure A.3	Comparison of measured data and 2D regression model of ASHP 2	232
Figure A.4	Comparison of measured data and 2D regression model of GSHP .	232

Figure A.5	Implementation of fit model with prescribed heat in Modelica . . . .	233
Figure A.6	Temperatures weighted with $Q_{con}$ at the evaporator inlet and outlet and condenser inlet and outlet for GSHP, monthly (m-av) and yearly (y-av) averages. . . . .	233
Figure A.7	Temperatures weighted with $Q_{con}$ at the evaporator inlet and outlet and condenser inlet and outlet for ASHP 2, monthly (m-av) and yearly (y-av) averages. . . . .	234
Figure A.8	Temperatures weighted with $Q_{con}$ at the evaporator inlet and outlet and condenser inlet and outlet for ASHP 1, monthly (m-av) and yearly (y-av) averages. . . . .	234
Figure A.9	Temperatures weighted with $Q_{con}$ at the evaporator inlet and outlet and condenser inlet and outlet for the Col-Dir system with $wcf=0.5$ and $A_{ap}$ of $6\text{ m}^2$ per $\dot{Q}_{demand,biv}$ ( $17.3\text{ kW}$ ), monthly (m-av) and yearly (y-av) averages. . . . .	235
Figure A.10	Seasonal performance factors $SPF_{HP}$ , $SPF_{HP,ext}$ , $SPF_{SYS}$ and $SPF_{SYS,ext}$ of reference systems, Col-Dir systems for different ratios $A_{ap}/\dot{Q}_{demand,biv}$ ( $wcf = 0.5$ ) and different Col-Ice systems. . . . .	236
Figure A.11	Drawing of Solardach AS (ColRef), excerpt of handbook of Energie Solaire SA [45]. . . . .	241
Figure A.12	Results of TABSOLAR system simulation during the first TABSOLAR project [74] . . . . .	246
Figure A.13	Yearly global warming potential of the system components and the operation per floor area $A_f$ on the base of 25 years of operation with $\text{CO}_2$ emissions factors following [55]. . . . .	247
Figure A.14	Global warming potential in the course of operating time. The time of amortization of global warming potential of the Col-Ice systems referred to the ASHP systems is indicated with $t_{x,ry}$ , exemplary savings on the right axis with $\text{Sav}_{x,y}$ . The first index refers to Col1-Ice70 (1) or Col2-Ice80 (2), the second index refers to ASHP 1 + ETICS (r1) or ASHP 2 + ETICS (r2). . . . .	248
Figure A.15	Global warming potential in the course of operating time. The time of amortization of global warming potential of the Col-Dir systems referred to the ASHP systems is indicated with $t_{x,ry}$ , exemplary savings on the right axis with $\text{Sav}_{x,y}$ . The first index refers to	



Col1-Dir (1) or Col2-Dir (2), the second index refers to ASHP 1 +  
ETICS (r1) or ASHP 2 + ETICS (r2). . . . . 249



## List of Tables

Table 4.2.1	Calculation of the effective heat capacity of collector variants according to ISO 9806 (2018)[36] for a collector with $A = 1.75 \text{ m}^2$ .	72
Table 4.3.1	Composition of a simulated building wall. It was assumed that an old building wall with a U-value of $1.13 \text{ W}/(\text{m}^2 \text{ K})$ would be renovated with thermal insulation and a rear-ventilated façade. The U-value of the renovated wall construction is $0.23 \text{ W}/(\text{m}^2 \text{ K})$ . . . . .	78
Table 4.3.2	Input data for collector model in Modelica according to DIN EN ISO 9806 (2018)[36]. Col1 and Col2 were simulated and prepared for a collector with an aperture area of $A = 1.16 \text{ m}^2$ . The reference steel collector (ColRef) has an aperture area of $A = 2.03 \text{ m}^2$ . . . . .	97
Table 4.3.3	Technical data of simulated glazing . . . . .	101
Table 5.3.1	Fitted input data for zone model in Modelica according to DIN EN ISO 13790:2008-09 [125]. . . . .	121
Table 5.4.1	Dimensions and parameter setting of hot storage tanks . . . . .	135
Table 6.1.1	Inventory of $1 \text{ m}^2$ external thermal insulation system (ETICS) with mineral wool with a U-value of the wall of $0.28 \text{ W}/(\text{m}^2 \text{ K})$ for renovation based on datasheets [21, 24, 22, 23] and [38] . . . . .	162
Table 6.1.2	Inventory of $1 \text{ m}^2$ <i>TABSOLAR</i> <sup>®</sup> collectors. The basic inventory accounts for the variant <i>Design</i> , other parts accounting for different variants are labeled “optional”. . . . .	164
Table 6.1.3	Inventory of $1 \text{ m}^3$ ultra-high performance concrete (UHPC), mixed (“UHPC, mixed, custom”) based on Fehling et al. [49] . . . . .	167
Table 6.1.4	Inventory of 1 kg “superplasticizer production, custom” based on Stengel and Schießl [153]. . . . .	167
Table 6.1.5	Inventory of deep-drawing of $1 \text{ m}^2$ <i>TABSOLAR</i> <sup>®</sup> element, custom process, based on experience during the production development (“deep-drawing UHPC, custom”) . . . . .	169

Table 6.1.6	Inventory of the substructure for 1 m <sup>2</sup> of a UHPC cladding (active or passive) (“substructure, custom”) . . . . .	170
Table 6.1.7	Inventory of 1 m <sup>2</sup> spectrally selective coating of UHPC. This dataset is based on “selective coating, copper sheet, sputtering [DE]”. The electricity value was doubled to account for the long operating time of the vacuum pump. Furthermore, aluminum and titanium dioxide were added to account for the used layers (“selective coating of UHPC, custom”). . . . .	170
Table 6.1.8	Inventory of pre-drying of 1 m <sup>2</sup> TABSOLAR panel, according to laboratory tests at Fraunhofer ISE. This process has to be revised as soon as the necessary drying parameters are better known. . . . .	172
Table 6.1.9	Inventory of one of four fluid connectors for a TABSOLAR design panel (“fluid connectors, custom”) . . . . .	172
Table A.1	Technical data of simulated building for TRNSYS simulation . . . . .	226
Table A.2	Characteristic curve for $\dot{Q}_{con}$ of air-source heat pump model “Ochsner GMLW 19” in [W], referred to as “ASHP 2” . . . . .	228
Table A.3	Characteristic curve for $P_{el}$ of air-source heat pump model “Ochsner GMLW 19” in [W], referred to as “ASHP 2” . . . . .	229
Table A.4	Characteristic curve for $\dot{Q}_{con}$ of air-source heat pump model “Ochsner GMLW 19 plus” in [W], referred to as “ASHP 1” . . . . .	229
Table A.5	Characteristic curve for $P_{el}$ of air-source heat pump model “Ochsner GMLW 19 plus” in [W], referred to as “ASHP 1” . . . . .	229
Table A.6	Characteristic curve for $\dot{Q}_{con}$ of ground-source heat pump model “Waterkotte Ecotouch DS 5056.5T” in [W] . . . . .	230
Table A.7	Characteristic curve for $P_{el}$ of ground-source heat pump model “Waterkotte Ecotouch DS 5056.5T” in [W] . . . . .	230
Table A.8	Fit parameters for heat pumps . . . . .	231
Table A.9	Annual energy flows of the Col1-Dir/Col1-Ice70 with Gray, uninsulated collector and Col2-Dir/Col2-Ice80 with spectrally selective coating and back insulation. Both Col-Dir and Col-Ice systems with $A_{ap}/\dot{Q}_{demand,biv} = 9 \text{ m}^2/\text{kW}$ and $wcf = 0.5$ . . . . .	237
Table A.10	Annual energy flows of systems with both ASHPs, GSHP, and the collector reference system ColRef-Dir. The shown	

	ColRef-Dir-system was simulated with the entire south façade ( $A_{ap}/\dot{Q}_{demand,biv} = 9 \text{ m}^2/\text{kW}$ ) and $wcf = 0.5$ . . . . .	238
Table A.11	Inventory of $1 \text{ m}^2$ flat plate collector with aluminum-copper absorber following Stucki and Jungbluth [150] and updated to Ecoinvent 3.6. Copper was modeled following table A.13, aluminum following table A.14. . . . .	239
Table A.12	Inventory of $1 \text{ m}^2$ unglazed flat plate collector with steel absorber Philippen et al. [131]. Aluminum was modeled following table A.14.	241
Table A.13	Inventory of 1 kg copper pipe based on the copper production mix “copper, at regional storage [RER]” from Ecoinvent v2 [2] with increased percentage of secondary copper (from 44 % to 65 %) following the description in the EPD of a representative manufacturer of copper pipes [83]. The original data set was transferred and adapted to Ecoinvent v3.3. . . . .	242
Table A.14	Inventory for 1 kg of aluminum (“aluminum, production mix, wrought alloy, at plant [RER] (custom)”) . . . . .	243
Table A.15	Inventory for an ice storage of $20 \text{ m}^3$ . . . . .	243